Unravelling the drivers of short- and long-term variability in the Amazon hydrological cycle using tree-ring oxygen isotopes

Jessica Charlotte Anne Baker

Submitted in accordance with the requirements for the degree of
Doctor of Philosophy

The University of Leeds
School of Geography

May 2017

The candidate confirms that the work submitted is her own, except where work which has formed part of jointly authored publications has been included. The contribution of the candidate and the other authors to this work has been explicitly indicated below. The candidate confirms that appropriate credit has been given within the thesis where reference has been made to the work of others.

Chapter 3

Baker, J.C.A., Santos, G.M., Gloor, M. & Brienen, R.J.W. *In review* in Trees. Does *Cedrela* always form annual rings? Testing ring periodicity across South America using radiocarbon dating.

JCAB (the candidate) and RJWB devised the manuscript and conducted tree-ring analysis. JCAB cut up rings, extracted cellulose and packed samples for radiocarbon analysis, prepared all figures and wrote the manuscript. GMS performed the radiocarbon dating and helped to write the section of the methods detailing the radiocarbon analysis. RJWB collected tree-ring samples and RJWB and MG helped with data interpretation. All authors gave critical feedback on a draft of the manuscript.

Chapter 4

Baker, J.C.A., Hunt, S.F.P., Clerici, S.J., Newton, R.J., Bottrell, S.H., Leng, M.J., Heaton, T.H.E., Helle, G., Argollo, J., Gloor, M. & Brienen, R.J.W. 2015. Oxygen isotopes in tree rings show good coherence between species and sites in Bolivia. *Global and Planetary Change*, 133, 298-308.

JCAB performed tree-ring analysis, cut up rings, conducted the cellulose extraction and prepared samples for isotope analysis and radiocarbon dating for all species apart from *Cedrela odorata*. JCAB also crossdated the isotope series, performed the data analysis, made all the figures presented in the manuscript and wrote the manuscript. SFPH performed the lab work outlined above for the samples of *C. odorata*. SJC, MJL and THEH conducted the isotope analysis. GH conducted isotope analysis of another data series (from Brienen et al., 2012) that is also included in the paper. JA provided the *Polylepis tarapacana* wood sample. RJWB collected all other samples from the field, conducted preliminary tree-ring analysis and guided the project. All authors commented

on a draft of the manuscript, with more extensive feedback from MG and RJWB (PhD supervisors).

Chapter 5

Baker, J.C.A., Gloor, M., Spracklen, D.V., Arnold, S.R., Tindall, J.C., Clerici, S. J., Leng, M.J. & Brienen, R.J.W. 2016. What drives interannual variation in tree-ring oxygen isotopes in the Amazon? *Geophysical Research Letters*, 43, 11831-11840.

JCAB conducted all analysis presented in the paper including trajectory simulations, calculations and climate data analysis, prepared all figures and wrote the manuscript. DVS and SRA provided support and training in how to use the trajectory model and output, and helped guide the analysis. MJ Leng analysed the isotope series presented in the paper. All authors contributed to discussion and/or provided critical feedback on a draft of the manuscript. MG and RJWB provided guidance and supervision throughout the process.

Chapter 6

Baker, J.C.A., Gloor, M., Boom, A., Cintra, B.B.L., Tindall, J.C., Clerici, S.J., Leng M.J., & Brienen, R.J.W. *In preparation.* The changing Amazon hydrological cycle – inferences from over 200 years of tree-ring oxygen isotope data.

JCAB helped with fieldwork, prepared samples and performed tree-ring analysis, cut up rings, extracted cellulose, crossdated isotope series, conducted all of the data analysis, made the figures and wrote the manuscript. AB and MJ conducted the isotope analysis. RJW, BC and SJC helped with fieldwork including sample collection. JCT provided guidance on data interpretation. MG and RJWB provided advice and guidance throughout and gave feedback on a draft of the manuscript.

Thesis by Alternative Format Rationale

This thesis is submitted as an alternative style of doctoral thesis including published material. This format is appropriate for the thesis because two out of the four data chapters have already been published in peer-reviewed journals, and a third is currently in review. The four manuscripts are preceded by an introduction (Chapter 1), which includes a review of the literature to give context to the work, the rationale for the project and an outline of the main research questions. The novelty of the research will also be highlighted here. The methodologies are described in Chapter 2. A discussion section (Chapter 7) follows the research articles, and weaves together the findings of all four manuscripts, placing them in the context of the literature and providing further in-depth critical analysis. Overarching conclusions from the work are also included in this section. This format adheres to the Faculty of Environment protocol for the format and presentation of an alternative style of doctoral thesis including published material.

Acknowledgments

This research would not have been possible without the help and support of numerous people. First and foremost, I would like to thank my fantastic supervision team, Roel Brienen and Manuel Gloor. Ever generous with their time, they have offered stimulating guidance, ideas and encouragement throughout this process, and have helped me to achieve more than I ever thought I could.

This thesis is founded on many thousands of tree-ring isotope measurements, and I am incredibly grateful to all of those whose hard work has helped to generate this data. Specifically, I would like to thank Arnoud Boom, Melanie Leng and Timothy Heaton, who conducted the majority of the isotope measurements, and Sarah Hunt for her assistance with the lab analysis. Special thanks go to Santiago Clerici who has helped me extensively – particularly during our trip to Ecuador and with many hours of lab work and isotope analysis since, always with characteristic good humour.

In addition to my main supervisors, I am thankful to Dominick Spracklen and Steve Arnold for sharing their expertise and helping me to develop new skills, and to Julia Tindall for her insightful comments and sage advice. Thanks also go to the many other researchers who have helped me at various points along the way: Jochen Schöngart, David Neill, Rob Newton, Simon Bottrell, Gerhard Helle and John Methven. I would also like to acknowledge the Natural Environment Research Council for providing the funding for this research.

Much of the fieldwork for this project was conducted before I began my PhD studentship. Therefore, I would like to thank those who assisted with sample collection and logistical planning, including Vincent Vos, Guido Pardo, Don Nico Divico and Nazareno Martinez.

I have been privileged to work alongside many talented people during the course of this PhD, many of whom have now become close friends. Their advice, moral support and enthusiasm have played an important part in helping me through the past three and a half years! Greta Dargie, Adriane Esquivel-Muelbert, Sophie Fauset and Fernanda Coelho deserve a special thank you, for inspiring me from the beginning. I would also like to thank the rest of my EGC family: Bruno Cintra (my tree-ring buddy), Marta Giannichi, Karina Melgaço, Georgia Pickavance, Freddie Draper, Michelle

Johnson, Yunxia Wang, Suzanne Stas, Martin Sullivan, Michelle Kalamandeen, Julia Tavares and Martin Gilpin. Thanks also go to my friends from other areas of research for reminding me of the world beyond tropical forests, including Magaly Valencia, Ana Cabrera Pacheco, James Bell, Alice Noble, Annie Connolly, Sarah Fell, Samuel Eze and Sarah Letsinger.

I must also thank those who have supported me for many years beyond the duration of my PhD. Thank you to Jane and Mark, my parents, for their love and unconditional support throughout my seemingly endless years in education; my siblings, Ruth, Tom, Hannah and Alexander for making me laugh and keeping me grounded; and Jimmy for making my world a more colourful place. Finally, I dedicate this thesis to the memory of June and Mac Baker, who are dearly missed.

Abstract

The Amazon hydrological cycle has intensified since approximately 1990, and yet long-term meteorological data from the region are limited, making it difficult to determine the cause of current variability. Proxy records can be used to reconstruct past climate, thus providing useful historical context for recent changes. This thesis focuses on the climate insights that can be gained from oxygen isotopes in tree rings ($\delta^{18}O_{TR}$). The consistency of annual ring formation was tested first, as this is an important prerequisite for constructing a well-dated proxy record. *Cedrela* trees were found to form annual rings across most of the species' natural range, but biannual rings in Suriname (Chapter 3). Next, new $\delta^{18}O_{TR}$ records were developed from *Cedrela* and seven other tree species from northern Bolivia. $\delta^{18}O_{TR}$ signals were shown to correlate between different species, and between sites large distances apart (<1000 km), indicating a large-scale environmental control on $\delta^{18}O_{TR}$ (Chapter 4). Following this, atmospheric back-trajectory modelling and basin-scale vapour transport analysis were used to confirm that rainout of heavy isotopes during moisture transport across the continent is the primary control on interannual $\delta^{18}O_{TR}$ signals in the western Amazon (Chapter 5). Finally, new *Cedrela* $\delta^{18}O_{TR}$ chronologies from Ecuador and Bolivia were developed. These records show an increase in $\delta^{18}O_{TR}$ from the early 1800s until approximately 1950, indicating a change in hydrological functioning over this period, with a reversal in the trend over the last 1–2 decades. The increase is most likely driven by a reduction in the fraction of incoming water vapour that rains out over the Amazon, which could be caused by a reduction in precipitation, or an increase in the volume of imported vapour. Overall, these results provide evidence for long-term changes in Amazon hydrology over the past 200 years, and make an important contribution to the field of tropical dendroclimatology.

Contents

Acknowledgments ..... **v**

Abstract ..... **vii**

Contents ..... **viii**

List of Tables ..... **xii**

List of Figures ..... **xiii**

List of Appendices ..... **xv**

List of Abbreviations ..... **xvii**

Chapter 1: Introduction **3**

1.1 The Changing Amazon Hydrological Cycle **4**

1.2 Literature Review **7**

1.2.1 Isotopes in the hydrological cycle 7

1.2.2 Global patterns in precipitation isotopes 11

1.2.3 Isotopes in Amazon precipitation 12

1.2.4 Oxygen isotope proxy records 14

1.2.5 Physiological effects on $\delta^{18}O_{TR}$ 18

1.2.6 Biochemical effects on $\delta^{18}O_{TR}$ 20

1.2.7 $\delta^{18}O_{TR}$ research in the Amazon 21

1.3 The Principle of Uniformitarianism **23**

1.4 Aims and Research Questions **26**

1.4.1 Test tree-ring periodicity across different sites in tropical South America 26

1.4.2 Develop and compare interannual $\delta^{18}O_{TR}$ series between different tropical tree species 27

1.4.3 Investigate spatial coherence between $\delta^{18}O_{TR}$ signatures from the Amazon 28

1.4.4 Identify the mechanisms controlling $\delta^{18}O_{TR}$ in the Amazon 29

1.4.5 Extend Amazon $\delta^{18}O_{TR}$ records back in time 30

1.4.6 Research questions 31

1.5 Thesis Outline **31**

1.6 References **32**

Chapter 2: Materials and Methods **43**

2.1 *Cedrela* growth and cambial dynamics 43
2.2 Sampling Strategy 43
2.3 Tree-Ring Analysis 44
2.3.1 Sample preparation 44
2.3.2 Radiocarbon dating 48
2.3.3 Oxygen isotope analysis 49
2.4 Data Processing 49
2.4.1 Processing isotope data 49
2.4.2 Data analysis 50
2.5 Towards a More Mechanistic Understanding of Amazon $\delta^{18}O_{TR}$ Records 51
2.5.1 Introduction to air parcel trajectory modelling 51
2.5.2 Back-trajectory analysis 53
2.5.3 Large-scale water vapour transport analysis 55
2.6 References 55

Chapter 3: Does *Cedrela* always form annual rings? Testing ring periodicity across South America using radiocarbon dating 59
3.1 Introduction 59
3.2 Methods 62
3.3 Results and Discussion 66
3.4 Summary and Outlook 73
3.5 References 74

Chapter 4: Oxygen isotopes in tree rings show good coherence between species and sites in Bolivia 79
4.1 Introduction 80
4.2 Materials and Methods 84
4.2.1 Study species 84
4.2.2 Regional setting 87
4.2.3 Oxygen isotope analysis 87
4.2.4 Dating calibration and radiocarbon verification 89
4.2.5 Statistical analysis 91
4.3 Results and Discussion 91
4.3.1 Crossdating tree-ring oxygen isotope series 91
4.3.2 *Cedrela* chronology 94
4.3.3. Inter-specific coherence in tree-ring oxygen isotopes 95

4.3.4 Spatial coherence of oxygen isotopes in tree rings 99
4.4 Conclusions 101
4.5 References 102

Chapter 5: What drives interannual variation in tree-ring oxygen isotopes in the Amazon? 107
5.1 Introduction 107
5.2 Data and Methodology 110
5.3 Results 113
5.4 Discussion 116
5.5 Summary 121
5.6 References 121

Chapter 6: The changing Amazon hydrological cycle – inferences from over 200 years of tree-ring oxygen isotope data 125
6.1 Introduction 126
6.2 Methods 128
6.2.1 Sample collection 128
6.2.2 Sample preparation 130
6.2.3 Oxygen isotope analysis 131
6.2.4 Dating $\delta^{18}O_{TR}$ series 132
6.2.5 Data analysis 132
6.3 Results and Discussion 134
6.3.1 Record description and inter-comparison 134
6.3.2 What drives interannual and decadal variation in $\delta^{18}O_{TR}$ from Ecuador? 136
6.4 Long-Term Trends in $\delta^{18}O_{TR}$ 142
6.4.1 Testing for an ontogenetic influence on $\delta^{18}O_{TR}$ 144
6.4.2 Tree-level response to rising CO_2 145
6.4.3 Changes in leaf-to-air vapour pressure difference 147
6.4.4 Increase in seawater $\delta^{18}O$ at moisture origin 148
6.4.5 Effect of increasing SSTs on fractionation during evaporation from the ocean surface 149
6.4.6 Change in the lapse rate 149
6.4.7 A change in local amount effects 150
6.4.8 A reduction in rainout fraction over the Amazon 151
6.5 The Recent Intensification of the Amazon Hydrological Cycle 153

6.6 Summary **154**
6.7 References **155**

Chapter 7: Discussion **161**
7.1 Overview of Findings and General Discussion **162**
7.1.1 Chapter summaries 162
7.1.2 Synthesis of results 164
7.2 Appraisal of Thesis Aims **173**
7.2.1 How consistent is annual tree-ring periodicity across the Amazon? 173
7.2.2 Do different tropical tree species show similar $\delta^{18}O_{TR}$ signatures? 174
7.2.3 Do $\delta^{18}O_{TR}$ records from the Amazon show coherence at large spatial scales? 174
7.2.4 Can a network of $\delta^{18}O_{TR}$ chronologies from sites across the basin provide further information about interannual variation in basin rainout, or changes in the precipitation-recycling ratio? 175
7.2.5 What are the most important mechanisms driving interannual variation in Amazon $\delta^{18}O_{TR}$? 178
7.2.6 What can new long $\delta^{18}O_{TR}$ records presented in this thesis tell us about the Amazon hydrological cycle over the past two centuries? 179
7.3 How Useful Are Amazon $\delta^{18}O_{TR}$ Proxy Records? **180**
7.4 Research Implications and Suggestions for Future Research **182**
7.5 Conclusions **185**
7.6 References **186**

Appendices **193**

List of Tables

Table 1.1 – Typical $\delta^{18}O$ values in some of the natural reservoirs of water in the global hydrological cycle 12
Table 4.1 – Traits of different tropical tree species 86
Table 4.2 – "Bomb-peak" radiocarbon dating results 92
Table 4.3 – Errors during analysis of tree rings in different tropical species 93
Table 6.1 – Summary of factors that may contribute to the long-term increase in $\delta^{18}O_{TR}$ 144

List of Figures

Figure 1.1 – The Craig-Gordon model of isotope effects in the hydrological cycle..... 10
Figure 1.2 – Continental rainout and precipitation recycling over the Amazon..... 13
Figure 1.3 – Processes affecting the oxygen isotope composition of cellulose..... 18
Figure 1.4 – Tree rings in *Cedrela*..... 28
Figure 2.1 – Network of tree-ring sampling sites across South America. 44
Figure 2.2 – Photos showing the apparatus for two different cellulose extraction techniques..... 45
Figure 2.3 – Cellulose extraction method comparison..... 47
Fig. 3.1 – Map of *Cedrela* study sites and their climate diagrams 64
Fig. 3.2 – Results from radiocarbon (^{14}C) analysis 67
Fig. 3.3 – Annotated high-resolution scans of tree-ring samples 70
Figure 3.4 – Precipitation and insolation data from Cameroon and Suriname 73
Figure 4.1 – Map of sample sites in the southwest Amazon..... 85
Figure 4.2 – $\delta^{18}O_{TR}$ time series from nine *Cedrela odorata* trees from Selva Negra, Bolivia..... 95
Figure 4.3 – Comparing $\delta^{18}O_{TR}$ signatures between tropical tree species. 97
Figure 4.4 – A comparison of *Cedrela* $\delta^{18}O_{TR}$ chronologies from two distant sites in Bolivia..... 100
Figure 4.5 – A comparison of tree-ring and ice-core $\delta^{18}O$ records from the Altiplano 101
Figure 5.1 – Annual climate for the tree-ring sample site in northern Bolivia, and example wet and dry season back trajectories. 112
Figure 5.2 – Relationships between $\delta^{18}O_{TR}$ and precipitation along air-mass back-trajectories..... 114
Figure 5.3 – Relationship between $\delta^{18}O_{TR}$ and mean wet season Amazon basin moisture balance..... 118
Figure 6.1 – Map of $\delta^{18}O$ proxy records from the Amazon..... 129
Figure 6.2 – New $\delta^{18}O_{TR}$ chronologies from Ecuador and Bolivia..... 135
Figure 6.3 – Correlations between $\delta^{18}O_{TR}$ and gridded precipitation..... 136
Figure 6.4 – Effect of Amazon precipitation and runoff on $\delta^{18}O_{TR}$ from Ecuador..... 138

Figure 6.5 – Correlation between $\delta^{18}O_{TR}$ from Ecuador and sea surface temperature data 140
Figure 6.6 – Testing the effect of sunspots on Amazon hydrology 142
Figure 6.7 – Long-term trends in different $\delta^{18}O$ proxy records from the Amazon 146
Figure 6.8 – Relationship between $\delta^{18}O_{TR}$ from Ecuador and sea surface temperatures in the North Atlantic 153
Figure 7.1 – Preliminary $\delta^{18}O_{TR}$ data from other sites in the Amazon 177
Figure 7.2 – Example of wedging tree rings in *Cedrela montana* from Ecuador 181

List of Appendices

Appendix 2.1 – Cellulose extraction method comparison 193
Appendix 4.1 – Raw isotope data with original and adjusted tree-ring dates 194
Appendix 5.1 – Altitude sensitivity analysis 209
Appendix 5.2 – Supplementary methods for Chapter 5 210
Appendix 5.3 – Determining whether basin climate or air transport pathway has a more important influence on $\delta^{18}O_{TR}$ 214
Appendix 5.4 – Relationships between tree-ring oxygen isotope composition ($\delta^{18}O_{TR}$) and leaf area index accumulated along back trajectories 215
Appendix 5.5 – Wind and moisture transport anomalies over the Amazon in years with high and low tree-ring oxygen isotope ($\delta^{18}O_{TR}$) values 216
Appendix 5.6 – Comparing interannual variation in vapour inflow to and outflow from the Amazon basin with variation in Amazon River discharge 218
Appendix 5.7 – Interannual variation in air transport pathways to sample site in northern Bolivia 219
Appendix 5.8 – Spatial variation in isotope composition at moisture origin 220
Appendix 5.9 – Rayleigh-based simulation of interannual variation in tree-ring oxygen isotope composition ($\delta^{18}O_{TR}$) 221
Appendix 6.1 – Number of climate stations in CRU precipitation dataset over time 224
Appendix 6.2 – Statistical analysis of tree-ring oxygen isotope ($\delta^{18}O_{TR}$) chronology quality 225
Appendix 6.3 – Correlation between tree-ring oxygen isotope ($\delta^{18}O_{TR}$) records from Ecuador and Bolivia 227
Appendix 6.4 – Air transport pathways to sample sites in Ecuador and Bolivia 228
Appendix 6.5 – Effect of Amazon precipitation and runoff on the tree-ring oxygen isotope ($\delta^{18}O_{TR}$) record from Bolivia 229
Appendix 6.6 – Testing for local and regional temperature effects on tree-ring oxygen isotopes ($\delta^{18}O_{TR}$) from Ecuador 230
Appendix 6.7 – Split-period regression statistics 230
Appendix 6.8 – Correlating the tree-ring oxygen isotope ($\delta^{18}O_{TR}$) record from Bolivia with sea surface temperature (SST) data 231

Appendix 6.9 – Comparing trajectory-inferred moisture origins with the ocean regions that influence tree-ring oxygen isotopes ($\delta^{18}O_{TR}$) in Ecuador 232
Appendix 6.10 – Effect of sea surface temperatures (SSTs) on Amazon precipitation 233
Appendix 6.11 – Testing for ontogenetic effects on tree-ring oxygen isotopes ($\delta^{18}O_{TR}$) from Bolivia and Ecuador 234
Appendix 6.12 – The Péclet-modified Craig-Gordon (PMCG) model 235
Appendix 7.1 – Preliminary $\delta^{18}O_{TR}$ data from Venezuela, Brazil and Suriname 237
Appendix 7.2 – References for the Appendices 238

List of Abbreviations

^{14}C – radiocarbon
α^* – equilibrium fractionation factor
$\alpha_{B/A}$ – the ratio of isotope ratios in pool B with respect to pool A
α_k – kinetic fractionation factor
ε^* – enrichment due to equilibrium fractionation ($\varepsilon^* = \alpha^* - 1$)
$\varepsilon_{B/A}$ – enrichment of the rare isotope in pool B with respect to pool A ($\varepsilon_{B/A} = \alpha_{B/A} - 1$)
ε_k – enrichment due to kinetic fractionation ($\varepsilon_k = \alpha_k - 1$)
δ_E – isotope composition of the evaporative flux
δ_L – isotope composition of liquid water
δ_V – isotope composition of atmospheric water vapour
$\delta^{13}C$ – carbon-13 isotope composition
$\delta^{18}O$ – oxygen-18 isotope composition
$\delta^{18}O_E$ – oxygen-18 isotope composition of water in the evaporative pool
$\delta^{18}O_{ICE}$ – oxygen-18 isotope composition of ice cores
$\delta^{18}O_L$ – oxygen-18 isotope composition of bulk leaf water
$\delta^{18}O_P$ – oxygen-18 isotope composition of precipitation
$\delta^{18}O_S$ – oxygen-18 isotope composition of source or stem water
$\delta^{18}O_{CARB}$ – oxygen-18 isotope composition of carbohydrates synthesised in the leaf
$\delta^{18}O_{SW}$ – oxygen-18 isotope composition of seawater
$\delta^{18}O_{TR}$ – oxygen-18 isotope composition of tree-ring cellulose
$\delta^{18}O_V$ – oxygen-18 isotope composition of water vapour
ρ – Péclet number
$\sum$LAI – leaf area index accumulated along a trajectory
$\sum$Precip – precipitation accumulated along a trajectory
ϕ – fraction of carbohydrate $\delta^{18}O$ that exchanges with local stem water during cellulose synthesis
AMS – accelerator mass spectrometry
ANA – Agência Nacional de Águas
C – concentration of water
CMIP5 – Coupled Model Intercomparison Project Phase 5
CO_2 – carbon dioxide
CRU – Climatic Research Unit
D – diffusivity of $H_2{}^{18}O$ in water
DBH – diameter at breast height
e_a – vapour pressure of ambient air
ECMWF – European Centre for Medium-Range Weather Forecasts
e_i – vapour pressure of intercellular air spaces
ENSO – El Niño-Southern Oscillation
EPS – Expressed Population Signal
ERSST – Extended Reconstruction Sea Surface Temperature
ET – evapotranspiration
f – fraction of water vapour in atmosphere
$F^{14}C$ – fraction modern carbon (see also pMC)
FACE – Free Air CO_2 Enrichment
FIRI – Fourth International Radiocarbon Intercomparison

GCM – general circulation model
GFZ – German Research Centre for Geosciences
GHCN-M – Global Historical Climatology Network-Monthly
g_{max} – maximum stomatal conductance
GNIP – Global Network of Isotopes in Precipitation
g_s – stomatal conductance
hPa – hectopascal
HPLC – high performance liquid chromatography
HT – high temperature
IAEA – International Atomic Energy Agency
IDL – Interactive Data Language
INAMHI – Instituto Nacional de Meteorología e Hidrología
IRMS – isotope-ratio mass spectrometry / isotope-ratio mass spectrometer
ITCZ – inter-tropical convergence zone
ITRDB – International Tree-Ring Data Bank
KCCAMS – Keck Carbon Cycle Accelerator Mass Spectrometer
KNMI – Koninklijk Nederlands Meteorologisch Instituut
L – effective path length in a leaf
LAI – leaf area index
LGM – Last Glacial Maximum
m.a.s.l. – metres above sea level
n or N – number
$NaClO_2$ – sodium chlorite
NaOH – sodium hydroxide
NERC – Natural Environment Research Council
NH – Northern Hemisphere
NIGF – NERC Isotope Geosciences Facilities
NIST – National Institute of Standards and Technology
NOAA – National Oceanic and Atmospheric Administration
p – *p*-value
PDO – Pacific Decadal Oscillation
Pg – petagram
pMC – per cent modern carbon (see also $F^{14}C$)
ppm – parts per million
PTFE – polytetrafluoroethylene
r – Pearson's product moment correlation coefficient
R – isotope ratio
r_{mean} – mean inter-tree correlation coefficient
RH – relative humidity
RH_N – relative humidity, normalised to account for temperature
RMSE – root mean square error
ROTRAJ – Reading Offline TRAJectory model
SASM – South American summer monsoon
SD – standard deviation
SEE – School of Earth and Environment
SH – Southern Hemisphere
SIDC – Solar Influences Data Analysis Centre
SST – sea surface temperature

t – time
T – temperature
TC/EA – temperature conversion elemental analyzer
TNA – tropical North Atlantic
TRMM – Tropical Rainfall Monitoring Mission
TRW – tree-ring width
VPD – vapour pressure difference
VSMOW – Vienna Standard Mean Ocean Water
WUE – water-use efficiency

Chapter 1: Introduction

The Amazon basin in South America is the world's largest watershed and forms a major component of the global hydrological (Richey et al., 1989, Salati et al., 1979) and carbon cycles (Pan et al., 2011). Estimates of annual precipitation averaged across the whole basin range from 1895–2322 mm (Costa and Foley, 1998) and mean annual Amazon River discharge to the oceans is around 200,000 m^3s^{-1} (Callède et al., 2010). The Amazon is also home to the world's largest tropical rainforest, which covers more than five million square kilometres and represents 40% of tropical forest worldwide (Aragão et al., 2014). This expanse of vegetation has been estimated to contain 16,000 tree species (ter Steege et al., 2013) and store approximately 17% of global terrestrial carbon (Feldpausch et al., 2012, Cao and Woodward, 1998). The forest also provides an interface for extensive biosphere-atmosphere interactions, including exchanges of carbon, water, trace gases, biogenic aerosols and energy (e.g. Silva Dias et al., 2002), which in turn affect the functioning of the climate. For example, water recycling through evapotranspiration accounts for roughly 28% of regional precipitation, though there is a spatial gradient and the far southwest corner of the basin receives the highest proportion (~70%) of precipitation originating from within the basin (van der Ent et al., 2010, van der Ent and Savenije, 2011).

The Amazon forest is currently a major terrestrial carbon sink (Pan et al., 2011), though long-term monitoring has revealed that the strength of the sink is weakening over time (Brienen et al., 2015). Severe drought events have caused substantial carbon losses from the region. For example, the droughts in 2005 and 2010 are estimated to have driven carbon fluxes to the atmosphere of 1.6 and 1.1 Pg respectively (Phillips et al., 2009, Feldpausch et al., 2016). These estimates are in line with results from CO_2 vertical profile analysis, which indicate that such extreme negative precipitation anomalies may temporarily neutralise the Amazon carbon sink, through increased biomass burning and reduced forest productivity (Gatti et al., 2014), with potential consequences for global climate. Furthermore, forest logging and land-use change, driven by a growing demand for agricultural expansion, may exacerbate these climate impacts by increasing forest susceptibility to fire and droughts (Nepstad et al., 2008), and reducing evaporative recycling and thus precipitation downstream (Spracklen et al.,

2012, Spracklen and Garcia-Carreras, 2015). For example, forest conversion to pasture reduces evaporative cooling, thus simultaneously warming and drying the local climate (Bonan, 2008). Indeed, the Amazon forest has been labelled a 'tipping element' in the Earth's climate system, because climate-driven forest loss could possibly escalate if certain critical thresholds (e.g. in annual precipitation and dry season length) are surpassed (Lenton et al., 2008). The complex interactions between the forest and the climate require careful monitoring as anthropogenic pressures on the region increase, since perturbations to these highly interconnected systems could have important global implications.

1.1 The Changing Amazon Hydrological Cycle

Sea surface temperature (SST) anomalies in the ocean basins surrounding the Amazon are known to control precipitation variability (Garreaud et al., 2009). For example, the influence of interannual variation in Pacific SSTs, particularly the El Niño-Southern Oscillation (ENSO), on Amazon hydrology is well established (e.g. Kousky et al., 1984, Marengo, 1992, Ronchail et al., 2002 and references therein). During positive (negative) ENSO years anomalously warm (cool) SSTs in the equatorial Pacific increase (reduce) convection over the ocean, thus suppressing (enhancing) convection over the Amazon (e.g. Foley et al., 2002, Garreaud et al., 2009). This mechanism differs from the influence of Atlantic SSTs on Amazon hydrology, which has been recognised more recently and is thought to be of comparable magnitude to the Pacific influence (Yoon and Zeng, 2010). Warm (cool) SST anomalies in the tropical North Atlantic cause the northward (southward) displacement of the inter-tropical convergence zone (ITCZ, a band of heavy precipitation which follows the thermal equator), therefore reducing (increasing) rainfall over the Amazon region (Yoon and Zeng, 2010, Zeng et al., 2008, Marengo et al., 2011). Changes to Pacific or Atlantic SSTs may therefore force changes to the functioning of the Amazon hydrological cycle.

Evidence is amassing which suggests that Amazon hydrology is currently in a state of flux. Dry seasons are becoming longer and more severe, possibly driven by rising SSTs in the tropical North Atlantic (Fu et al., 2013, Marengo et al., 2011). Meanwhile a recent analysis of river flows and rain gauges indicates that wet season

precipitation has risen between 1990–2010, with increased wet season river fluxes and greater variability between wet and dry season moisture regimes (Gloor et al., 2013). This amplification of the Amazon hydrological cycle is consistent with a rise in the volume of moisture being transported into the basin and a switch to the cold phase of the Pacific Decadal Oscillation (PDO), a low-frequency SST mode with a similar spatial pattern to ENSO (Gloor et al., 2015). This shift reversed a trend of declining moisture import to the basin over the period 1976–1996 (Costa and Foley, 1999). The reversal in moisture transport trends illustrates the variability of the Amazon climate system and highlights a need for longer hydrological records to adequately assess on-going changes.

Extreme drought and flood events in the Amazon have also tended to become more frequent in recent decades (Marengo and Espinoza, 2016). For example, there were major droughts in 2005, 2010 and 2015/16 (Marengo et al., 2008, Marengo et al., 2011, Jiménez-Muñoz et al., 2016), while intense precipitation caused severe flooding in 2009 and 2012–2014 (Espinoza et al., 2013, Espinoza et al., 2014, Marengo and Espinoza, 2016). Droughts have the potential to cause increased tree mortality and associated carbon release (Phillips et al., 2009), and may also drive shifts in floristic composition, particularly in wet areas where species may be more sensitive to drought (Esquivel-Muelbert, 2017). On the other hand, floodplain species already living at the edge of their physiological limits may be susceptible to increases in the flood height or inundation length (Wittmann et al., 2004, Gloor et al., 2015). It follows that accurately projecting future changes in the frequency of extreme events is important for predicting how the forest will respond to anthropogenic climate change.

Some modelling studies have suggested the Amazon may experience a substantial drying and consequential rainforest ‘dieback’ under future warming (e.g. Cox et al., 2004, Huntingford et al., 2008), though these studies were based on a single general circulation model (GCM), which underestimates current Amazon wet season precipitation and overestimates dry season length (Cox et al., 2004). An analysis of 29 GCMs in the Coupled Model Intercomparison Project phase 5 (CMIP5) ensemble showed that temperature-driven increases in moisture convergence would rather increase precipitation over monsoon regions globally, including the South American monsoon domain (Kitoh et al., 2013). Another recent study, involving 36 CMIP5 GCMs

and focussing specifically on the Amazon basin, showed that while models simulate a large spread of trends in precipitation over the next century, precipitation seasonality is mostly projected to increase, following the current trend in observations (Boisier et al., 2015). The increasing seasonality could reduce rainforest cover in regions where the dry season becomes longer than three months. However, there are concerns that current model ensembles could be underestimating the impact of drying in the Amazon, due to dry biases in the models (Boisier et al., 2015) and an inability to reproduce observed increases in dry season length since 1979 (Fu et al., 2013).

It is also important to consider the spatial heterogeneity of future hydrological shifts. Models generally project an east-west divide, with stronger drying in the eastern Amazon, and a possible transition to seasonal forest in this region (Malhi et al., 2009, Duffy et al., 2015). This pattern is supported to an extent by remote sensing observations of precipitation and terrestrial water storage, which both show declines in the eastern Amazon since 2000 (Hilker et al., 2014). However, river records show a slightly different pattern, with basins in the northwest and centre of the Amazon showing an increase in runoff, while basins in the south are following a drying trend (Espinoza et al., 2009: analysed period 1974–2004, Gloor et al., 2015: analysed period ~1980–2012). Using a novel water recycling network approach, Zemp et al. (2017) simulated a change pattern more in line with the river discharge data, with land-atmosphere interactions driving increased forest instability and tree cover losses, predominantly over the south of the Amazon by the end of the 21st century. Given the current uncertainties in model forecasts, and the potential negative impacts of climate change, it is vital to develop a better understanding of the underlying controls on Amazon hydrology and the natural patterns of variability.

The overarching aim of this thesis is to develop a more complete understanding of the Amazon hydrological cycle using a palaeoclimate approach. Although meteorological stations are scarce in this region, and there are few long-term instrumental climate records, proxy climate data may offer helpful insights (Boninsegna et al., 2009). For example, stable oxygen isotopes in tree-rings ($\delta^{18}O_{TR}$) have recently been shown to record $\delta^{18}O$ in precipitation ($\delta^{18}O_P$) and be a good proxy for precipitation across the whole Amazon basin (Brienen et al., 2012). Reconstructions of historical climate using such proxy data could clarify whether the recent amplification of Amazon

hydrology is part of natural climatic variability, or linked to global climate change. In this chapter, an overview of the relevant literature for the thesis topic is provided (section 1.2). This will include an introduction to stable isotopes in the hydrological cycle (1.2.1), an overview of global patterns in $\delta^{18}O_P$ (1.2.2), a summary of the main controls on $\delta^{18}O_P$ over the Amazon (1.2.3), and a description of how $\delta^{18}O_P$ signals preserved in natural archives can provide valuable information on Amazon climate (1.2.4). The physiological (1.2.5) and biochemical (1.2.6) factors that influence the isotope signature stored in tree rings are described, and $\delta^{18}O_{TR}$ research in the Amazon to date is reviewed (1.2.7). The principle of uniformitarianism, which is fundamental to palaeoclimate reconstructions, is defined in section 1.3, with a discussion on why anthropogenic impacts need to be considered for the correct interpretation of $\delta^{18}O_{TR}$ chronologies. Section 1.4 sets out the project aims and the key research questions, and the structure of the whole thesis is outlined in section 1.5.

1.2 Literature Review

1.2.1 Isotopes in the hydrological cycle

One way to gain a better understanding of the hydrological cycle is to use stable (i.e. non-radioactive) water isotopes (Galewsky et al., 2016). Isotopes are forms of the same element with different numbers of neutrons in the nucleus of the atom, and many elements have at least two. Given the difficulties of measuring isotope abundances directly, the isotope composition of a substance, such as water, is usually expressed using delta notation (δ). Isotope composition (in units of per mil, ‰) is given as the isotope ratio (R) in a sample relative to that in a standard reference material (e.g. Mook, 2000):

$$\delta = \left(\frac{R_{sample}}{R_{standard}} - 1\right) \times 1000 \quad \text{where} \quad R = \frac{\text{abundance of the rare isotope}}{\text{abundance of the common isotope}} \qquad (1)$$

With an increase in the number of neutrons in the nucleus there is a corresponding increase in an element's atomic mass, so different isotopes have slightly different chemical and physical properties. In particular, heavy isotopes form stronger bonds with other atoms than their light counterparts do, and they are also less mobile. These differences in behaviour between heavy and light isotopes result in mass-dependent isotope fractionation (Mook, 2000, Galewsky et al., 2016). Mass-dependent

fractionation (also called isotope discrimination) causes differences in the isotope composition of compounds before and after a chemical or physical reaction (Gat et al., 2001). The symbol α is used to denote the fractionation factor, which can be defined as the ratio of isotope ratios in two pools of compounds (A and B, for the reaction A→ B):

$$\alpha_{B/A} = \frac{R(B)}{R(A)} \qquad (2)$$

As isotope fractionation effects are small, α has a value close to 1. Therefore, fractionation may also be expressed as difference between α and 1:

$$\varepsilon_{B/A} = (\alpha_{B/A} - 1) \qquad (3)$$

where $\varepsilon_{B/A}$ represents the enrichment or depletion of the rare isotope in pool B relative to pool A, and is usually given in units of per mil.

Fractionation effects can be grouped into two categories: i) equilibrium (thermodynamic) fractionation during reversible reactions, and ii) kinetic fractionation during irreversible reactions, or as a result of slightly different diffusion coefficients (Mook, 2000). Equilibrium fractionation is controlled by temperature, with fractionation decreasing as temperatures become warmer (Bottinga and Craig, 1968, Majoube, 1971). This is because the difference between the amount of energy needed to react light and heavy isotopes becomes smaller as temperatures increase. The equation to describe the relationship between equilibrium fractionation (ε^*) and temperature (T, in kelvin) can be written as follows (from Bottinga and Craig, 1968):

$$\varepsilon^* = 2.644 - 3.206\left(\frac{10^3}{T}\right) + 1.534\left(\frac{10^6}{T^2}\right) \qquad (4)$$

Conversely, kinetic fractionation effects are temperature-independent. Most natural processes will involve multiple types of fractionation, though the magnitude of kinetic fractionation effects tends to exceed that of equilibrium fractionation effects (Gat et al., 2001).

Oxygen has three naturally occurring stable isotopes (^{16}O, ^{17}O and ^{18}O), which combine with hydrogen to form the water isotopologues $H_2{}^{16}O$, $H_2{}^{17}O$ and $H_2{}^{18}O$. The rare heavy isotopologues of water ($H_2{}^{17}O$ and $H_2{}^{18}O$) have higher binding energies and lower diffusivities than the abundant $H_2{}^{16}O$ form (Galewsky et al., 2016). These properties result in fractionation during phase changes and transport through the hydrological cycle, causing different natural reservoirs of water on Earth to have

different oxygen isotope compositions ($\delta^{18}O$; see Table 1.1). This makes it possible to trace water as it moves between these reservoirs (Gat et al., 2001, Mook, 2000).

Figure 1.1 shows a simple schematic of the fractionation processes that occur during evaporation, condensation and precipitation over the ocean (modified from Fig. 15 in Craig and Gordon, 1965). First, temperature-dependent equilibrium fractionation occurs during evaporation from the surface of the ocean into a very thin boundary layer of saturated air at the liquid/air interface (step 1 in Fig. 1.1). The water vapour that forms is isotopically lighter (i.e. depleted) relative to the liquid source water (Dansgaard, 1964). Water molecules then move via molecular diffusion through the unsaturated diffusive layer (step 2 in Fig. 1.1). Kinetic fractionation occurs here, because the lighter vapour molecules diffuse faster than the heavier vapour molecules. Kinetic fractionation is not affected by temperature but rather determined by the isotope composition of atmospheric water vapour and the relative humidity (RH) of the ambient air. Equilibrium and kinetic fractionation effects together determine the isotope composition of the evaporative flux ($\delta^{18}O_E$). Craig and Gordon (1965) developed a model (henceforth referred to as the Craig-Gordon model) to describe the fractionation processes during evaporation as a function of environmental parameters. The model, simplified by Gat et al (2001; equation 3.4), can be written:

$$\delta^{18}O_E = \frac{(\alpha^* \times \delta^{18}O_L) - (RH_N * \delta^{18}O_V) + \varepsilon^* + \varepsilon_k}{(1 - RH_N) - \varepsilon_k} \quad (5)$$

where α^* is the equilibrium fractionation factor between vapour and liquid water, $\delta^{18}O_L$ is the isotope composition of the liquid water, RH_N is the relative humidity, normalised to account for temperature, $\delta^{18}O_V$ is the isotope composition of atmospheric water vapour, $\varepsilon^*$is the enrichment due to equilibrium fractionation (equal to $\alpha^* - 1$), and ε_k is the enrichment due to kinetic fractionation (in this case diffusion). The model assumes that atmospheric water vapour is in isotopic equilibrium with the source water at the liquid/air interface, that both water bodies are well mixed, and that water volume remains constant over time.

The evaporative flux is transported by turbulent diffusion through the free atmosphere (step 3 in Fig. 1.1). It is usually assumed that there is no isotope fractionation during this turbulent transport of moisture (Gat et al., 2001, Galewsky et al., 2016). As air masses rise and cool, clouds form, and further isotope fractionation takes place. In-cloud isotope processes are complex (e.g. Ciais and Jouzel, 1994, Risi et

al., 2008), though fractionation during condensation has the strongest effect on the isotope composition of precipitation (Dansgaard, 1964). Since the air inside a cloud is saturated, the phase change from vapour to liquid is affected by equilibrium fractionation, which is dependent on the temperature of the cloud and thus largely determined by the altitude of condensation (step 4 in Fig. 1.1). The condensate that forms is isotopically heavier (i.e. enriched) relative to the surrounding water vapour (Dansgaard, 1964). Finally, water droplets coalesce and fall to the ground, becoming further isotopically enriched as they fall (step 5 in Fig. 1.1). This is due to partial re-evaporation and diffusive exchange with atmospheric water vapour. These fractionation processes are kinetic, since the rain is falling through the air and there is no time for isotope equilibration to occur. Therefore, fractionation during precipitation is affected by $\delta^{18}O_V$ and RH, but not influenced by temperature.

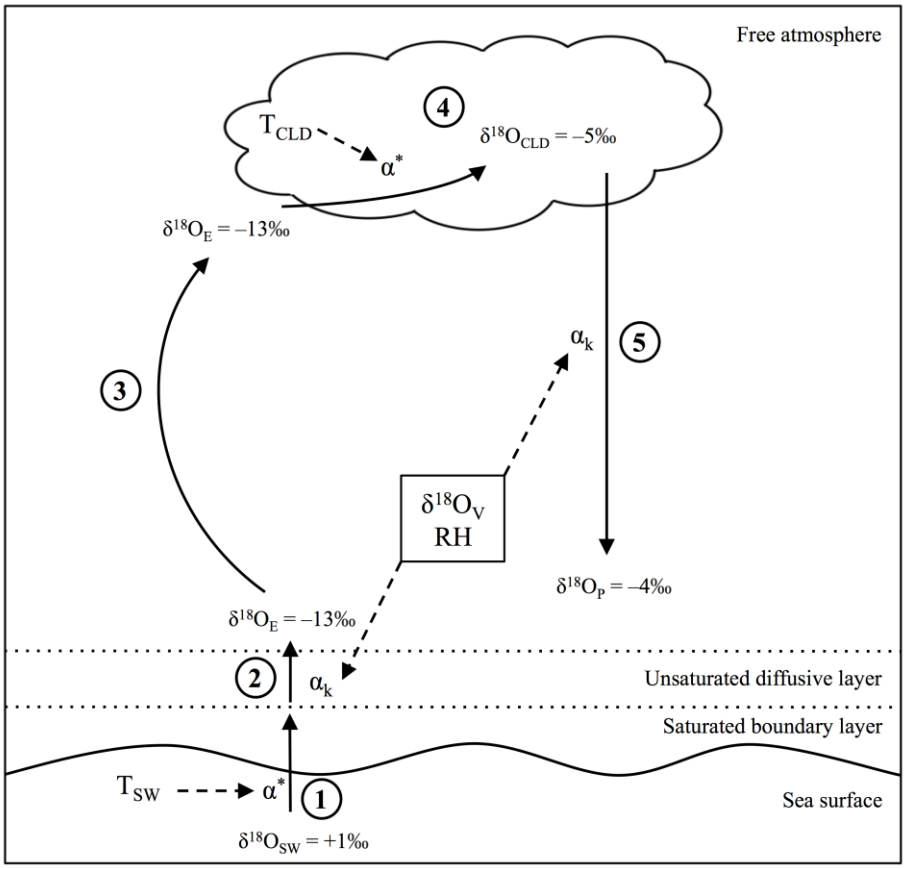

Figure 1.1 – The Craig-Gordon model of isotope effects in the hydrological cycle. Numbers indicate evaporation (1), molecular diffusion (2), turbulent diffusion (no fractionation, 3), condensation (4) and precipitation (5) over the ocean. Equilibrium (α^*) and kinetic (α_k) fractionation effects are indicated. α^* is controlled by temperature (T), while α_k is influenced by relative humidity (RH) and the isotope composition of atmospheric vapour ($\delta^{18}O_V$). Example oxygen isotope values are given for seawater ($\delta^{18}O_{SW}$), the evaporative flux ($\delta^{18}O_E$), cloud condensate ($\delta^{18}O_{CLD}$) and precipitation ($\delta^{18}O_P$). Modified from Fig. 15 in Craig and Gordon, 1965 and Fig. 3.4 in Gat et al., 2001.

1.2.2 Global patterns in precipitation isotopes

The fractionation processes outlined above affect the isotope composition of precipitation ($\delta^{18}O_P$), which is of particular relevance to this thesis. In addition, there are four large-scale effects that cause considerable spatial variation in $\delta^{18}O_P$ across the globe: the latitude effect, the amount effect, the continental effect and the altitude effect. These effects are described in detail by Rozanski et al. (1993), and will be briefly summarised here. First, the latitude effect is the observed reduction in $\delta^{18}O_P$ with increasing latitude. This is because the tropical oceans are the primary global source of atmospheric water vapour, and moisture is transported from here towards the poles. Air masses cool during poleward transport, causing water vapour to condense, and heavy isotopes to be progressively removed (Gat et al., 2001). Furthermore, temperature-dependent equilibrium fractionation effects increase as temperatures decline at higher latitudes, thus enhancing the latitude effect.

The amount effect refers to the negative relationship between the amount of rain in a single rainfall event and the $\delta^{18}O_P$ of the rainfall, and is particularly important in the tropics (Dansgaard, 1964). Risi et al. (2008) outlined the main physical processes contributing to this phenomenon: first, as explained above, the temperature, and thus the altitude of condensation, affects the degree to which the condensate is enriched through equilibrium fractionation. Next, kinetic fractionation occurs as raindrops fall from the cloud to the ground, through re-evaporation from the falling water droplets and isotope exchanges between the liquid water and atmospheric vapour. These processes tend to further enrich the falling rain, but are less effective during strong precipitation events, since rain falls more quickly and RH is high. Conversely, during light precipitation events raindrops fall more slowly through less humid air, and kinetic fractionation effects are stronger, thus raindrops become more isotopically enriched. This explains the observed inverse relationship between $\delta^{18}O_P$ and local precipitation amount.

Finally, the continental effect and the altitude effect can be considered together as they are effectively controlled by the same mechanism (Rozanski et al., 1993). The continental effect refers to the tendency for $\delta^{18}O_P$ to become more depleted with increasing distance from the coast, while the altitude effect is the reduction in $\delta^{18}O_P$ that occurs with increasing surface elevation. As described in section 1.2.1, temperature-dependent equilibrium fractionation effects within a raincloud result in the heavier

Table 1.1 – Typical $\delta^{18}O$ values in some of the natural reservoirs of water in the global hydrological cycle. Values come from Fig. 7.9 in Mook (2000).

Natural reservoir	$\delta^{18}O$ (‰)
Lake Chad	+8 to +15
Dead Sea	+2 to +5
Arctic sea ice	–3 to +3
Ocean water	–2 to +1
Subtropical/tropical zone precipitation	–8 to –2
Temperate zone precipitation	–16 to –4
Alpine glaciers	–18 to –11
Greenland glaciers	–39 to –25
Antarctic ice	–60 to –25

isotopologues of water condensing and raining out first (Dansgaard, 1964). Therefore, successive precipitation events during the transport of moisture over continents, or as air masses rise and cool during orographic uplift, result in the cumulative depletion of water vapour isotopes remaining in the atmosphere. Therefore, precipitation further inland, or at higher altitudes, will tend to have lower $\delta^{18}O_P$ values.

1.2.3 Isotopes in Amazon precipitation

Having reviewed the large-scale effects on $\delta^{18}O_P$ across the globe, the most important processes controlling $\delta^{18}O_P$ in the Amazon basin will now be discussed. Amazon $\delta^{18}O_P$ are influenced by three main factors: i) local amount effects, ii) continental rainout, and iii) precipitation recycling. These factors will each be discussed, and their relative importance in the Amazon highlighted. First, as explained in section 1.2.2, the amount effect has an important influence on $\delta^{18}O_P$ across the tropics, including the Amazon (Dansgaard, 1964, Rozanski et al., 1993). Models show that local amount effects are strongest over the tropical Atlantic Ocean, which is the major source of water vapour transported into the Amazon (Stohl and James, 2005, Drumond et al., 2014), and its control on $\delta^{18}O_P$ declines inland with increasing distance from the moisture source (Vimeux et al., 2005, Vuille et al., 2012). It should be noted that there is often a lack of clarity in the literature between the amount effect described here, and the large-scale inverse relationships between $\delta^{18}O_P$ and Amazon precipitation caused by continental rainout, which is described in the next paragraph. Henceforth, to avoid ambiguity, the phrase ‘local amount effects’ is used to refer to the amount effect in this thesis.

The second important factor influencing $\delta^{18}O_P$ in the Amazon is continental rainout, which is sometimes also referred to as Rayleigh rainout, or simply rainout. A schematic representation of this process is shown in Figure 1.2. The gradual removal of moisture from air masses during transport over the basin causes a gradient in $\delta^{18}O_P$ from the east to the west of the Amazon (Salati et al., 1979). The more rainout that occurs during moisture transport, the more isotopically light the rainfall at the western margins of the basin will be, often with little influence of the local climate at the site of condensation (e.g. Vimeux et al., 2005, Villacís et al., 2008). Indeed, the influence of rainout on $\delta^{18}O_P$ becomes stronger with increasing distance from the coast, which contrasts with the influence of local amount effects on Amazon $\delta^{18}O_P$ (see above). The gradual isotope depletion of atmospheric vapour over the course of multiple precipitation events can be mathematically described using Rayleigh distillation equations (Dansgaard, 1964, Salati et al., 1979). Due to their relative simplicity, and their ability to adequately describe most variability in $\delta^{18}O_P$ in the Amazon, Rayleigh distillation models have been employed in many studies over the past few decades (e.g. Grootes et al., 1989, Pierrehumbert, 1999, Gonfiantini et al., 2001, Vimeux et al., 2005, Samuels-Crow et al., 2014, Hurley et al., 2016). Further details on Rayleigh distillation are provided in Chapters 5 and 6.

A third important control on $\delta^{18}O_P$ in the Amazon is precipitation recycling through vegetation. At the global scale, transpiration contributions to terrestrial water

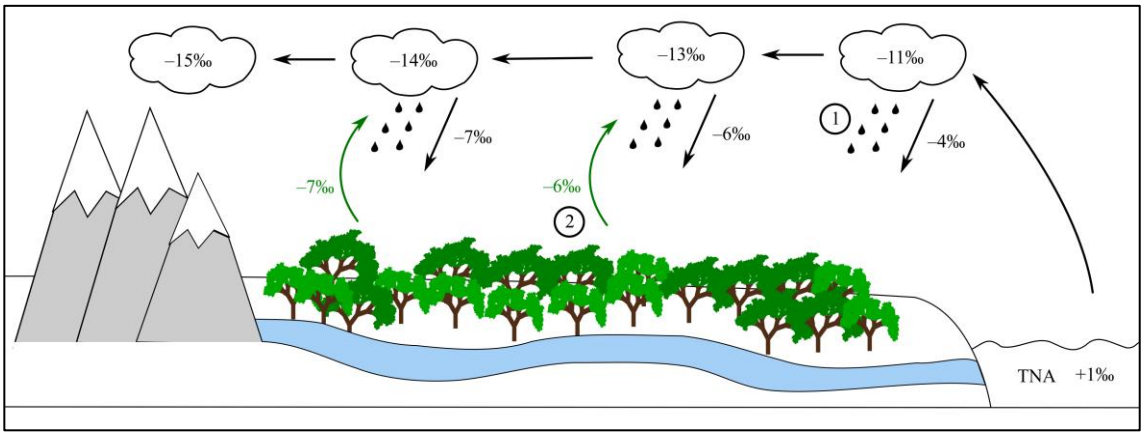

Figure 1.2 – Continental rainout and precipitation recycling over the Amazon. Water vapour is transported into the Amazon basin from the tropical North Atlantic (TNA). During moisture transport over the basin precipitation events preferentially remove heavy isotopes from the atmosphere (1), resulting in a gradient in the isotope composition of precipitation ($\delta^{18}O_P$) from east to west across the basin. Non-fractionating transpiration returns heavy isotopes back to the atmosphere (2), thus reducing the effective rainout and weakening the $\delta^{18}O_P$ gradient. Example oxygen isotope values in the ocean source water, atmospheric vapour, precipitation and transpired water are shown.

fluxes remain uncertain, but may be in the range of 35–80% (Jasechko et al., 2013, Coenders-Gerrits et al., 2014). Steady-state transpiration, which is generally assumed to be reached over longer timescales, such as over the course of a wet season (Jasechko et al., 2013; Welp et al., 2008; Yakir and Wang, 1996), has been shown to be isotopically non-fractionating (Flanagan and Ehleringer, 1991). Therefore, when plants transpire and return water vapour to the atmosphere that has the same isotope composition as precipitation, the effective rainout of heavy isotopes is reduced, thus weakening continental gradients in $\delta^{18}O_P$ (see Fig. 1.2). Indeed, Salati et al. (1979) measured $\delta^{18}O_P$ along an east-west gradient in the Amazon and observed that the inland gradient was weaker than that observed over Europe due to the significant contribution of water transpired through tropical forest, particularly during the dry season. Running a precipitation-recycling model with two different datasets, Eltahir and Bras (1994) estimated recycling ratios (i.e. the proportion of rain originating from evaporation within the region) of 25% and 35% for the Amazon. Other studies support these findings, with van der Ent et al. (2010) calculating that approximately 28% of precipitation in the Amazon originated from evapotranspiration within the region, which is in close accordance with Bosilovich and Chern's (2006) estimate of 27.2%. The precipitation-recycling ratio increases with distance from the Atlantic coast, and may be up to 70% in the southwest Amazon (van der Ent and Savenije, 2011). Finally, although transpiration is the dominant process by which water is returned to the atmosphere in the Amazon, evaporation from open water bodies and partial re-evaporation of rainwater trapped in the canopy (both fractionating processes, i.e. the evaporative flux is isotopically depleted relative to the source) are also important (Martinelli et al., 1996, Victoria et al., 1991). Henderson-Sellers et al. (2002) illustrate that the correct partitioning of fractionating evaporation relative to non-fractionating transpiration is necessary for accurate representation of Amazon $\delta^{18}O_P$ in GCMs.

1.2.4 Oxygen isotope proxy records

Instrumental climate records are temporally and spatially limited, particularly across regions of South America (Boninsegna et al., 2009, Rosenblüth et al., 1997, Villalba et al., 2003). In order to assess recent climatic changes in the context of historic variability it is helpful to extend these records further back in time, which can be done

using palaeoclimate proxies. Bradley (2011) reviewed the prerequisites for reconstructing palaeoclimate from proxy data. In summary, these include: i) the ability to establish an precisely dated chronology, which will usually require sufficient sample replication, ii) the possibility to sample at high (e.g. annual) resolution, iii) a good understanding of how climate influences the proxy signal, iv) confidence that the climate-signal relationship has been uniform over time (i.e. the principle of uniformitarianism, for further details see section 1.3), and v) an awareness of the different timescales of variation captured in the proxy signal. However, in reality different proxy archives have different strengths and weaknesses, and may not necessarily meet all of these requirements.

A variety of archives from South America have been shown to preserve $\delta^{18}O_P$, including ice cores (e.g. Thompson et al., 1995, Hoffmann, 2003, Vimeux et al., 2009, Thompson et al., 2013, Hurley et al., 2016), speleothems (e.g. Cruz et al., 2009, Reuter et al., 2009, Strikis et al., 2011, Kanner et al., 2013, Moquet et al., 2016, Novello et al., 2016), lake and palaeo-lake sediments (e.g. Baker et al., 2001, Wolfe et al., 2001, Bird et al., 2011a), marine sediments (Maslin and Burns, 2000) and also peat bogs (Skrzypek et al., 2011), which have all previously been used to reconstruct changes in climate across the Amazon. These records are a valuable source of information, and may provide insights on palaeoclimate over very long periods of time. For example, speleothems from southern Brazil have been used to reconstruct variation in convective activity over South America controlled by the precessional insolation cycle, which has a period of approximately 26,000 years (Cruz et al., 2005). However, there are also specific problems associated with each of these proxy records, which are outlined below.

First, replication may be limited, either due to the challenge of finding samples (e.g. speleothems are relatively rare), or because of the substantial cost and effort required to collect the samples, particularly ice cores (Bradley, 2011). In addition, several of these proxies may have fairly coarse or variable temporal resolution, for example, the resolution of isotope sampling in speleothems or peat can be as low as 40 or 50 years (e.g. Strikis et al., 2011, Skrzypek et al., 2011). While layer counting is possible in some archives, in the absence of clear annual stratification dating must be achieved using other methods, including the construction of age models, which are

subject to a degree of uncertainty (e.g. Thompson et al., 1998, Hardy et al., 2003, Kanner et al., 2013, Bird et al., 2011b). Furthermore, it can sometimes be difficult to isolate the source water $\delta^{18}O$ signal from post-depositional processes, limiting the conclusions that can be drawn (Cruz et al., 2005, Hoffmann, 2003, Pierrehumbert, 1999). For example, the $\delta^{18}O$ of speleothem calcite is affected by the isotope composition of drip water and modified by temperature-dependent fractionation, which can only be disentangled by analysing drip water preserved in fluid inclusions (e.g. van Breukelen et al., 2008). Similarly, ice-cores are affected by post-depositional processes during firnification, including evaporative enrichment at the surface and percolation of melted water through older ice, thus smoothing the signal (Grootes et al., 1989). Hardy et al. (2003) note that ice cores may be seasonally biased as they only preserve the signal during periods of net accumulation (i.e. the wet season). For instance, they estimate that just two thirds of the annual snowfall on the Sajama ice cap in Bolivia accumulates on the summit, with the rest lost due to melting and wind scour. Furthermore, reductions in wet season precipitation during extreme ENSO events may result in zero net annual accumulation, thus limiting the ability of ice cores to record these important climate anomalies. Other problems include the fact that ice cores are biased to high elevation sites, which are likely to be influenced by the altitude effect (see section 1.2.2), and tropical ice sheets are also under threat from anthropogenic warming (Thompson et al., 2000, Thompson et al., 2006).

More recently, tree-ring cellulose has been identified as another useful tropical $\delta^{18}O_P$ archive (Brienen et al., 2012, Ballantyne et al., 2011). Cellulose is used because it is immobile and produces a less noisy signal than lignin or whole wood (Gray and Thompson, 1977). Although it was once widely believed that tropical trees do not form annual growth rings due to the lack of temperature and daylight seasonality at low latitudes (e.g. Whitmore, 1998), at least 230 tropical tree species are now known to form demonstrably annual rings, and this number is continuing to rise with the expansion of tropical dendrochronology (Brienen et al., 2016). Rings can form in tropical trees that experience either an extreme dry (Dünisch et al., 2002) or an extreme wet (i.e. flooded) period (Worbes, 1995, Worbes and Junk, 1989), which both result in cessation of cambial growth. Tree-ring samples are relatively cheap and quick to collect; so, adequate replication is easily attainable. Furthermore, many species known

to form annual rings are ubiquitous across the Amazon basin, reducing the geographic limitations found with other archives. In sites where rings are known to be annual, dating can be achieved by simple ring counting and crossdating ring width (i.e. Douglass, 1941, Stokes and Smiley, 1968), or isotope measurements, between samples. Tree-ring records are likely to be subject to seasonal biases as $\delta^{18}O_P$ signals are only preserved during the period of tree growth, for example, *Cedrela odorata* from the Amazon primarily record wet season $\delta^{18}O_P$ (Brienen et al., 2012). However, once cellulose has formed the signal is retained and does not degrade, as may sometimes occur with ice cores. Finally, tree-ring $\delta^{18}O$ analysis can be conducted at annual resolution and higher, with some studies measuring $\delta^{18}O$ in sections only a few hundred micrometres wide to evaluate seasonal variability (e.g. Ohashi et al., 2016). One drawback of using tree-ring records is that tree lifespan may limit the length of palaeoclimate reconstructions, unless sufficient well-preserved wood can be found to extend the reconstruction back in time. In the tropics trees are widely thought to reach a maximum of 400–500 years old (Worbes and Junk, 1999), though the mean maximum age of tropical trees estimated by counting annual rings is 207 years (Brienen et al., 2016). However, some studies have reported finding trees much older than this (e.g. Chambers et al., 1998).

As with other proxy records, it is vital to have a mechanistic understanding of the controls on variation in Amazon tree-ring $\delta^{18}O$ ($\delta^{18}O_{TR}$), and whether they may have changed over time, before $\delta^{18}O_{TR}$ records can be used to reliably reconstruct palaeoclimate (see section 1.3). The $\delta^{18}O$ signature recorded in cellulose reflects the isotope composition of source water taken up by the plant, modified, to a greater or lesser extent, by plant physiology (Roden et al., 2000). Climate signals can be imprinted in $\delta^{18}O_{TR}$ either by an influence on source water $\delta^{18}O$, or by affecting leaf-level enrichment (McCarroll and Loader, 2004). In order to correctly interpret $\delta^{18}O_{TR}$ records it is necessary to develop a detailed understanding of how the $\delta^{18}O$ signal alters between water uptake and cellulose formation. The modification can be separated into physiological and biochemical fractionation effects (Sternberg, 2009), which will be described in detail in the sections that follow.

1.2.5 Physiological effects on $\delta^{18}O_{TR}$

Figure 1.3 shows the key processes that affect the $\delta^{18}O_{TR}$ signal (modified from Fig. 1 in Roden et al., 2000). First, precipitation (step 1 in Fig. 1.3) determines the isotope composition of the source water available to the tree in the top layers of soil. Next, water uptake and stem transport (steps 2 & 3 in Fig. 1.3) are non-fractionating processes so water entering the leaf has the same isotopic signal as the source/stem water ($\delta^{18}O_S$; White et al., 1985). In the leaf, preferential transpiration of isotopically light water through the stomata leads to enrichment at the site of evaporation (step 4 in Fig. 1.3; Roden et al., 2000, Barbour et al., 2004). The enrichment of the evaporative pool inside the leaf ($\delta^{18}O_E$) has been described using the Craig-Gordon model (Eqn. 5), since modified to include the effects of a boundary layer at the leaf surface and diffusion through the stomata (Craig and Gordon, 1965, Dongmann et al., 1974,

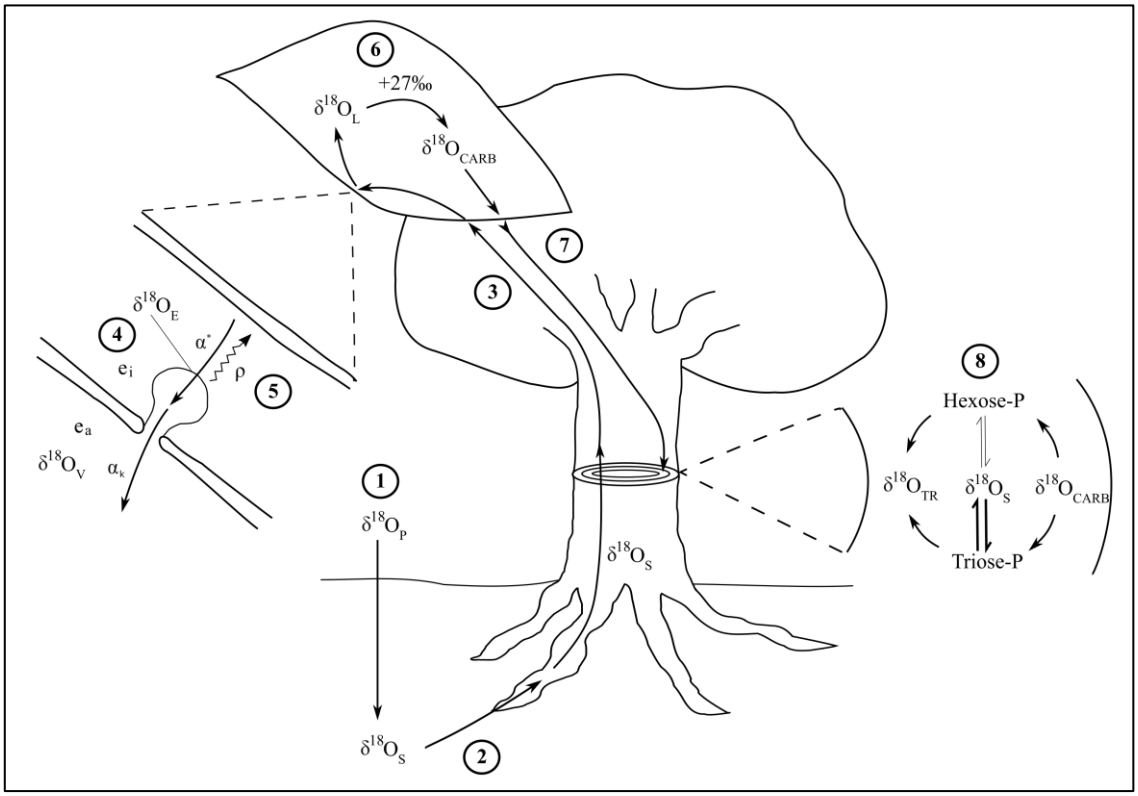

Figure 1.3 – Processes affecting the oxygen isotope composition of cellulose ($\delta^{18}O_{TR}$). Numbers indicate precipitation (1), non-fractionating uptake of source water (2), water transport to the leaf (3), enrichment at the site of evaporation (4), the Péclet effect (5), enrichment during synthesis of carbohydrate molecules in the leaf (6), the transport of carbohydrates to the stem (7) and oxygen atom exchange with stem water in phosphate recycling reactions during cellulose synthesis (8). Important $\delta^{18}O$ pools are labelled, including precipitation ($\delta^{18}O_P$), source/stem water ($\delta^{18}O_S$), water at the site of evaporation in the leaf ($\delta^{18}O_E$), bulk leaf water ($\delta^{18}O_L$) and synthesised carbohydrates ($\delta^{18}O_{CARB}$). Finally, e_i and e_a represent the intercellular and ambient vapour pressures respectively. Modified from Fig. 1 in Roden et al. (2000).

Farquhar and Lloyd, 1993, Sternberg, 2009):

$$\delta^{18}O_E = \varepsilon^* + (\delta^{18}O_S + \varepsilon_k)\left(\frac{e_i - e_a}{e_i}\right) + \delta^{18}O_V\left(\frac{e_a}{e_i}\right) \quad (6)$$

In this equation, hereafter referred to as the Dongmann model, ε^* represents the enrichment at the site of evaporation due to equilibrium fractionation, during the phase change from liquid to vapour (NB: $\varepsilon^* = \alpha^* - 1$). This process is dependent on the temperature (T) of the leaf, though the effect of T is relatively small (Majoube, 1971). In the second term of the model, $\delta^{18}O_S$ represents the isotope composition of the source/stem water, and ε_k is the enrichment through kinetic fractionation during molecular diffusion through the stomata and the leaf boundary layer (NB: $\varepsilon_k = \alpha_k - 1$; Barbour and Farquhar, 2000, Barbour et al., 2001, Roden et al., 2000). In the third term, $\delta^{18}O_V$ is the isotope composition of atmospheric vapour. The second and third terms are strongly influenced by RH, which determines the difference between the intercellular (e_i) and ambient (e_a) vapour pressures (i.e. the leaf-to-air vapour pressure difference). Under humidity-controlled conditions RH decreases with increasing T. RH is inversely related to $\delta^{18}O_E$, thus when RH is low (high), $\frac{e_i - e_a}{e_i}$ is high (low) and thus $\delta^{18}O_E$ is more (less) enriched through kinetic fractionation effects, while $\frac{e_a}{e_i}$ is low (high) and thus $\delta^{18}O_V$ (which would tend to have a depleting effect) has a weaker (stronger) influence on $\delta^{18}O_E$.

Flanagan and Ehleringer (1991) observed that the above model overestimated leaf water enrichment. This is because the Dongmann model only considers advective transport of water and its isotopes, however, the rate of diffusive backflow of water from the site of evaporation into the rest of the leaf is also important. The extent to which $\delta^{18}O_E$ affects bulk leaf water isotope composition ($\delta^{18}O_L$) depends on the ratio between the advective transport rate and diffusive transport rate, which is called the Péclet number (ρ; step 5 in Fig. 1.3; Farquhar and Lloyd, 1993). For rate of water loss via evapotranspiration through the stomata (ET, in kg m^{-2} s^{-1}), and the effective path length (L, in m) for advection through the leaf veins, the Péclet number can be calculated:

$$\rho = \frac{ET \times L}{C \times D} \quad (7)$$

where C is the concentration of water (in kg m^{-3}) and D is the diffusivity of $H_2{}^{18}O$ in water (in m^2 s^{-1}; $D=2.275\times10^9$ at 25 °C; Easteal et al., 1984). A low Péclet number

means that diffusive backflow from the evaporative site is important, while a large number means that diffusive back transport is not important (e.g. Barbour et al., 2004). $\delta^{18}O_L$ can then be modelled as a function of $\delta^{18}O_S$, $\delta^{18}O_E$ and the Péclet number (Eqn. 3 in Sternberg, 2009):

$$\delta^{18}O_L = \left[\left(1 - \left(\frac{1-e^{-\rho}}{\rho}\right)\right) \times \delta^{18}O_S\right] + \left[\left(\frac{1-e^{-\rho}}{\rho}\right) \times \delta^{18}O_E\right] \quad (8)$$

Plants respond to variation in local T and RH by modulating their stomatal conductance, which in turn affects the rate of ET and thus the Péclet number (Barbour et al., 2000, Barbour and Farquhar, 2000, Cernusak and Kahmen, 2013). Therefore, in addition to the effects on fractionation described above, T and RH are inversely related to $\delta^{18}O_L$ via their influence on ET. When RH is low (high), stomatal conductance is reduced (increased), ET and thus the Péclet number are low (high), resulting in a higher (lower) $\delta^{18}O_L$. However, subsequent biochemical reactions may prevent the $\delta^{18}O_L$ signal from being transferred to cellulose (e.g. Treydte et al., 2014).

1.2.6 Biochemical effects on $\delta^{18}O_{TR}$

The $\delta^{18}O_L$ signal is not directly recorded in tree rings but is first modified via biochemical fractionation effects during the synthesis of carbohydrates and then cellulose (Roden et al., 2000). The carbohydrates produced during photosynthesis are enriched in $\delta^{18}O$ by approximately 27 ‰ relative to the surrounding leaf water (step 6 in Fig. 1.3; Sternberg, 2009, Yakir and DeNiro, 1990):

$$\delta^{18}O_{CARB} = \delta^{18}O_L + 27\ ‰ \quad (9)$$

where $\delta^{18}O_{CARB}$ is the $\delta^{18}O$ of the synthesized carbohydrate molecules. The enrichment occurs through isotope fractionation during the hydration of carbonyl groups in the Calvin cycle (Sternberg and DeNiro, 1983). Furthermore, experiments have proven that $\delta^{18}O$ in synthesised carbohydrates are determined by $\delta^{18}O_L$ only, and are not affected at all by the $\delta^{18}O$ of CO_2 taken up by the plant (Deniro and Epstein, 1979). The carbohydrates are then transported to the stem for cellulose synthesis (step 7 in Fig. 1.3).

Oxygen exchange between carbohydrates and the water containing them is important in determining the final isotope signature recorded in cellulose (Roden et al., 2000). A recent study suggested that exchange of oxygen atoms with unenriched stem

water during phloem loading in conifers could contribute to the observed reduction in $\delta^{18}O$ in phloem sugars relative to those in the leaf (Gessler et al., 2013). However, no such decrease was observed for two deciduous broadleaf species (*Fagus* and *Quercus*) in the same study. Oxygen exchange predominantly occurs during triose phosphate recycling during cellulose synthesis (step 8 in Fig. 1.3; Hill et al., 1995). A proportion of the oxygen atoms in the carbohydrate precursors re-exchange with the local stem water ($\delta^{18}O_S$), causing some decoupling of the $\delta^{18}O_{TR}$ signal from that of the enriched leaf water, effectively reinforcing the source water isotope signal. The final $\delta^{18}O_{TR}$ value can therefore be modelled as (Eqn. 7 in Sternberg, 2009):

$$\delta^{18}O_{TR} = \phi \times (\delta^{18}O_S + 27) + (1 - \phi)(\delta^{18}O_{CARB}) \qquad (10)$$

where ϕ represents the fraction of carbohydrate $\delta^{18}O$ that exchanges with local stem water during cellulose synthesis, on average 42% (Roden et al., 2000). Work has shown that ϕ is positively related to the turnover time of non-structural carbohydrates (Song et al., 2014). This may be because more carbohydrate molecules pass through the triose phosphate recycling pathway when turnover time is high, or due to another biochemical mechanism that has not yet been accounted for (Song et al., 2014). Furthermore, Cheesman and Cernusak (2016) recently suggested that ϕ might be inversely related to variation in RH. They measured leaf and branch cellulose $\delta^{18}O$ in eucalypts growing along an aridity gradient and found that while leaf cellulose $\delta^{18}O$ became less enriched relative to source water with increasing RH, branch cellulose showed little or no variation. Increasing oxygen atom exchange between cellulose precursors and unenriched stem water with increasing dryness masked the influence of RH on branch cellulose $\delta^{18}O$. This work has cast doubt on the ability of cellulose to record interannual variation in local climate (i.e. T and RH), but supports the interpretation of $\delta^{18}O_{TR}$ as a reliable record of source water $\delta^{18}O$ (Voelker and Meinzer, 2017).

1.2.7 $\delta^{18}O_{TR}$ research in the Amazon

Due to the misconception that tropical trees do not form annual growth rings, there have been relatively few dendrochronological studies in the tropics in comparison with temperate regions (International Tree-Ring Data Bank, ITRDB, 2015), and tree-ring isotope studies are even scarcer. The first study analysing $\delta^{18}O$ in tropical trees from South America was by Evans and Schrag (2004), who measured $\delta^{18}O$ at high-

resolution in a *Prosopis* sp. tree from a coastal plantation in Peru. Although the tree did not form clear annual rings, the authors associated a strong excursion of approximately 8 ‰ in the isotope data to the 1997/98 ENSO event, thus highlighting the sensitivity of cellulose $\delta^{18}O$ from Peru to a pantropical climate oscillation. Subsequently, Ballantyne et al. (2011) analysed $\delta^{18}O$ in annual tree rings of *Tachigali myrmecophila*, *C. odorata* and *Polylepis tarapacana* from Brazil, Peru, and Argentina respectively. They identified negative relationships between $\delta^{18}O_{TR}$ and regional precipitation, though since the authors only analysed one individual from each site, it was not possible to develop robust climate reconstructions from the data.

More recently, Brienen et al. (2012) developed a $\delta^{18}O_{TR}$ chronology spanning 1901–2001 from eight *C. odorata* trees from a single site in northern Bolivia. The $\delta^{18}O_{TR}$ record was found to be significantly anticorrelated with precipitation over the whole Amazon basin during the wet season, and with Amazon River discharge measured at Óbidos (Pearson correlation coefficients >0.5), which integrates precipitation over approximately 80% of the Amazon basin (Callède et al., 2004). Meanwhile, local environmental variables had little influence on the $\delta^{18}O_{TR}$ signal. The authors hypothesised that the negative relationship with whole-basin precipitation was driven by rainout of heavy isotopes during moisture transport across the basin determining $\delta^{18}O_P$ (i.e. the continental effect, sections 1.2.2 & 1.2.3), with this signal being transferred to the tree rings.

In another recent study Volland et al. (2016) developed a well-replicated chronology from *Cedrela montana* trees growing in the mountain rainforest of southern Ecuador. Trees here were also shown to record $\delta^{18}O_P$, though there was more variability between individual trees than in the Brienen et al. (2012) study. Volland et al. (2016) related $\delta^{18}O_{TR}$ to precipitation over the Andes and found negative associations, but did not test for relationships with precipitation over a larger area. The fact that $\delta^{18}O_{TR}$ records from two different sites in the Amazon primarily record the isotope signature of source water is an important finding, and illustrates the potential for $\delta^{18}O_{TR}$ to be used for high-resolution palaeoclimate reconstructions in the region. However, both Brienen et al. (2012) and Volland et al. (2016) also report strong positive relationships between SSTs in the ENSO region of the Pacific and $\delta^{18}O_{TR}$, which could indicate a remote control on the signal, which is independent of the direct effect of precipitation on

$\delta^{18}O_{TR}$. Thus, before $\delta^{18}O_{TR}$ can be reliably used to reconstruct climate, a deeper understanding of the mechanisms driving Amazon $\delta^{18}O_{TR}$-climate relationships is required, beyond that suggested by correlation analyses.

1.3 The Principle of Uniformitarianism

Palaeoclimate reconstructions from tree rings rely on the principle of uniformitarianism, which is the assumption that relationships between climate and proxy data are constant over time (e.g. Speer, 2010). However, anthropogenic impacts on the environment have likely resulted in a violation of this principle. Although $\delta^{18}O_{TR}$ have been shown to be strongly related to precipitation over the Amazon (Brienen et al., 2012), the $\delta^{18}O$ signal recorded in cellulose is in fact very complex, and integrates information across different hydrological and plant physiological processes, potentially hindering the interpretation as a direct proxy for basin-wide rainout. For example, changes in the environmental conditions during evaporation from the ocean surface (e.g. Craig and Gordon, 1965, Pfahl and Sodemann, 2014), water recycling during moisture transport (e.g. Sturm et al., 2007), the degree of soil evaporation before plant water uptake (e.g. Kanner et al., 2014), and the various factors influencing plant physiology (e.g. Roden et al., 2000) could all add noise to the $\delta^{18}O_{TR}$ signal. It is therefore important to be aware of any trends in these various influences, in order to correctly interpret $\delta^{18}O_{TR}$ from the Amazon as a proxy for $\delta^{18}O_P$ and rainout processes over the basin.

The first factors to consider are changes in the location of, and conditions at, the oceanic origin of moisture. Surface seawater salinity measurements have been used to infer spatial variation in seawater $\delta^{18}O$ across the globe, with the highest values in the tropical and subtropical Atlantic (LeGrande and Schmidt, 2006). A change in atmospheric circulation patterns could possibly cause a change in the location of the primary moisture source and thus affect the $\delta^{18}O$ of source water, and although modelling work suggests this is not an important source of interannual variability in $\delta^{18}O_P$ over the Andes, for which the Amazon is the main source of moisture (Vuille et al., 2003), long-term changes in ocean $\delta^{18}O$ could possibly affect $\delta^{18}O_{TR}$ over longer timescales. Environmental conditions during evaporation from the ocean are also

important, as shown in the Craig-Gordon model (Fig. 1.1). For example, the increase in SSTs over the past few decades and longer (Stocker et al., 2013) will have reduced isotope fractionation during evaporation (Mook, 2000), though the effect of this on $\delta^{18}O_V$ is likely to be small (Majoube, 1971). Changes in RH at the ocean origin have also been observed to affect precipitation isotopes (Aemisegger et al., 2014, Pfahl and Sodemann, 2014), though in general RH over the oceans has remained relatively constant with increasing global temperatures (Hartmann et al., 2013).

Deforestation and increasing atmospheric CO_2 may have altered surface moisture fluxes in the Amazon and could thus have affected the $\delta^{18}O_{TR}$ signal. Lathuillière et al. (2012) observed that deforestation in Mato Grosso, Brazil, reduced evapotranspiration from forest by a quarter between 2000 and 2009 alone. Furthermore, rising atmospheric CO_2 may have led to reductions in transpiration fluxes over the Amazon, by reducing stomatal conductance (de Boer et al., 2011a, Keenan et al., 2013). Reductions in the ratio of non-fractionating transpiration versus fractionating evaporation would result in steeper continental gradients in $\delta^{18}O_P$ as the effective rainout volume is higher when moisture recycling is reduced (see Fig. 1.2; Salati et al., 1979). However, it should also be noted that most deforestation to date has been along the southern border of the Amazon rainforest (Hansen et al., 2013), and approximately 80% of the original forest remains intact (Davidson et al., 2012). Therefore, deforestation is not yet expected to have had much impact on recycling over the core of the basin.

The importance of evaporation from the soil prior to plant water uptake should also be considered, and will be briefly discussed here. Evaporation is a fractionating process so could cause the water taken up by plants to be enriched relative to the original precipitation (Ehleringer and Dawson, 1992). Increases in soil evaporation, which may result from rising global temperatures, could increase the isotope signature of source water and thus affect $\delta^{18}O_{TR}$. Kanner et al. (2014) used a modelling approach to identify regions where soil evaporation might potentially obscure the $\delta^{18}O_P$ signal, and thus interfere with palaeoclimate reconstructions from $\delta^{18}O_{TR}$. Their results suggest that soil water evaporation in the humid Amazon is not strong enough to have an important influence on $\delta^{18}O_{TR}$, relative to the stronger controlling effects of $\delta^{18}O_P$ and $\delta^{18}O_V$.

Changes in leaf functioning and environment could impact leaf water enrichment, as described in section 1.2.5. In addition to impacting basin-scale water recycling and thus $\delta^{18}O_P$ in areas downstream (i.e. the south and southwest of the Amazon basin), reductions in stomatal conductance in response to increased atmospheric CO_2 (e.g. de Boer et al., 2011b, Lammertsma et al., 2011, Keenan et al., 2013) could have a direct effect on $\delta^{18}O_L$ of the trees being sampled. For example, reduced transpiration rates would allow more back diffusion of isotopically enriched water from the site of evaporation, lowering the Péclet number (e.g. Farquhar and Lloyd, 1993), and resulting in higher $\delta^{18}O_L$ and potentially higher $\delta^{18}O_{TR}$ values in the tree-ring proxy records (e.g. step 5 in Fig. 1.3). Apart from CO_2, long-term changes in local climate may have also affected leaf-level enrichment (Cernusak et al., 2016). The effects of T and RH can be combined into a single factor influencing $\delta^{18}O_L$: the leaf-to-air vapour pressure difference (VPD; Kahmen et al., 2011). As VPD increases there is more isotopic fractionation and leaf water becomes more enriched (Barbour and Farquhar, 2000). VPD increases with increasing leaf temperature and decreasing ambient vapour pressure. Leaf temperatures are likely to have increased following reduced evaporative cooling with rising CO_2, which could be reflected in elevated $\delta^{18}O_{TR}$. Although several studies have suggested that local environmental effects on $\delta^{18}O_{TR}$ are small (e.g. Brienen et al., 2012, Treydte et al., 2014, Volland et al., 2016, Cheesman and Cernusak, 2016) the relative importance of controls may vary between sites and species, and all influencing factors must thus be taken into account.

Finally, trees also experience strong environmental changes as they grow from a small seedling in the understory, to become a large canopy tree (for a comprehensive summary see Meinzer et al., 2011). Particularly important are the substantial changes in the light environment and the hydraulic challenges associated with increasing tree height. Age-related growth trends are well known, and tree-ring width series require standardisation to remove these trends prior to palaeoclimate reconstructions (Cook and Kairiukstis, 1990). In addition, there are ontogenetic effects on carbon isotopes ($\delta^{13}C$) in tree rings, related to the many environmental and structural variables affecting photosynthesis and gas exchange, which co-vary with height (McDowell et al., 2011). Ontogenetic effects in $\delta^{18}O_{TR}$ might therefore also be expected, as changes in leaf temperature and transpiration rate with height may influence $\delta^{18}O_L$. However, studies

show that age-related $\delta^{18}O_{TR}$ biases vary in direction between species and sites (Treydte et al., 2006, Esper et al., 2010, Labuhn et al., 2014), and many studies find no significant ontogenetic effect on $\delta^{18}O_{TR}$ (Young et al., 2011, Sano et al., 2013, Kilroy et al., 2016, Xu et al., 2016). From these variable findings, it is clear that $\delta^{18}O_{TR}$ chronologies from new species and locations must be explicitly tested for ontogenetic effects.

In summary, to extract meaningful climate data from $\delta^{18}O_{TR}$ it is important to be aware of the complex nature of the recorded signal, and understand that environmental conditions have not been uniform over the lifetimes of the sampled trees. These long-term environmental trends are particularly important to consider when interpreting low-frequency changes in $\delta^{18}O_{TR}$.

1.4 Aims and Research Questions

The primary aim of this thesis is to develop a deeper understanding of the Amazon hydrological cycle using $\delta^{18}O_{TR}$ as a proxy for historical climate. This will provide valuable insight on natural hydrological variability and help to contextualise current climatic changes in the region. Stable isotope dendrochronology is still a relatively new field in the Amazon and thus this thesis will begin with some fundamental questions about the nature of tropical tree rings, before progressing to investigate $\delta^{18}O_{TR}$ signatures and what they can tell us about Amazon climate. Specific aims and research questions are formulated below.

1.4.1 Test tree-ring periodicity across different sites in tropical South America

The first step when undertaking dendrochronological research in a new site is to prove that trees form only one ring per year, as this is an important prerequisite for crossdating (Stokes and Smiley, 1968). Indeed, one of the advantages of using tree-ring $\delta^{18}O$ instead of other $\delta^{18}O$ records (e.g. speleothems or ice cores) for palaeoclimate reconstructions is that they can be reliably dated at an annual resolution (Bradley, 2011). However, false (i.e. non-annual) tree rings may form in some tropical tree species and/or locations (e.g. Worbes, 1995, Borchert, 1999, Pearson et al., 2011). Previous work has shown that cambial dormancy and ring formation in *C. odorata*

occur during the dry season (Dünisch et al., 2002), although the precise environmental signal to which trees respond remains unclear. Furthermore, spatial variation in rainfall seasonality has been shown to cause *C. odorata* trees to differ in their period of growth, resulting in variation in the timing of ring formation across different sites (e.g. Costa et al., 2013). Since rainfall seasonality is not strictly annual across all parts of the basin, it might then be expected that ring formation is not always annual. Therefore, the first aim of this thesis is to check the annual character of tree rings in different sites across the Amazon basin. Radiocarbon dating will be used to check tree-ring dates in *C. odorata* samples from Bolivia, Venezuela and Suriname, as well as samples of the closely related *C. montana* from Ecuador (see Fig. 1.4 for examples of the rings in these two species).

1.4.2 Develop and compare interannual $\delta^{18}O_{TR}$ series between different tropical tree species

Brienen et al. (2012) showed that a $\delta^{18}O_{TR}$ chronology developed from *C. odorata* (which has very clear rings) was an effective proxy for basin-wide precipitation. *C. odorata* has shallow roots and therefore the source water it takes up is predominantly recent precipitation, and the $\delta^{18}O_P$ signal is preserved in cellulose. In principle, $\delta^{18}O_{TR}$ chronologies could also be constructed from other shallow-rooted species that do not have access to deep groundwater (which may contain water from precipitation events across several years, and would therefore have a smoother climate signal). Several tropical tree species besides *C. odorata* are known to form annual growth rings, some more distinctly than others (Worbes, 1999), though to date few have been analysed for $\delta^{18}O_{TR}$. Ballantyne et al. (2011) measured $\delta^{18}O_{TR}$ in *T. myrmecophila*, *P. tarapacana,* and *C. odorata*, each from different countries in South America, Volland et al. (2016) constructed a robust $\delta^{18}O_{TR}$ chronology from *C. montana* from Ecuador, and Ohashi et al. (2016) studied intra-annual $\delta^{18}O_{TR}$ signals in *Eschweilera coriacea*, *Iryanthera coriacea* and *Protium hebetatum* from Brazil. The extent to which $\delta^{18}O_{TR}$ signals correspond between tree species will be investigated in this thesis, which will improve our understanding of how the signal is determined, and indicate whether other species may be suitable for developing palaeoclimate proxy records. $\delta^{18}O_{TR}$ signals in *C. odorata*, *Tachigali vasquezii*, *Amburana cearensis*, *Peltogyne heterophylla*, *Bertholletia*

excelsa, *Cedrelinga catenaeformis*, *Couratari macrosperma* and *P. tarapacana* from Bolivia will be measured and compared, thus substantially increasing the number of species used to develop $\delta^{18}O_{TR}$ series. Each species will be investigated to determine whether it shows a similar interannual $\delta^{18}O_{TR}$ signature to *C. odorata*. The results from this analysis could potentially improve the potency of $\delta^{18}O_{TR}$ as a palaeoclimate proxy in the Amazon, as longer-lived species could facilitate the extension of $\delta^{18}O_{TR}$ records back in time, and other species may be useful in regions where there are no natural *C. odorata* populations.

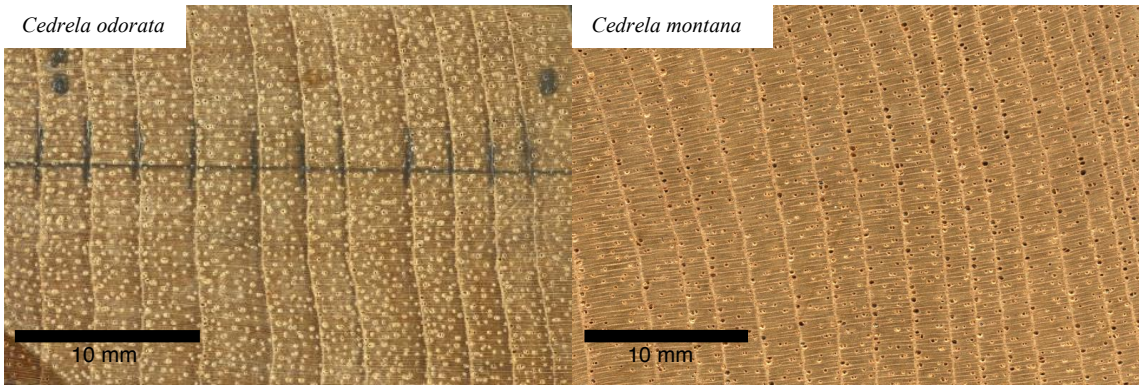

Figure 1.4 – Tree rings in *Cedrela*. High-resolution scans show the tree-ring structures in *Cedrela odorata* and *Cedrela montana,* the two main study species in this thesis.

1.4.3 Investigate spatial coherence between $\delta^{18}O_{TR}$ signatures from the Amazon

Work in tropical and sub-tropical Southeast Asia has shown that regional variation in climate can cause correlations between $\delta^{18}O_{TR}$ records from distant sites. For example, $\delta^{18}O_{TR}$ chronologies from sites 150 km apart in Laos and Vietnam were found to correlate strongly at interannual timescales (r=0.77; Sano et al., 2012). In addition, three $\delta^{18}O_{TR}$ records from the southeast Tibetan Plateau show weaker but significant coherence between sites <800 km apart (r values ranged between 0.37–0.49; Liu et al., 2014). If, as hypothesised, $\delta^{18}O_{TR}$ signals in the Amazon are controlled by large-scale rainout processes during moisture transport (Brienen et al., 2012), one might expect to see coherence between $\delta^{18}O_{TR}$ chronologies from sites large distances apart. Furthermore, a greater understanding of the Amazon hydrological cycle can possibly be gained by developing $\delta^{18}O_{TR}$ records from different sites along the moisture transport pathway. For example, $\delta^{18}O_{TR}$ from sites on the Atlantic coast, and in the central and western Amazon, could offer insights into changes in the basin $\delta^{18}O_P$ gradient, and thus

whether precipitation-recycling ratios and patterns of rainout have changed over time. Furthermore, the difference between $\delta^{18}O_{TR}$ signals from the east and west of the basin may relate better to interannual variation in rainout over the basin than just a single $\delta^{18}O_{TR}$ chronology from the west (i.e. Brienen et al., 2012).

To increase the spatial coverage of $\delta^{18}O_{TR}$ records in the Amazon, the first step will be to develop a second $\delta^{18}O_{TR}$ chronology from a new lowland rainforest site in northern Bolivia to see whether $\delta^{18}O_{TR}$ records cohere between sites several hundreds of kilometres apart. This would provide further support for a large-scale control on Amazon $\delta^{18}O_{TR}$. In addition to the new lowland Bolivian site, tree-ring samples have also been collected from the Bolivian Altiplano, and sites in Suriname, Venezuela, Brazil and Ecuador for analysis in this thesis. Suriname represents the point at which air masses enter the basin from the Atlantic, the Venezuelan site is in northernmost South America, the Brazil site is in centre of the Amazon basin, and the sites in Bolivia and Ecuador are in the far west of the basin, on the margins of the Andes (see Fig. 2.1 in Chapter 2). Initially, pilot analyses will be conducted in sites that have not previously been studied, to test the potential for $\delta^{18}O_{TR}$ chronology development. The pilot $\delta^{18}O_{TR}$ time series will then be extended in sites that show good coherence between trees, as coherence indicates that trees can be precisely dated and that there is a common climate control on the $\delta^{18}O_{TR}$ signal.

1.4.4 Identify the mechanisms controlling $\delta^{18}O_{TR}$ in the Amazon

Although correlation analysis has shown that a $\delta^{18}O_{TR}$ chronology from northern Bolivia is a good proxy for precipitation over the whole Amazon region (Brienen et al., 2012), the mechanism driving this relationship is not yet fully understood. In particular, it is not yet clear whether the relationship is definitely caused by rainout processes happening over the Amazon basin, or whether there could be a pan-tropical control on the signal (see 1.2.7). Clarification on this point is needed before $\delta^{18}O_{TR}$ records can be reliably used to reconstruct Amazon precipitation. This uncertainty will be addressed using two independent approaches: i) air-parcel trajectory modelling and ii) large-scale water vapour transport analysis. First, back-trajectories can be used to gain a better understanding of the controls on interannual variation in $\delta^{18}O_{TR}$, by relating isotope signatures to processes such as the amount of upstream rainout, air mass exposure to

vegetation and temperature changes during transport. For example, a change in the amount of rainout along trajectories is expected to affect the degree of isotopic depletion (Dansgaard, 1964, Salati et al., 1979), and therefore influence $\delta^{18}O_{TR}$ signatures. In the second approach, reanalysis data will be used to calculate Amazon basin moisture inflow and outflow, and thus see whether $\delta^{18}O_{TR}$ records are able to capture large-scale patterns in the regional moisture balance. These analyses will show the extent to which interannual variation in $\delta^{18}O_{TR}$ is indeed controlled by processes happening over the basin.

1.4.5 Extend Amazon $\delta^{18}O_{TR}$ records back in time

At present $\delta^{18}O_{TR}$ chronologies from the Amazon do not extend beyond the limit of instrumental climate data (rainfall data are available from 1901 (e.g. Harris et al., 2014), and the earliest river records begin in 1902 (e.g. HidroWeb, 2017)) and therefore cannot provide additional insights about historical hydrological variability. The published record from Brienen et al. (2012) spans a century, from 1901–2001, and the chronology from Volland et al. (2016) is from 1905–2011 (with a minimum replication of three trees). It would be valuable to extend Amazon $\delta^{18}O_{TR}$ records further back in time, ideally, far enough back to allow comparisons between $\delta^{18}O_{TR}$ signatures before and after anthropogenic impacts on the atmosphere became significant. Long records can be used to investigate drivers of Amazon hydrology at interannual, decadal and potentially even centennial scales. Insights on drivers of low-frequency climate variability are of particular interest, and may be gained from long $\delta^{18}O_{TR}$ records, provided there is no evidence for age-related effects on $\delta^{18}O_{TR}$ that would necessitate statistical de-trending (Loader et al., 2013). Finally, extending Amazon $\delta^{18}O_{TR}$ records will allow observed changes in Amazon climate, such as the intensification of the hydrological cycle since approximately 1990 (Gloor et al., 2013), and the recent severe droughts and floods (e.g. Zeng et al., 2008, Lewis et al., 2011, Marengo et al., 2011, Marengo and Espinoza, 2016), to be assessed in the context of historical change. This will help to evaluate whether these changes are within the bounds of natural variability or driven by anthropogenic influences.

1.4.6 Research questions

The research questions relating to the aforementioned aims can be summarised as follows:

1. How consistent is annual tree-ring periodicity across the Amazon?
2. Do different tropical tree species show similar $\delta^{18}O_{TR}$ signatures?
3. Do $\delta^{18}O_{TR}$ records from the Amazon show coherence at large spatial scales?
4. Can a network of $\delta^{18}O_{TR}$ chronologies from sites across the basin provide further information about interannual variation in basin rainout, or changes in the precipitation-recycling ratio?
5. What are the most important mechanisms driving interannual variation in Amazon $\delta^{18}O_{TR}$?
6. What can new long $\delta^{18}O_{TR}$ records presented in this thesis tell us about the Amazon hydrological cycle over the past two centuries?

1.5 Thesis Outline

As detailed in section 1.4, the aims of this thesis are to expand tree-ring research in Amazonia, and develop new $\delta^{18}O_{TR}$ chronologies that can be used to improve our understanding of the Amazon hydrological cycle. Chapter 1 has provided an overview of the literature to give context to the research, provided a rationale for the work and outlined the key aims and main research questions to be addressed. The rest of the thesis consists of six chapters: a chapter describing the methods, four research manuscripts, and a discussion section.

The methodologies used in the thesis are summarised in Chapter 2. The chapter includes an overview of the sample sites, the procedures for tree-ring and isotope analysis, and an outline of the main statistical techniques used. Background on air-mass trajectory modelling and the methods for trajectory computation are also provided.

It is important to verify the annual nature of tropical tree rings before they can be used to make inferences about climate. Thus, Chapter 3 uses radiocarbon dating to test ring periodicity in samples from Bolivia, Ecuador, Venezuela and Suriname, and uses

additional data from the literature to investigate what drives variability in growth across tropical South America.

The $\delta^{18}O_{TR}$ signals from different species and sites in Bolivia are investigated in chapter 4. The level of synchronicity between records from different species or between samples from distant locations will indicate how powerful $\delta^{18}O_{TR}$ is as a palaeoclimate proxy. Possible causes for observed differences and/or similarities between records will be discussed.

Chapter 5 seeks to better understand the mechanisms controlling $\delta^{18}O_{TR}$ signatures from the Amazon. This is necessary if $\delta^{18}O_{TR}$ records are to be reliably used to reconstruct palaeoclimate. Atmospheric back-trajectories are calculated and combined with remote sensing observations, and large-scale water vapour transport analysis is conducted, to determine whether basin-intrinsic processes control $\delta^{18}O_{TR}$ signals in trees from north Bolivia.

In Chapter 6 two long $\delta^{18}O_{TR}$ chronologies from Bolivia and Ecuador are presented. These chronologies span 1799–2014 and are the longest and best-replicated $\delta^{18}O_{TR}$ records from tropical South America to date. The records are compared with each other, and against climate observations to identify controls on variation on short- and long-term timescales. Long-term trends in $\delta^{18}O_{TR}$ and other $\delta^{18}O$ proxy records are evaluated and possible drivers discussed.

The main findings from chapters 3–6 are drawn together and discussed in Chapter 7. This section contains further in-depth critical analysis of the results and places them in the context of the literature. The key aims of the thesis are re-examined to see to whether they have been achieved, and any problems encountered during the research are discussed. Finally, the overall conclusions from the thesis are summarised.

1.6 References

Aemisegger, F., Pfahl, S., Sodemann, H., Lehner, I., Seneviratne, S. I. & Wernli, H. 2014. Deuterium excess as a proxy for continental moisture recycling and plant transpiration. *Atmospheric Chemistry and Physics Discussions,* 13**,** 29721-29784.

Aragão, L. E. O. C., Poulter, B., Barlow, J. B., Anderson, L. O., Malhi, Y., Saatchi, S., Phillips, O. L. & Gloor, M. 2014. Environmental change and the carbon balance of Amazonian forests. *Biological Reviews,* 89**,** 913-931.

Baker, P. A., Rigsby, C. A., Seltzer, G. O., Fritz, S. C., Lowenstein, T. K., Bacher, N. P. & Veliz, C. 2001. Tropical climate changes at millennial and orbital timescales on the Bolivian Altiplano. *Nature,* 409**,** 698-701.

Ballantyne, A. P., Baker, P. A., Chambers, J. Q., Villalba, R. & Argollo, J. 2011. Regional differences in South American monsoon precipitation inferred from the growth and isotopic composition of tropical trees. *Earth Interactions,* 15**,** 1-35.

Barbour, M. M., Fischer, R. A., Sayre, K. D. & Farquhar, G. D. 2000. Oxygen isotope ratio of leaf and grain material correlates with stomatal conductance and grain yield in irrigated wheat. *Functional Plant Biology,* 27**,** 625-637.

Barbour, M. M. & Farquhar, G. D. 2000. Relative humidity- and ABA-induced variation in carbon and oxygen isotope ratios of cotton leaves. *Plant, Cell and Environment,* 23**,** 473-485.

Barbour, M. M., Andrews, T. J. & Farquhar, G. D. 2001. Correlations between oxygen isotope ratios of wood constituents of *Quercus* and *Pinus* samples from around the world. *Functional Plant Biology,* 28**,** 335-348.

Barbour, M. M., Roden, J. S., Farquhar, G. D. & Ehleringer, J. R. 2004. Expressing leaf water and cellulose oxygen isotope ratios as enrichment above source water reveals evidence of a Péclet effect. *Oecologia,* 138**,** 426-35.

Bird, B. W., Abbott, M. B., Vuille, M., Rodbell, D. T., Stansell, N. D. & Rosenmeier, M. F. 2011a. A 2,300-year-long annually resolved record of the South American summer monsoon from the Peruvian Andes. *Proceedings of the National Academy of Sciences,* 108**,** 8583-8588.

Bird, B. W., Abbott, M. B., Rodbell, D. T. & Vuille, M. 2011b. Holocene tropical South American hydroclimate revealed from a decadally resolved lake sediment $\delta^{18}O$ record. *Earth and Planetary Science Letters,* 310**,** 192-202.

Boisier, J. P., Ciais, P., Ducharne, A. & Guimberteau, M. 2015. Projected strengthening of Amazonian dry season by constrained climate model simulations. *Nature Climate Change,* 5**,** 656-660.

Bonan, G. B. 2008. Forests and Climate Change: Forcings, Feedbacks, and the Climate Benefits of Forests. *Science,* 320**,** 1444-1449.

Boninsegna, J. A., Argollo, J., Aravena, J., Barichivich, J., Christie, D., Ferrero, M., Lara, A., Le Quesne, C., Luckman, B. & Masiokas, M. 2009. Dendroclimatological reconstructions in South America: A review. *Palaeogeography, Palaeoclimatology, Palaeoecology,* 281**,** 210-228.

Borchert, R. 1999. Climatic periodicity, phenology, and cambium activity in tropical dry forest trees. *IAWA Journal,* 20**,** 239-247.

Bosilovich, M. G. & Chern, J.-D. 2006. Simulation of water sources and precipitation recycling for the MacKenzie, Mississippi, and Amazon River basins. *Journal of Hydrometeorology,* 7**,** 312-329.

Bottinga, Y. & Craig, H. 1968. Oxygen isotope fractionation between CO_2 and water, and the isotopic composition of marine atmospheric CO_2. *Earth and Planetary Science Letters,* 5**,** 285-295.

Bradley, R. S. 2011. High-Resolution Paleoclimatology. *In:* HUGHES, M. K., SWETNAM, T. W. & DIAZ, H. F. (eds.) *Dendroclimatology: Progress and Prospects.* Dordrecht: Springer Netherlands.

Brienen, R. J. W., Helle, G., Pons, T. L., Guyot, J. L. & Gloor, M. 2012. Oxygen isotopes in tree rings are a good proxy for Amazon precipitation and El Niño-Southern Oscillation variability. *Proceedings of the National Academy of Sciences,* 109**,** 16957-16962.

Brienen, R. J. W., Phillips, O. L., Feldpausch, T. R., Gloor, E., Baker, T. R., Lloyd, J., Lopez-Gonzalez, G., Monteagudo-Mendoza, A., Malhi, Y., Lewis, S. L., Vasquez Martinez, R., Alexiades, M., Alvarez Davila, E., Alvarez-Loayza, P., Andrade, A., Aragao, L. E. O. C., Araujo-Murakami, A., Arets, E. J. M. M., Arroyo, L., Aymard C, G. A., Banki, O. S., Baraloto, C., Barroso, J., Bonal, D., Boot, R. G. A., Camargo, J. L. C., Castilho, C. V., Chama, V., Chao, K. J., Chave, J., Comiskey, J. A., Cornejo Valverde, F., Da Costa, L., De Oliveira, E. A., Di Fiore, A., Erwin, T. L., Fauset, S., Forsthofer, M., Galbraith, D. R., Grahame, E. S., Groot, N., Herault, B., Higuchi, N., Honorio Coronado, E. N., Keeling, H., Killeen, T. J., Laurance, W. F., Laurance, S., Licona, J., Magnussen, W. E., Marimon, B. S., Marimon-Junior, B. H., Mendoza, C., Neill, D. A., Nogueira, E. M., Nunez, P., Pallqui Camacho, N. C., Parada, A., Pardo-Molina, G., Peacock, J., Pena-Claros, M., Pickavance, G. C., Pitman, N. C. A., Poorter, L., Prieto, A., Quesada, C. A., Ramirez, F., Ramirez-Angulo, H., Restrepo, Z., Roopsind, A., Rudas, A., Salomao, R. P., Schwarz, M., Silva, N., Silva-Espejo, J. E., Silveira, M., Stropp, J., Talbot, J., Ter Steege, H., Teran-Aguilar, J., Terborgh, J., Thomas-Caesar, R., Toledo, M., Torello-Raventos, M., Umetsu, R. K., Van Der Heijden, G. M. F., Van Der Hout, P., Guimaraes Vieira, I. C., Vieira, S. A., Vilanova, E., Vos, V. A. & Zagt, R. J. 2015. Long-term decline of the Amazon carbon sink. *Nature,* 519**,** 344-348.

Brienen, R. J. W., Schöngart, J. & Zuidema, P. A. 2016. Tree Rings in the Tropics: Insights into the Ecology and Climate Sensitivity of Tropical Trees. *In:* GOLDSTEIN, G. & SANTIAGO, L. S.

(eds.) *Tropical Tree Physiology: Adaptations and Responses in a Changing Environment.* Cham: Springer International Publishing.
Callède, J., Guyot, J. L., Ronchail, J., L'hôte, Y., Niel, H. & De Oliveira, E. 2004. Evolution of the River Amazon's discharge at Óbidos from 1903 to 1999. *Hydrological Sciences Journal,* 49**,** 85-97.
Callède, J., Cochonneau, G., Alves, F. V., Guyot, J.-L., Guimarães, V. S. & De Oliveira, E. 2010. Les apports en eau de l'Amazone à l'Océan Atlantique. *Revue des sciences de l'eau/Journal of Water Science,* 23**,** 247-273.
Cao, M. & Woodward, F. I. 1998. Net primary and ecosystem production and carbon stocks of terrestrial ecosystems and their responses to climate change. *Global Change Biology,* 4**,** 185-198.
Cernusak, L. A. & Kahmen, A. 2013. The multifaceted relationship between leaf water O enrichment and transpiration rate. *Plant, Cell and Environment,* 36**,** 1239-1241.
Cernusak, L. A., Barbour, M. M., Arndt, S. K., Cheesman, A. W., English, N. B., Feild, T. S., Helliker, B. R., Holloway-Phillips, M. M., Holtum, J. A., Kahmen, A., McInerney, F. A., Munksgaard, N. C., Simonin, K. A., Song, X., Stuart-Williams, H., West, J. B. & Farquhar, G. D. 2016. Stable isotopes in leaf water of terrestrial plants. *Plant, Cell and Environment,* 39**,** 1087-1102.
Chambers, J. Q., Higuchi, N. & Schimel, J. P. 1998. Ancient trees in Amazonia. *Nature,* 391**,** 135-136.
Cheesman, A. & Cernusak, L. 2016. Infidelity in the outback: climate signal recorded in $\Delta^{18}O$ of leaf but not branch cellulose of eucalypts across an Australian aridity gradient. *Tree Physiology***,** 1-11.
Ciais, P. & Jouzel, J. 1994. Deuterium and oxygen 18 in precipitation: Isotopic model, including mixed cloud processes. *Journal of Geophysical Research,* 99**,** 16793-16803.
Coenders-Gerrits, A. M. J., Van Der Ent, R. J., Bogaard, T. A., Wang-Erlandsson, L., Hrachowitz, M. & Savenije, H. H. G. 2014. Uncertainties in transpiration estimates. *Nature,* 506**,** E1-E2.
Cook, E. R. & Kairiukstis, L. A. 1990. *Methods of dendrochronology: applications in the environmental sciences*, Dordrecht, The Netherlands, Kluwer Academic Publishers.
Costa, M. H. & Foley, J. A. 1998. A comparison of precipitation datasets for the Amazon basin. *Geophysical Research Letters,* 25**,** 155-158.
Costa, M. H. & Foley, J. A. 1999. Trends in the hydrologic cycle of the Amazon basin. *Journal of Geophysical Research: Atmospheres,* 104**,** 14189-14198.
Costa, M. S., De Vasconcellos, T. J., Barros, C. F. & Callado, C. H. 2013. Does growth rhythm of a widespread species change in distinct growth sites? *IAWA Journal,* 34**,** 498 – 509.
Cox, P. M., Betts, R. A., Collins, M., Harris, P. P., Huntingford, C. & Jones, C. D. 2004. Amazonian forest dieback under climate-carbon cycle projections for the 21st century. *Theoretical and applied climatology,* 78**,** 137-156.
Craig, H. & Gordon, L. I. 1965. Deuterium and oxygen 18 variations in the ocean and the marine atmosphere. *In:* TONGIOGI, E. (ed.) *Stable Isotopes in Oceanographic Studies and Paleotemperatures.* Spoleto, Italy: Consiglio nazionale delle richerche, Laboratorio de geologia nucleare.
Cruz, F. W., Burns, S. J., Karmann, I., Sharp, W. D., Vuille, M., Cardoso, A. O., Ferrari, J. A., Dias, P. L. S. & Viana, O. 2005. Insolation-driven changes in atmospheric circulation over the past 116,000 years in subtropical Brazil. *Nature,* 434**,** 63-66.
Cruz, F. W., Vuille, M., Burns, S. J., Wang, X., Cheng, H., Werner, M., Edwards, R. L., Karmann, I., Auler, A. S. & Nguyen, H. 2009. Orbitally driven east–west antiphasing of South American precipitation. *Nature Geoscience,* 2**,** 210-214.
Dansgaard, W. 1964. Stable isotopes in precipitation. *Tellus,* 16**,** 436-468.
Davidson, E. A., De Araujo, A. C., Artaxo, P., Balch, J. K., Brown, I. F., C. Bustamante, M. M., Coe, M. T., Defries, R. S., Keller, M., Longo, M., Munger, J. W., Schroeder, W., Soares-Filho, B. S., Souza, C. M. & Wofsy, S. C. 2012. The Amazon basin in transition. *Nature,* 481**,** 321-328.
De Boer, H. J., Lammertsma, E. I., Wagner-Cremer, F., Dilcher, D. L., Wassen, M. J. & Dekker, S. C. 2011a. Climate forcing due to optimization of maximal leaf conductance in subtropical vegetation under rising CO_2. *Proceedings of the National Academy of Sciences,* 108**,** 4041-4046.
De Boer, H. J., Lammertsma, E. I., Wagner-Cremer, F., Dilcher, D. L., Wassen, M. J. & Dekker, S. C. 2011b. Climate forcing due to optimization of maximal leaf conductance in subtropical vegetation under rising CO2. *Proc Natl Acad Sci U S A,* 108**,** 4041-6.
Deniro, M. J. & Epstein, S. 1979. Relationship between the oxygen isotope ratios of terrestrial plant cellulose, carbon dioxide, and water. *Science,* 204**,** 51-53.
Dongmann, G., Nürnberg, H., Förstel, H. & Wagener, K. 1974. On the enrichment of $H_2{}^{18}O$ in the leaves of transpiring plants. *Radiation and Environmental Biophysics,* 11**,** 41-52.
Douglass, A. E. 1941. Crossdating in dendrochronology. *Journal of Forestry,* 39**,** 825-831.

Drumond, A., Marengo, J., Ambrizzi, T., Nieto, R., Moreira, L. & Gimeno, L. 2014. The role of the Amazon Basin moisture in the atmospheric branch of the hydrological cycle: a Lagrangian analysis. *Hydrology and Earth System Sciences,* 18**,** 2577-2598.

Duffy, P. B., Brando, P., Asner, G. P. & Field, C. B. 2015. Projections of future meteorological drought and wet periods in the Amazon. *Proceedings of the National Academy of Sciences,* 112**,** 13172-13177.

Dünisch, O., Bauch, J. & Gasparotto, L. 2002. Formation of increment zones and intraannual growth dynamics in the xylem of *Swietenia macrophylla*, *Carapa guianensis*, and *Cedrela odorata* (Meliaceae). *IAWA Journal,* 23**,** 101-120.

Easteal, A. J., Edge, A. V. J. & Woolf, L. A. 1984. Isotope effects in water. Tracer diffusion coefficients for $H_2{}^{18}O$ in ordinary water. *The Journal of Physical Chemistry,* 88**,** 6060-6063.

Ehleringer, J. & Dawson, T. 1992. Water uptake by plants: perspectives from stable isotope composition. *Plant, Cell and Environment,* 15**,** 1073-1082.

Eltahir, E. A. & Bras, R. L. 1994. Precipitation recycling in the Amazon basin. *Quarterly Journal of the Royal Meteorological Society,* 120**,** 861-880.

Esper, J., Frank, D. C., Battipaglia, G., Büntgen, U., Holert, C., Treydte, K., Siegwolf, R. & Saurer, M. 2010. Low-frequency noise in $\delta^{13}C$ and $\delta^{18}O$ tree ring data: A case study of *Pinus uncinata* in the Spanish Pyrenees. *Global Biogeochemical Cycles,* 24**,** 1-11.

Espinoza, J. C., Guyot, J. L., Ronchail, J., Cochonneau, G., Filizola, N., Fraizy, P., Labat, D., De Oliveira, E. A., Ordoñez, J. J. & Vauchel, P. 2009. Contrasting regional discharge evolutions in the Amazon basin (1974–2004). *Journal of Hydrology,* 375**,** 297-311.

Espinoza, J. C., Ronchail, J., Frappart, F., Lavado, W., Santini, W. & Guyot, J. L. 2013. The Major Floods in the Amazonas River and Tributaries (Western Amazon Basin) during the 1970–2012 Period: A Focus on the 2012 Flood. *Journal of Hydrometeorology,* 14**,** 1000-1008.

Espinoza, J. C., Marengo, J. A., Ronchail, J., Carpio, J. M., Flores, L. N. & Guyot, J. L. 2014. The extreme 2014 flood in south-western Amazon basin: the role of tropical-subtropical South Atlantic SST gradient. *Environmental Research Letters,* 9**,** 1-9.

Esquivel-Muelbert, A., Galbraith, D., Dexter, K. G., Baker, T. R., Lewis, S. L., Meir, P., Rowland, L., Costa, A. C. L. D., Nepstad, D. & Phillips, O. L. 2017. Biogeographic distributions of neotropical trees reflect their directly measured drought tolerances. *Scientific Reports*, 7, 8334.

Evans, M. N. & Schrag, D. P. 2004. A stable isotope-based approach to tropical dendroclimatology. *Geochimica et Cosmochimica Acta,* 68**,** 3295-3305.

Farquhar, G. & Lloyd, J. 1993. Carbon and oxygen isotope effects in the exchange of carbon dioxide between terrestrial plants and the atmosphere. *Stable isotopes and plant carbon-water relations,* 40**,** 47-70.

Feldpausch, T. R., Lloyd, J., Lewis, S. L., Brienen, R. J. W., Gloor, M., Monteagudo Mendoza, A., Lopez-Gonzalez, G., Banin, L., Abu Salim, K., Affum-Baffoe, K., Alexiades, M., Almeida, S., Amaral, I., Andrade, A., Aragão, L. E. O. C., Araujo Murakami, A., Arets, E. J. M. M., Arroyo, L., Aymard C, G. A., Baker, T. R., Bánki, O. S., Berry, N. J., Cardozo, N., Chave, J., Comiskey, J. A., Alvarez, E., De Oliveira, A., Di Fiore, A., Djagbletey, G., Domingues, T. F., Erwin, T. L., Fearnside, P. M., França, M. B., Freitas, M. A., Higuchi, N., C, E. H., Iida, Y., Jiménez, E., Kassim, A. R., Killeen, T. J., Laurance, W. F., Lovett, J. C., Malhi, Y., Marimon, B. S., Marimon-Junior, B. H., Lenza, E., Marshall, A. R., Mendoza, C., Metcalfe, D. J., Mitchard, E. T. A., Neill, D. A., Nelson, B. W., Nilus, R., Nogueira, E. M., Parada, A., Peh, K. S. H., Pena Cruz, A., Peñuela, M. C., Pitman, N. C. A., Prieto, A., Quesada, C. A., Ramírez, F., Ramírez-Angulo, H., Reitsma, J. M., Rudas, A., Saiz, G., Salomão, R. P., Schwarz, M., Silva, N., Silva-Espejo, J. E., Silveira, M., Sonké, B., Stropp, J., Taedoumg, H. E., Tan, S., Ter Steege, H., Terborgh, J., Torello-Raventos, M., Van Der Heijden, G. M. F., Vásquez, R., Vilanova, E., Vos, V. A., White, L., Willcock, S., Woell, H. & Phillips, O. L. 2012. Tree height integrated into pantropical forest biomass estimates. *Biogeosciences,* 9**,** 3381-3403.

Feldpausch, T. R., Phillips, O. L., Brienen, R. J. W., Gloor, E., Lloyd, J., Lopez-Gonzalez, G., Monteagudo-Mendoza, A., Malhi, Y., Alarcón, A., Álvarez Dávila, E., Alvarez-Loayza, P., Andrade, A., Aragao, L. E. O. C., Arroyo, L., Aymard C, G. A., Baker, T. R., Baraloto, C., Barroso, J., Bonal, D., Castro, W., Chama, V., Chave, J., Domingues, T. F., Fauset, S., Groot, N., Honorio Coronado, E., Laurance, S., Laurance, W. F., Lewis, S. L., Licona, J. C., Marimon, B. S., Marimon-Junior, B. H., Mendoza Bautista, C., Neill, D. A., Oliveira, E. A., Oliveira Dos Santos, C., Pallqui Camacho, N. C., Pardo-Molina, G., Prieto, A., Quesada, C. A., Ramírez, F., Ramírez-Angulo, H., Réjou-Méchain, M., Rudas, A., Saiz, G., Salomão, R. P., Silva-Espejo, J.

E., Silveira, M., Ter Steege, H., Stropp, J., Terborgh, J., Thomas-Caesar, R., Van Der Heijden, G. M. F., Vásquez Martinez, R., Vilanova, E. & Vos, V. A. 2016. Amazon forest response to repeated droughts. *Global Biogeochemical Cycles,* 30**,** 964-982.

Flanagan, L. & Ehleringer, J. 1991. Stable isotope composition of stem and leaf water: applications to the study of plant water use. *Functional Ecology,* 5**,** 270-277.

Foley, J. A., Botta, A., Coe, M. T. & Costa, M. H. 2002. El Niño–Southern oscillation and the climate, ecosystems and rivers of Amazonia. *Global Biogeochemical Cycles,* 16**,** 1-20.

Fu, R., Yin, L., Li, W., Arias, P. A., Dickinson, R. E., Huang, L., Chakraborty, S., Fernandes, K., Liebmann, B., Fisher, R. A. & Myneni, R. B. 2013. Increased dry-season length over southern Amazonia in recent decades and its implication for future climate projection. *Proceedings of the National Academy of Sciences,* 110**,** 18110-18115.

Galewsky, J., Steen-Larsen, H. C., Field, R. D., Worden, J., Risi, C. & Schneider, M. 2016. Stable isotopes in atmospheric water vapor and applications to the hydrologic cycle. *Reviews of Geophysics,* 54**,** 809-865.

Garreaud, R. D., Vuille, M., Compagnucci, R. & Marengo, J. 2009. Present-day South American climate. *Palaeogeography, Palaeoclimatology, Palaeoecology,* 281**,** 180-195.

Gat, J. R., Mook, W. G. & Meijer, H. a. J. 2001. *Environmental isotopes in the hydrological cycle: Volume II Atmospheric water*, International Atomic Energy Agency and United Nations Educational, Scientific and Cultural Organization.

Gatti, L., Gloor, M., Miller, J., Doughty, C., Malhi, Y., Domingues, L., Basso, L., Martinewski, A., Correia, C. & Borges, V. 2014. Drought sensitivity of Amazonian carbon balance revealed by atmospheric measurements. *Nature,* 506**,** 76-80.

Gessler, A., Brandes, E., Keitel, C., Boda, S., Kayler, Z. E., Granier, A., Barbour, M., Farquhar, G. D. & Treydte, K. 2013. The oxygen isotope enrichment of leaf-exported assimilates–does it always reflect lamina leaf water enrichment? *New Phytologist,* 200**,** 144-157.

Gloor, M., Brienen, R. J. W., Galbraith, D., Feldpausch, T. R., Schöngart, J., Guyot, J. L., Espinoza, J. C., Lloyd, J. & Phillips, O. L. 2013. Intensification of the Amazon hydrological cycle over the last two decades. *Geophysical Research Letters,* 40**,** 1729-1733.

Gloor, M., Barichivich, J., Ziv, G., Brienen, R. J. W., Schöngart, J., Peylin, P., Cintra, B. B. L., Feldpausch, T. R., Phillips, O. L. & Baker, J. C. A. 2015. Recent Amazon climate as background for possible ongoing and future changes of Amazon humid forests. *Global Biogeochemical Cycles,* 29**,** 1384-1399.

Gonfiantini, R., Roche, M.-A., Olivry, J.-C., Fontes, J.-C. & Zuppi, G. M. 2001. The altitude effect on the isotopic composition of tropical rains. *Chemical Geology,* 181**,** 147-167.

Gray, J. & Thompson, P. 1977. Climatic information from $^{18}O/^{16}O$ analysis of cellulose, lignin and whole wood from tree rings. *Nature,* 270**,** 708-709.

Grootes, P., Stuiver, M., Thompson, L. & Mosley-Thompson, E. 1989. Oxygen isotope changes in tropical ice, Quelccaya, Peru. *Journal of Geophysical Research: Atmospheres,* 94**,** 1187-1194.

Hansen, M. C., Potapov, P. V., Moore, R., Hancher, M., Turubanova, S. A., Tyukavina, A., Thau, D., Stehman, S. V., Goetz, S. J., Loveland, T. R., Kommareddy, A., Egorov, A., Chini, L., Justice, C. O. & Townshend, J. R. G. 2013. High-Resolution Global Maps of 21st-Century Forest Cover Change. *Science,* 342**,** 850-853.

Hardy, D., Vuille, M. & Bradley, R. 2003. Variability of snow accumulation and isotopic composition on Nevado Sajama, Bolivia. *Journal of Geophysical Research: Atmospheres* 108**,** 1-10.

Harris, I., Jones, P. D., Osborn, T. J. & Lister, D. H. 2014. Updated high-resolution grids of monthly climatic observations–the CRU TS3.10 Dataset. *International Journal of Climatology,* 34**,** 623-642.

Hartmann, D. L., Klein tank, A. M. G., Rusticucci, M., Alexander, L. V., BröNnimann, S., Charabi, Y., Dentener, F. J., Dlugokencky, E. J., Easterling, D. R., Kaplan, A., Soden, B. J., Thorne, P. W., Wild, M. & Zhai, P. M. 2013. Observations: Atmosphere and Surface. *In:* STOCKER, T. F., QIN, D., PLATTNER, G.-K., TIGNOR, M., ALLEN, S. K., BOSCHUNG, J., NAUELS, A., XIA, Y., BEX, V. & MIDGLEY, P. M. (eds.) *Climate Change 2013: The Physical Science Basis. Contribution of Working Group I to the Fifth Assessment Report of the Intergovernmental Panel on Climate Change.* Cambridge, United Kingdom and New York, NY, USA: Cambridge University Press.

Henderson-Sellers, A., McGuffie, K. & Zhang, H. 2002. Stable isotopes as validation tools for global climate model predictions of the impact of Amazonian deforestation. *Journal of Climate,* 15**,** 2664-2677.

HidroWeb [Online]. Agência Nacional de Águas. Available: http://hidroweb.ana.gov.br [Accessed 2017].
Hilker, T., Lyapustin, A. I., Tucker, C. J., Hall, F. G., Myneni, R. B., Wang, Y., Bi, J., Mendes De Moura, Y. & Sellers, P. J. 2014. Vegetation dynamics and rainfall sensitivity of the Amazon. *Proceedings of the National Academy of Sciences,* 111**,** 16041-16046.
Hill, S., Waterhouse, J., Field, E., Switsur, V. & Ap Rees, T. 1995. Rapid recycling of triose phosphates in oak stem tissue. *Plant, Cell and Environment,* 18**,** 931-936.
Hoffmann, G. 2003. Coherent isotope history of Andean ice cores over the last century. *Geophysical Research Letters,* 30**,** 1-4.
Huntingford, C., Fisher, R. A., Mercado, L., Booth, B. B. B., Sitch, S., Harris, P. P., Cox, P. M., Jones, C. D., Betts, R. A., Malhi, Y., Harris, G. R., Collins, M. & Moorcroft, P. 2008. Towards quantifying uncertainty in predictions of Amazon 'dieback'. *Philosophical Transactions of the Royal Society B: Biological Sciences,* 363**,** 1857-1864.
Hurley, J., Vuille, M. & Hardy, D. 2016. Forward modeling of $\delta^{18}O$ in Andean ice cores. *Geophysical Research Letters,* 43**,** 8178-8188.
International Tree Ring Data Bank (ITRDB) [Online]. Available: http://www.ncdc.noaa.gov/data-access/paleoclimatology-data/datasets/tree-ring [Accessed 1 March 2015].
Jasechko, S., Sharp, Z. D., Gibson, J., Birks, S. J., Yi, Y. & Fawcett, P. J. 2013. Terrestrial water fluxes dominated by transpiration. *Nature,* 496**,** 347-350.
Jiménez-Muñoz, J. C., Mattar, C., Barichivich, J., Santamaría-Artigas, A., Takahashi, K., Malhi, Y., Sobrino, J. A. & Schrier, G. V. D. 2016. Record-breaking warming and extreme drought in the Amazon rainforest during the course of El Niño 2015–2016. *Scientific Reports,* 6**,** 33130.
Kahmen, A., Sachse, D., Arndt, S. K., Tu, K. P., Farrington, H., Vitousek, P. M. & Dawson, T. E. 2011. Cellulose $\delta^{18}O$ is an index of leaf-to-air vapor pressure difference (VPD) in tropical plants. *Proceedings of the National Academy of Sciences,* 108**,** 1981-1986.
Kanner, L. C., Burns, S. J., Cheng, H., Edwards, R. L. & Vuille, M. 2013. High-resolution variability of the South American summer monsoon over the last seven millennia: insights from a speleothem record from the central Peruvian Andes. *Quaternary Science Reviews,* 75**,** 1-10.
Kanner, L. C., Buenning, N. H., Stott, L. D., Timmermann, A. & Noone, D. 2014. The role of soil processes in $\delta^{18}O$ terrestrial climate proxies. *Global Biogeochemical Cycles,* 28**,** 239-252.
Keenan, T. F., Hollinger, D. Y., Bohrer, G., Dragoni, D., Munger, J. W., Schmid, H. P. & Richardson, A. D. 2013. Increase in forest water-use efficiency as atmospheric carbon dioxide concentrations rise. *Nature,* 499**,** 324-327.
Kilroy, E., McCarroll, D., Young, G. H., Loader, N. J. & Bale, R. J. 2016. Absence of juvenile effects confirmed in stable carbon and oxygen isotopes of European larch trees. *Acta Silvae et Ligni***,** 27-33.
Kitoh, A., Endo, H., Krishna Kumar, K., Cavalcanti, I. F. A., Goswami, P. & Zhou, T. 2013. Monsoons in a changing world: A regional perspective in a global context. *Journal of Geophysical Research: Atmospheres,* 118**,** 3053-3065.
Kousky, V. E., Kagano, M. T. & Cavalcanti, I. F. A. 1984. A review of the Southern Oscillation: oceanic-atmospheric circulation changes and related rainfall anomalies. *Tellus A,* 36A**,** 490-504.
Labuhn, I., Daux, V., Pierre, M., Stievenard, M., Girardclos, O., Feron, A., Genty, D., Masson-Delmotte, V. & Mestre, O. 2014. Tree age, site and climate controls on tree ring cellulose delta O-18: A case study on oak trees from south-western France. *Dendrochronologia,* 32**,** 78-89.
Lammertsma, E. I., De Boer, H. J., Dekker, S. C., Dilcher, D. L., Lotter, A. F. & Wagner-Cremer, F. 2011. Global CO_2 rise leads to reduced maximum stomatal conductance in Florida vegetation. *Proceedings of the National Academy of Sciences,* 108**,** 4035-4040.
Lathuillière, M. J., Johnson, M. S. & Donner, S. D. 2012. Water use by terrestrial ecosystems: temporal variability in rainforest and agricultural contributions to evapotranspiration in Mato Grosso, Brazil. *Environmental Research Letters,* 7**,** 1-12.
Legrande, A. N. & Schmidt, G. A. 2006. Global gridded data set of the oxygen isotopic composition in seawater. *Geophysical Research Letters,* 33**,** 1-5.
Lenton, T. M., Held, H., Kriegler, E., Hall, J. W., Lucht, W., Rahmstorf, S. & Schellnhuber, H. J. 2008. Tipping elements in the Earth's climate system. *Proceedings of the National Academy of Sciences,* 105**,** 1786-1793.
Lewis, S. L., Brando, P. M., Phillips, O. L., Van Der Heijden, G. M. & Nepstad, D. 2011. The 2010 amazon drought. *Science,* 331**,** 554-554.
Liu, X., Xu, G., Grießinger, J., An, W., Wang, W., Zeng, X., Wu, G. & Qin, D. 2014. A shift in cloud cover over the southeastern Tibetan Plateau since 1600: evidence from regional tree-ring $\delta^{18}O$

and its linkages to tropical oceans. *Quaternary Science Reviews,* 88**,** 55-68.
Loader, N. J., Young, G. H. F., McCarroll, D. & Wilson, R. J. S. 2013. Quantifying uncertainty in isotope dendroclimatology. *The Holocene,* 23**,** 1221-1226.
Majoube, M. 1971. Fractionnement en oxygène-18 et en deutérium entre l'eau et sa vapeur. *Journal de Chimie Physique et de Physico-Chimie Biologique,* 58**,** 1423-1435.
Malhi, Y., Aragão, L. E., Galbraith, D., Huntingford, C., Fisher, R., Zelazowski, P., Sitch, S., McSweeney, C. & Meir, P. 2009. Exploring the likelihood and mechanism of a climate-change-induced dieback of the Amazon rainforest. *Proceedings of the National Academy of Sciences,* 106**,** 20610-20615.
Marengo, J. A. 1992. Interannual variability of surface climate in the Amazon basin. *International Journal of Climatology,* 12**,** 853-863.
Marengo, J. A., Nobre, C. A., Tomasella, J., Oyama, M. D., Sampaio De Oliveira, G., De Oliveira, R., Camargo, H., Alves, L. M. & Brown, I. F. 2008. The drought of Amazonia in 2005. *Journal of Climate,* 21**,** 495-516.
Marengo, J. A., Tomasella, J., Alves, L. M., Soares, W. R. & Rodriguez, D. A. 2011. The drought of 2010 in the context of historical droughts in the Amazon region. *Geophysical Research Letters,* 38**,** 1-5.
Marengo, J. A. & Espinoza, J. C. 2016. Extreme seasonal droughts and floods in Amazonia: causes, trends and impacts. *International Journal of Climatology,* 36**,** 1033-1050.
Martinelli, L. A., Victoria, R. L., Silveira Lobo Sternberg, L., Ribeiro, A. & Zacharias Moreira, M. 1996. Using stable isotopes to determine sources of evaporated water to the atmosphere in the Amazon basin. *Journal of Hydrology,* 183**,** 191-204.
Maslin, M. A. & Burns, S. J. 2000. Reconstruction of the Amazon Basin effective moisture availability over the past 14,000 years. *Science,* 290**,** 2285-2287.
McCarroll, D. & Loader, N. J. 2004. Stable isotopes in tree rings. *Quaternary Science Reviews,* 23**,** 771-801.
McDowell, N. G., Bond, B. J., Dickman, L. T., Ryan, M. G. & Whitehead, D. 2011. Relationships between tree height and carbon isotope discrimination. *Size-and age-related changes in tree structure and function.* Springer Science & Business Media.
Meinzer, F. C., Lachenbruch, B. & Dawson, T. E. 2011. *Size-and age-related changes in tree structure and function*, Springer Science & Business Media.
Mook, W. G. 2000. *Environmental isotopes in the hydrological cycle: Volume I Introduction (Theory, Methods, Review)*, International Atomic Energy Agency and United Nations Educational, Scientific and Cultural Organization.
Moquet, J., Cruz, F., Novello, V., Stríkis, N., Deininger, M., Karmann, I., Santos, R. V., Millo, C., Apaestegui, J., Guyot, J.-L., Siffedine, A., Vuille, M., Cheng, H., Edwards, R. & Santini, W. 2016. Calibration of speleothem $\delta^{18}O$ records against hydroclimate instrumental records in Central Brazil. *Global and Planetary Change,* 139**,** 151-164.
Nepstad, D. C., Stickler, C. M., Filho, B. S.-. & Merry, F. 2008. Interactions among Amazon land use, forests and climate: prospects for a near-term forest tipping point. *Philosophical Transactions of the Royal Society B: Biological Sciences,* 363**,** 1737-1746.
Novello, V. F., Vuille, M., Cruz, F. W., Stríkis, N. M., De Paula, M. S., Edwards, R. L., Cheng, H., Karmann, I., Jaqueto, P. F., Trindade, R. I. F., Hartmann, G. A. & Moquet, J. S. 2016. Centennial-scale solar forcing of the South American Monsoon System recorded in stalagmites. *Scientific Reports,* 6**,** 1-8.
Ohashi, S., Durgante, F. M., Kagawa, A., Kajimoto, T., Trumbore, S. E., Xu, X., Ishizuka, M. & Higuchi, N. 2016. Seasonal variations in the stable oxygen isotope ratio of wood cellulose reveal annual rings of trees in a Central Amazon terra firme forest. *Oecologia,* 180**,** 685-696.
Pan, Y., Birdsey, R. A., Fang, J., Houghton, R., Kauppi, P. E., Kurz, W. A., Phillips, O. L., Shvidenko, A., Lewis, S. L. & Canadell, J. G. 2011. A large and persistent carbon sink in the world's forests. *Science,* 333**,** 988-993.
Pearson, S., Hua, Q., Allen, K. & Bowman, D. M. 2011. Validating putatively cross-dated *Callitris* tree-ring chronologies using bomb-pulse radiocarbon analysis. *Australian Journal of Botany,* 59**,** 7-17.
Pfahl, S. & Sodemann, H. 2014. What controls deuterium excess in global precipitation? *Climate of the Past,* 10**,** 771–781.
Phillips, O. L., Aragão, L. E., Lewis, S. L., Fisher, J. B., Lloyd, J., López-González, G., Malhi, Y., Monteagudo, A., Peacock, J. & Quesada, C. A. 2009. Drought sensitivity of the Amazon

rainforest. *Science,* 323**,** 1344-1347.
Pierrehumbert, R. T. 1999. Huascaran $\delta^{18}O$ as an indicator of tropical climate during the Last Glacial Maximum. *Geophysical Research Letters,* 26**,** 1345-1348.
Reuter, J., Stott, L., Khider, D., Sinha, A., Cheng, H. & Edwards, R. L. 2009. A new perspective on the hydroclimate variability in northern South America during the Little Ice Age. *Geophysical Research Letters,* 36**,** 1-5.
Richey, J. E., Nobre, C. & Deser, C. 1989. Amazon river discharge and climate variability: 1903 to 1985. *Science,* 246**,** 101-103.
Risi, C., Bony, S. & Vimeux, F. 2008. Influence of convective processes on the isotopic composition ($\delta^{18}O$ and δD) of precipitation and water vapor in the tropics: 2. Physical interpretation of the amount effect. *Journal of Geophysical Research: Atmospheres,* 113**,** 1-12.
Roden, J. S., Lin, G. & Ehleringer, J. R. 2000. A mechanistic model for interpretation of hydrogen and oxygen isotope ratios in tree-ring cellulose. *Geochimica et Cosmochimica Acta,* 64**,** 21-35.
Ronchail, J., Cochonneau, G., Molinier, M., Guyot, J.-L., De Miranda Chaves, A. G., Guimarães, V. & De Oliveira, E. 2002. Interannual rainfall variability in the Amazon basin and sea-surface temperatures in the equatorial Pacific and the tropical Atlantic Oceans. *International Journal of Climatology,* 22**,** 1663-1686.
Rosenblüth, B., Fuenzalida, H. A. & Aceituno, P. 1997. Recent Temperature Variations in Southern South America. *International Journal of Climatology,* 17**,** 67-85.
Rozanski, K., Araguás-Araguás, L. & Gonfiantini, R. 1993. Isotopic patterns in modern global precipitation. *Climate change in continental isotopic records***,** 1-36.
Salati, E., Dall'olio, A., Matsui, E. & Gat, J. R. 1979. Recycling of water in the Amazon basin: an isotopic study. *Water Resources Research,* 15**,** 1250-1258.
Samuels-Crow, K. E., Galewsky, J., Hardy, D. R., Sharp, Z. D., Worden, J. & Braun, C. 2014. Upwind convective influences on the isotopic composition of atmospheric water vapor over the tropical Andes. *Journal of Geophysical Research: Atmospheres,* 119**,** 7051-7063.
Sano, M., Xu, C. & Nakatsuka, T. 2012. A 300-year Vietnam hydroclimate and ENSO variability record reconstructed from tree ring $\delta^{18}O$. *Journal of Geophysical Research: Atmospheres,* 117**,** 1-11.
Sano, M., Tshering, P., Komori, J., Fujita, K., Xu, C. & Nakatsuka, T. 2013. May–September precipitation in the Bhutan Himalaya since 1743 as reconstructed from tree ring cellulose $\delta^{18}O$. *Journal of Geophysical Research: Atmospheres,* 118**,** 8399-8410.
Silva Dias, M. a. F., Rutledge, S., Kabat, P., Silva Dias, P. L., Nobre, C., Fisch, G., Dolman, A. J., Zipser, E., Garstang, M., Manzi, A. O., Fuentes, J. D., Rocha, H. R., Marengo, J., Plana-Fattori, A., Sá, L. D. A., Alvalá, R. C. S., Andreae, M. O., Artaxo, P., Gielow, R. & Gatti, L. 2002. Cloud and rain processes in a biosphere-atmosphere interaction context in the Amazon Region. *Journal of Geophysical Research: Atmospheres,* 107**,** 1-18.
Skrzypek, G., Engel, Z., Chuman, T. & Šefrna, L. 2011. *Distichia* peat — A new stable isotope paleoclimate proxy for the Andes. *Earth and Planetary Science Letters,* 307**,** 298-308.
Song, X., Farquhar, G. D., Gessler, A. & Barbour, M. M. 2014. Turnover time of the non-structural carbohydrate pool influences $\delta^{18}O$ of leaf cellulose. *Plant, Cell and Environment,* 37**,** 2500-2507.
Speer, J. H. 2010. *Fundamentals of tree-ring research*, The University of Arizona Press.
Spracklen, D. V., Arnold, S. R. & Taylor, C. M. 2012. Observations of increased tropical rainfall preceded by air passage over forests. *Nature,* 489**,** 282-285.
Spracklen, D. V. & Garcia-Carreras, L. 2015. The impact of Amazonian deforestation on Amazon basin rainfall. *Geophysical Research Letters,* 42**,** 9546-9552.
Sternberg, L. D. S. L. & Deniro, M. J. 1983. Biogeochemical implications of the isotopic equilibrium fractionation factor between the oxygen atoms of acetone and water. *Geochimica et Cosmochimica Acta,* 47**,** 2271-2274.
Sternberg, L. D. S. L. 2009. Oxygen stable isotope ratios of tree-ring cellulose: the next phase of understanding. *New Phytologist,* 181**,** 553-562.
Stocker, T., Qin, D. & Platner, G. 2013. Climate Change 2013: The Physical Science Basis. *Working Group I Contribution to the Fifth Assessment Report of the Intergovernmental Panel on Climate Change. Summary for Policymakers (IPCC, 2013)*.
Stohl, A. & James, P. 2005. A Lagrangian Analysis of the Atmospheric Branch of the Global Water Cycle. Part II: Moisture Transports between Earth's Ocean Basins and River Catchments. *Journal of Hydrometeorology,* 6**,** 961-984.
Stokes, M. & Smiley, T. 1968. *An introduction to tree-ring dating*, University of Arizona Press.

Strikis, N. M., Cruz, F. W., Cheng, H., Karmann, I., Edwards, R. L., Vuille, M., Wang, X., De Paula, M. S., Novello, V. F. & Auler, A. S. 2011. Abrupt variations in South American monsoon rainfall during the Holocene based on a speleothem record from central-eastern Brazil. *Geology,* 39**,** 1075-1078.

Sturm, C., Hoffmann, G. & Langmann, B. 2007. Simulation of the stable water isotopes in precipitation over South America: Comparing regional to global circulation models. *Journal of Climate,* 20**,** 3730-3750.

Ter Steege, H., Pitman, N. C. A., Sabatier, D., Baraloto, C., Salomão, R. P., Guevara, J. E., Phillips, O. L., Castilho, C. V., Magnusson, W. E., Molino, J.-F., Monteagudo, A., Núñez Vargas, P., Montero, J. C., Feldpausch, T. R., Coronado, E. N. H., Killeen, T. J., Mostacedo, B., Vasquez, R., Assis, R. L., Terborgh, J., Wittmann, F., Andrade, A., Laurance, W. F., Laurance, S. G. W., Marimon, B. S., Marimon, B.-H., Guimarães Vieira, I. C., Amaral, I. L., Brienen, R., Castellanos, H., Cárdenas López, D., Duivenvoorden, J. F., Mogollón, H. F., Matos, F. D. D. A., Dávila, N., García-Villacorta, R., Stevenson Diaz, P. R., Costa, F., Emilio, T., Levis, C., Schietti, J., Souza, P., Alonso, A., Dallmeier, F., Montoya, A. J. D., Fernandez Piedade, M. T., Araujo-Murakami, A., Arroyo, L., Gribel, R., Fine, P. V. A., Peres, C. A., Toledo, M., Aymard C., G. A., Baker, T. R., Cerón, C., Engel, J., Henkel, T. W., Maas, P., Petronelli, P., Stropp, J., Zartman, C. E., Daly, D., Neill, D., Silveira, M., Paredes, M. R., Chave, J., Lima Filho, D. D. A., Jørgensen, P. M., Fuentes, A., Schöngart, J., Cornejo Valverde, F., Di Fiore, A., Jimenez, E. M., Peñuela Mora, M. C., Phillips, J. F., Rivas, G., Van Andel, T. R., Von Hildebrand, P., Hoffman, B., Zent, E. L., Malhi, Y., Prieto, A., Rudas, A., Ruschell, A. R., Silva, N., Vos, V., Zent, S., Oliveira, A. A., Schutz, A. C., Gonzales, T., Trindade Nascimento, M., Ramirez-Angulo, H., Sierra, R., Tirado, M., Umaña Medina, M. N., Van Der Heijden, G., Vela, C. I. A., Vilanova Torre, E., Vriesendorp, C., Wang, O., et al. 2013. Hyperdominance in the Amazonian Tree Flora. *Science,* 342.

Thompson, L. G., Mosley-Thompson, E. & Davis, M. E. 1995. Late glacial stage and Holocene tropical ice core records from Huascaran, Peru. *Science,* 269**,** 46-50.

Thompson, L. G., Davis, M. E., Mosley-Thompson, E., Sowers, T. A., Henderson, K. A., Zagorodnov, V. S., Lin, P.-N., Mikhalenko, V. N., Campen, R. K., Bolzan, J. F., Cole-Dai, J. & Francou, B. 1998. A 25,000-Year Tropical Climate History from Bolivian Ice Cores. *Science,* 282**,** 1858-1864.

Thompson, L. G., Mosley-Thompson, E. & Henderson, K. A. 2000. Ice-core palaeoclimate records in tropical South America since the Last Glacial Maximum. *Journal of Quaternary Science,* 15**,** 377-394.

Thompson, L. G., Mosley-Thompson, E., Brecher, H., Davis, M., León, B., Les, D., Lin, P.-N., Mashiotta, T. & Mountain, K. 2006. Abrupt tropical climate change: Past and present. *Proceedings of the National Academy of Sciences,* 103**,** 10536-10543.

Thompson, L. G., Mosley-Thompson, E., Davis, M. E., Zagorodnov, V. S., Howat, I. M., Mikhalenko, V. N. & Lin, P. N. 2013. Annually resolved ice core records of tropical climate variability over the past ~1800 years. *Science,* 340**,** 945-950.

Treydte, K., Boda, S., Graf Pannatier, E., Fonti, P., Frank, D., Ullrich, B., Saurer, M., Siegwolf, R., Battipaglia, G. & Werner, W. 2014. Seasonal transfer of oxygen isotopes from precipitation and soil to the tree ring: source water versus needle water enrichment. *New Phytologist,* 202**,** 772-783.

Treydte, K. S., Schleser, G. H., Helle, G., Frank, D. C., Winiger, M., Haug, G. H. & Esper, J. 2006. The twentieth century was the wettest period in northern Pakistan over the past millennium. *Nature,* 440**,** 1179-1182.

Van Breukelen, M. R., Vonhof, H. B., Hellstrom, J. C., Wester, W. C. G. & Kroon, D. 2008. Fossil dripwater in stalagmites reveals Holocene temperature and rainfall variation in Amazonia. *Earth and Planetary Science Letters,* 275**,** 54-60.

Van Der Ent, R. J., Savenije, H. H., Schaefli, B. & Steele-Dunne, S. C. 2010. Origin and fate of atmospheric moisture over continents. *Water Resources Research,* 46**,** 1-12.

Van Der Ent, R. J. & Savenije, H. H. G. 2011. Length and time scales of atmospheric moisture recycling. *Atmospheric Chemistry and Physics,* 11**,** 1853-1863.

Victoria, R. L., Martinelli, L. A., Jefferson, M. & Jeffrey, R. 1991. Mechanisms of Water Recycling in the Amazon Basin: Isotopic Insights. *Ambio,* 20**,** 384-387.

Villacís, M., Vimeux, F. & Taupin, J. D. 2008. Analysis of the climate controls on the isotopic composition of precipitation ($\delta^{18}O$) at Nuevo Rocafuerte, 74.5 W, 0.9 S, 250 m, Ecuador.

Comptes Rendus Geoscience, 340**,** 1-9.
Villalba, R., Lara, A., Boninsegna, J. A., Masiokas, M., Delgado, S., Aravena, J. C., Roig, F. A., Schmelter, A., Wolodarsky, A. & Ripalta, A. 2003. Large-scale temperature changes across the southern Andes: 20th-century variations in the context of the past 400 years. *Climate Variability and Change in High Elevation Regions: Past, Present & Future.* Springer.
Vimeux, F., Gallaire, R., Bony, S., Hoffmann, G. & Chiang, J. C. 2005. What are the climate controls on δD in precipitation in the Zongo Valley (Bolivia)? Implications for the Illimani ice core interpretation. *Earth and Planetary Science Letters,* 240**,** 205-220.
Vimeux, F., Ginot, P., Schwikowski, M., Vuille, M., Hoffmann, G., Thompson, L. G. & Schotterer, U. 2009. Climate variability during the last 1000 years inferred from Andean ice cores: A review of methodology and recent results. *Palaeogeography, Palaeoclimatology, Palaeoecology,* 281**,** 229-241.
Voelker, S. L. & Meinzer, F. C. 2017. Where and when does stem cellulose $\delta^{18}O$ reflect a leaf water enrichment signal? *Tree Physiology,* 00**,** 1-3.
Volland, F., Pucha, D. & Braeuning, A. 2016. Hydro-climatic variability in southern Ecuador reflected by tree-ring oxygen isotopes. *Erdkunde,* 70**,** 69-82.
Vuille, M., Bradley, R. S., Werner, M., Healy, R. & Keimig, F. 2003. Modeling $\delta^{18}O$ in precipitation over the tropical Americas: 1. Interannual variability and climatic controls. *Journal of Geophysical Research: Atmospheres,* 108**,** 1-24.
Vuille, M., Burns, S., Taylor, B., Cruz, F., Bird, B., Abbott, M., Kanner, L., Cheng, H. & Novello, V. 2012. A review of the South American monsoon history as recorded in stable isotopic proxies over the past two millennia. *Climate of the Past,* 8**,** 1309-1321.
Welp, L. R., Lee, X., Kim, K., Griffis, T. J., Billmark, K. A. & Baker, J. M. 2008. $\delta^{18}O$ of water vapour, evapotranspiration and the sites of leaf water evaporation in a soybean canopy. *Plant, Cell & Environment,* 31**,** 1214-1228.
White, J. W., Cook, E. R., Lawrence, J. R. & Wallace S, B. 1985. The DH ratios of sap in trees: Implications for water sources and tree ring DH ratios. *Geochimica et Cosmochimica Acta,* 49**,** 237-246.
Whitmore, T. 1998. *An Introduction To Tropical Rain Forests*, Clarendon Press.
Wittmann, F., Junk, W. J. & Piedade, M. T. F. 2004. The várzea forests in Amazonia: flooding and the highly dynamic geomorphology interact with natural forest succession. *Forest Ecology and Management,* 196**,** 199-212.
Wolfe, B. B., Aravena, R., Abbott, M. B., Seltzer, G. O. & Gibson, J. J. 2001. Reconstruction of paleohydrology and paleohumidity from oxygen isotope records in the Bolivian Andes. *Palaeogeography, Palaeoclimatology, Palaeoecology,* 176**,** 177-192.
Worbes, M. & Junk, W. J. 1989. Dating tropical trees by means of ^{14}C from bomb tests. *Ecology,* 70**,** 503-507.
Worbes, M. 1995. How to measure growth dynamics in tropical trees a review. *IAWA Journal,* 16**,** 337-351.
Worbes, M. 1999. Annual growth rings, rainfall-dependent growth and long-term growth patterns of tropical trees from the Caparo Forest Reserve in Venezuela. *Journal of Ecology,* 87**,** 391-403.
Worbes, M. & Junk, W. J. 1999. How old are tropical trees? The persistence of a myth. *IAWA Journal,* 20**,** 255-260.
Xu, C. X., Ge, J. Y., Nakatsuka, T., Yi, L., Zheng, H. Z. & Sano, M. 2016. Potential utility of tree ring delta O-18 series for reconstructing precipitation records from the lower reaches of the Yangtze River, southeast China. *Journal of Geophysical Research: Atmospheres,* 121**,** 3954-3968.
Yakir, D. & Deniro, M. J. 1990. Oxygen and hydrogen isotope fractionation during cellulose metabolism in *Lemna gibba* L. *Plant Physiology,* 93**,** 325-332.
Yakir, D. & Wang, X.-F. 1996. Fluxes of CO_2 and water between terrestrial vegetation and the atmosphere estimated from isotope measurements. *Nature*, 380, 515.
Yoon, J.-H. & Zeng, N. 2010. An Atlantic influence on Amazon rainfall. *Climate Dynamics,* 34**,** 249-264.
Young, G. H. F., Demmler, J. C., Gunnarson, B. E., Kirchhefer, A. J., Loader, N. J. & McCarroll, D. 2011. Age trends in tree ring growth and isotopic archives: A case study of *Pinus sylvestris* L. from northwestern Norway. *Global Biogeochemical Cycles,* 25**,** 1-6.
Zemp, D. C., Schleussner, C.-F., Barbosa, H. M. J., Hirota, M., Montade, V., Sampaio, G., Staal, A., Wang-Erlandsson, L. & Rammig, A. 2017. Self-amplified Amazon forest loss due to vegetation-atmosphere feedbacks. *Nature Communications,* 8**,** 1-10.
Zeng, N., Yoon, J.-H., Marengo, J. A., Subramaniam, A., Nobre, C. A., Mariotti, A. & Neelin, J. D. 2008.

Causes and impacts of the 2005 Amazon drought. *Environmental Research Letters,* 3**,** 1-9.

Chapter 2: Materials and Methods

2.1 *Cedrela* Growth and Cambial Dynamics

Cedrela odorata, the main tropical tree species analysed in this thesis, is an obligate deciduous species that has been observed to shed its leaves once per year throughout most of its natural range, which extends from Mexico to Argentina (Pennington et al., 1981). Leaf shedding coincides with the start of the annual dry season, which is followed by a period of cambial dormancy that may persist for several months (Dünisch et al., 2002). Ring structure in *Cedrela* is described as ring-porous or semi-ring-porous as large vessels form during the reactivation of the cambium when the tree flushes its leaves at the start of the new growing season (Dünisch et al., 2002). As growth begins, an abundance of wide vessels is embedded in a band of paratracheal parenchyma, while the wood which forms later in the growing season contains fewer, narrower vessels (Dünisch et al., 2002; Vetter and Botosso, 1989). The parenchyma bands, which mark the end of cambial dormancy, clearly delineate one tree ring from the next, and thus make *C. odorata* a suitable tree species for tropical dendrochronology (Worbes, 1999, Brienen and Zuidema, 2005).

2.2 Sampling Strategy

Whole stem discs and increment cores were collected from sites across the Amazon basin for analysis in this thesis. Samples were collected from sites in Suriname, Brazil and Venezuela, as well as Bolivia and Ecuador to represent different points along the moisture transport pathway, from the Atlantic coast through to the interior and far west of the basin (Fig. 2.1). Most of the samples come from lowland tropical rainforest sites (0–200 m above sea level (a.s.l.)), though samples were also collected from a montane rainforest in Ecuador (2950 m a.s.l.) and from the Bolivian Altiplano (4400–4500 m a.s.l.). Discs were collected from trees that had already been felled for timber or during the installation of overhead power lines. Cores were taken using an increment borer, with trees sampled in 2–4 directions around the circumference of the trunk, at a height of approximately 130 cm from the ground.

Figure 2.1 – Network of tree-ring sampling sites across South America. The Amazon basin is indicated by a thick black line. The black arrow on the inset map indicates the mean wet season wind flow over the Amazon region.

Several tropical tree species were sampled across the different sites. *Cedrela odorata* was sampled in all of the lowland sites, *Cedrela montana* and *Polylepis tarapacana* were sampled in the Ecuador and Bolivia highland sites respectively, while *Tachigali vasquezii, Amburana cearensis, Peltogyne heterophylla, Bertholletia excelsa, Cedrelinga catenaeformis* and *Couratari macrosperma* were sampled from lowland sites in northern Bolivia only. These Amazon tree species have all previously been shown to form annual rings in Bolivia (Argollo et al., 2004, Brienen and Zuidema, 2005), Ecuador (Bräuning et al., 2009) and Brazil (Dünisch et al., 2002), apart from *C. macrosperma*, which has not previously been studied.

2.3 Tree-Ring Analysis

2.3.1 Sample preparation

Loader et al. (2013) suggest a minimum of 10 trees should be used to construct reliable isotope chronologies for use in palaeoclimate reconstructions, particularly when

analysing low-frequency variation in climate. However, for sites that had not previously been analysed for $\delta^{18}O$, trial runs of approximately 30 rings from 3 different trees were conducted. For the species inter-comparison, a single individual was analysed from each species (e.g. Ballantyne et al., 2011) to maximise the number of species investigated. This pilot data was used to determine whether further analyses should be conducted. To prepare a good surface for ring analysis discs were polished with a mechanical sander using sandpaper up to 600 grit. Using a stereomicroscope to improve visibility, rings were marked along 2–4 radii for each disc, interconnecting every 10^{th} ring between radii to ensure dating accuracy. Cores were prepared using a core-microtome (Gärtner and Nievergelt, 2010) and rings marked along 2–4 radii from each tree. Rings were measured using a LINTAB measuring stage to the nearest 0.01 mm and visually crossdated (e.g. Stokes and Smiley, 1968) using the tree-ring analysis software TSAP-Win. Radii with the widest and clearest rings were selected for isotope analysis. These samples were scanned to preserve a copy of the ring markings for future reference. A bandsaw was used to cut up the discs and cores, separating a layer of wood 1 mm deep. Extraction of α-cellulose then followed one of two possible methodologies:

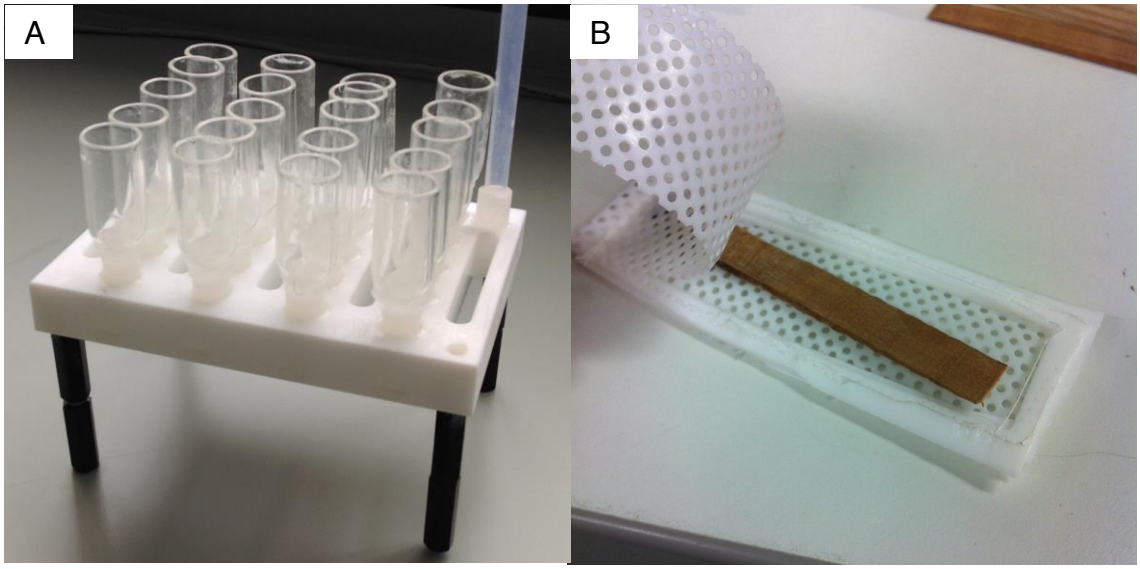

Figure 2.2 – Photos showing the apparatus for two different cellulose extraction techniques. (a) The filter funnels and drainage module used for the batch extraction method from Wieloch et al. (2011), and **(b)** sample lath and perforated PTFE case used for the cross-section extraction method from Kagawa et al. (2015).

1. Rings along the 1 mm wood section were cut up into small pieces using a scalpel, making sure to take an equal amount of wood along the entire width of the ring so that the sample would not be not biased towards a particular period of growth. The extraction of α-cellulose then followed the batch method of Wieloch et al. (2011). First, the wood from each ring was transferred to a glass filter funnel, fitted with fine glass micromesh. Funnels were then inserted into a polytetrafluoroethylene (PTFE) 'drainage module' (see Fig. 2.2a), to enable the fluids to be easily exchanged during the extraction process, and placed into a water bath set to 60 °C. Samples were treated with 5% sodium hydroxide (NaOH) solution to remove resins, fatty acids and tannins from the wood. After 2 hours, the chemicals were drained using a vacuum pump and the step was repeated with fresh NaOH solution. Samples were then washed with boiling water to neutralise the pH, before being treated with acidified 7.5% sodium chlorite ($NaClO_2$) solution. The $NaClO_2$ solution was refreshed four times (approximately every 10 hours), and the expended solution pumped out each time. Once cellulose extraction was complete, the samples were white in appearance. Samples were washed again with boiling water until pH neutral, and then the material from each ring was rinsed with deionised water from the funnel into an Eppendorf labelled with the tree number and ring year. Next, samples were homogenised in a Retsch MM 301 mixer mill before being frozen and desiccated in the freeze-dryer. Finally, dried cellulose samples were weighed and packed into silver cups ready for $\delta^{18}O$ analysis.

2. In the second methodology, cellulose extraction preceded the isolation of material from each ring (e.g. Loader et al., 2002, Li et al., 2011, Kagawa et al., 2015). First, the 1 mm wood cross-sections (laths) were enclosed in cases made from perforated PTFE, ensuring that there was sufficient space around the wood for chemicals to circulate (see Fig. 2.2b). The encased laths were then placed into a PTFE container in a water bath set at 60 °C. Chemicals were added to the PTFE container, following the same steps described above, and ensuring that the encased wood laths were fully submerged. After the final washing step the samples were freeze-dried while still inside the PTFE cases. The fragile cellulose laths were then carefully removed from their cases and inspected with a stereomicroscope capable of transmitting light, as this helped to visualise the ring boundaries. Material from each ring was then separated using a scalpel and transferred to a labelled Eppendorf with 1–2 mL of deionised water.

Samples were then homogenised, freeze-dried (for a second time) and weighed into silver cups ready for $\delta^{18}O$ analysis, as detailed above.

The cross-section extraction method (2) was found to be much faster than the batch extraction method (1). The main time cost came from preparing the PTFE cases, but these could be re-used in later extractions. The time-consuming step of cutting up each ring into small slivers was no longer necessary, and the chemical solutions were added to a single container, rather than individual funnels. Thus, in one week it was possible to extract cellulose from 1074 tree rings, which is approximately four times more than could be processed in a week using the batch extraction method. This accelerated throughput of samples thus permitted higher replication. However, ring boundaries in the cellulose laths were slightly less distinct than in the polished surface of whole wood, and it was sometimes challenging to distinguish between, and isolate material from, very narrow rings. The cross-section extraction method is therefore suggested to be most appropriate for samples with wide and clear rings.

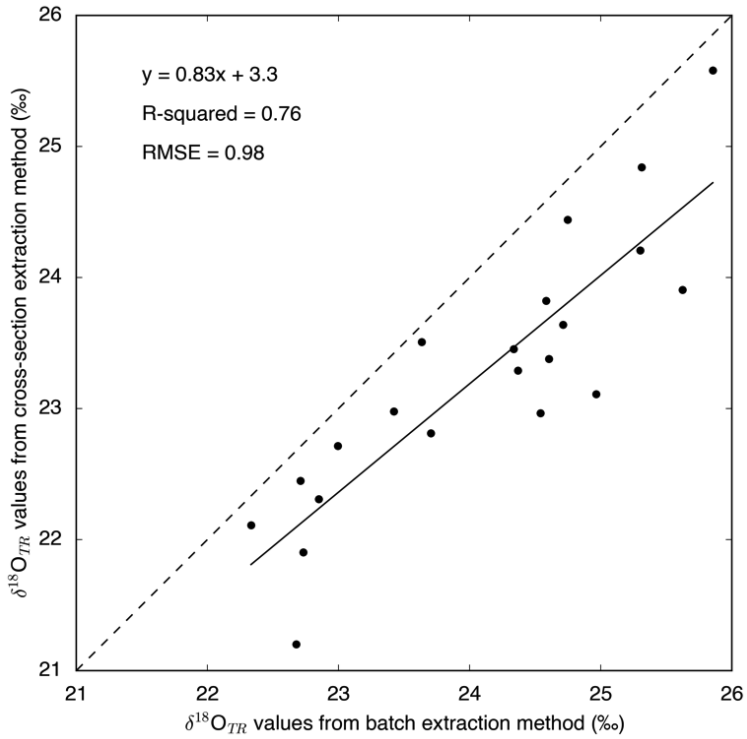

Figure 2.3 – Cellulose extraction method comparison. $\delta^{18}O_{TR}$ values obtained using two different methods for cellulose extraction are compared. The dashed black line shows the expected 1:1 relationship and the solid black line shows the ordinary least squares regression relationship, the equation for which is given in the top left corner of the plot, along with the R-squared and root mean square error (RMSE).

A brief method comparison was conducted with a series of 21 rings from a tree from Cuyuja, Ecuador (see Fig. 2.3 and Appendix 2.1). $\delta^{18}O_{TR}$ values from the two methods correlate reasonably well (R^2=0.76) and the slope and intercept of the regression do not differ significantly from 1 and 0 respectively (slope=0.83±0.22, intercept=3.33±5.33, 95% confidence intervals). However, the cross-section method gave consistently lower $\delta^{18}O_{TR}$ values, (mean offset = 0.8 ‰, root mean square error (RMSE)=0.98 ‰, n=21). It should be emphasised that the only difference between the two methods is whether the tree rings were separated before or after chemical treatment. Therefore, the offset must be caused by the reduced ability of the chemicals to permeate the wood in the cross-section method, possibly resulting in incomplete extraction (though all of the samples had a white appearance). Kagawa et al. (2015) found a stronger relationship and a negligible offset between values derived from standard and the cross-section extraction methods (R^2=0.96, mean offset = 0.046 ‰, n=93), and an earlier study by Li et al. (2011) reported an offset of 0.2 ‰ (n=8), which was within the bounds of experimental error. Although, it must be noted that a slightly different standard extraction method was employed in both of these studies (i.e. following the Jayme and Wise method detailed by Loader et al., 1997). One potential cause for the larger offset observed in this study, is that cross-sections were cut using a bandsaw rather than the recommended diamond saw wheel, as these are costly and there was not one available. This meant that it was slightly harder to regulate section thickness. If the wood laths were slightly thicker than the recommended 1 mm then cellulose extraction may not have proceeded as effectively. Finally, although the method comparison did show a strong relationship between isotope values of cellulose extracted following the two different methods, due to the offset it was decided that either one or the other of these methods would be used for each site in the study, and cellulose $\delta^{18}O$ values from the two methods would not be combined into a single $\delta^{18}O_{TR}$ chronology.

2.3.2 Radiocarbon dating

"Bomb-peak" radiocarbon (^{14}C) dating was performed on selected samples from species and/or sites that had not previously been analysed for $\delta^{18}O$. Nuclear tests during the late 1950s caused an artificial peak in atmospheric ^{14}C, which has since declined since the implementation of the Test Ban Treaty. The atmospheric ^{14}C distribution from

1950 to the present is relatively well established (e.g. Hua et al., 2013), and thus organic material formed during this time can be dated with an accuracy of 1–2 years. Measuring the ^{14}C content of tree rings has been shown to be a useful, independent method for validating the ages of crossdated tree rings (Worbes and Junk, 1989, Pearson et al., 2011, Andreu-Hayles et al., 2015, Santos et al., 2015). In this study, ^{14}C dating was used to check the annual character of tree rings in species and locations that had not previously been studied, as this is an important prerequisite for dendrochronological research.

2.3.3 Oxygen isotope analysis

The $\delta^{18}O$ of each sample was measured using isotope-ratio mass spectrometry (IRMS). Isotope measurements were performed at the School of Earth and Environment at the University of Leeds, the NERC Isotope Geosciences Facilities at Keyworth in Nottingham, and the Department of Geography at the University of Leicester. Since the analysis protocols vary slightly between each of these institutions, a laboratory inter-comparison was conducted to check the consistency of results.

2.4 Data Processing

2.4.1 Processing isotope data

Raw $\delta^{18}O_{TR}$ measurements were compiled and checked prior to crossdating and chronology construction. First, any clearly anomalous results from the IRMS analysis (e.g. negative values) were deleted. $\delta^{18}O_{TR}$ series from a particular site were then crossdated between each other by pattern matching in the same way that ring-width data are usually crossdated (Douglass, 1941). Precise dating is essential for reliable palaeoclimate reconstructions but can sometimes be difficult in tropical trees, which may have challenging wood anatomy (Worbes, 2002). Problems include indistinct ring boundaries, false (non-annual) or discontinuous rings, and wedging rings (for examples of each see Fig. 2 in Brienen et al., 2016). The established $\delta^{18}O_{TR}$ chronology from Brienen et al. (2012) was used as a benchmark for dating. Where dating errors were identified through crossdating, or from radiocarbon analysis (2.3.2), the original samples (or high-resolution scans) were re-examined to see where mistakes had been

made during the initial ring counting. Finally, in sites where the trees showed a good match, chronologies were constructed by averaging data across the trees, with a minimum sample depth of three at any point along the chronology.

2.4.2 Data analysis

Data analysis was conducted to address the research questions listed in section 1.4.6. The analysis was separated into three distinct stages: i) assessment of chronology quality, ii) chronology inter-comparison and iii) chronology interpretation. First, assessment of chronology quality involved measuring the reliability or robustness of the record, by measuring inter-tree variability. Records with more consistent signals between trees were considered to be more reliable. Signal consistency was assessed by calculating the expressed population signal (EPS), as defined by Wigley et al. (1984). An EPS threshold of 0.85 was used to distinguish between chronologies dominated by individual tree-level or stand-level signals.

Records from different species and different sites were compared to determine the correspondence of $\delta^{18}O_{TR}$ signals. The Pearson's product-moment correlation method was primarily used to compare $\delta^{18}O_{TR}$ series at interannual timescales. In addition, low-pass Butterworth filters were applied to the records to determine, visualise and compare decadal variation in $\delta^{18}O_{TR}$. Low-pass Butterworth filters are designed to remove the high frequency signal components, and are calculated using a specified order and cut-off frequency. In this study, second order filters with a cut-off frequency of 0.2 (removing variation at five-yearly timescales), were applied, with symmetrical padding at the start and end of the time series to avoid end effects.

Finally, it was necessary to develop a thorough understanding of the climate signal contained in $\delta^{18}O_{TR}$ data, in order to correctly interpret the proxy record. To achieve this, correlation analyses between $\delta^{18}O_{TR}$ records and climate data were combined with a more process-based methodology involving back-trajectory modelling and water vapour transport analysis (see section 2.5). Together, these approaches helped to provide a clear understanding of how climate drives variation in $\delta^{18}O_{TR}$ records from the Amazon, and were used to support palaeoclimate inferences from long $\delta^{18}O_{TR}$ records.

All data analysis and visualisation was conducted using a combination of statistical software, including R version 3.2.2 (R Development Core Team, 2015), Interactive Data Language (IDL) version 8.2.3, and Python version 3.5.2 in the Scientific PYthon Development EnviRonment (Spyder) 3.1.2.

2.5 Towards a More Mechanistic Understanding of Amazon $\delta^{18}O_{TR}$ Records

Air parcel trajectory modelling and water vapour transport analysis was used to develop a more thorough understanding of how the history of an air parcel influences the isotopic composition of precipitation, and therefore the isotope signature recorded in Amazon tree rings. This section provides a brief background to trajectory modelling and explains how it has already been used to improve understanding of water vapour transport and isotope records from the Amazon (2.5.1). In addition, the specific methodologies for air-mass trajectory analysis (2.5.2), and the basin-scale water vapour transport analysis (2.5.3) applied in this thesis are described.

2.5.1 Introduction to air parcel trajectory modelling

The various methods of trajectory computation and application, and the errors associated with trajectory modelling, were summarised in a review by Stohl (1998). Trajectories are calculated using wind data, which can be observation-based or derived from models (Stohl, 1998). Back-trajectories, as the name suggests, describe the movement of air particles back in time from a defined location, and they have been widely used to monitor and predict the dispersal and long-range transport of atmospheric pollutants (e.g. Jaffe et al., 1999, Moy et al., 1994, Stohl, 1996). Back-trajectories have also been employed to monitor the transport of atmospheric moisture (Aemisegger et al., 2014, Gimeno et al., 2010, Sodemann et al., 2008, Sodemann and Stohl, 2009). For example, Sodemann et al. (2008) developed a moisture source diagnostic to locate the origin of precipitation falling over Greenland. The authors traced humidity changes in parcels of air along transport pathways as the net difference between moisture uptake (from evaporation) and moisture loss (through precipitation events). This study used a Lagrangian framework, which means that each air parcel

trajectory was estimated as a function of its position coordinates and instantaneous velocity at different points in time (Berlemont et al., 1990).

Lagrangian trajectory models have been used in several studies to quantify contributions to the water budget in the Amazon. For example, they have been used to track changes in atmospheric water vapour along back-trajectories and thus diagnose moisture source and sink regions (Stohl and James, 2005, Drumond et al., 2014). Also using back-trajectory analysis, Spracklen et al. (2012) found that the volume of precipitation produced by an air parcel was significantly related to the amount of vegetation the air parcel had encountered along the transport pathway. This study highlights the important contribution of evapotranspiration to atmospheric moisture in the Amazon, and elsewhere in the tropics. Furthermore, the authors estimate that current deforestation trends in the Amazon could reduce wet season and dry season precipitation by 12% and 21% respectively by 2050. In another recent study Bagley et al. (2014) applied forward trajectory modelling to determine spatial patterns of deforestation-induced precipitation reductions across the Amazon basin. Their results indicate that almost the whole of the central and western parts of the basin, and large areas in the south have already been affected by reductions in precipitation resulting from forest loss. Furthermore, precipitation-recycling ratios calculated using back-trajectories were 7.3% higher in the dry season in drought years relative to wet years, suggesting that deforestation may lead to increases in drought severity (Bagley et al., 2014). These studies illustrate how trajectory modelling can provide useful insights on water recycling in the Amazon.

Trajectory modelling has also been used to gain a more mechanistic understanding of the factors controlling interannual variation in precipitation isotopes (both $\delta^{18}O$ and δD) over the Amazon. This could be by simply characterising variability in the direction of transport pathways, and thus relating variation in precipitation isotopes to inferred variation in moisture origin (e.g. Vimeux et al., 2011, Insel et al., 2013, Fiorella et al., 2015), or by comparing satellite observations of water vapour isotopes between trajectory-inferred moisture origins and observations over the Amazon (Brown et al., 2008). Other studies have related isotopes in precipitation to remote sensing observations of precipitation, or outgoing longwave radiation (OLR), which is inversely related to convective activity, along water vapour transport pathways over the

Amazon (Vimeux et al., 2005, Samuels-Crow et al., 2014). Lastly, more complex representation of water vapour isotope composition along trajectories may be achieved by combining trajectories with simulated (Sturm et al., 2007) or observed (Brown et al., 2013) isotope data.

While useful, there are a few uncertainties associated with using trajectories to investigate Amazon isotope signatures. First, by definition, they primarily capture advection (i.e. transport by winds) and thus disregard (at least in their usual formulation) the full complexity of tropical atmospheric transport processes, including small-scale convective transport and atmospheric mixing (Stohl, 1998). Furthermore, Sturm et al. (2007) suggest that trajectory-based Rayleigh fractionation models may not be able to adequately describe the processes controlling isotopes in tropical rainfall, due to the large number of factors influencing the isotopic composition of precipitation. These include: the predominance of convective precipitation, evaporative input from vegetation, high moisture source variation and local topographical effects. Convective precipitation is potentially problematic because as air moves vertically, isotope exchanges occur between condensed water and vapour in the surrounding air (Dansgaard, 1964, Risi et al., 2008), processes which are unlikely to be captured in a simple Rayleigh rainout model. Furthermore, for a fixed volume of precipitation, variation in the strength of convection controls the extent to which an air parcel is depleted in heavy isotopes (i.e. local amount effects; Risi et al., 2008). In addition, variation in moisture origin may alter the initial isotope composition of vapour entering the basin, the volume of non-fractionating water fluxes from vegetation will vary through the year, and topography may influence temperature and therefore local fractionation effects. However, the simplicity of trajectories is also advantageous as they can be calculated with modest computational cost and can provide easily accessible information about air origin, which is not directly available from more complex general circulation models.

2.5.2 Back-trajectory analysis

The Reading Offline TRAJectory model (ROTRAJ), a Lagrangian atmospheric transport model, was used to calculate air-mass back-trajectories (Methven, 1997). Trajectories were calculated as follows: particles were released at a specified point in

space and time, and at each 30-minute time step gridded wind velocity data were read and interpolated to calculate the next position of the particle. Linear interpolation was used in the horizontal direction, and in time, and cubic interpolation was used in the vertical direction. In addition to particle position, other trajectory attributes, such as temperature, pressure and specific humidity, were determined using the same integration scheme. Trajectory position and attribute data were output every six hours. The back-trajectories calculated using ROTRAJ are kinematic (i.e. three-dimensional), and these have been shown to be more accurate than trajectories computed using other methods (Stohl and Seibert, 1998). However, the limitations of simple trajectory modelling must also be acknowledged (see section 2.5.1).

In this work, gridded wind and attribute data were retrieved from the European Centre for Medium-Range Weather Forecasts (ECMWF) ERA-Interim reanalysis dataset (Dee et al., 2011). The ERA-Interim dataset spans 1979–present and incorporates observations with model data. For each analysis cycle during data assimilation, information from the previous model cycle is combined with observational data to estimate the state of the climate system at a particular moment in time (Dee et al., 2011, Uppala et al., 2005). ERA-Interim data have a horizontal resolution of approximately 79 km and there are 60 vertical levels (<0.1 hPa). The hydrological cycle is thought to be better represented in ERA-Interim compared with previous ECMWF reanalyses, due to an improved atmospheric model and humidity analysis scheme (Dee et al., 2011).

Ten-day back-trajectories arriving once a day (12:00) at Selva Negra, Bolivia (10˚5'S, 66˚18'W) were computed for the period 1998–present. Trajectories were initiated approximately 2 km above the surface (800 hPa), close to the height of low-level moisture advection over the Amazon. Sensitivity analyses were conducted to test how variation in trajectory initiation height influenced the results. Following the methods of Spracklen et al. (2012) each trajectory was combined with remote sensing observations of precipitation and leaf area index (LAI), which was used as a proxy for evapotranspiration. Precipitation data were from the Tropical Rainfall Measuring Mission (TRMM; Huffman et al., 2007) and LAI data were from the Moderate Resolution Imaging Spectroradiometer (MODIS; Myneni et al., 2002). These variables were summed along each trajectory during its time over land to calculate either the total

amount of precipitation during transport over the basin (∑Precip), or exposure to vegetation (∑LAI). ∑Precip, ∑LAI and other trajectory attribute data were then related to $\delta^{18}O_{TR}$.

2.5.3 Large-scale water vapour transport analysis

Finally, following the methods of Gloor et al. (2015), a basin-scale analysis of water vapour transport was conducted, using column-integrated water vapour flux data from the ERA-Interim reanalysis dataset. The amount of water vapour entering (inflow) and leaving (outflow) the Amazon basin were calculated to investigate whether $\delta^{18}O_{TR}$ records are able to capture interannual variability in the net moisture balance of the region. Inflow is an important variable, as it controls how much water vapour there is in the atmosphere over the basin, and thus has an effect on regional precipitation. Outflow, on the other hand, is itself controlled by the amount of precipitation over the basin. The difference between the water vapour inflow and outflow should be approximately equal to Amazon precipitation and runoff. Therefore, these variables provide an independent measure of the hydrological status of the Amazon basin.

2.6 References

Aemisegger, F., Pfahl, S., Sodemann, H., Lehner, I., Seneviratne, S. I. & Wernli, H. 2014. Deuterium excess as a proxy for continental moisture recycling and plant transpiration. *Atmospheric Chemistry and Physics Discussions,* 13**,** 29721-29784.

Andreu-Hayles, L., Santos, G. M., Herrera-Ramírez, D. A., Martin-Fernández, J., Ruiz-Carrascal, D., Boza-Espinoza, T. E., Fuentes, A. F. & Jorgensen, P. M. 2015. Matching dendrochronological dates with the Southern Hemisphere ^{14}C bomb curve to confirm annual tree rings in *Pseudolmedia rigida* from Bolivia. *Radiocarbon,* 57**,** 1-13.

Argollo, J., Soliz, C. & Villalba, R. 2004. Potencialidad dendrocronológica de *Polylepis tarapacana* en los Andes Centrales de Bolivia. *Ecología en Bolivia,* 39**,** 5-24.

Bagley, J. E., Desai, A. R., Harding, K. J., Snyder, P. K. & Foley, J. A. 2014. Drought and Deforestation: Has land cover change influenced recent precipitation extremes in the Amazon? *Journal of Climate,* 27**,** 345-361.

Ballantyne, A. P., Baker, P. A., Chambers, J. Q., Villalba, R. & Argollo, J. 2011. Regional differences in South American monsoon precipitation inferred from the growth and isotopic composition of tropical trees. *Earth Interactions,* 15**,** 1-35.

Berlemont, A., Desjonqueres, P. & Gouesbet, G. 1990. Particle Lagrangian simulation in turbulent flows. *International Journal of Multiphase Flow,* 16**,** 19-34.

Bräuning, A., Volland-Voigt, F., Burchardt, I., Ganzhi, O., Nauss, T. & Peters, T. 2009. Climatic control of radial growth of *Cedrela montana* in a humid mountain rainforest in southern Ecuador. *Erdkunde,* 63**,** 337-345.

Brienen, R. J. W. & Zuidema, P. A. 2005. Relating tree growth to rainfall in Bolivian rain forests: a test for six species using tree ring analysis. *Oecologia,* 146**,** 1-12.

Brienen, R. J. W., Helle, G., Pons, T. L., Guyot, J. L. & Gloor, M. 2012. Oxygen isotopes in tree rings are a good proxy for Amazon precipitation and El Niño-Southern Oscillation variability.

Proceedings of the National Academy of Sciences, 109**,** 16957-16962.
Brienen, R. J. W., Schöngart, J. & Zuidema, P. A. 2016. Tree Rings in the Tropics: Insights into the Ecology and Climate Sensitivity of Tropical Trees. *In:* GOLDSTEIN, G. & SANTIAGO, L. S. (eds.) *Tropical Tree Physiology: Adaptations and Responses in a Changing Environment.* Cham: Springer International Publishing.
Brown, D., Worden, J. & Noone, D. 2008. Comparison of atmospheric hydrology over convective continental regions using water vapor isotope measurements from space. *Journal of Geophysical Research: Atmospheres,* 113**,** 1-17.
Brown, D., Worden, J. & Noone, D. 2013. Characteristics of tropical and subtropical atmospheric moistening derived from Lagrangian mass balance constrained by measurements of HDO and H_2O. *Journal of Geophysical Research: Atmospheres,* 118**,** 54-72.
Dansgaard, W. 1964. Stable isotopes in precipitation. *Tellus,* 16**,** 436-468.
Dee, D., Uppala, S., Simmons, A., Berrisford, P., Poli, P., Kobayashi, S., Andrae, U., Balmaseda, M., Balsamo, G. & Bauer, P. 2011. The ERA-Interim reanalysis: Configuration and performance of the data assimilation system. *Quarterly Journal of the Royal Meteorological Society,* 137**,** 553-597.
Douglass, A. E. 1941. Crossdating in dendrochronology. *Journal of Forestry,* 39**,** 825-831.
Drumond, A., Marengo, J., Ambrizzi, T., Nieto, R., Moreira, L. & Gimeno, L. 2014. The role of the Amazon Basin moisture in the atmospheric branch of the hydrological cycle: a Lagrangian analysis. *Hydrology and Earth System Sciences,* 18**,** 2577-2598.
Dünisch, O., Bauch, J. & Gasparotto, L. 2002. Formation of increment zones and intraannual growth dynamics in the xylem of *Swietenia macrophylla*, *Carapa guianensis*, and *Cedrela odorata* (Meliaceae). *IAWA Journal,* 23**,** 101-120.
Fiorella, R. P., Poulsen, C. J., Pillco Zolá, R. S., Barnes, J. B., Tabor, C. R. & Ehlers, T. A. 2015. Spatiotemporal variability of modern precipitation $\delta^{18}O$ in the central Andes and implications for paleoclimate and paleoaltimetry estimates. *Journal of Geophysical Research: Atmospheres,* 120**,** 4630-4656.
Gärtner, H. & Nievergelt, D. 2010. The core-microtome: a new tool for surface preparation on cores and time series analysis of varying cell parameters. *Dendrochronologia,* 28**,** 85-92.
Gimeno, L., Drumond, A., Nieto, R., Trigo, R. M. & Stohl, A. 2010. On the origin of continental precipitation. *Geophysical Research Letters,* 37**,** 1-7.
Gloor, M., Barichivich, J., Ziv, G., Brienen, R. J. W., Schöngart, J., Peylin, P., Cintra, B. B. L., Feldpausch, T. R., Phillips, O. L. & Baker, J. C. A. 2015. Recent Amazon climate as background for possible ongoing and future changes of Amazon humid forests. *Global Biogeochemical Cycles,* 29**,** 1384-1399.
Hua, Q., Barbetti, M. & Rakowski, A. Z. 2013. Atmospheric radiocarbon for the period 1950–2010. *Radiocarbon,* 55**,** 2059-2072.
Huffman, G. J., Bolvin, D. T., Nelkin, E. J., Wolff, D. B., Adler, R. F., Gu, G., Hong, Y., Bowman, K. P. & Stocker, E. F. 2007. The TRMM multisatellite precipitation analysis (TMPA): Quasi-global, multiyear, combined-sensor precipitation estimates at fine scales. *Journal of Hydrometeorology,* 8**,** 38-55.
Insel, N., Poulsen, C. J., Sturm, C. & Ehlers, T. A. 2013. Climate controls on Andean precipitation $\delta^{18}O$ interannual variability. *Journal of Geophysical Research: Atmospheres,* 118**,** 9721-9742.
Jaffe, D., Anderson, T., Covert, D., Kotchenruther, R., Trost, B., Danielson, J., Simpson, W., Berntsen, T., Karlsdottir, S. & Blake, D. 1999. Transport of Asian air pollution to North America. *Geophysical Research Letters,* 26**,** 711-714.
Kagawa, A., Sano, M., Nakatsuka, T., Ikeda, T. & Kubo, S. 2015. An optimized method for stable isotope analysis of tree rings by extracting cellulose directly from cross-sectional laths. *Chemical Geology,* 393**,** 16-25.
Li, Z.-H., Labbé, N., Driese, S. G. & Grissino-Mayer, H. D. 2011. Micro-scale analysis of tree-ring $\delta^{18}O$ and $\delta^{13}C$ on α-cellulose spline reveals high-resolution intra-annual climate variability and tropical cyclone activity. *Chemical Geology,* 284**,** 138-147.
Loader, N. J., Robertson, I., Lucke, A. & Helle, G. 2002. Preparation of holocellulose from standard increment cores for stable carbon isotope analysis. *Swansea Geographer,* 37**,** 1-9.
Loader, N. J., Young, G. H. F., McCarroll, D. & Wilson, R. J. S. 2013. Quantifying uncertainty in isotope dendroclimatology. *The Holocene,* 23**,** 1221-1226.
Methven, J. 1997. Offline trajectories: Calculation and accuracy. UK Universities Global Atmospheric Modelling Programme.

Moy, L. A., Dickerson, R. R. & Ryan, W. F. 1994. Relationship between back trajectories and tropospheric trace gas concentrations in rural Virginia. *Atmospheric Environment,* 28**,** 2789-2800.

Myneni, R., Hoffman, S., Knyazikhin, Y., Privette, J., Glassy, J., Tian, Y., Wang, Y., Song, X., Zhang, Y. & Smith, G. 2002. Global products of vegetation leaf area and fraction absorbed PAR from year one of MODIS data. *Remote sensing of environment,* 83**,** 214-231.

Pearson, S., Hua, Q., Allen, K. & Bowman, D. M. 2011. Validating putatively cross-dated *Callitris* tree-ring chronologies using bomb-pulse radiocarbon analysis. *Australian Journal of Botany,* 59**,** 7-17.

Pennington, T., Styles, B. & Taylor, D. 1981. Meliaceae, Flora Neotropica Monograph. *The New York Botanical Garden, Bronx, New York, USA,* 28**,** 1-470.

R Development Core Team 2015. R: A language and environment for statistical computing. Vienna, Austria: R Foundation for Statistical Computing.

Risi, C., Bony, S. & Vimeux, F. 2008. Influence of convective processes on the isotopic composition ($\delta^{18}O$ and δD) of precipitation and water vapor in the tropics: 2. Physical interpretation of the amount effect. *Journal of Geophysical Research: Atmospheres,* 113**,** 1-12.

Samuels-Crow, K. E., Galewsky, J., Hardy, D. R., Sharp, Z. D., Worden, J. & Braun, C. 2014. Upwind convective influences on the isotopic composition of atmospheric water vapor over the tropical Andes. *Journal of Geophysical Research: Atmospheres,* 119**,** 7051-7063.

Santos, G. M., Linares, R., Lisi, C. S. & Tomazello Filho, M. 2015. Annual growth rings in a sample of Paraná pine (*Araucaria angustifolia*): Toward improving the ^{14}C calibration curve for the Southern Hemisphere. *Quaternary Geochronology,* 25**,** 96-103.

Sodemann, H., Schwierz, C. & Wernli, H. 2008. Interannual variability of Greenland winter precipitation sources: Lagrangian moisture diagnostic and North Atlantic Oscillation influence. *Journal of Geophysical Research,* 113**,** 1-17.

Sodemann, H. & Stohl, A. 2009. Asymmetries in the moisture origin of Antarctic precipitation. *Geophysical Research Letters,* 36**,** 1-5.

Spracklen, D. V., Arnold, S. R. & Taylor, C. M. 2012. Observations of increased tropical rainfall preceded by air passage over forests. *Nature,* 489**,** 282-285.

Stohl, A. 1996. Trajectory statistics-a new method to establish source-receptor relationships of air pollutants and its application to the transport of particulate sulfate in Europe. *Atmospheric Environment,* 30**,** 579-587.

Stohl, A. & Seibert, P. 1998. Accuracy of trajectories as determined from the conservation of meteorological tracers. *Quarterly Journal of the Royal Meteorological Society,* 124**,** 1465-1484.

Stohl, A. 1998. Computation, accuracy and applications of trajectories—a review and bibliography. *Atmospheric Environment,* 32**,** 947-966.

Stohl, A. & James, P. 2005. A Lagrangian Analysis of the Atmospheric Branch of the Global Water Cycle. Part II: Moisture Transports between Earth's Ocean Basins and River Catchments. *Journal of Hydrometeorology,* 6**,** 961-984.

Stokes, M. & Smiley, T. 1968. *An introduction to tree-ring dating*, University of Arizona Press.

Sturm, C., Hoffmann, G. & Langmann, B. 2007. Simulation of the stable water isotopes in precipitation over South America: Comparing regional to global circulation models. *Journal of Climate,* 20**,** 3730-3750.

Uppala, S. M., Kållberg, P., Simmons, A., Andrae, U., Bechtold, V., Fiorino, M., Gibson, J., Haseler, J., Hernandez, A. & Kelly, G. 2005. The ERA-40 re-analysis. *Quarterly Journal of the Royal Meteorological Society,* 131**,** 2961-3012.

Vetter, R. E. & Botosso, P. C. 1989. Remarks on age and growth rate determination of Amazonian trees. *IAWA Journal,* 10**,** 133-145.

Vimeux, F., Gallaire, R., Bony, S., Hoffmann, G. & Chiang, J. C. 2005. What are the climate controls on δD in precipitation in the Zongo Valley (Bolivia)? Implications for the Illimani ice core interpretation. *Earth and Planetary Science Letters,* 240**,** 205-220.

Vimeux, F., Tremoy, G., Risi, C. & Gallaire, R. 2011. A strong control of the South American SeeSaw on the intra-seasonal variability of the isotopic composition of precipitation in the Bolivian Andes. *Earth and Planetary Science Letters,* 307**,** 47-58.

Wieloch, T., Helle, G., Heinrich, I., Voigt, M. & Schyma, P. 2011. A novel device for batch-wise isolation of α-cellulose from small-amount wholewood samples. *Dendrochronologia,* 29**,** 115-117.

Wigley, T. M., Briffa, K. R. & Jones, P. D. 1984. On the average value of correlated time series, with

applications in dendroclimatology and hydrometeorology. *Journal of Climate and Applied Meteorology,* 23**,** 201-213.
Worbes, M. & Junk, W. J. 1989. Dating tropical trees by means of ^{14}C from bomb tests. *Ecology,* 70**,** 503-507.
Worbes, M. 1999. Annual growth rings, rainfall-dependent growth and long-term growth patterns of tropical trees from the Caparo Forest Reserve in Venezuela. *Journal of Ecology,* 87**,** 391-403.
Worbes, M. 2002. One hundred years of tree-ring research in the tropics–a brief history and an outlook to future challenges. *Dendrochronologia,* 20**,** 217-231.

Chapter 3: Does *Cedrela* always form annual rings? Testing ring periodicity across South America using radiocarbon dating

In review in Trees

Jessica C.A. Baker[1], Guaciara M. Santos[2], Manuel Gloor[1] and Roel J.W. Brienen[1]

[1]School of Geography, University of Leeds, UK

[2] Earth System Science, University of California, Irvine, USA

Abstract

Tropical tree rings have the potential to yield valuable ecological and climate information, on the condition that rings are annual and accurately dated. It is important to understand the factors controlling ring formation, since regional variation in these factors could cause trees in different regions to form tree rings at different times. Here we use 'bomb-peak' radiocarbon (^{14}C) dating to test the periodicity of ring formation in *Cedrela* trees from four sites across tropical South America. We show that trees from Bolivia, Ecuador and Venezuela have reliably annual tree rings, while trees from Suriname regularly form two rings per year. This proves that while tree rings of a particular species may be demonstrably annual at one site, this does not imply that rings are formed annually in other locations. We explore possible drivers of variation in ring periodicity and find that *Cedrela* growth rhythms are most likely caused by precipitation seasonality, with a possible degree of genetic control. Therefore, tree-ring studies undertaken at new locations in the tropics require independent validation of the annual nature of tree rings, irrespective of how the studied species behaves in other locations.

3.1 Introduction

Tropical dendrochronology is a steadily growing field, and the number of species known to be suitable for tree-ring analysis is also rising. Annual ring formation has now been shown in 230 tropical tree species (Brienen et al., 2016a), providing a great

opportunity to further expand tropical tree-ring studies. Tropical tree rings and their associated characteristics can be used to reconstruct climate (e.g. Baker et al., 2016; Mendivelso et al., 2013; Schöngart et al., 2006; Vlam et al., 2014; Xu et al., 2015), inform sustainable forest management (e.g. Brienen and Zuidema, 2006; De Ridder et al., 2013; Schöngart, 2008), study forest dynamics (e.g. Brienen et al., 2010; Vlam et al., 2017) and monitor forest responses to climate change (e.g. van der Sleen et al., 2015; Zuidema et al., 2012) but cf. (Brienen et al., 2016b). With such important applications, it is vital to understand what drives ring formation and thus how growth dynamics might vary between sites, even within a single species.

Temperature, which induces cambial dormancy and ring formation at high latitudes, has limited seasonality in the tropics (Jacoby, 1989), and seasonal variation in rainfall is instead thought to be the most common cue for growth periodicity and tree-ring formation (Brienen et al., 2016a). During an extreme dry period, water stress can result in cambial dormancy and this may be accompanied by discernible changes to the structure of the xylem, thus resulting in a growth band or tree ring (Bräuning et al., 2008a; Dünisch et al., 2002; Mendivelso et al., 2013; Worbes, 1999, 2002). Deciduous trees shed their leaves in response to the water stress, only to flush their leaves again and thereby reactivate the cambium once tree water status has been restored (Borchert, 1999). Periodic flooding and the ensuing anoxia can provide a similar trigger for ring formation in floodplain tree species (Schöngart et al., 2002). However, several studies have also highlighted the important influence of seasonality in daily insolation (amount of solar radiation per unit area) and photoperiod on tropical tree phenology, with phenological changes (such as shedding/flushing leaves) sometimes occurring in advance of the climate changes (such as water stress/onset of rains) that the trees might be expected to be responding to (Borchert et al., 2005; Borchert et al., 2015; Elliott et al., 2006; Lisi et al., 2008; Rivera et al., 2002). Furthermore, besides external cues, intrinsic plant rhythms are also likely to play some role in governing cambial activity (e.g. Callado et al., 2013; Villalba, 1985). This shows that identifying the trigger factor for growth rhythms in tropical trees is not always straightforward, as different tropical tree species respond to different cues (Borchert et al., 2015), and there could also be differences in response between sub-populations of the same species (e.g. Ruiz et al., 2013; Stubblebine et al., 1978).

Although the exact environmental trigger for ring formation in tropical trees may still be under discussion, it follows that regional variation in the stimulus may cause variation in growth periodicity. Indeed, previous work in the tropics has shown that a single species may have different growth rhythms under different environmental regimes (Costa et al., 2013). A species that forms distinct annual rings at a location with seasonal precipitation may form vague or false (non-annual) rings at a location with low or irregular precipitation seasonality, or may not form visible growth rings at all (Borchert, 1999; Boysen et al., 2014; Pearson et al., 2011; Priya and Bhat, 1999). Tree-ring formation may therefore occur at regular intervals (i.e. annual/biannual rings) or at irregular intervals (intermittent false rings) depending on the seasonality of environmental conditions (Gourlay, 1995; Jacoby, 1989). Thus, care should be taken when analysing tree rings from a new species, or from a known species in a new location (Brienen et al., 2016a).

Tree-ring periodicity can be tested using 'bomb-peak' radiocarbon (^{14}C) dating. Thermonuclear tests during the late 1950s caused an artificial increase in atmospheric ^{14}C (peaking around 1963–64), which has slowly been removed from the atmosphere since the 1962 Test Ban Treaty (Levin et al., 2008). From 1950 onwards, atmospheric ^{14}C signatures have been recorded across the globe at sites away from localized emissions sources (such as large cities and volcanoes), and, despite small variations, such as at the onset of the thermonuclear tests, these signatures are mostly well-distributed across the hemispheres (Hua et al., 2013; Levin and Hesshaimer, 2000; Levin et al., 2008 and references therein). This means that organic material from the last 60 years can be dated with an accuracy of 1–2 years by measuring its ^{14}C content, providing a means to validate tree-ring dates (e.g. Andreu-Hayles et al., 2015; Bormann and Berlyn, 1982; Pearson et al., 2011; Santos et al., 2015; Worbes and Junk, 1989).

This study focuses on *Cedrela odorata* and its highland relative *Cedrela montana*. *Cedrela* spp. have been used extensively in tree-ring studies in South America and are widely believed to form annual rings (e.g. Ballantyne et al., 2011; Bräuning et al., 2009; Brienen and Zuidema, 2005; Costa et al., 2013; Dünisch et al., 2002; Espinoza et al., 2014; Tomazello-Filho. et al., 2000; Worbes, 1999). The aim is to use bomb-peak ^{14}C dating to test the annual character of tree rings from four sites across the Amazon basin that vary in their precipitation and insolation seasonality. We complement this analysis

with tree-ring and growth rhythm data of *Cedrela* from various additional sites from Central and South America, and discuss what might be driving the observed variability in tree-ring periodicity.

3.2 Methods

The samples used in this study came from four locations across the Amazon basin: Reserva Forestal de Caparo in Venezuela (7.45°N, 70.98°W, 150 m above sea level (a.s.l.)), a logging concession near Matapi, Suriname (4.90°N, 56.85°W; 60 m a.s.l.), Cuyuja, Ecuador (0.45°S, 78.04°W; 2950 m a.s.l.), and Selva Negra, Bolivia (10.10°S, 66.31°W; 160 m a.s.l.). These locations and their corresponding climate diagrams are shown in Figure 3.1. Four additional sites where *Cedrela* growth data are available from the literature are also shown for comparison: Manaus, Amazonas State, Brazil (Dünisch and Morais, 2002), Aripuanã, Mato Grosso State, Brazil (Dünisch et al., 2003), Nova Iguaçu, Rio de Janeiro State, Brazil (Costa et al., 2013) and Ejido Pich, Campeche State, Mexico (Brienen et al., 2010). Temperature and precipitation data are from local weather stations or extracted from the Climatic Research Unit (CRU) TS3.24 0.5° x 0.5° dataset (Harris et al., 2014) and downloaded via Climate Explorer (Trouet and Van Oldenborgh, 2013). Daily insolation data were downloaded from the NASA (National Aeronautics and Space Administration) website (http://data.giss.nasa.gov/ar5/srlocat.html) and averaged over the period 1990–2000. Growth and phenology data are also shown in Figure 3.1. Sources of these data are as follows: Mexico (Brienen et al., 2010), Venezuela (Worbes, 1999), Suriname (personal communication, P. Teunissen), Ecuador (Bräuning et al., 2009), Bolivia (Brienen and Zuidema, 2005) and Brazil (e.g. Manaus (Dünisch and Morais, 2002), Aripuanã (Dünisch et al., 2003) and Nova Iguaçu (Costa et al., 2013)).

The main climatic features of each site will now be briefly summarised. While temperature shows little seasonality at any of the sites, there is some variability in rainfall regime. Mexico, Venezuela, Bolivia, Aripuanã and Nova Iguaçu all have one pronounced dry season, with precipitation falling below 50 mm for three consecutive months or more (Fig. 3.1a, b, f–h). Ecuador and Manaus also have a single distinct dry season when monthly precipitation falls below 100 mm for at least three consecutive

months (Fig. 3.1d, e). In Suriname, precipitation has a bimodal distribution, peaking in January and June, and does not fall below 100 mm in any month (Fig. 3.1c). Insolation distributions also vary, with sites furthest from the Equator experiencing a single annual insolation peak (i.e. Fig. 3.1a, f–h) and sites close to the Equator experiencing two insolation peaks in each year (i.e. Fig. 3.1b–e).

C. odorata was sampled in Bolivia, Venezuela and Suriname, and the closely related species *C. montana* was sampled in the high elevation site in Ecuador (hereafter referred to by genus name only). Stem discs were collected in 2011 (Bolivia), 2013 (Ecuador) and 2014 (Suriname) from trees felled for timber or during the installation of overhead power lines. The Venezuelan samples were collected in 2012, using an increment borer to collect cores from living trees. Discs were polished using an orbital sander with sandpaper up to grit 600 to improve ring visibility. On each disc rings were marked on 2–4 radii and every 10th ring was interconnected between radii to crosscheck counting accuracy, and account for wedging rings (Brienen et al., 2016a). A core-microtome (Gärtner and Nievergelt, 2010) was used to prepare the surface of the cores from Venezuela. Rings on the cores were then marked, measured using a LINTAB measuring stage to the nearest 0.01 mm, and visually crossdated across 2–3 radii. Disc sections (cut using a bandsaw) and cores were then scanned at high resolution using an Epson Expression 11000XL scanner (Fig. 3.3a–c). As the rings were particularly narrow on the samples from Suriname, the microtome was used to cut thin sections (~10 µm thick) that were scanned with an Epson Perfection V700 Photo scanner (Fig. 3.3d) to optimise ring visibility. Rings on the samples from Suriname were observed to frequently follow a regular pattern of a narrow ring followed by a wide ring, possibly indicating the presence of non-annual rings (e.g. Gourlay, 1995). Where this pattern was identified the narrow rings were assumed to be false and thus the wide and narrow rings were initially counted together as a single annual ring and dated accordingly. All rings were dated following the convention of Schulman (1956), where the assigned calendar date corresponds with the year that the tree started growing.

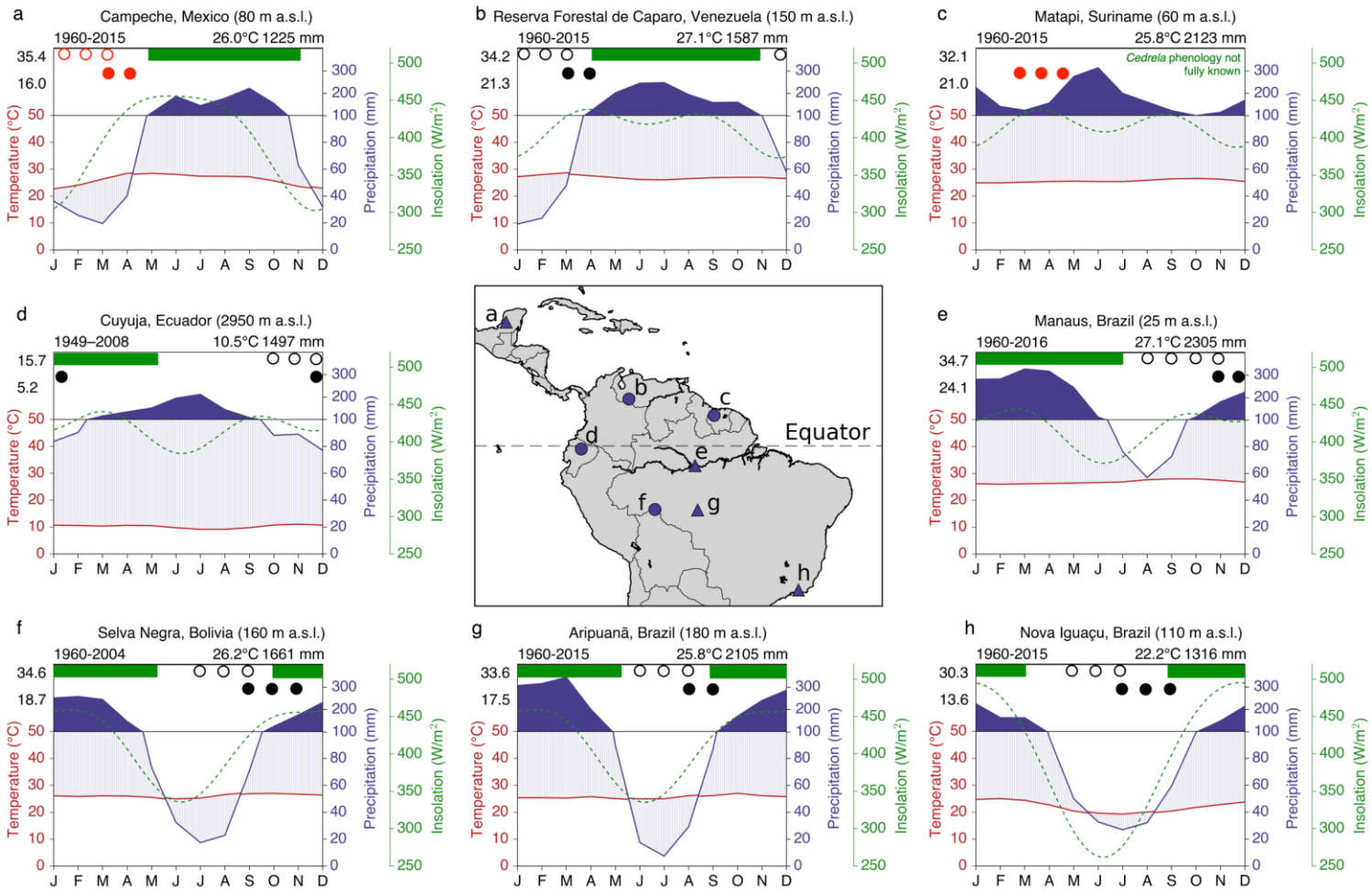

Fig. 3.1 – Map of *Cedrela* study sites and their climate diagrams. The four sites sampled in this study (dark blue circles) and four sites where *Cedrela* growth periodicity data are available from the literature (dark blue triangles) are shown. The altitude of each site is given in m above sea level (m a.s.l.). The date range at the top left of each climate diagram is the period of temperature and precipitation observations. The values in black at the top right are the mean annual temperature and the total annual precipitation. Values in black on the left side of each diagram are the maximum and minimum annual temperatures. Note that the precipitation scale changes above 100 mm, indicated by a change to solid blue fill. Average daily insolation data are also shown (dashed green line). Horizontal green bars at the top of each graph show the main growing period for *Cedrela* at each of the sites. Open and filled black circles show the periods of *Cedrela* leaf-fall and leaf-flush respectively, with data from systematic monitoring. Open and filled red circles show the periods of *Cedrela* leaf-fall and leaf-flush respectively, with data from casual observations. Sources for the climate, insolation, growth and phenology data used for each site are given in the Methods.

To independently validate this initial ring age-assignment, between one and three trees from each site were selected for bomb-peak ^{14}C dating. This approach is a useful method for validating crossdated tree-ring samples (e.g. Andreu-Hayles et al., 2015; Baker et al., 2015; Bormann and Berlyn, 1982; Pearson et al., 2011; Santos et al., 2015; Worbes and Junk, 1989). All measurements were performed on α-cellulose or holocellulose extracts rather than whole wood, as these wood fractions are immobile and will thus produce more precise radiocarbon dates than if whole wood were used (Leavitt and Bannister, 2009). For each sample, 2–4 rings putatively dated from 1955 to 1985 were selected for analysis, and the wood cut from each individual ring using a scalpel (in total 25 samples from 8 different trees). Cellulose extraction for the Suriname samples was conducted in Leeds, following the batch method of Wieloch et al. (2011). These samples were then sent for ^{14}C analysis by means of accelerator mass spectrometry (AMS) in Bothell, USA by DirectAMS (http://www.directams.com). AMS analysis used NIST Ox-II standards (Stuiver, 1983) for normalization, and IAEA-C7 as secondary standards (Le Clercq et al., 1997). Graphitisation of CO2 produced by combustion of organic materials was via the zinc reduction method (Vogel, 1992). All other samples were analysed at the W. M. Keck Carbon Cycle Accelerator Mass Spectrometer (KCCAMS Facility) located at the Earth System Science Department at the University of California in Irvine, USA. At KCCAMS holocellulose was isolated following a method adapted from Leavitt and Danzer (1993) with AnkomTM F57 Dacron filter bags (25 μm effective pore size) used as sample pouches. Wood samples loaded in pouches were lined up in a Soxhlet apparatus and initially treated with a 2:1 mixture of >99.5 % toluene and HPLC grade ethanol for 24 hours, and later by pure HPLC ethanol for another 24 hours. Subsequent processing used hot Milli-Q water to remove solvent residues, followed by bleaching at 70 °C with a sodium chlorite solution acidified with 2 ml of 100% glacial acetic acid. Once samples turned white, they were washed with Milli-Q water and gently dried at 50 °C in a conventional drying oven. After extraction of holocellulose, samples were removed from pouches, combusted and graphitized following established protocols (Santos et al., 2007). Wood blank (^{14}C-free) and secondary standards (FIRI-J and FIRI-H; Scott, 2003), as well as cellulose extract (IAEA-C3; Rozanski et al., 1992) were processed alongside samples for background corrections and quality control purposes. High-precision ^{14}C measurements were

conducted at an in-house modified AMS compact instrument (Beverly et al., 2010) via multiple analyses of the primary and normalizing standard Oxalic Acid I (OX-I). All ^{14}C results were corrected for background effects and isotopic fractionation due to photosynthesis, sample processing and spectrometer analysis, with δ13C measured on prepared graphite directly at the spectrometer, as described by Santos et al. (2007).

To check the accuracy of the individual tree-ring dates their respective fraction modern carbon values ($F^{14}C$, defined as the ratio of the radioactivity of the sample to the radioactivity of the modern standard; Reimer et al., 2004) were plotted alongside atmospheric radiocarbon bomb-peak calibration curves from designated zones in the Northern and Southern Hemispheres (e.g. NHZ2 and SHZ3; Hua et al., 2013). The calendar dates that had been assigned initially (following Schulman's convention, see above) were converted to a decimal date that was centred in the middle of the growing season for each site (green bars in Fig. 3.1), as this is when trees photosynthesise atmospheric $^{14}CO_2$ and form tree-ring cellulose. For example, the ring 2000 would be adjusted to 2001.0, 2001.25 and 2000.5 in samples from Bolivia, Ecuador, and Venezuela respectively, as these dates fall within the growing season at each location (see growth data sources above). Samples from Suriname were not adjusted relative to the initial assigned dates, as the main growing period for *Cedrela* is unknown for this site.

3.3 Results and Discussion

The measured $F^{14}C$ values were plotted alongside the atmospheric ^{14}C calibration curves from Hua et al. (2013). The samples from Bolivia, Ecuador and Venezuela all fall on or between these curves (Fig. 3.2a–c), indicating that these trees have been accurately dated by counting rings and that *Cedrela* forms annual growth rings at each of these locations. High-resolution scans of samples from these locations illustrate the correspondence between tree-ring dates (black annotations) and radiocarbon dates (blue annotations, Fig. 3.3a–c). These results are consistent with previous tree-ring studies, which report annual ring formation in *Cedrela* spp. from Bolivia (Brienen and Zuidema, 2005), Ecuador (Bräuning et al., 2009) and Venezuela (Worbes, 1999). Furthermore, the excellent agreement between ^{14}C in tree rings and

existing bomb-peak calibration curves shows that well-dated tropical tree-ring records can potentially be used to refine low-latitude intra-hemispheric ^{14}C calibration curves between 1950 and 1970, when distributions of atmospheric ^{14}C were more variable across the globe, as previously described. This could lead to present intra-hemispheric ^{14}C calibration curves being redefined in tropical regions.

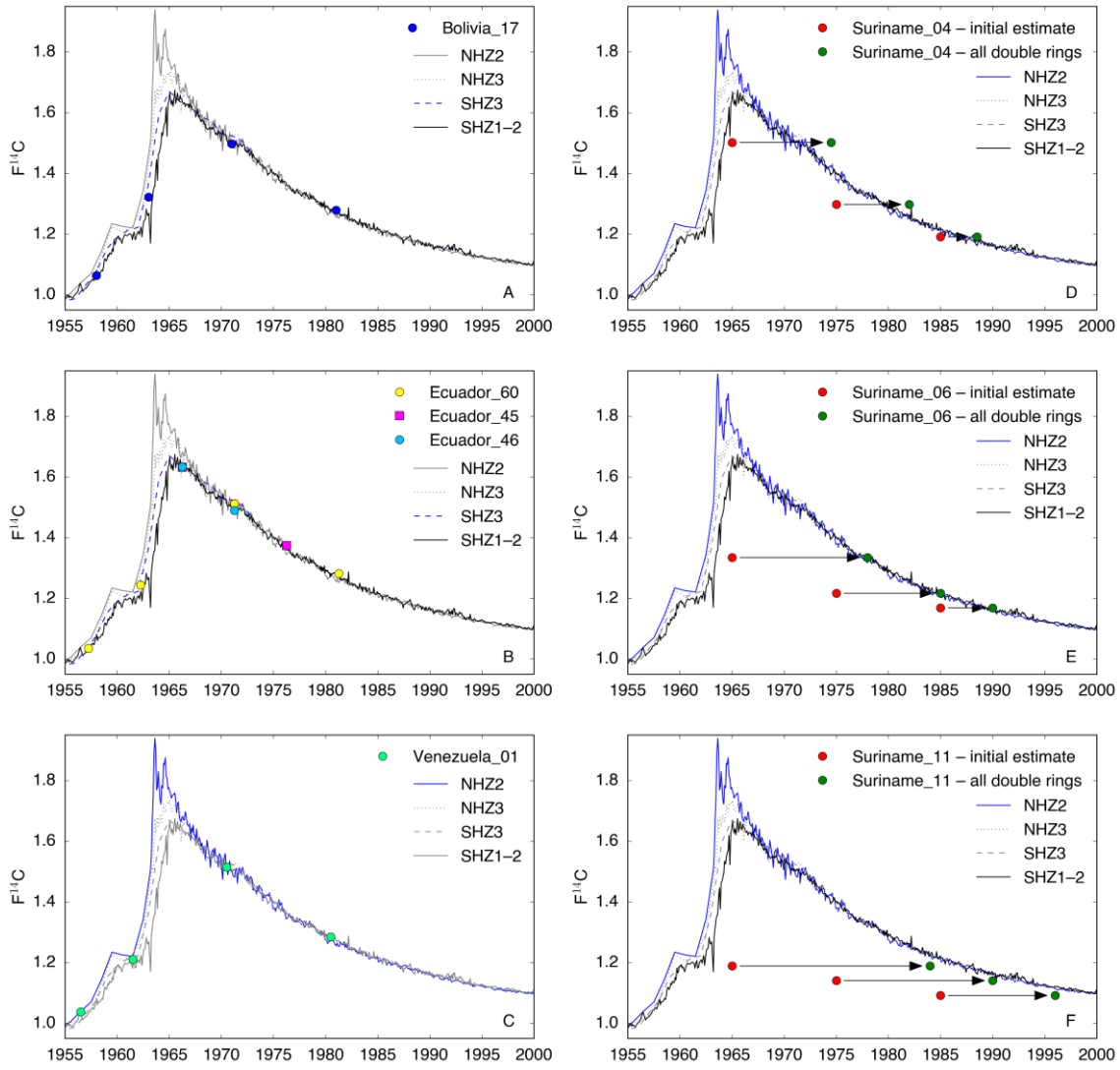

Fig. 3.2 – Results from radiocarbon (^{14}C) analysis. Measured $F^{14}C$ values (circles) plotted over the northern hemisphere (NH) and southern hemisphere (SH) ^{14}C bomb datasets compiled by Hua et al. (2013). **(a–c)** Samples from Bolivia (tree 17), Ecuador (trees 45, 46 and 60) and Venezuela (tree 01) all fall on top or between these calibration curves. **(d–f)** Samples from Suriname (trees 04, 06 and 11) plotted using the initial sample age estimates (red circles) and the age estimates if trees are assumed to regularly form two rings per year (green circles). In each panel, the location-specific atmospheric ^{14}C calibration curve presently accepted by the radiocarbon community (as per Hua et al., 2013), is highlighted in blue.

The Suriname samples were initially dated using a 'best-guess' approach, based on the assumption that a narrow ring followed by a wide ring should be counted as one single year. The initial estimated calendar dates fall far from the calibration curves (red circles, Fig. 3.2d–f), showing that the initial ring dating was inaccurate. The original samples were then re-inspected and the rings were dated assuming that the trees formed i) a single ring each year and ii) consistently two rings per year. Figure 3.3d shows a scan of Suriname sample 06 with the revised dates from these two approaches annotated in red (approach i) and green (approach ii). Only the second approach produced any sample dates close to the results from ^{14}C analysis (blue annotations). When plotted against these adjusted dates (green circles), the $F^{14}C$ values fall either exactly on (Suriname_06, Fig. 3.2e) or closer to (Suriname_04 and Suriname_11, Fig. 3.2d & f) the bomb calibration curves. Samples from Suriname_04 appear to be overestimated by 1–3 years, while samples from Suriname_11 appear to be underestimated by 2–3 years. Nevertheless, these results are a strong indication that in Suriname *Cedrela* forms two rings every (or nearly every) year. The slight offsets that remain for Suriname_04 and Suriname_11 suggest there could still be some minor dating errors with either one or two rings missed or miscounted. For example, in Figure 3.2f the green circles fall to the left of the radiocarbon calibration curves, suggesting that there may have been one or two false rings in the Suriname_11 sample. To the authors' knowledge this is the first time that the formation of two rings per year has been reported in *Cedrela*, and shows that dendrochronologists should take a cautious approach when analysing samples from new sites in the tropics. Furthermore, if a species regularly forms two rings per year at a particular site then conventional dendrochronological crossdating methods (see Stokes and Smiley, 1968) may not detect that ring formation is not annual. Ring periodicity thus needs to be validated using radiocarbon dating, or by correlating a robust ring-width or isotope chronology against climate data over a sufficiently long period.

To explore what might be driving the observed spatial variation in growth periodicity it is first necessary to understand how tree rings form in *Cedrela*. *Cedrela* is an obligate deciduous species and throughout most of its natural range (from Mexico to northern Argentina; Pennington et al., 1981) leaf shedding and associated dormancy occur strictly once per year, during the annual dry season (Fig. 3.1; Brienen and Zuidema, 2005; Costa et al., 2013; Worbes, 1999). Thus, in Bolivia, trees are leafless

from July to September (Brienen and Zuidema, 2005), in Ecuador from October to December (Bräuning et al., 2009) and in Venezuela from December to March (Worbes, 1999), although the exact dates of leaf-fall and leaf-flush may vary between years. The cambium is inactive during this leafless period and a marginal parenchyma band marks the cessation of growth (Brienen and Zuidema, 2005; Dünisch et al., 2002; Marcati et al., 2006). Ring structure in *Cedrela* is described as ring-porous or semi-ring-porous as large vessels form during reactivation of the cambium, resulting in an abundance of wide vessels embedded within the parenchyma band, and fewer, narrower vessels in the wood which forms later in the growing season (Dünisch et al., 2002; Vetter and Botosso, 1989). This pattern is clear in samples from all of the sites in this study (side panels, Fig. 3.3). Leaf-fall behaviour of *Cedrela* in Suriname has not been systematically monitored so it is not known whether biannual ring formation corresponds to (or is induced by) biannual leaf exchange. Casual observations have been made of trees flowering and fruiting at the turn of the year (from September/October to February/March), and in 2010 and 2015, trees were observed to flush their leaves between March and May (personal communication, P. Teunissen). This is broadly similar to neighbouring Guyana where *Cedrela* flowers from August to November and fruiting occurs in January to March (Polak, 1992; ter Steege and Persaud, 1991), though leaf-fall behaviour has also not been consistently observed here. Despite this knowledge gap, the factors controlling growth dynamics of tropical trees can still be explored in an attempt to understand the regional variation in Cedrela ring formation reported here.

Growth periodicity in *Cedrela* may be driven by variation in an external environmental signal (e.g. precipitation or insolation), or by an intrinsic biological rhythm. These candidate drivers will be discussed in turn, using data from each of the sample sites complemented with data from the literature. First, rainfall and insolation distributions are compared with periodicity of ring formation in *Cedrela*. In Suriname, where *Cedrela* forms two rings each year, rainfall has a bimodal distribution. This is likely due to the oscillating position of the inter-tropical convergence zone (ITCZ) which follows maximum solar radiation and thus moves southward across the continent during austral summer and northward again during austral winter (Garreaud et al., 2009). For this reason, at the ‘climatic equator’, which in South America centres around

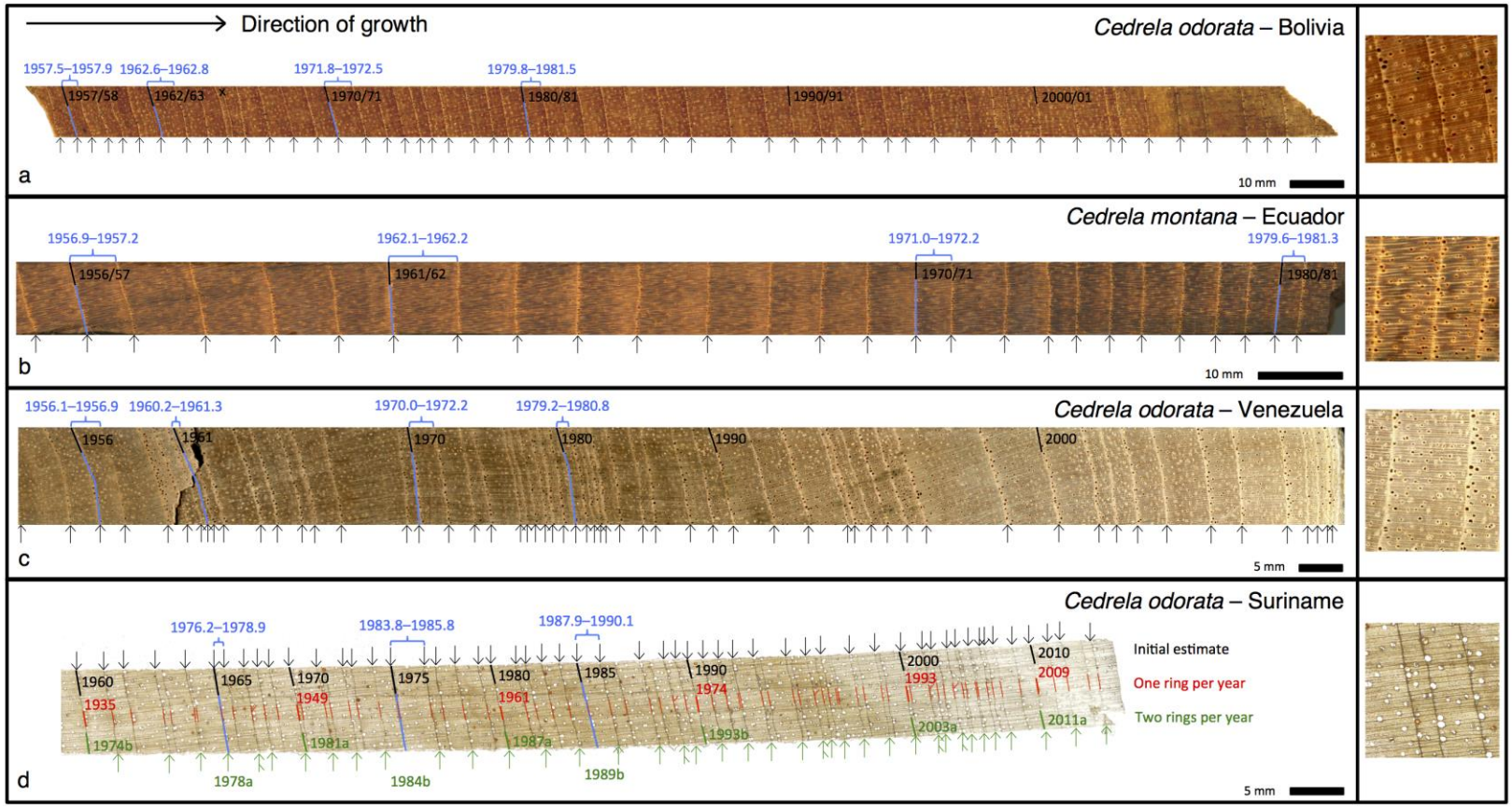

Fig. 3.3 – Annotated high-resolution scans of tree-ring samples. One tree each from **(a)** Bolivia (tree 17), **(b)** Ecuador (tree 60), **(c)** Venezuela (tree 01) and **(d)** Suriname (tree 06). Black arrows indicate the parenchyma bands counted as ring boundaries during the initial tree-ring dating process. For Suriname only we show two extra annotations: ring boundaries if a tree forms one ring per year (red markings) or two rings per year (green arrows). Blue brackets and lines indicate the tree rings selected for ^{14}C analysis with their initial assigned years shown in black. Note that a tree ring may grow across two calendar years (e.g. 2000/01), depending on the main growing period at a particular location (see Fig. 1). Radiocarbon-derived calendar age ranges (±2σ) are shown in blue and were translated from the $F^{14}C$ values and uncertainties obtained from ^{14}C-AMS using the free online CALIBomb software (http://calib.org/CALIBomb/) and the available intra-hemispheric datasets of Hua et al. (2013), e.g. SHZ3 (Bolivia and Ecuador) and NHZ2 (Venezuela and Suriname). New age estimates (assuming trees form two rings per year) are in green. When marking 2 rings per year the first and second rings are denoted *a* and *b* respectively.

4–5°N, there may be two wet seasons as the ITCZ passes over two times in each year (Borchert et al., 2005). In contrast, the other seven sites show only one distinct wet and dry season per year, and at all of these seven sites *Cedrela* has been shown to form one ring each year. At these seven sites the trees grow mainly during the wet season and are leafless during the driest part of the year (Fig. 3.1a, b, d–h). This provides a strong indication that tree rings at these sites are formed in response to seasonal water availability. The phenology of Suriname *Cedrela* has not been studied, so it is not known whether the species changes its leaves twice a year here, but it is possible that one of the two rings forms during a period of temporary cambial dormancy when the trees are still in leaf (Borchert, 1999). However, it should also be noted that the seasonal water deficit in Suriname is much less pronounced than at the other sites, with monthly precipitation never falling below 100 mm. A recent analysis used remote sensing data to show that tropical forests in central and north-eastern Amazonia, where mean annual precipitation exceeds 2000 mm, are able to sustain or enhance photosynthetic activity during the dry season (Guan et al., 2015), contrasting the notion of growth being limited by drought.

The second potential environmental stimulus for ring formation is insolation, which is known to have an important influence on tropical tree phenology (Borchert et al., 2005; Borchert et al., 2015). For example, some species have been observed flushing their leaves twice a year at the Equator in response to two insolation peaks per year, and only once a year farther from the Equator where insolation has just one peak per year (Borchert et al., 2015; Calle et al., 2010). Daily insolation data are shown in Figure 3.1 (green lines). The Suriname site is closest to the 'insolation equator' which, at ~3°N, is the latitude where insolation has the lowest year-round variation (Borchert et al., 2015). Across the other study sites, where *Cedrela* is known to exchange its leaves once per year and form annual rings, there is no clear relationship between insolation seasonality and *Cedrela* growth rhythm. Of these seven sites, some have two peaks of insolation per year (Ecuador, Venezuela and Manaus), and some just one peak of insolation per year (Bolivia, Aripuanã, Nova Iguaçu and Campeche; Fig. 3.1). Therefore, we believe that solar insolation is not the primary driver of the distinct biannual ring formation of *Cedrela* in Suriname. Furthermore, periods of leaf-fall do not consistently coincide with increasing, decreasing, peak or minimum insolation, though

leaf-flush occurs more commonly when insolation is increasing or nearing its annual maximum (Fig. 3.1).

Controls on growth periodicity can also be endogenous (Bräuning et al., 2008b). Ring formation may not be a plastic response to an external cue but could instead be driven by a biologically-determined growth rhythm. In other words, different populations of *Cedrela* may be adapted to shed their leaves at a specific time each year, coinciding with the local seasonality in water deficit. This is supported by observations of Costa et al. (2013) who showed that *Cedrela* growing in southern Brazil exhibited regular cambial dormancy during the dry season, even in years when there was no water deficit, thus implying some conservatism in growth behaviour. Furthermore, providence trials (where seeds sourced from different origins are grown under the same conditions) have shown that *Cedrela* from drier sites show more pronounced leaf-fall behaviour than *Cedrela* from wetter sites, indicating that variation in phenology is at least partly controlled by phylogeny (Newton et al., 1999). As *Cedrela odorata* is also known to have one of the highest levels of population differentiation of any tree species yet to be tested, with moist- and dry-adapted lineages (Cavers et al., 2003; Muellner et al., 2009), it seems feasible that regional differences in ring periodicity might be associated with phylogenetic differences.

Finally, a comparison with *Cedrela* growing in plantations in Cameroon at a similar latitude (3.5°N) to the Suriname *Cedrela* (4.90°N) can provide further clues as to what controls tree growth in this species. The *Cedrela* trees from Cameroon are known to form annual rings (Détienne and Mariaux, 1977), and as the annual course of insolation in Cameroon is almost identical to that in Suriname (Fig. 3.4) where rings are biannual, it is unlikely that insolation is the primary driver of *Cedrela* ring formation. Therefore, the differences in growth rhythm between Cameroon and Suriname must either be due to differences in climate or due to some internal (i.e., genetically controlled) growth rhythm of the plantation trees in Cameroon. As in Suriname, rainfall has a bimodal distribution in Cameroon (Fig. 3.4) but the dry periods in Cameroon are more extreme and trees only stop growing during the long dry season from December to February (Détienne and Mariaux, 1977). As the Cameroon trees were most likely introduced from central America (most commercial *Cedrela* trees are), and as trees in Central America stop growing during the same period (December to February, e.g.

Mexico, Fig. 3.1a), the distinct annual growth rhythm of the Cameroon trees may thus also be a genetic relict from the original population of these plantation trees. In conclusion, the available evidence suggests that insolation is unlikely to be a driver of growth periodicity in *Cedrela*, but climate seasonality and/or genetics are likely to be important.

3.4 Summary and Outlook

Radiocarbon dating has been used to confirm that *Cedrela*, a tree widely used in tropical tree-ring studies, forms annual rings in Bolivia, Ecuador and Venezuela but two rings per year in Suriname. This result shows that annual tree-ring formation in a species at one site cannot automatically be extrapolated elsewhere. The rhythm of tree-ring formation at new locations needs to be established if tree rings are to be used for dating, especially in tropical sites with low climatic seasonality. With incomplete phenological data it is difficult to draw definite conclusions about what controls *Cedrela* growth rhythms, though it seems that rainfall seasonality, not solar insolation, is the environmental cue triggering tree-ring formation, with a probable genetic influence. In sites with relatively aseasonal climates, like in Suriname, phenological

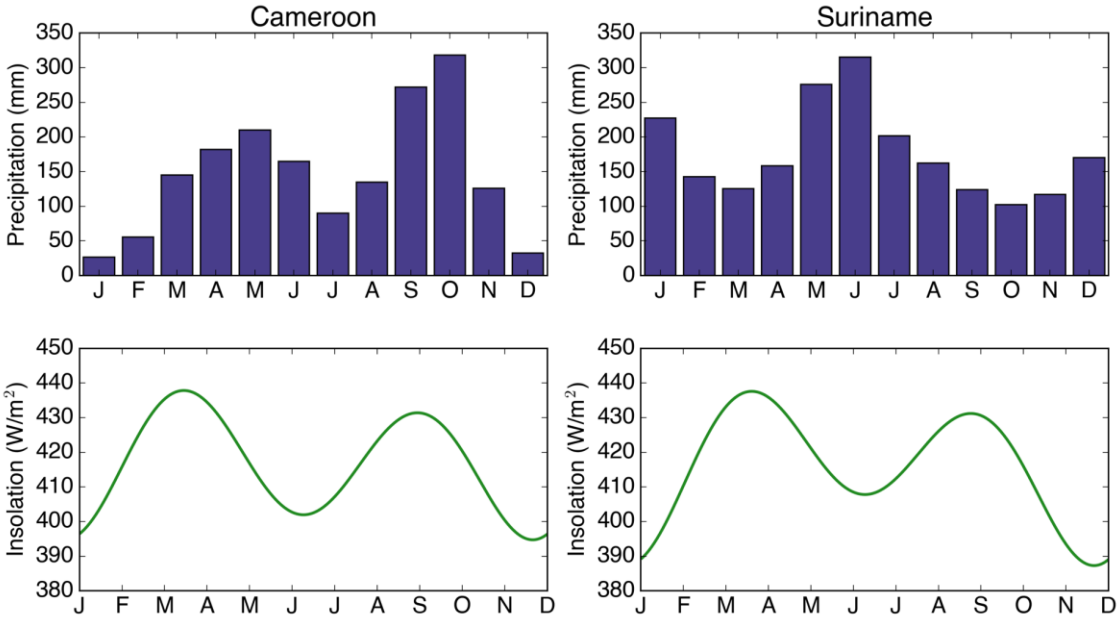

Figure 3.4 – Precipitation and insolation data from Cameroon and Suriname. Annual precipitation (upper panels) and insolation (lower panels) in Cameroon and Suriname. Precipitation data are from CRU TS3.24 0.5° x 0.5° and insolation data were downloaded from http://data.giss.nasa.gov/ar5/srlocat.html.

observations and dendrometer measurements of *Cedrela* cambial dynamics, possibly combined with relocation experiments, would help us to better understand the spatial differences in growth dynamics of this scientifically and commercially important species.

3.5 References

Andreu-Hayles, L., Santos, G. M., Herrera-Ramírez, D. A., Martin-Fernández, J., Ruiz-Carrascal, D., Boza-Espinoza, T. E., Fuentes, A. F. & Jorgensen, P. M. 2015. Matching dendrochronological dates with the Southern Hemisphere ^{14}C bomb curve to confirm annual tree rings in *Pseudolmedia rigida* from Bolivia. *Radiocarbon,* 57**,** 1-13.

Baker, J. C. A., Hunt, S. F. P., Clerici, S. J., Newton, R. J., Bottrell, S. H., Leng, M. J., Heaton, T. H. E., Helle, G., Argollo, J., Gloor, M. & Brienen, R. J. W. 2015. Oxygen isotopes in tree rings show good coherence between species and sites in Bolivia. *Global and Planetary Change,* 133**,** 298-308.

Baker, J. C. A., Gloor, M., Spracklen, D. V., Arnold, S. R., Tindall, J. C., Clerici, S. J., Leng, M. J. & Brienen, R. J. W. 2016. What drives interannual variation in tree ring oxygen isotopes in the Amazon? *Geophysical Research Letters,* 43**,** 11831-11840.

Ballantyne, A. P., Baker, P. A., Chambers, J. Q., Villalba, R. & Argollo, J. 2011. Regional differences in South American monsoon precipitation inferred from the growth and isotopic composition of tropical trees. *Earth Interactions,* 15**,** 1-35.

Beverly, R. K., Beaumont, W., Tauz, D., Ormsby, K. M., Von Reden, K. F., Santos, G. M. & Southon, J. R. 2010. The Keck Carbon Cycle AMS Laboratory, University of California, Irvine: status report. *Radiocarbon,* 52**,** 301-309.

Borchert, R. 1999. Climatic periodicity, phenology, and cambium activity in tropical dry forest trees. *IAWA Journal,* 20**,** 239-247.

Borchert, R., Renner, S. S., Calle, Z., Navarrete, D., Tye, A., Gautier, L., Spichiger, R. & Von Hildebrand, P. 2005. Photoperiodic induction of synchronous flowering near the Equator. *Nature,* 433**,** 627-629.

Borchert, R., Calle, Z., Strahler, A. H., Baertschi, A., Magill, R. E., Broadhead, J. S., Kamau, J., Njoroge, J. & Muthuri, C. 2015. Insolation and photoperiodic control of tree development near the equator. *New Phytologist,* 205**,** 7-13.

Bormann, F. H. & Berlyn, G. 1982. Age and growth rate of tropical trees. New directions for research. *Forest Science,* 28**,** 422.

Boysen, B. M. M., Evans, M. N. & Baker, P. J. 2014. $\delta^{18}O$ in the tropical conifer *Agathis robusta* records ENSO-related precipitation variations. *Plos One,* 9**,** 1-9.

Bräuning, A., Von Schnakenburg, P., Volland-Voigt, F. & Peters, T. 2008a. Seasonal growth dynamics and its climate forcing in a tropical mountain rain forest in southern Ecuador. *TRACE—tree rings in Archaeology. Climatol Ecol,* 6**,** 27-30.

Bräuning, A., Homeier, J., Cueva, E., Beck, E. & Günter, S. 2008b. Growth dynamics of trees in tropical mountain ecosystems. *Gradients in a Tropical Mountain Ecosystem of Ecuador.* Springer.

Bräuning, A., Volland-Voigt, F., Burchardt, I., Ganzhi, O., Nauss, T. & Peters, T. 2009. Climatic control of radial growth of *Cedrela montana* in a humid mountain rainforest in southern Ecuador. *Erdkunde,* 63**,** 337-345.

Brienen, R. J. W. & Zuidema, P. A. 2005. Relating tree growth to rainfall in Bolivian rain forests: a test for six species using tree ring analysis. *Oecologia,* 146**,** 1-12.

Brienen, R. J. W. & Zuidema, P. A. 2006. Lifetime growth patterns and ages of Bolivian rain forest trees obtained by tree ring analysis. *Journal of Ecology,* 94**,** 481-493.

Brienen, R. J. W., Zuidema, P. A. & Martínez-Ramos, M. 2010. Attaining the canopy in dry and moist tropical forests: strong differences in tree growth trajectories reflect variation in growing conditions. *Oecologia,* 163**,** 485-496.

Brienen, R. J. W., Gloor, M. & Ziv, G. 2016a. Tree demography dominates long-term growth trends

inferred from tree rings. *Global Change Biology,* 23**,** 474-484.
Brienen, R. J. W., Schöngart, J. & Zuidema, P. A. 2016b. Tree Rings in the Tropics: Insights into the Ecology and Climate Sensitivity of Tropical Trees. *In:* GOLDSTEIN, G. & SANTIAGO, L. S. (eds.) *Tropical Tree Physiology: Adaptations and Responses in a Changing Environment.* Cham: Springer International Publishing.
Callado, C. H., Roig, F. A., Tomazello Filho, M. & Barros, C. F. 2013. Cambial growth periodicity studies of South American woody species–A review. *IAWA Journal,* 34**,** 213-230.
Calle, Z., Schlumpberger, B. O., Piedrahita, L., Leftin, A., Hammer, S. A., Tye, A. & Borchert, R. 2010. Seasonal variation in daily insolation induces synchronous bud break and flowering in the tropics. *Trees,* 24**,** 865-877.
Cavers, S., Navarro, C. & Lowe, A. J. 2003. Chloroplast DNA phylogeography reveals colonization history of a Neotropical tree, *Cedrela odorata* L., in Mesoamerica. *Molecular Ecology,* 12**,** 1451-1460.
Costa, M. S., De Vasconcellos, T. J., Barros, C. F. & Callado, C. H. 2013. Does growth rhythm of a widespread species change in distinct growth sites? *IAWA Journal,* 34**,** 498 – 509.
De Ridder, M., Van Den Bulcke, J., Van Acker, J. & Beeckman, H. 2013. Tree-ring analysis of an African long-lived pioneer species as a tool for sustainable forest management. *Forest Ecology and Management,* 304**,** 417-426.
Détienne, P. & Mariaux, A. 1977. Nature et périodicité des cernes dans les bois rouges de méliacées africaines. *Bois et forets des tropiques***,** 52-61.
Dünisch, O. & Morais, R. R. 2002. Regulation of xylem sap flow in an evergreen, a semi-deciduous, and a deciduous Meliaceae species from the Amazon. *Trees,* 16**,** 404-416.
Dünisch, O., Bauch, J. & Gasparotto, L. 2002. Formation of increment zones and intraannual growth dynamics in the xylem of *Swietenia macrophylla*, *Carapa guianensis*, and *Cedrela odorata* (Meliaceae). *IAWA Journal,* 23**,** 101-120.
Dünisch, O., Montóia, V. R. & Bauch, J. 2003. Dendroecological investigations on *Swietenia macrophylla* King and *Cedrela odorata* L.(Meliaceae) in the central Amazon. *Trees,* 17**,** 244-250.
Elliott, S., Baker, P. J. & Borchert, R. 2006. Leaf flushing during the dry season: the paradox of Asian monsoon forests. *Global Ecology and Biogeography,* 15**,** 248-257.
Espinoza, M. J. P., Guillen, G. J. I., Morales, M. S. & Arisméndiz, R. R. 2014. *Cedrela odorata* (Meliaceae) potential for dendrochronological studies in the Selva Central of Perú. *Revista de Biología Tropical/International Journal of Tropical Biology and Conservation,* 62**,** 783-793.
Garreaud, R. D., Vuille, M., Compagnucci, R. & Marengo, J. 2009. Present-day South American climate. *Palaeogeography, Palaeoclimatology, Palaeoecology,* 281**,** 180-195.
Gärtner, H. & Nievergelt, D. 2010. The core-microtome: a new tool for surface preparation on cores and time series analysis of varying cell parameters. *Dendrochronologia,* 28**,** 85-92.
Gourlay, I. D. 1995. Growth ring characteristics of some African *Acacia* species. *Journal of Tropical Ecology,* 11**,** 121-140.
Guan, K., Pan, M., Li, H., Wolf, A., Wu, J., Medvigy, D., Caylor, K. K., Sheffield, J., Wood, E. F., Malhi, Y., Liang, M., Kimball, J., Saleska, S., Berry, J., Joiner, J. & Lyapustin, A. 2015. Photosynthetic seasonality of global tropical forests constrained by hydroclimate. *Nature Geoscience,* 8**,** 284-289.
Harris, I., Jones, P. D., Osborn, T. J. & Lister, D. H. 2014. Updated high-resolution grids of monthly climatic observations–the CRU TS3.10 Dataset. *International Journal of Climatology,* 34**,** 623-642.
Hua, Q., Barbetti, M. & Rakowski, A. Z. 2013. Atmospheric radiocarbon for the period 1950–2010. *Radiocarbon,* 55**,** 2059-2072.
Jacoby, G. C. 1989. Overview of tree-ring analysis in tropical regions. *IAWA Journal,* 10**,** 99-108.
Leavitt, S. W. & Danzer, S. R. 1993. Method for batch processing small wood samples to holocellulose for stable-carbon isotope analysis. *Analytical Chemistry,* 65**,** 87-89.
Leavitt, S. W. & Bannister, B. 2009. Dendrochronology and radiocarbon dating: The laboratory of tree-ring research connection. *Radiocarbon,* 51**,** 373-384.
Levin, I. & Hesshaimer, V. 2000. Radiocarbon–a unique tracer of global carbon cycle dynamics. *Radiocarbon,* 42**,** 69-80.
Levin, I., Hammer, S., Kromer, B. & Meinhardt, F. 2008. Radiocarbon observations in atmospheric CO_2: Determining fossil fuel CO_2 over Europe using Jungfraujoch observations as background. *Science of the Total Environment,* 391**,** 211-216.

Lisi, C. S., Fo, M. T., Botosso, P. C., Roig, F. A., Maria, V. R., Ferreira-Fedele, L. & Voigt, A. R. 2008. Tree-ring formation, radial increment periodicity, and phenology of tree species from a seasonal semi-deciduous forest in southeast Brazil. *IAWA Journal,* 29**,** 189-207.

Marcati, C. R., Angyalossy, V. & Evert, R. F. 2006. Seasonal variation in wood formation of *Cedrela fissilis* (Meliaceae). *IAWA Journal,* 27**,** 199-211.

Mendivelso, H. A., Camarero, J. J., Obregón, O. R., Gutiérrez, E. & Toledo, M. 2013. Differential growth responses to water balance of coexisting deciduous tree species are linked to wood density in a Bolivian tropical dry forest. *PloS One,* 8**,** 1-11.

Muellner, A. N., Pennington, T. D. & Chase, M. W. 2009. Molecular phylogenetics of Neotropical *Cedreleae* (mahogany family, Meliaceae) based on nuclear and plastid DNA sequences reveal multiple origins of "*Cedrela odorata*". *Molecular Phylogenetics and Evolution,* 52**,** 461-469.

Newton, A. C., Watt, A. D., Lopez, F., Cornelius, J. P., Mesén, J. F. & Corea, E. A. 1999. Genetic variation in host susceptibility to attack by the mahogany shoot borer, *Hypsipyla grandella* (Zeller). *Agricultural and Forest Entomology,* 1**,** 11-18.

Pearson, S., Hua, Q., Allen, K. & Bowman, D. M. 2011. Validating putatively cross-dated *Callitris* tree-ring chronologies using bomb-pulse radiocarbon analysis. *Australian Journal of Botany,* 59**,** 7-17.

Pennington, T., Styles, B. & Taylor, D. 1981. Meliaceae, Flora Neotropica Monograph. *The New York Botanical Garden, Bronx, New York, USA,* 28**,** 1-470.

Polak, A. 1992. *Major timber trees of Guyana: a field guide,* Wageningen, The Netherlands, Tropenbos Foundation.

Priya, P. & Bhat, K. 1999. Influence of rainfall, irrigation and age on the growth periodicity and wood structure in teak (*Tectona grandis*). *IAWA journal,* 20**,** 181-192.

Reimer, P. J., Brown, T. A. & Reimer, R. W. 2004. Discussion: reporting and calibration of post-bomb ^{14}C data. *Radiocarbon,* 46**,** 1299-1304.

Rivera, G., Elliott, S., Caldas, L. S., Nicolossi, G., Coradin, V. T. & Borchert, R. 2002. Increasing day-length induces spring flushing of tropical dry forest trees in the absence of rain. *Trees,* 16**,** 445-456.

Ruiz, V. E., Meloni, D. A., Fornes, L. F., Ordano, M., Hilal, M. & Prado, F. E. 2013. Seedling growth and water relations of three *Cedrela* species sourced from five provenances: response to simulated rainfall reductions. *Agroforestry systems,* 87**,** 1005-1021.

Santos, G. M., Moore, R. B., Southon, J. R., Griffin, S., Hinger, E. & Zhang, D. 2007. AMS ^{14}C sample preparation at the KCCAMS/UCI Facility: status report and performance of small samples. *Radiocarbon,* 49**,** 255-269.

Santos, G. M., Linares, R., Lisi, C. S. & Tomazello Filho, M. 2015. Annual growth rings in a sample of Paraná pine (*Araucaria angustifolia*): Toward improving the ^{14}C calibration curve for the Southern Hemisphere. *Quaternary Geochronology,* 25**,** 96-103.

Schöngart, J., Piedade, M. T. F., Ludwigshausen, S., Horna, V. & Worbes, M. 2002. Phenology and stem-growth periodicity of tree species in Amazonian floodplain forests. *Journal of Tropical Ecology,* 18**,** 581-597.

Schöngart, J., Orthmann, B., Hennenberg, K. J., Porembski, S. & Worbes, M. 2006. Climate–growth relationships of tropical tree species in West Africa and their potential for climate reconstruction. *Global Change Biology,* 12**,** 1139-1150.

Schöngart, J. 2008. Growth-Oriented Logging (GOL): A new concept towards sustainable forest management in Central Amazonian várzea floodplains. *Forest Ecology and Management,* 256**,** 46-58.

Schulman, E. 1956. *Dendroclimatic changes in semiarid America,* Tucson, University of Arizona Press.

Scot, E. M. 2003. The Fourth International Radiocarbon Intercomparison (FIRI). *Radiocarbon,* 45**,** 135-291.

Stokes, M. & Smiley, T. 1968. *An introduction to tree-ring dating*, University of Arizona Press.

Stubblebine, W., Langenheim, J. H. & Lincoln, D. 1978. Vegetative response to photoperiod in the tropical leguminous tree *Hymenaea courbaril* L. *Biotropica,* 10**,** 18-29.

Ter Steege, H. & Persaud, C. A. 1991. The phenology of Guyanese timber species: a compilation of a century of observations. *Vegetatio,* 95**,** 177-198.

Tomazello Filho, M., Botosso, P. & Lisi, C. 2000. Potencialidade da família Meliaceae para dendrocronologia em regiões tropicais e subtropicais. *F.A. Roig (ed.) Dendrocronología em América Latina. EDIUNC, Mendoza***,** 381-431.

Van Der Sleen, P., Groenendijk, P., Vlam, M., Anten, N. P., Boom, A., Bongers, F., Pons, T. L., Terburg,

G. & Zuidema, P. A. 2015. No growth stimulation of tropical trees by 150 years of CO2 fertilization but water-use efficiency increased. *Nature Geoscience,* 8**,** 24-28.
Vetter, R. E. & Botosso, P. C. 1989. Remarks on age and growth rate determination of Amazonian trees. *IAWA Journal,* 10**,** 133-145.
Villalba, R. 1985. Xylem structure and cambial activity in *Prosopis flexuosa* DC. *IAWA Bulletin,* 6**,** 119-130.
Vlam, M., Baker, P. J., Bunyavejchewin, S. & Zuidema, P. A. 2014. Temperature and rainfall strongly drive temporal growth variation in Asian tropical forest trees. *Oecologia,* 174**,** 1449-1461.
Vlam, M., Van Der Sleen, P., Groenendijk, P. & Zuidema, P. A. 2017. Tree Age Distributions Reveal Large-Scale Disturbance-Recovery Cycles in Three Tropical Forests. *Frontiers in Plant Science,* 7**,** 1-12.
Vogel, J. S. 1992. Rapid production of graphite without contamination for biomedical AMS. *Radiocarbon,* 34**,** 344-350.
Wieloch, T., Helle, G., Heinrich, I., Voigt, M. & Schyma, P. 2011. A novel device for batch-wise isolation of α-cellulose from small-amount wholewood samples. *Dendrochronologia,* 29**,** 115-117.
Worbes, M. & Junk, W. J. 1989. Dating tropical trees by means of ^{14}C from bomb tests. *Ecology,* 70**,** 503-507.
Worbes, M. 1999. Annual growth rings, rainfall-dependent growth and long-term growth patterns of tropical trees from the Caparo Forest Reserve in Venezuela. *Journal of Ecology,* 87**,** 391-403.
Worbes, M. 2002. One hundred years of tree-ring research in the tropics–a brief history and an outlook to future challenges. *Dendrochronologia,* 20**,** 217-231.
Xu, C., Pumijumnong, N., Nakatsuka, T., Sano, M. & Li, Z. 2015. A tree-ring cellulose $\delta^{18}O$-based July–October precipitation reconstruction since AD 1828, northwest Thailand. *Journal of Hydrology,* 529**,** 433-441.
Zuidema, P. A., Brienen, R. J. W. & Schöngart, J. 2012. Tropical forest warming: looking backwards for more insights. *Trends in Ecology and Evolution,* 27**,** 193-194.

Chapter 4: Oxygen isotopes in tree rings show good coherence between species and sites in Bolivia

Published in Global and Planetary Change

Jessica C. A. Baker[1], Sarah F. P. Hunt[1], Santiago J. Clerici[1], Robert J. Newton[2], Simon H. Bottrell[2], Melanie J. Leng[3], Timothy H. E. Heaton[3], Gerhard Helle[4], Jaime Argollo[5], Manuel Gloor[1], Roel J. W. Brienen[1]

[1] School of Geography, University of Leeds, Leeds, UK

[2] School of Earth and Environment, University of Leeds, Leeds, UK

[3] NERC Isotope Geosciences Facilities, British Geological Survey, UK

[4] GFZ - German Research Centre for Geosciences, Germany

[5] Laboratorio de Dendrocronologia e Historia Ambiental, Universidad Mayor de San Andres, Bolivia

Abstract

A tree-ring oxygen isotope ($\delta^{18}O_{TR}$) chronology developed from one species (*Cedrela odorata)* growing in a single site has been shown to be a sensitive proxy for rainfall over the Amazon basin, thus allowing reconstructions of precipitation in a region where meteorological records are short and scarce. Although these results suggest there should be large-scale (>100 km) spatial coherence of $\delta^{18}O_{TR}$ records in the Amazon, this has not been tested. Furthermore, it is of interest to investigate whether other, possibly longer-lived, species similarly record interannual variation of Amazon precipitation, and can be used to develop climate-sensitive isotope chronologies. In this study, we measured $\delta^{18}O$ in tree rings from seven lowland and one highland tree species from Bolivia. We found that crossdating with $\delta^{18}O_{TR}$ gave more accurate tree-ring dates than using ring width. Our "isotope crossdating approach" is confirmed with radiocarbon "bomb-peak" dates, and has the potential to greatly facilitate development of $\delta^{18}O_{TR}$ records in the tropics, identify dating errors, and check annual ring formation in tropical trees. Six of the seven lowland species correlated significantly with *C. odorata*, showing that variation in $\delta^{18}O_{TR}$ has a coherent imprint across very different

species, most likely arising from a dominant influence of source water $\delta^{18}O$ on $\delta^{18}O_{TR}$. In addition, we show that $\delta^{18}O_{TR}$ series cohere over large distances, within and between species. Comparison of two *C. odorata* $\delta^{18}O_{TR}$ chronologies from sites several hundreds of kilometres apart showed a very strong correlation (0.80, $p<0.001$, 1901-2001), and a significant (but weaker) relationship was found between lowland *C. odorata* trees and a *Polylepis tarapacana* tree growing in the distant Altiplano ($r=0.39$, $p<0.01$, 1931-2001). This large-scale coherence of $\delta^{18}O_{TR}$ records is probably triggered by a strong spatial coherence in precipitation $\delta^{18}O$ due to large-scale controls. These results highlight the strength of $\delta^{18}O_{TR}$ as a precipitation proxy, and open the way for temporal and spatial expansion of precipitation reconstructions in South America.

4.1 Introduction

Palaeo proxies allow reconstruction of past climates beyond the limit of instrumental records, and thus help the interpretation of recent and on-going climatic changes. Tree rings have the potential to be particularly useful climate archives since they are widely distributed and often allow reconstructions at annual resolution or higher (Briffa, 1999). In the tropics, however, it has long been assumed that trees do not form visible growth rings (e.g. Whitmore, 1998). Nonetheless, studies in recent decades show that in fact many tropical tree species do form annual rings, in response to seasonal variation in rainfall (Worbes, 1999), or an annual flood-pulse (Schöngart et al., 2002). Indeed, annual ring formation has been observed and verified in 67 tree species from tropical lowland rainforest alone (Zuidema et al., 2012). Despite these advances, useful tree-ring-based climate reconstructions are notably scarce in the tropics (see the International Tree-Ring Data Bank; Grissino-Mayer and Fritts, 1997), an important region in terms of global climate. This is due in part to the difficulty of developing climate-sensitive proxies from tropical tree species; ring-width patterns often match poorly between trees, making crossdating a challenge (Groenendijk et al., 2014, Stahle, 1999), and growth responses to interannual climate variation are often relatively weak (e.g. Brienen and Zuidema, 2005, Schollaen et al., 2013, van der Sleen et al., 2015, Worbes, 1999) due to generally favourable growth conditions, especially in warm and

humid climates. Alternative methods are therefore required in the tropics to extract useful climate information from tree rings.

One promising approach is to use the oxygen isotope composition of tree rings ($\delta^{18}O_{TR}$) to reconstruct past precipitation. Unlike variation in ring width, $\delta^{18}O_{TR}$ in several tropical sites have been shown to be highly sensitive to variations in rainfall amount, at local and regional scales (e.g. Anchukaitis and Evans, 2010, Brienen et al., 2012, 2013, Schollaen et al., 2013, Xu et al., 2011). In a particularly successful study, a $\delta^{18}O_{TR}$ chronology constructed from eight *Cedrela odorata* trees from a single site in northern Bolivia showed a clear signal of precipitation integrated over the whole Amazon basin, demonstrated by a close correlation between Amazon River discharge at Obidos, Brazil and the $\delta^{18}O_{TR}$ record (r=0.58; Brienen et al., 2012). This correlation suggests that *C. odorata* is an excellent recorder of the isotopic composition of precipitation ($\delta^{18}O_P$), which in turn is a good proxy for basin-wide precipitation. *C. odorata* is a shallow-rooted species (Cintron, 1990), only using water from the top soil layers (Schwendenmann et al., 2014). Thus, the water taken up by the tree (source water) predominantly comes from recent precipitation, and this is probably the reason it so precisely records year-to-year variation in $\delta^{18}O_P$ (Brienen et al., 2012). $\delta^{18}O_P$ is itself influenced by several factors which affect the rate of rainout and return of isotopes to the atmosphere, including the continental effect, altitude effect, amount effect and recycling of water by vegetation (see Dansgaard, 1964, Rozanski et al., 1993, Risi et al., 2008, and Salati et al., 1979). In the lowland forest of northern Bolivia, the location of the trees used in this study, cumulative rainout of heavy isotopes during transport of water vapour across the continent from the Atlantic seems to be the dominant control of variation in $\delta^{18}O_P$ (i.e. the continental effect; Brienen et al., 2012, Pierrehumbert, 1999, Salati et al., 1979, Sturm et al., 2007). Equilibrium fractionation during condensation in rainclouds results in preferential removal of heavy isotopes during rain events (Dansgaard, 1964) and leads effectively to a Rayleigh distillation process, such that precipitation downwind becomes more and more isotopically depleted. If *C. odorata* indeed records such large-scale effects, one would expect trees from sites several hundreds of kilometres apart to show the same interannual variation in $\delta^{18}O_{TR}$. Such coincidence of isotopic variation would not only be helpful in tree-ring dating and

construction of tree-ring chronologies, but would also confirm the case for large-scale effects controlling $\delta^{18}O_P$ in the Amazon basin.

Apart from *C. odorata*, the potential for the development of isotope chronologies has thus far been tested for very few tree species in tropical South America (see Ballantyne et al., 2011). Using additional, possibly longer-lived tree species allows for an increase in the spatial and temporal coverage of precipitation reconstructions in South America and beyond. However, it is currently not known to what degree other tree species (with similar and different rooting behaviours) show the same $\delta^{18}O_{TR}$ signals, because other factors influence $\delta^{18}O_{TR}$ besides source water isotopic composition ($\delta^{18}O_S$). Several of these factors are conceptualized in the mechanistic model presented by Roden et al. (2000), which we briefly summarize here.

Starting at the roots, water uptake from the soil is a non-fractionating process, so water reaching the leaves has a very similar isotopic composition to soil water (Ehleringer and Dawson, 1992). In the leaf, water is isotopically enriched relative to the source water. There are two components to this process: enrichment of heavy water at the site of evaporation in the leaf (due to preferential transpiration of isotopically light water) and back diffusion of some of this heavy water to the rest of the leaf (Barbour et al., 2004, Roden et al., 2000). This second component, the back diffusion of heavy water from the evaporative site, affects the isotope ratio of bulk leaf water ($\delta^{18}O_L$) and consequently the isotopic signal in cellulose precursors, which form throughout the leaf (Sternberg, 2009). The magnitude of back diffusion of heavy water is primarily determined by the rate of transpiration: under high (low) transpiration rates, advection of unenriched water from the vein is higher (lower), reducing (increasing) back diffusion, and thus causing $\delta^{18}O_L$ to be more similar to (more enriched than) $\delta^{18}O_S$ (Song et al., 2013). The ratio of advective to diffusive transport is known as the Péclet number (Farquhar and Lloyd, 1993) and this has an important moderating influence on $\delta^{18}O_L$ (and thus the $\delta^{18}O$ of fixed sugars).

In a final step, the $\delta^{18}O$ signal of sugars produced in the leaf further changes before conversion to cellulose. Sugars formed in the leaf are transported to the stem where some of the oxygen atoms may exchange with stem water oxygen during cellulose synthesis, determining the final isotope signature (Hill et al., 1995). This exchange is important, as it acts to partially "uncouple" $\delta^{18}O_{TR}$ from leaf physiology

(Offermann et al., 2011), and reinforces the signal of the source water. Experimental evidence shows that the degree of exchange is positively related to the turnover time of non-structural carbohydrates (Song et al., 2014a), thus leading to differences between species in the degree to which $\delta^{18}O_{TR}$ represents $\delta^{18}O_S$ (Song et al., 2014b).

Several studies have examined how interannual $\delta^{18}O_{TR}$ records vary between different temperate tree species, and within and between sites (Li et al., 2015, Marshall and Monserud, 2006, Saurer et al., 2008, Singer et al., 2013, Reynolds-Henne et al., 2009). Coherence in $\delta^{18}O_{TR}$ records between species varies considerably. Saurer et al. (2008) analysed six tree species in Switzerland and found a weak common interspecies signal in $\delta^{18}O_{TR}$ (mean inter-series correlation=0.23), with the strongest relationship between spruce and beech (r=0.68). The authors attribute these correlations to temperature influencing $\delta^{18}O_S$ and an influence of precipitation through its effect on local humidity. Li et al. (2015) found a strong relationship between pine and oak $\delta^{18}O_{TR}$ records in Japan (r=0.67), driven by summer precipitation amount controlling $\delta^{18}O_S$. In other temperate studies trends in $\delta^{18}O_{TR}$ differed strongly between species (Marshall and Monserud, 2006, Reynolds-Henne et al., 2009, Singer et al., 2013). These inter-species differences were variously attributed to species-specific partitioning of source water within the soil profile (Marshall and Monserud, 2006, Saurer et al., 2008, Singer et al., 2013), differences in plant physiology (Reynolds-Henne et al., 2009, Saurer et al., 2008), and differences in phenology (Saurer et al., 2008), although isolating the drivers of inter-specific differences in $\delta^{18}O_{TR}$ can be a challenge.

This paper focuses on tropical South America and aims: i) to determine whether or not an established Bolivian $\delta^{18}O_{TR}$ chronology can be used as a reference curve to verify dating of new isotope records, ii) to assess how well $\delta^{18}O_{TR}$ signals correspond between species, and iii) to investigate coherence of $\delta^{18}O_{TR}$ signals between distant sites. For this purpose, we analyse multi-decadal $\delta^{18}O_{TR}$ records for eight tropical tree species from three lowland moist forest sites and one site in the Bolivian Altiplano. Among these are five light-demanding tree species, two shade-tolerant tree species and one high altitude shrub. To address the first question, isotope series that were dated by ring counting were compared with a well-replicated and verified $\delta^{18}O_{TR}$ record from Brienen et al. (2012). Dating of re-aligned series was verified using radiocarbon "bomb-peak" dating (e.g. Worbes and Junk, 1989). The $\delta^{18}O_{TR}$ record for each lowland species

was then compared with the geographically closest *C. odorata* chronology to assess interspecies signal correlations. Finally, to assess spatial coherence of $\delta^{18}O_{TR}$ signals, *C. odorata* records from lowland sites >300 km apart were first compared with each other, and then with a *Polylepis tarapacana* series from the Altiplano (>1000 km away).

4.2 Materials and Methods

4.2.1 Study species

We selected eight tropical tree species that form clear and annual rings (Brienen and Zuidema, 2005, Argollo et al., 2004): seven are Bolivian lowland rainforest tree species (*Cedrela odorata*, *Tachigali vasquezii*, *Amburana cearensis*, *Peltogyne heterophylla*, *Bertholletia excelsa*, *Cedrelinga catenaeformis* and *Couratari macrosperma*), while one species (*Polylepis tarapacana*) only grows at high altitudes in the Bolivian Altiplano. Hereafter species will be referred to by their generic names only. Ring anatomy for the lowland species (except for *Couratari*) is described in Brienen and Zuidema (2005), and for *Polylepis* in Argollo et al. (2004). Relevant ecological characteristics are described below, and summarized in Table 4.1.

The lowland species vary in their growth rates and regeneration requirements. *Cedrela*, *Tachigali* and *Cedrelinga* reach the highest diameter growth rates (3.2–4.8 cm $year^{-1}$), while *Amburana*, *Peltogyne* and *Bertholletia* show slower diameter growth rates (e.g. ~1.8 cm $year^{-1}$, Table 4.1). All of the lowland species, except for *Peltogyne* and *Couratari*, seem to require gaps at some stage during their regeneration, and are classified as light-demanding (Brienen and Zuidema, 2006). *Peltogyne* is the most shade-tolerant species with the densest wood. Leaf phenology differs between species, from obligate deciduous leaf habit in *Cedrela* and *Amburana*, which lose their leaves for several months, to evergreen or brevi-deciduous in other species. *Cedrela* prefers well-drained soils, has a superficial root system (Cintron, 1990), and predominantly uses water from the top 30 cm of the soil profile (Schwendenmann et al., 2014). *Amburana* is often found on deep, well-drained or otherwise calcareous soils (Leite, 2005) and *Bertholletia* also seems to favour well-drained sites. For the other species, we have very little information on soil preferences or rooting depth. Species also vary in their adult stature - *Bertholletia* and *Cedrelinga* are the tallest species, reaching over 2

m in diameter and heights of up to 50 m (classified as “emergents”), while the other lowland species are canopy trees, growing to maximum heights of 25–35 m.

The only species in this study from the Altiplano, *Polylepis,* has the highest altitudinal range of any tree in the world, growing from 3900–5200 m elevation (Solíz et al., 2009). These trees grow slowly due to the cold and dry climate, and can live for over 700 years (Solíz et al., 2009). Precipitation is the main growth-limiting factor in these dry highlands (Morales et al., 2004), making *Polylepis* particularly useful for climate reconstructions (Morales et al., 2004, Solíz et al., 2009). Trees at these altitudes remain small (rarely exceeding 7m in height; Domic and Capriles, 2009), and radial growth patterns are often highly eccentric.

Figure 4.1 – Map of sample sites in the southwest Amazon. The locations of sample sites in this study (circles) and the location of the *Polylepis* chronology from Ballantyne et al. (2011; triangle) are indicated. The species sampled at each site are as follows: *Cedrela* and *Couratari* from Selva Negra, *Amburana* from Purisima, *Tachigali*, *Peltogyne*, *Bertholletia* and *Cedrelinga* from Riberalta and *Polylepis* from Sajama. The Amazon basin catchment area is shaded in pale green. Lowland sites are shown in black and Altiplano sites are shown in red.

Table 4.1 – Traits of different tropical tree species. Growth strategy, leaf-fall behaviour, adult stature, maximum observed age, maximum growth rate, rooting depth and habitat of the eight study species are given. Maximum diameter growth rate is the mean of the five highest annual growth rates observed in different trees.

Species name	Family	Growth strategy	Leaf-fall behaviour	Adult stature	Max. observed age (years)	Max. growth rate (cm year^{-1})	Rooting depth	Habitat
Cedrela odorata	Meliaceae	Light-demanding	Obligate deciduous	Canopy	308[a]	3.2[a]	Shallow	Evergreen - seasonally dry forest
Amburana cearensis	Leguminosae	Light-demanding	Obligate deciduous	Canopy	243[a]	1.8[a]	?	Evergreen - seasonally dry forest
Peltogyne heterophylla	Leguminosae	Shade-tolerant	Brevi-deciduous	Canopy	254[a]	1.8[a]	?	Tropical lowland moist forest
Tachigali vasquezii	Leguminosae	Light-demanding	Brevi-deciduous	Canopy	35[a]	4.8[a]	?	Tropical lowland moist forest
Couratari macrosperma	Lecythidaceae	Shade-tolerant	?	Canopy-Emergent	?	?	?	Tropical lowland moist forest
Cedrelinga catenaeformis	Leguminosae	Light-demanding	Brevi-deciduous	Emergent	123[a]	3.7[a]	?	Tropical lowland moist forest
Bertholletia excelsa	Lecythidaceae	Light-demanding	Obligate deciduous	Emergent	427[a]	1.9[a]	?	Tropical lowland moist forest
Polylepis tarapacana	Rosaceae	High altitude shrub	Evergreen	?	705[b]	?	?	Cold, high altitude desert

[a] Brienen and Zuidema (2005)
[b] Solíz et al. (2009)

4.2.2 Regional setting

Tree-ring samples for this study come from lowland rainforest sites in northern Bolivia, except for the *Polylepis* sample which originated from the Bolivian Altiplano, close to the Sajama volcano at an altitude of 4400–4500 m (Fig. 4.1; 18°06'S, 68°53'W; Solíz et al., 2009). The *Amburana* sample is from the private property Purisima, in Pando (11°24'S, 68°43'W; 170 m.a.s.l.), while the *Tachigali*, *Peltogyne*, *Bertholletia* and *Cedrelinga* samples were obtained from logging concession areas approximately 40 km to the east of the town Riberalta (10°55'S, 65°40'W; 160 m.a.s.l.). These two sites are described by Brienen and Zuidema (2005). The *Couratari* and *Cedrela* samples are from a third lowland site, Selva Negra (10°5'S, 66°18'W; 160 m.a.s.l.), 90 km north of Riberalta and approximately 325 km northeast of the Purisima site. All of the lowland sites have a similar climatology, with total annual precipitation between 1675 - 1850 mm (Cobija and Riberalta station data, GHCN-Monthly version 2, Peterson and Vose, 1997, accessed from Climate Explorer (http://climexp.knmi.nl)), and a distinct dry period during the austral winter (June–August) with less than 100 mm of rain per month. For *Amburana, Tachigali*, *Peltogyne*, *Bertholletia* and *Cedrelinga* stem discs were collected between October 2002 and September 2003 from trees that had been felled, or that had died of natural causes (see Brienen and Zuidema, 2005 for sampling protocols). Discs of *Couratari* and *Cedrela* were collected in 2011 from trees felled for timber. The *Polylepis* disc was collected in 2003. Between 5 and 31 discs were collected per species. Sampling height varied from 0.5–2.0 m above the ground, and discs ranged from 30–200 cm in diameter.

4.2.3 Oxygen isotope analysis

Stem discs were collected and polished with sandpaper up to grit 600 using a mechanical sander. Rings were then marked and crossdated (see section 4.2.4 for full description). Old trees with good internal crossdating were selected for isotope analysis. For *Cedrela* we selected nine trees, while for the other species only one tree was selected. While we acknowledge that a single individual is not sufficient to develop a climate sensitive chronology, this approach is well suited to explore coherence in $\delta^{18}O_{TR}$ between different species and a well-developed chronology. Using one tree per species allowed us to maximize the number of species included in this study (see also

Ballantyne et al., 2011, Saurer et al., 2008). Each ring was individually cut up using a scalpel, sampling equally from the entire width of the ring to ensure even representation of the whole growing season. In some instances where rings were very narrow it was not possible to isolate sufficient wood for analysis, and the final isotope series therefore show some missing data-points. We extracted α-cellulose from the wood following the batch method of Wieloch et al. (2011). Cellulose was homogenized using a mixer mill (Retsch MM 301) and then freeze-dried. Samples were then weighed into silver capsules for isotope analysis.

Oxygen isotope data presented here were measured at three different labs: the British Geological Survey's Stable Isotope Facility (part of the NERC Isotope Geosciences Facilities) (NIGF; Keyworth, Nottingham, UK); the School of Earth and Environment (SEE) at the University of Leeds, UK; and the German Research Centre for Geosciences (GFZ; Potsdam, Germany). Analysis of the *Cedrela* samples was performed at NIGF utilising a ThermoFinnigan (Bremen, Germany) TC/EA linked to a Delta+XL isotope ratio mass spectrometer (IRMS) at 1400 °C. $^{18}O/^{16}O$ ratios were converted to $\delta^{18}O$ values with reference to VSMOW by comparison with co-run IAEA-CH-3 cellulose (assuming $\delta^{18}O$=+31.9±0.5 ‰ (mean±1SD); Hunsinger et al., 2010). The within-run precision of IAEA-CH-3 $\delta^{18}O$ was ≤0.2 ‰ (1 SD). Standards were included at an interval of every eight samples. For the other species (*Tachigali*, *Amburana*, *Peltogyne*, *Bertholletia*, *Cedrelinga, Couratari* and *Polylepis*) $^{18}O/^{16}O$ ratios were measured in SEE at the University of Leeds, using continuous flow mass-spectrometry. Cellulose samples were thermally decomposed in an Elementar Vario Pyrocube in the absence of oxygen at 1450 °C, prior to analysis by an Isoprime continuous flow mass spectrometer. $^{18}O/^{16}O$ ratios were converted to $\delta^{18}O$ values versus VSMOW with reference to cellulose from Sigma-Aldrich, UK (Lot#SLBD2972V; for clarity hereafter referred to as Leeds Sigma cellulose). The Leeds Sigma cellulose was analysed at SEE against IAEA-CH-3 cellulose (assuming $\delta^{18}O$=+31.9±0.5 ‰; Hunsinger et al., 2010) and assigned a value of 29.2±0.2 ‰. Standards were included at an interval of every twelve samples. The "reference" $\delta^{18}O_{TR}$ chronology from Brienen et al (2012; hereafter referred to as *Cedrela*$_{2012}$) was analysed at GFZ utilising a "low" temperature pyrolysis (1080 °C) in an element analyser (Carlo Erba) coupled to an OPTIMA (Micromass Ltd., UK) IRMS. Two standards, IAEA-CH-3 and Merck

cellulose (Darmstadt, Germany), were included at an interval of every eight samples. At the time, their $\delta^{18}O$ values were defined as +32.6±0.3 ‰ and +28.7±0.3 ‰ (Boettger et al., 2007). This method is no longer in use at GFZ. Currently, a ThermoFinnigan (Bremen, Germany) TC/EA set to 1400 °C, coupled to a Delta V Advantage IRMS is utilized. Re-analysis of IAEA-CH-3 and Merck cellulose resulted in $\delta^{18}O$ values of +32.95±0.3 ‰ and +28.20±0.3 ‰ respectively, after calibration against a different batch of Sigma-Aldrich cellulose (Lot#92F0243; +27.3 ±0.3 ‰, Boettger et al., 2007, Loader et al., 2015), IAEA-601 (benzoic acid; $\delta^{18}O$ = +23.15±0.3 ‰) and IAEA-602 (benzoic acid; $\delta^{18}O$ = +71.28±0.5 ‰; Brand et al., 2009). For an inter-laboratory comparison, the Leeds Sigma-Aldrich cellulose was analysed at each of the labs, yielding the following values: +29.1±0.2 ‰ (NIGF; n=23), +29.2±0.2 ‰ (SEE; n=20), and +30.2±0.35 ‰ (GFZ; n=17). Note that the ca. 1 ‰ offset between Leeds Sigma cellulose analysed at GFZ and the other two laboratories is consistent with the ca. 1 ‰ difference between the $\delta^{18}O$ values assigned to IAEA-CH-3. Hence the *Cedrela*$_{2012}$ chronology measured at GFZ is likely to be offset by approximately 1 ‰ from the other datasets. However, we abstained from applying a correction to *Cedrela*$_{2012}$ as interannual variance of $\delta^{18}O$ is of greater importance in this study than absolute values.

4.2.4 Dating calibration and radiocarbon verification

Exact dating of tree rings is a necessity for palaeoclimate reconstructions. In tree rings this is often done by matching ring-width patterns between dated and undated chronologies, also called crossdating (Speer, 2010). Dating of tropical tree rings through this technique poses a particular challenge, as ring anatomy is often less clear in comparison with temperate trees, and regularly presents wedging (locally absent) or false rings (e.g. Priya and Bhat, 1998, Worbes, 2002). In addition, interannual variation in climate may not be the main driver of variation in growth, thus resulting in low common signals in ring width, and poor crossdating statistics (Brienen and Zuidema, 2005). Here we use a different approach to correct for dating errors, through crossdating the isotope series from each species with an established isotope chronology. The method and approach are outlined below.

First, tree rings were cross-dated using the standard ring-width approach: rings were marked and visually cross-dated across 2–4 radii on intact discs, ensuring every

tenth ring interconnected between radii to detect errors. Rings were measured and a quality control was conducted using correlation analysis (program COFECHA; Grissino-Mayer, 2001, Holmes, 1983). Ring-width series were de-trended using a flexible cubic spline method, and a tree-ring chronology was built with ARSTAN, only using series that passed the quality control. For several species, inter-tree correlations were low (r<0.3; Brienen and Zuidema, 2005), and they presented a varying degree of problems during crossdating using standard ring-width. As a result, for most species only approximately half of the trees were incorporated in the ring-width chronologies. For full details see Brienen and Zuidema, (2005).

Second, $\delta^{18}O_{TR}$ records developed in this study were aligned against the published *C. odorata* $\delta^{18}O_{TR}$ chronology from Brienen et al. (2012, i.e. *Cedrela*$_{2012}$). We initially performed a visual comparison, allowing the identification of tree-ring sections where mistakes in the original dating could have been made due to missing rings or the inclusion of false rings. The original sample of wood was then re-inspected to see whether any rings had been missed (to support adding in a ring), or falsely identified (to support ring deletion from the series; see Table 4.3). Curves were only shifted if wood anatomical features in the original sample suggested false or wedging rings.

Finally, the dating of the newly aligned chronologies was verified using radiocarbon "bomb-peak" dating for species *Bertholletia*, *Couratari*, *Amburana*, *Peltogyne* and *Cedrelinga*. This methodology utilizes the near doubling of atmospheric ^{14}C during the nuclear tests of the 1960s to date modern organic material (e.g. Worbes and Junk, 1989). Cellulose extracted from the rings dated as 1975 (using the isotope crossdating approach described above) were analysed in Bothell, USA by DirectAMS. The ^{14}C concentrations were normalized to a value of $\delta^{13}C$=–25 ‰ to correct for isotopic fractionation during photosynthesis. The SHCal13 radiocarbon calibration curve from Hogg et al. (2013) was used alongside the bomb extension curve from Hua et al. (2013) to convert pMC (per cent Modern Carbon) values to actual calendar dates using the free online CALIBomb software (http://calib.qub.ac.uk). Calendar dates were assigned to rings according to the year in which the growth started. Thus, the ring spanning calendar years 1975 to 1976 is here called 1975. The original and adjusted tree-ring dates of all the trees analysed in this study are presented in Appendix 4.1,

together with plots showing the original and adjusted data series of those trees where dating changes were applied.

4.2.5 Statistical analysis

Using the $\delta^{18}O_{TR}$ data from the nine *Cedrela* trees, we constructed an isotope chronology for the period 1901–2001 (hereafter referred to as *Cedrela$_{2015}$)*. The minimum number of samples at any point along the chronology is three. "Expressed Population Signal" (EPS) values were calculated according to Wigley et al. (1984), using the formula $(N*r_{mean})/(1+(N-1)*r_{mean})$, where N is the number of time series and r_{mean} is the mean inter-series correlation coefficient. An EPS threshold of 0.85 is generally used to determine whether individual tree-level (<0.85) or stand-level (>0.85) signals dominate a chronology (Wigley et al., 1984). We correlated the *Cedrela$_{2015}$* chronology with the *Cedrela$_{2012}$* chronology, and the different species' $\delta^{18}O_{TR}$ records were correlated with either *Cedrela$_{2012}$* or *Cedrela$_{2015}$*, depending on which was geographically closest to the sample site of that species. The *Polylepis* series was also compared with the Navado Sajama ice-core record (data extracted from Hardy et al., 2003), and the published *Polylepis* $\delta^{18}O_{TR}$ chronology from Ballantyne et al. (2011). All correlations used the "Pearson's product-moment correlation" method and were calculated in the statistical program *R* (R Development Core Team, 2015). This method uses the formula $r_{XY} = (cov(X,Y))/(\sigma_X\sigma_Y)$ where r_{XY} is the correlation coefficient, cov is the covariance and σ_X and σ_Y are the standard deviations of the time series X and Y respectively. To visualise decadal trends, a second order, low-pass Butterworth filter with a cut-off frequency of 0.2 was applied in both the forward and reverse directions for each series, using the *R* package "signal" (Ligges et al., 2015).

4.3 Results and Discussion

4.3.1 Crossdating tree-ring oxygen isotope series

Radiocarbon dating proves that $\delta^{18}O$ can be used to date tree rings more accurately than simple ring counting (Table 4.2). For three out of the five species tested for radiocarbon (*Couratari*, *Amburana*, and *Cedrelinga*) the $\delta^{18}O_{TR}$-adjusted ring dates match the radiocarbon age estimates. For these species mistakes made during the initial

Table 4.2 – "Bomb-peak" radiocarbon dating results. Calendar dates were assigned to tree rings according to the year in which the growth started. Thus, a ring may be correctly dated if the radiocarbon age estimate encompasses the $\delta^{18}O_{TR}$-adjusted age estimate plus one year. Per cent Modern Carbon (pMC) values were converted to calendar dates using the free online CALIBomb software (http://calib.qub.ac.uk).

Species	$\delta^{13}C$	pMC	1 σ error	Ring counting age estimate	$\delta^{18}O_{TR}$-adjusted age estimate	Radiocarbon age (1SD)	Radiocarbon age (2SD)	Correctly dated?
Couratari	–22.9	134.73	0.37	1979	1975	1976.5–1977	1976–1978	Yes
Amburana	–21.2	135.16	0.36	1979	1975	1976–1977	1975.5–1978	Yes
Cedrelinga	–20.5	136.81	0.37	1978	1975	1975.5–1976.5	1974.5–1976.5	Yes
Bertholletia	–23.0	146.51	0.38	1975	1975	1973	1972.5–1974	1–4 years out
Peltogyne	–21.6	159.81	0.42	1975	1975	1964 or 1967	1964 or 1967–8	7–12 years out

ring counting were correctly identified through comparison of their $\delta^{18}O_{TR}$-series with the *Cedrela*$_{2012}$ reference chronology. The validation of this technique is an important result, since it shows that $\delta^{18}O_{TR}$ can help with the detection of false or missing rings, potentially offering a simple way to correct for minor dating inaccuracies. The ability to precisely crossdate $\delta^{18}O_{TR}$ series over different sites and species could also facilitate the construction of new chronologies. A similar method was used to date dead tropical wood through crossdating high-resolution $\delta^{13}C$ series with precipitation records (Fichtler et al., 2010), and other tropical studies have highlighted the utility of high-resolution isotope measurements in cases where ring detection is difficult (e.g. Boysen et al., 2014, Pons and Helle, 2011) or rings are not visible at all (e.g. Anchukaitis and Evans, 2010, Poussart et al., 2004). In a comparison of pine and oak $\delta^{18}O_{TR}$ from Japan, Li et al. (2015) suggest that oxygen isotopes can also be used to crossdate between angiosperm and gymnosperm species. Nevertheless, crossdating interannual $\delta^{18}O_{TR}$ variability with an established chronology for dating verification has not, to the best of our knowledge, been previously applied in a tropical context.

For all species, except *Tachigali* and *Polylepis*, our analysis indicates that rings must have been missed during the initial ring counting based purely on macroscopical wood anatomy (i.e., before comparison of the oxygen isotope series with the reference chronology, see Table 4.3). The exact number of rings missed in the *Bertholletia* record is unknown, although radiocarbon dating suggests a disparity of 1–4 years up to 1975. It was not possible to use $\delta^{18}O_{TR}$ to correct the dating of *Bertholletia* or *Peltogyne*, as these species showed a low degree of synchronicity with the reference isotope curve

making curve fitting impossible. Of all the species *Peltogyne* and *Couratari* had the highest number of dating errors, as revealed by radiocarbon dating (Table 4.3). For *Peltogyne* 13 rings were missed in the outermost part of the sample, the sapwood, where rings are markedly less distinct (Brienen and Zuidema, 2005), while for *Couratari* eight rings were identified which had been missed during the original mark-up, predominantly in sections with reduced ring visibility, or where rings were very narrow. Additional mistakes arose due to misidentification of resin bands as rings, particularly in *Cedrela*, a species that is known to form non-annual resin bands (Dünisch et al., 2002). These problems in ring dating using only standard, anatomical ring detection methods confirm the continuing challenges in tropical tree-ring analysis (Groenendijk et al., 2014, Stahle, 1999).

Table 4.3 – Errors during analysis of tree rings in different tropical species. Dating corrections were applied following verification from radiocarbon (^{14}C) analysis. Columns indicate the number of rings that were inserted or deleted based on comparison of the respective $\delta^{18}O_{TR}$ series with the reference *Cedrela*$_{2012}$ $\delta^{18}O_{TR}$ chronology, or corrections made due to ^{14}C dating (only for *Peltogyne*). The mistake rate was calculated by dividing the number of corrected rings by the length of the series.

Species	Record period	Dating with $\delta^{18}O_{TR}$		Radiocarbon dating		Mistake rate
		Rings inserted	Rings deleted	Rings inserted	Rings deleted	
Cedrela						
Tree 11	1920–2010	1	3	-	-	0.0444
Tree 12	1941–2010	0	0	-	-	0
Tree 13	1915–2010	2	1	-	-	0.0316
Tree 14	1908–2010	0	3	-	-	0.0294
Tree 16	1884–2010	0	0	-	-	0
Tree 20	1904–2010	4	3	-	-	0.0660
Tree 21	1898–2010	0	1	-	-	0.00893
Tree 23	1897–2010	8	1	-	-	0.0796
Tree 27	1903–2010	0	0	-	-	0
Tachigali	1990–2002	0	0	-	-	0
Amburana	1897–2000	2	0	0	0	0.0194
Couratari	1892–2008	8	0	0	0	0.0690
Peltogyne	1929–1990	-	-	13	0	0.2131
Cedrelinga	1950–1999	3	0	0	0	0.0612
Bertholletia	1896–2001	-	-	-	-	?
Polylepis	1931–2002	0	0	-	-	0

4.3.2 *Cedrela* chronology

The nine *Cedrela* trees from Selva Negra show high synchronicity in their $\delta^{18}O_{TR}$ (Fig. 4.2; mean inter-tree correlation (r_{mean}) for 1901–2001 is 0.71), and a high "Expressed Population Signal" (EPS; Wigley et al., 1984) of 0.96, suggesting that $\delta^{18}O_{TR}$ is dominated by a strong external control (N.B. EPS calculated using the raw, unadjusted series = 0.73). The signal becomes noisier further back in time, most likely due to an accumulation of undetected dating errors. This has been observed before in tropical $\delta^{18}O_{TR}$ records (e.g. van der Sleen et al., 2015). The r_{mean} and EPS values for the *Cedrela* record presented here are highly comparable with the results for *Cedrela*$_{2012}$ (Brienen et al., 2012; r_{mean}=0.63, EPS=0.97, 1900–2001), and suggest similar drivers to the *Cedrela*$_{2012}$ chronology, i.e. $\delta^{18}O_P$ (Brienen et al. 2012). It indicates that *Cedrela* is a well-suited species for reconstructing $\delta^{18}O_P$. *Cedrela* trees are shallow-rooted and favour sites with good drainage (Cintron 1990), using water from the top 30 cm of the soil profile (Schwendenmann et al., 2014). We thus expect $\delta^{18}O_{TR}$ of *Cedrela* to predominantly reflect the isotopic composition of recent rainfall, and be only minimally influenced by groundwater, which could potentially dampen the interannual variability of the chronology.

In contrast to $\delta^{18}O_{TR}$, inter-tree correlation and EPS values for tree-ring width were much lower for the nine *Cedrela*$_{2015}$ trees (r_{mean}=0.17, EPS=0.64). This has been found for other tree species across the tropics. For example, *Fokienia hodginsii* in Laos (Xu et al., 2011), *Entandrophragma utile* in Cameroon (van der Sleen et al., 2015) and *Mimosa acantholoba* in Mexico (Brienen et al., 2013) all show better coherence in $\delta^{18}O_{TR}$ than in growth. These studies show that in the tropics $\delta^{18}O_{TR}$ are often more sensitive than ring width to external climate forcings, and therefore make a better climate proxy. One exception is *Tectona grandis* (teak) in Indonesia, where inter-tree synchronization in $\delta^{18}O_{TR}$ and ring width are more comparable (e.g. Poussart et al., 2004, Schollaen et al., 2013).

Given the high cost of isotope measurements it is of interest to quantify the minimum number of trees needed to establish a robust $\delta^{18}O_{TR}$ chronology. An EPS above 0.85 has been suggested to imply good internal coherence, with the minimum number of cores needed to exceed this threshold dependent on the strength of the common signal (i.e. when the inter-series correlation is low, more cores are required to

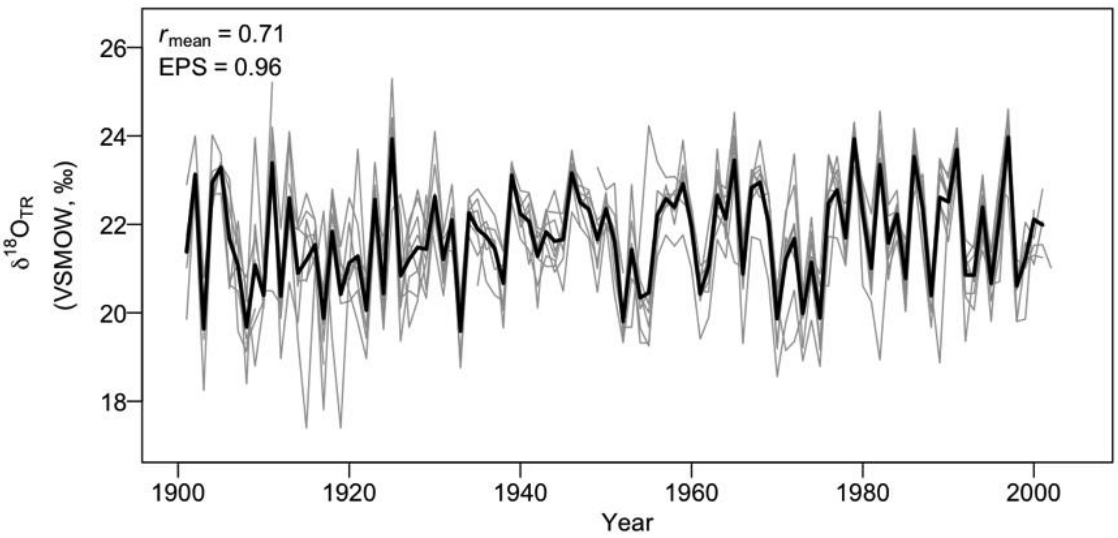

Figure 4.2 – $\delta^{18}O_{TR}$ time series from nine *Cedrela odorata* trees from Selva Negra, Bolivia. Grey lines represent individual trees, and the black line shows the mean composite chronology from 1901 to 2001. The mean inter-tree correlation for the period 1901–2001 is 0.71 and the Expressed Population Signal (EPS) is 0.96.

build a satisfactory chronology; Wigley et al., 1984). The results of *Cedrela* imply that this threshold would have been exceeded with just three trees when using $\delta^{18}O_{TR}$. In contrast, to create a standard ring-width chronology approximately 28 trees would have been required to reach an EPS of 0.85 (see Cook and Kairiukstis, 1990).

4.3.3. Inter-specific coherence in tree-ring oxygen isotopes

The $\delta^{18}O_{TR}$ records of five of the six lowland species showed significant correlations with the closest *Cedrela* $\delta^{18}O_{TR}$ chronology (Fig. 4.3). Only *Bertholletia* showed no significant relationship (r=–0.15, p=0.14, 1901–2001, n=96). Although the *Tachigali* series only spans a short period (13 years), it showed the strongest relationship with *Cedrela*$_{2015}$ (r=0.90, p<0.001, 1990–2001, n=13), approximately 100 km away. *Peltogyne* also correlated quite well with *Cedrela*$_{2015}$ (r=0.39, p<0.01, 1929–1990, n=60), but had a stronger relationship with the *Cedrela*$_{2012}$ curve from the more distant Purisima site (r=0.58, p<0.001, 1929–1990, n=60). *Amburana* also correlated well with *Cedrela*$_{2012}$ from the same location (r=0.41, p<0.001, 1901–2000, n=98). The relationship between *Cedrelinga* and *Cedrela*$_{2015}$ was slightly weaker (r=0.33, p<0.05, 1950–1999, n=50), as was the correlation between *Couratari* and *Cedrela*$_{2015}$ (r=0.27, p<0.05, 1901–2001, n=89). These close inter-species relationships most likely arise from a dominant imprint of interannual variation in $\delta^{18}O_P$ on $\delta^{18}O_{TR}$, via a strong influence of $\delta^{18}O_S$.

Correlations between the different lowland tree species were also evaluated. *Bertholletia* was excluded from the analysis due to the uncertainties with regard to its dating precision. The mean inter-species correlation coefficient for six species including *Cedrela*$_{2015}$ is 0.37. This value is slightly higher than that found by Saurer et al. (2008) for trees in a temperate region (r_{mean}=0.23), comparing records from sites with smaller distances between them (<160 km vs. <325 km in this study). The observed differences in correlations between these studies can possibly be explained by higher levels of precipitation during the growing season for our Amazon site compared to the temperate study, thus reducing the influence of residual soil water which may dampen variation in $\delta^{18}O_S$ (Treydte et al., 2014). In addition, the sites in the Saurer et al. (2008) study are situated in a heterogeneous mountainous environment with varying altitudes (480–1400 m.a.s.l.), and as $\delta^{18}O_P$ varies strongly with altitude (Dansgaard, 1964), this may explain the lower correspondence between their trees.

Despite showing similar trends in $\delta^{18}O_{TR}$, we observed a degree of variation between the isotope series for the different species. The two most likely causes for this variation are differences in partitioning of water sources between species, and species-specific differences in plant physiology. Differences in partitioning of water sources arise due to differences in rooting structure/depth (spatial partitioning), due to differences between species' growing season, or due to timing of wood formation (temporal partitioning). Rooting depth affects $\delta^{18}O_S$ due to the existence of isotopic gradients in soil water. These arise from surface evaporation enriching the isotope signal at the surface, and mixing of precipitation with residual pools of groundwater in lower soil layers (Ehleringer and Dawson, 1992, Tang and Feng, 2001). While model simulation experiments suggest that the influence of soil evaporation on $\delta^{18}O_{TR}$ is likely to be minimal in the Amazon basin (Kanner et al., 2014), xylem water $\delta^{18}O$ of tropical trees in Panama show inter-species variation up to 7 ‰, reflecting downward isotopic gradients in soil water, and differences between species in water uptake depth (Schwendenmann et al., 2014). For the species in this study, little is known about the rooting depth (Table 4.1), but differences in phenology may provide some indication. Retention of leaves during the dry season could indicate that trees have access to deeper groundwater (Borchert, 1994, Jackson et al., 1995, Schwendenmann et al., 2014), and

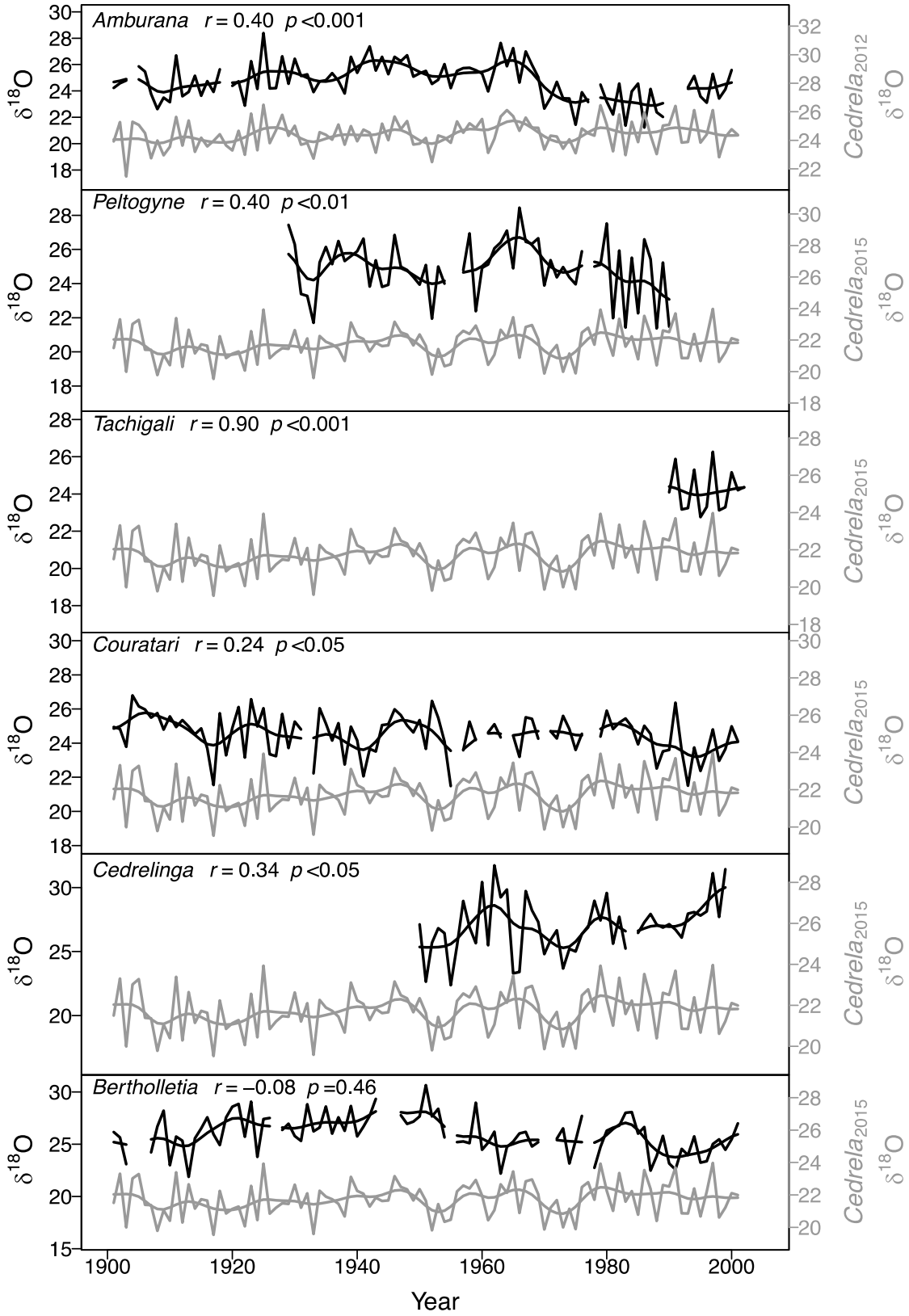

Figure 4.3 – Comparing $\delta^{18}O_{TR}$ signatures between tropical tree species. Grey lines show *Cedrela* $\delta^{18}O_{TR}$ signatures and black lines show $\delta^{18}O_{TR}$ signatures in six other tropical tree species. Pearson correlation coefficients and significance levels are shown at the top of each panel. In some cases, records are discontinuous because there was insufficient sample material for isotope analysis in years with very narrow rings. A low-pass Butterworth filter was applied to each series to visualise decadal variation.

water uptake from deeper soil layers during this dry period may affect the interannual $\delta^{18}O$ signal recorded in cellulose. For example, *Cedrelinga,* which is brevi-deciduous with a gradual turnover of leaves at the end of the dry season (Brienen and Zuidema, 2005), showed only a weak correlation with *Cedrela*.

In addition to spatial partitioning of source water, species may also vary in timing of their water uptake and wood formation through the year. This temporal partitioning may be as important, since seasonal variation in $\delta^{18}O_P$ is large in Bolivia (i.e. approx. 9 ‰, data from the Global Network of Isotopes in Precipitation (GNIP; see also Brienen et al., 2012), and studies elsewhere have shown that such variability can be reflected in $\delta^{18}O_{TR}$ (e.g. Schollaen et al., 2013). Differences in timing of water uptake and wood formation could mean species record $\delta^{18}O_P$ over slightly different timeframes. *Amburana* and *Cedrela* are strictly deciduous, with defoliation occurring from July to October for both species (Brienen and Zuidema, 2005). These species are therefore likely to use water during the same period in the year, possibly causing the good correspondence between their $\delta^{18}O_{TR}$ records. *Bertholletia*, another deciduous species, showed no relationship with the *Cedrela* $\delta^{18}O_{TR}$ record at interannual or decadal timescales, but this may be because it retains its leaves well into the start of the dry season, suggesting it may grow for longer and use water from the start of the dry season. This could also be true for the other brevi-deciduous species, which never appear completely leafless for extended periods (see Table 4.1).

Differences in plant physiology may also explain some of the variability seen between $\delta^{18}O_{TR}$ records. For example, "effective path length" (the pathway of water movement through the leaf to the site of evaporation and an important determinant of the Péclet effect), has been found to drive variation in $\delta^{18}O_L$ within and between species (e.g. Kahmen et al., 2008, Song et al., 2013). In addition, interspecific variation in transpiration rates and transpiration responses to changes in relative humidity (RH) may affect the degree to which variation in $\delta^{18}O_S$ is maintained in $\delta^{18}O_{TR}$ for the different species. For example, leaf water enrichment may have a relatively greater influence on $\delta^{18}O_{TR}$ than source water influences for those species with generally lower transpiration rates, or for species whose growing season extends into the dry season when RH is expected to be lower. This may be another reason why *Bertholletia* shows no

correlation with *Cedrela* $\delta^{18}O_{TR}$. However, exchange of oxygen atoms between cellulose-precursors and non-enriched stem water during phloem loading (Gessler et al., 2013) and/or cellulose synthesis (Song et al., 2013) reinforces the signature of source water on $\delta^{18}O_{TR}$ such that short-term variation in $\delta^{18}O_L$ may not be reflected in the final $\delta^{18}O_{TR}$ signal (Treydte et al., 2014). The extent of exchange may vary between species, and is thought to explain why oak $\delta^{18}O_{TR}$ records from Japan showed lower sensitivity to changes in RH than pine $\delta^{18}O_{TR}$ records (Li et al., 2015). The degree of exchange is positively related to the time between carbohydrate production in the leaf and cellulose synthesis in the stem (i.e the turnover time of carbohydrates, Song et al., 2014a), and may itself vary considerably between species. These physiological processes may all contribute, in part, to the variation observed between $\delta^{18}O_{TR}$ records in this study.

4.3.4 Spatial coherence of oxygen isotopes in tree rings

Despite the considerable distance between sites (approx. 325 km), there is a strong correlation between the *Cedrela*$_{2015}$ chronology and the published *Cedrela*$_{2012}$ record (Brienen et al., 2012; Fig. 4.4; r=0.80, p<0.001, 1901–2001, n=101). This suggests that factors influencing $\delta^{18}O_{TR}$ in this part of the Amazon basin are acting at a large scale. Poussart et al. (2004) also report synchronization of $\delta^{18}O_{TR}$ in two *Samanea saman* trees thought to be from different forests in Java, Indonesia, although the precise origins of the trees are unknown. A strong correlation between $\delta^{18}O_{TR}$ records from relatively distant sites can arise from either a strong source water signal, or spatially coherent changes in RH influencing transpiration and thus the Péclet number and $\delta^{18}O_L$ (see section 4.1). Since RH depends on local climate conditions and may thus vary over short distances, we expect that the common interannual variation between the two chronologies is mostly driven by a dominant source water influence on $\delta^{18}O_{TR}$. Assuming that plant source water is predominantly recent precipitation, as opposed, for example, to groundwater, the strong coherence between these *Cedrela* records also reveals that $\delta^{18}O_P$ is itself coherent over wide areas. Thus $\delta^{18}O_P$ in the study region is primarily controlled by large-scale processes, such as Rayleigh rainout (continental effect) and evaporative recycling during moisture transport to the site of precipitation, rather than a local amount effect (Dansgaard, 1964, Salati et al., 1979, Rozanski et al., 1993). This hypothesis was previously suggested by Brienen et al. (2012), based on

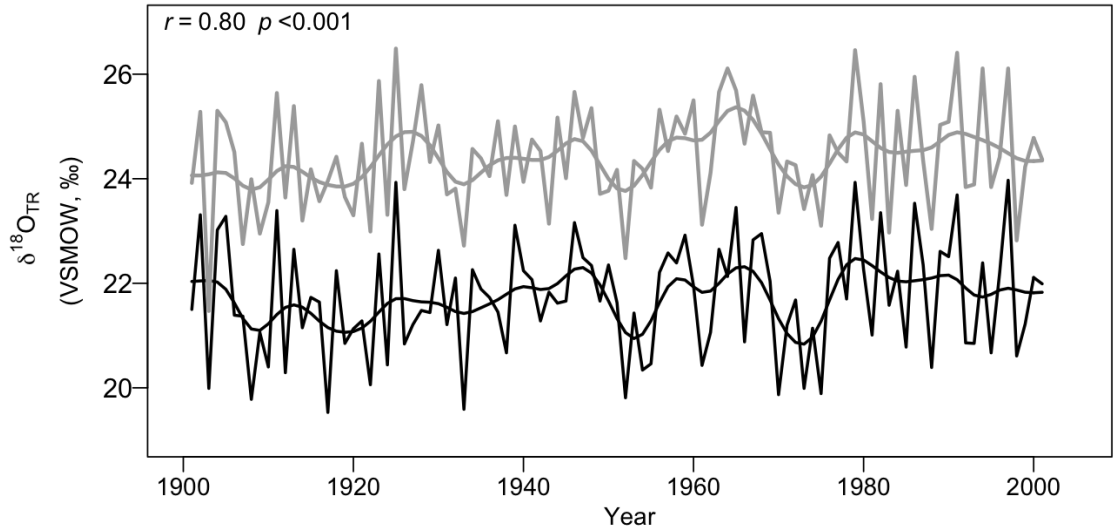

Figure 4.4 – A comparison of *Cedrela* $\delta^{18}O_{TR}$ chronologies from two distant sites in Bolivia. Interannual variation in the *Cedrela*$_{2015}$ chronology from Selva Negra is shown in black, and variation in the *Cedrela*$_{2012}$ chronology from Purisima is shown in grey (record from Brienen et al., 2012). The Pearson correlation coefficient is 0.80 for the full period, 1901–2001. A low-pass Butterworth filter was applied to each series to visualise decadal variation.

comparisons of $\delta^{18}O_{TR}$ with $\delta^{18}O_P$ records from the basin (from GNIP), and with local and basin-wide climate.

Further support for spatial coherence in $\delta^{18}O_{TR}$ comes from a comparison of the Altiplano *Polylepis* record and the lowland *Cedrela*$_{2015}$ chronology. The correlation between these two records is significant, but much weaker than the correlation between the two lowland *Cedrela* chronologies (i.e. r=0.39, p<0.01, 1931–2001, n=71). A weaker correlation is expected for several reasons. Firstly, the two records are simply further apart (approx. 1000 km). Secondly, *Polylepis* grows in the Altiplano, a very dry plateau with an average height of approximately 3800 m, and the factors controlling $\delta^{18}O_{TR}$ are likely to differ between the lowland and the highland trees. Thirdly, while the dominant source of moisture for the Altiplano is the Amazon basin (Garreaud, 2000), orographic precipitation as air masses rise over the foothills of the Andes will increase the rainout of heavy isotopes (i.e. the "altitude effect"; Dansgaard, 1964, Grootes et al., 1989, Rozanski et al., 1993), and subsequent transport of moisture over approximately 200 km of dry, high-altitude desert will further alter Altiplano $\delta^{18}O_P$ in comparison with the Amazon. These additional alterations to the $\delta^{18}O$ signal of moisture originating from the Amazon probably explain the greater variability in the Altiplano series (i.e. standard deviation for *Polylepis* is 2.3 ‰ vs. 1.07 ‰ for *Cedrela*). The

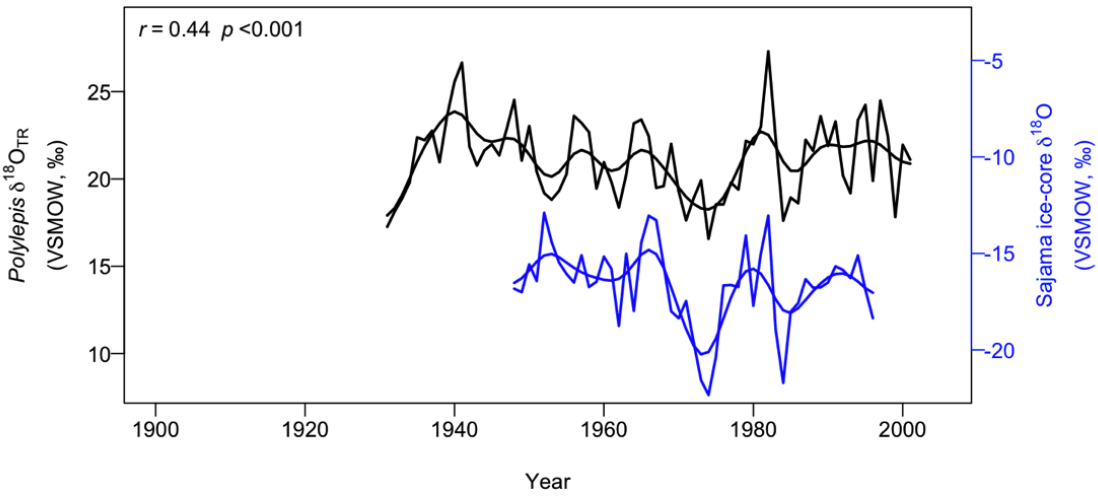

Figure 4.5 – A comparison of tree-ring and ice-core $\delta^{18}O$ records from the Altiplano. The *Polylepis* $\delta^{18}O_{TR}$ record is shown in black and the Sajama ice-core $\delta^{18}O$ record is shown in blue. The Pearson correlation coefficient is 0.44 for the period 1948–1996. A low-pass Butterworth filter was applied to each series to visualise decadal variation.

Polylepis series was also found to correlate with two other Altiplano isotope series: the nearby Nevado Sajama ice-core $\delta^{18}O$ record (r=0.44, p<0.001, 1948–1996, n=49; Fig. 4.5) and a *Polylepis* $\delta^{18}O_{TR}$ record from Volcan Granada, Argentina, approximately 500 km to the south (r=0.30, p<0.05, n=67; Ballantyne et al., 2011). This suggests that $\delta^{18}O_P$ retains a reasonable degree of coherence over the plateau. The spatial coherence of $\delta^{18}O$ records from distant sites provides further evidence for a broad common signal in $\delta^{18}O_P$, extending from the Amazon basin to the Altiplano, and confirms the interpretation of highland $\delta^{18}O$ records such as ice cores as, at least partially, a record of precipitation over the Amazon basin (Brienen et al., 2012, Hoffmann, 2003).

4.4 Conclusions

Comparison of $\delta^{18}O_{TR}$ series from eight tropical tree species from four sites ranging from lowland rainforest to the Bolivian Altiplano showed that $\delta^{18}O_{TR}$ can be used to crossdate tree-ring chronologies from the tropics with higher accuracy than simple ring-width measurements. Six of the seven lowland species analysed show matching interannual variation in $\delta^{18}O_{TR}$, suggesting they all preserve variation in source water isotopic composition. We found that $\delta^{18}O_{TR}$ records correlated well over large distances (<1000 km), which suggests a dominant influence of source water on the cellulose signal, and that $\delta^{18}O_P$ in this region is similar over large spatial scales. The

coherent imprint of $\delta^{18}O_{TR}$ across different species and sites has important implications for future studies in the Amazon, offering the potential to reconstruct $\delta^{18}O_{P,}$ and thus rainfall over a large and globally important area. In context of the recent hydrological intensification (Gloor et al., 2013) and uncertainties about the direction of future precipitation changes in the Amazon (Zhang et al., 2015), development of a network of extended $\delta^{18}O_{TR}$ records across the Amazon would be a significant step towards a better understanding of the region's complex hydrology.

4.5 References

Anchukaitis, K. J. & Evans, M. N. 2010. Tropical cloud forest climate variability and the demise of the Monteverde golden toad. *Proceedings of the National Academy of Sciences,* 107**,** 5036-5040.

Argollo, J., Soliz, C. & Villalba, R. 2004. Potencialidad dendrocronológica de *Polylepis tarapacana* en los Andes Centrales de Bolivia. *Ecología en Bolivia,* 39**,** 5-24.

Ballantyne, A. P., Baker, P. A., Chambers, J. Q., Villalba, R. & Argollo, J. 2011. Regional differences in South American monsoon precipitation inferred from the growth and isotopic composition of tropical trees. *Earth Interactions,* 15**,** 1-35.

Barbour, M. M., Roden, J. S., Farquhar, G. D. & Ehleringer, J. R. 2004. Expressing leaf water and cellulose oxygen isotope ratios as enrichment above source water reveals evidence of a Péclet effect. *Oecologia,* 138**,** 426-35.

Boettger, T., Haupt, M., Knöller, K., Weise, S. M., Waterhouse, J. S., Rinne, K. T., Loader, N. J., Sonninen, E., Jungner, H. & Masson-Delmotte, V. 2007. Wood cellulose preparation methods and mass spectrometric analyses of $\delta^{13}C$, $\delta^{18}O$, and nonexchangeable $\delta^{2}H$ values in cellulose, sugar, and starch: an interlaboratory comparison. *Analytical Chemistry,* 79**,** 4603-4612.

Borchert, R. 1994. Soil and stem water storage determine phenology and distribution of tropical dry forest trees. *Ecology,* 75**,** 1437-1449.

Boysen, B. M. M., Evans, M. N. & Baker, P. J. 2014. $\delta^{18}O$ in the tropical conifer *Agathis robusta* records ENSO-related precipitation variations. *Plos One,* 9**,** 1-9.

Brand, W. A., Coplen, T. B., Aerts-Bijma, A. T., Böhlke, J. K., Gehre, M., Geilmann, H., Gröning, M., Jansen, H. G., Meijer, H. a. J., Mroczkowski, S. J., Qi, H., Soergel, K., Stuart-Williams, H., Weise, S. M. & Werner, R. A. 2009. Comprehensive inter-laboratory calibration of reference materials for $\delta^{18}O$ versus VSMOW using various on-line high-temperature conversion techniques. *Rapid Communications in Mass Spectrometry,* 23**,** 999-1019.

Brienen, R. J. W. & Zuidema, P. A. 2005. Relating tree growth to rainfall in Bolivian rain forests: a test for six species using tree ring analysis. *Oecologia,* 146**,** 1-12.

Brienen, R. J. W. & Zuidema, P. A. 2006. Lifetime growth patterns and ages of Bolivian rain forest trees obtained by tree ring analysis. *Journal of Ecology,* 94**,** 481-493.

Brienen, R. J. W., Helle, G., Pons, T. L., Guyot, J. L. & Gloor, M. 2012. Oxygen isotopes in tree rings are a good proxy for Amazon precipitation and El Niño-Southern Oscillation variability. *Proceedings of the National Academy of Sciences,* 109**,** 16957-16962.

Brienen, R. J. W., Hietz, P., Wanek, W. & Gloor, M. 2013. Oxygen isotopes in tree rings record variation in precipitation $\delta^{18}O$ and amount effects in the south of Mexico. *Journal of Geophysical Research: Biogeosciences,* 118**,** 1604-1615.

Briffa, K. R. 1999. Interpreting high-resolution proxy climate data - the example of dendroclimatology. *Analysis of Climate Variability.* Springer.

Cintron, B. B. 1990. *Cedrela odorata* L. Cedro hembra, Spanish cedar. *Silvics of North America,* 2**,** 250.

Cook, E. R. & Kairiukstis, L. A. 1990. *Methods of dendrochronology: applications in the environmental sciences*, Dordrecht, The Netherlands, Kluwer Academic Publishers.

Dansgaard, W. 1964. Stable isotopes in precipitation. *Tellus,* 16**,** 436-468.

Domic, A. I. & Capriles, J. M. 2009. Allometry and effects of extreme elevation on growth velocity of the

Andean tree *Polylepis tarapacana* Philippi (Rosaceae). *Plant Ecology,* 205**,** 223-234.
Dünisch, O., Bauch, J. & Gasparotto, L. 2002. Formation of increment zones and intraannual growth dynamics in the xylem of *Swietenia macrophylla*, *Carapa guianensis*, and *Cedrela odorata* (Meliaceae). *IAWA Journal,* 23**,** 101-120.
Ehleringer, J. & Dawson, T. 1992. Water uptake by plants: perspectives from stable isotope composition. *Plant, Cell and Environment,* 15**,** 1073-1082.
Farquhar, G. & Lloyd, J. 1993. Carbon and oxygen isotope effects in the exchange of carbon dioxide between terrestrial plants and the atmosphere. *Stable isotopes and plant carbon-water relations,* 40**,** 47-70.
Fichtler, E., Helle, G. & Worbes, M. 2010. Stable-carbon isotope time series from tropical tree rings indicate a precipitation signal. *Tree-Ring Research,* 66**,** 35-49.
Garreaud, R. 2000. Intraseasonal variability of moisture and rainfall over the South American Altiplano. *Monthly Weather Review,* 128**,** 3337-3346.
Gessler, A., Brandes, E., Keitel, C., Boda, S., Kayler, Z. E., Granier, A., Barbour, M., Farquhar, G. D. & Treydte, K. 2013. The oxygen isotope enrichment of leaf-exported assimilates–does it always reflect lamina leaf water enrichment? *New Phytologist,* 200**,** 144-157.
Gloor, M., Brienen, R. J. W., Galbraith, D., Feldpausch, T. R., Schöngart, J., Guyot, J. L., Espinoza, J. C., Lloyd, J. & Phillips, O. L. 2013. Intensification of the Amazon hydrological cycle over the last two decades. *Geophysical Research Letters,* 40**,** 1729-1733.
Grissino-Mayer, H. D. & Fritts, H. C. 1997. The International Tree-Ring Data Bank: an enhanced global database serving the global scientific community. *The Holocene,* 7**,** 235-238.
Grissino-Mayer, H. D. 2001. Evaluating crossdating accuracy: a manual and tutorial for the computer program COFECHA. *Tree-Ring Research,* 57**,** 205-221.
Groenendijk, P., Sass-Klaassen, U., Bongers, F. & Zuidema, P. A. 2014. Potential of tree-ring analysis in a wet tropical forest: A case study on 22 commercial tree species in Central Africa. *Forest Ecology and Management,* 323**,** 65-78.
Grootes, P., Stuiver, M., Thompson, L. & Mosley-Thompson, E. 1989. Oxygen isotope changes in tropical ice, Quelccaya, Peru. *Journal of Geophysical Research: Atmospheres,* 94**,** 1187-1194.
Hardy, D., Vuille, M. & Bradley, R. 2003. Variability of snow accumulation and isotopic composition on Nevado Sajama, Bolivia. *Journal of Geophysical Research: Atmospheres* 108**,** 4693.
Hill, S., Waterhouse, J., Field, E., Switsur, V. & Ap Rees, T. 1995. Rapid recycling of triose phosphates in oak stem tissue. *Plant, Cell and Environment,* 18**,** 931-936.
Hoffmann, G. 2003. Coherent isotope history of Andean ice cores over the last century. *Geophysical Research Letters,* 30**,** 1-4.
Hogg, A. G., Hua, Q., Blackwell, P. G., Niu, M., Buck, C. E., Guilderson, T. P., Heaton, T. J., Palmer, J. G., Reimer, P. J., Reimer, R. W., Turney, C. S. & Zimmerman, S. R. 2013. SHCal13 Southern Hemisphere calibration, 0–50,000 years cal BP. *Radiocarbon,* 55**,** 1889-1903.
Holmes, R. L. 1983. Computer-assisted quality control in tree-ring dating and measurement. *Tree-Ring Bulletin,* 43**,** 69-78.
Hua, Q., Barbetti, M. & Rakowski, A. Z. 2013. Atmospheric radiocarbon for the period 1950–2010. *Radiocarbon,* 55**,** 2059-2072.
Hunsinger, G. B., Hagopian, W. M. & Jahren, A. H. 2010. Offline oxygen isotope analysis of organic compounds with high N: O. *Rapid Communications in Mass Spectrometry,* 24**,** 3182-3186.
Jackson, P., Cavelier, J., Goldstein, G., Meinzer, F. & Holbrook, N. 1995. Partitioning of water resources among plants of a lowland tropical forest. *Oecologia,* 101**,** 197-203.
Kahmen, A., Simonin, K., Tu, K. P., Merchant, A., Callister, A., Siegwolf, R., Dawson, T. E. & Arndt, S. K. 2008. Effects of environmental parameters, leaf physiological properties and leaf water relations on leaf water $\delta^{18}O$ enrichment in different *Eucalyptus* species. *Plant, Cell and Environment,* 31**,** 738-751.
Kanner, L. C., Buenning, N. H., Stott, L. D., Timmermann, A. & Noone, D. 2014. The role of soil processes in $\delta^{18}O$ terrestrial climate proxies. *Global Biogeochemical Cycles,* 28**,** 239-252.
Leite, E. J. 2005. State-of-knowledge on *Amburana cearensis* (Fr. Allem.) AC Smith (Leguminosae: Papilionoideae) for genetic conservation in Brazil. *Journal for Nature Conservation,* 13**,** 49-65.
Li, Z., Nakatsuka, T. & Sano, M. 2015. Tree-ring cellulose $\delta^{18}O$ variability in pine and oak and its potential to reconstruct precipitation and relative humidity in central Japan. *Geochemical Journal,* 49**,** 125-137.
Ligges, U., Short, T., Kienzle, P., Schnackenberg, S., Borchers, H.-W., Carezia, A., Dupuis, P., Eaton, J. W., Farhi, E., Habel, K., Hornik, K., Krey, S., Lash, B., Leisch, F., Mersmann, O., Neis, P.,

Ruohio, J., Smith Iii, J. O., Stewart, D. & Weingessel, A. 2015. Package 'signal': signal processing.

Loader, N. J., Street-Perrott, F. A., Daley, T. J., Hughes, P. D. M., Kimak, A., Levanič, T., Mallon, G., Mauquoy, D., Robertson, I., Roland, T. P., Van Bellen, S., Ziehmer, M. M. & Leuenberger, M. 2015. Simultaneous Determination of Stable Carbon, Oxygen, and Hydrogen Isotopes in Cellulose. *Analytical Chemistry,* 87**,** 376-380.

Marshall, J. D. & Monserud, R. A. 2006. Co-occurring species differ in tree-ring $\delta^{18}O$ trends. *Tree Physiology,* 26**,** 1055-1066.

Morales, M. S., Villalba, R., Grau, H. R. & Paolini, L. 2004. Rainfall-controlled tree growth in high-elevation subtropical treelines. *Ecology,* 85**,** 3080-3089.

Offermann, C., Ferrio, J. P., Holst, J., Grote, R., Siegwolf, R., Kayler, Z. & Gessler, A. 2011. The long way down—are carbon and oxygen isotope signals in the tree ring uncoupled from canopy physiological processes? *Tree Physiology,* 31**,** 1088-1102.

Peterson, T. C. & Vose, R. S. 1997. An overview of the Global Historical Climatology Network temperature database. *Bulletin of the American Meteorological Society,* 78**,** 2837-2849.

Pierrehumbert, R. T. 1999. Huascaran $\delta^{18}O$ as an indicator of tropical climate during the Last Glacial Maximum. *Geophysical Research Letters,* 26**,** 1345-1348.

Pons, T. L. & Helle, G. 2011. Identification of anatomically non-distinct annual rings in tropical trees using stable isotopes. *Trees,* 25**,** 83-93.

Poussart, P. F., Evans, M. N. & Schrag, D. P. 2004. Resolving seasonality in tropical trees: multi-decade, high-resolution oxygen and carbon isotope records from Indonesia and Thailand. *Earth and Planetary Science Letters,* 218**,** 301-316.

Priya, P. & Bhat, K. 1998. False ring formation in teak (*Tectona grandis* L.f.) and the influence of environmental factors. *Forest Ecology and Management,* 108**,** 215-222.

R Development Core Team 2015. R: A language and environment for statistical computing. Vienna, Austria: R Foundation for Statistical Computing.

Reynolds-Henne, C. E., Saurer, M. & Siegwolf, R. T. 2009. Temperature versus species-specific influences on the stable oxygen isotope ratio of tree rings. *Trees,* 23**,** 801-811.

Risi, C., Bony, S. & Vimeux, F. 2008. Influence of convective processes on the isotopic composition ($\delta^{18}O$ and δD) of precipitation and water vapor in the tropics: 2. Physical interpretation of the amount effect. *Journal of Geophysical Research: Atmospheres,* 113**,** 1-12.

Roden, J. S., Lin, G. & Ehleringer, J. R. 2000. A mechanistic model for interpretation of hydrogen and oxygen isotope ratios in tree-ring cellulose. *Geochimica et Cosmochimica Acta,* 64**,** 21-35.

Rozanski, K., Araguás-Araguás, L. & Gonfiantini, R. 1993. Isotopic patterns in modern global precipitation. *Climate change in continental isotopic records***,** 1-36.

Salati, E., Dall'olio, A., Matsui, E. & Gat, J. R. 1979. Recycling of water in the Amazon basin: an isotopic study. *Water Resources Research,* 15**,** 1250-1258.

Saurer, M., Cherubini, P., Reynolds-Henne, C., Treydte, K., Anderson, W. & Siegwolf, R. 2008. An investigation of the common signal in tree ring stable isotope chronologies at temperate sites. *Journal of Geophysical Research: Biogeosciences* 113**,** 1-11.

Schollaen, K., Heinrich, I., Neuwirth, B., Krusic, P. J., D'arrigo, R. D., Karyanto, O. & Helle, G. 2013. Multiple tree-ring chronologies (ring width, $\delta^{13}C$ and $\delta^{18}O$) reveal dry and rainy season signals of rainfall in Indonesia. *Quaternary Science Reviews,* 73**,** 170-181.

Schöngart, J., Piedade, M. T. F., Ludwigshausen, S., Horna, V. & Worbes, M. 2002. Phenology and stem-growth periodicity of tree species in Amazonian floodplain forests. *Journal of Tropical Ecology,* 18**,** 581-597.

Schwendenmann, L., Pendall, E., Sanchez-Bragado, R., Kunert, N. & Hölscher, D. 2014. Tree water uptake in a tropical plantation varying in tree diversity: interspecific differences, seasonal shifts and complementarity. *Ecohydrology,* 8**,** 1-12.

Singer, M. B., Stella, J. C., Dufour, S., Piégay, H., Wilson, R. J. & Johnstone, L. 2013. Contrasting water-uptake and growth responses to drought in co-occurring riparian tree species. *Ecohydrology,* 6**,** 402-412.

Solíz, C., Villalba, R., Argollo, J., Morales, M. S., Christie, D. A., Moya, J. & Pacajes, J. 2009. Spatio-temporal variations in *Polylepis tarapacana* radial growth across the Bolivian Altiplano during the 20th century. *Palaeogeography, Palaeoclimatology, Palaeoecology,* 281**,** 296-308.

Song, X., Barbour, M. M., Farquhar, G. D., Vann, D. R. & Helliker, B. R. 2013. Transpiration rate relates to within- and across-species variations in effective path length in a leaf water model of oxygen isotope enrichment. *Plant, Cell and Environment,* 36**,** 1338–1351.

Song, X., Farquhar, G. D., Gessler, A. & Barbour, M. M. 2014a. Turnover time of the non-structural carbohydrate pool influences $\delta^{18}O$ of leaf cellulose. *Plant, Cell and Environment,* 37**,** 2500-2507.

Song, X., Clark, K. S. & Helliker, B. R. 2014b. Interpreting species-specific variation in tree-ring oxygen isotope ratios among three temperate forest trees. *Plant, Cell and Environment,* 37**,** 2169-2182.

Speer, J. H. 2010. *Fundamentals of tree-ring research*, The University of Arizona Press.

Stahle, D. W. 1999. Useful strategies for the development of tropical tree-ring chronologies. *IAWA Journal,* 20**,** 249-253.

Sternberg, L. D. S. L. 2009. Oxygen stable isotope ratios of tree-ring cellulose: the next phase of understanding. *New Phytologist,* 181**,** 553-562.

Sturm, C., Hoffmann, G. & Langmann, B. 2007. Simulation of the stable water isotopes in precipitation over South America: Comparing regional to global circulation models. *Journal of Climate,* 20**,** 3730-3750.

Tang, K. & Feng, X. 2001. The effect of soil hydrology on the oxygen and hydrogen isotopic compositions of plants' source water. *Earth and Planetary Science Letters,* 185**,** 355-367.

Treydte, K., Boda, S., Graf Pannatier, E., Fonti, P., Frank, D., Ullrich, B., Saurer, M., Siegwolf, R., Battipaglia, G. & Werner, W. 2014. Seasonal transfer of oxygen isotopes from precipitation and soil to the tree ring: source water versus needle water enrichment. *New Phytologist,* 202**,** 772-783.

Van Der Sleen, P., Groenendijk, P. & Zuidema, P. A. 2015. Tree-ring $\delta^{18}O$ in African mahogany (*Entandrophragma utile*) records regional precipitation and can be used for climate reconstructions. *Global and Planetary Change,* 127**,** 58-66.

Whitmore, T. 1998. *An Introduction To Tropical Rain Forests*, Clarendon Press.

Wieloch, T., Helle, G., Heinrich, I., Voigt, M. & Schyma, P. 2011. A novel device for batch-wise isolation of α-cellulose from small-amount wholewood samples. *Dendrochronologia,* 29**,** 115-117.

Wigley, T. M., Briffa, K. R. & Jones, P. D. 1984. On the average value of correlated time series, with applications in dendroclimatology and hydrometeorology. *Journal of Climate and Applied Meteorology,* 23**,** 201-213.

Worbes, M. & Junk, W. J. 1989. Dating tropical trees by means of ^{14}C from bomb tests. *Ecology,* 70**,** 503-507.

Worbes, M. 1999. Annual growth rings, rainfall-dependent growth and long-term growth patterns of tropical trees from the Caparo Forest Reserve in Venezuela. *Journal of Ecology,* 87**,** 391-403.

Worbes, M. 2002. One hundred years of tree-ring research in the tropics–a brief history and an outlook to future challenges. *Dendrochronologia,* 20**,** 217-231.

Xu, C., Sano, M. & Nakatsuka, T. 2011. Tree ring cellulose $\delta^{18}O$ of *Fokienia hodginsii* in northern Laos: A promising proxy to reconstruct ENSO? *Journal of Geophysical Research,* 116.

Zhang, K., Almeida Castanho, A. D., Galbraith, D. R., Moghim, S., Levine, N. M., Bras, R. L., Coe, M. T., Costa, M. H., Malhi, Y. & Longo, M. 2015. The fate of Amazonian ecosystems over the coming century arising from changes in climate, atmospheric CO_2, and land use. *Global Change Biology*.

Zuidema, P. A., Brienen, R. J. W. & Schöngart, J. 2012. Tropical forest warming: looking backwards for more insights. *Trends in Ecology and Evolution,* 27**,** 193-194.

Chapter 5: What drives interannual variation in tree-ring oxygen isotopes in the Amazon?

Published in Geophysical Research Letters

J.C.A. Baker[1], M. Gloor[1], D.V. Spracklen[2], S.R. Arnold[2], J.C. Tindall[2], S.J. Clerici[1], M.J. Leng[3] and R.J.W. Brienen[1]

[1]School of Geography, University of Leeds, UK
[2]School of Earth and Environment, University of Leeds, UK
[3]NERC Isotope Geosciences Facilities, British Geological Survey, UK

Abstract

Oxygen isotope ratios in tree rings ($\delta^{18}O_{TR}$) from northern Bolivia record local precipitation $\delta^{18}O$ and correlate strongly with Amazon basin-wide rainfall. While this is encouraging evidence that $\delta^{18}O_{TR}$ can be used for palaeoclimate reconstructions, it remains unclear whether variation in $\delta^{18}O_{TR}$ is truly driven by within-basin processes, thus recording Amazon climate directly, or if the isotope signal may already be imprinted on incoming vapour, perhaps reflecting a pan-tropical climate signal. We use atmospheric back-trajectories combined with satellite observations of precipitation, together with water vapour transport analysis to show that $\delta^{18}O_{TR}$ in Bolivia are indeed controlled by basin-intrinsic processes, with rainout over the basin the most important factor. Furthermore, interannual variation in basin-wide precipitation and atmospheric circulation are both shown to affect $\delta^{18}O_{TR}$. These findings suggest $\delta^{18}O_{TR}$ can be reliably used to reconstruct Amazon precipitation, and have implications for the interpretation of other palaeoproxy records from the Amazon basin.

5.1 Introduction

Relationships between oxygen isotopes ($\delta^{18}O$) and environmental variables have often been the basis for palaeoclimate reconstructions, but relying on empirical

correlations alone without an understanding of the underlying mechanisms may lead to misinterpretations of proxy records (McCarroll and Loader, 2004). In the Amazon, $\delta^{18}O$ in palaeoarchives (including speleothems, lake and marine sediments, and ice cores; (e.g. Maslin and Burns, 2000, Thompson et al., 2013, Kanner et al., 2013, Moquet et al., 2016, Vuille et al., 2012 and references therein), offer valuable insights for climate in the absence of quality instrumental data. In addition to these, $\delta^{18}O$ in annual tree rings ($\delta^{18}O_{TR}$) have been identified as a useful tool for precipitation reconstructions (Ballantyne et al., 2011, Brienen et al., 2012, Baker et al., 2015). $\delta^{18}O_{TR}$ reflects soil water $\delta^{18}O$, modified, to a greater or lesser extent, by plant physiological influences, including leaf-water enrichment at the site of evaporation, back-diffusion of this enriched water to the rest of the leaf (the Péclet effect), and biological fractionation during metabolic processes (Barbour et al., 2004, Roden et al., 2000). Local climate can affect plant physiology, and thus $\delta^{18}O_{TR}$ (Kahmen et al., 2011), though Brienen et al. (2012) found $\delta^{18}O_{TR}$ from the warm, humid rainforest of northern Bolivia recorded local precipitation $\delta^{18}O$ ($\delta^{18}O_P$), with limited evidence of a local climate influence, possibly because leaf-water isotopic enrichment is low when relative humidity is high (Cernusak et al., 2016). Instead, $\delta^{18}O_{TR}$ was found to correlate with precipitation over the whole Amazon basin during the last century (Brienen et al., 2012). The authors hypothesize that this relationship is driven by rainout of heavy isotopes during moisture transport over the Amazon basin, although $\delta^{18}O_{TR}$ was also found to correlate with the El Niño-Southern Oscillation (ENSO), possibly indicating an alternative proximal driver of interannual variation. Similar relationships with ENSO have been reported for $\delta^{18}O_{TR}$ records elsewhere in the tropics, including Ecuador (Volland et al., 2016), Central America (Anchukaitis and Evans, 2010), northern Australia (Boysen et al., 2014) and several sites in Southeast Asia (Poussart et al., 2004, Xu et al., 2011, 2013, 2015, Sano et al., 2012, Schollaen et al., 2015). This leaves some doubt over the extent to which interannual variation in $\delta^{18}O_{TR}$ in Bolivia is driven by processes within the Amazon basin, or is more representative of processes occurring at the pan-tropical scale. This is important to clarify if such isotope data are to be reliably used to reconstruct climate and potentially validate output from general circulation models (GCMs) in the Amazon (Henderson-Sellers et al., 2002).

Contrasting interpretations of $\delta^{18}O$ in Andean ice cores ($\delta^{18}O_{ICE}$) suggest that the drivers of variation in $\delta^{18}O_P$ in the Amazon region are still not fully understood. It has been proposed that tropical ice cores record changes in temperature, as they do at higher latitudes (Thompson et al., 1995, 2000, 2006), but analyses using Rayleigh fractionation models instead suggest that ice cores primarily reflect changes in regional hydrology (Grootes et al., 1989, Pierrehumbert, 1999, Hoffmann, 2003a, Samuels-Crow et al., 2014). Rayleigh models predict the depletion of water vapour isotopes during moisture transport across the Amazon basin as heavy isotopes are preferentially removed during precipitation events (Dansgaard, 1964, Salati et al., 1979). A recent Rayleigh-based model, which included the influence of South American cold-air incursions (typically associated with positive precipitation anomalies in the western Amazon basin (Hurley et al., 2015)), was able to simulate ~74 % of the daily variability in Andean snowfall $\delta^{18}O$ (Hurley et al., 2016). However, studies have also shown Rayleigh models could be an oversimplification in tropical South America, not least due to large-scale water recycling by vegetation (Salati et al., 1979, Sturm et al., 2007, Brown et al., 2008). This is because transpiration at steady state is a non-fractionating process, which returns heavy isotopes to the atmosphere and accounts for the weak continental gradient in $\delta^{18}O_P$ over the Amazon (Salati et al., 1979, Insel et al., 2013). Transpiration therefore needs to be considered in an assessment of the controls on Amazon $\delta^{18}O_P$.

Several recent studies have used trajectory modelling as a tool to develop a better understanding of Amazon water vapour transport. Trajectory analysis can be used to identify moisture origins and detect changes in atmospheric transport/circulation that might influence $\delta^{18}O_P$ (van der Ent et al., 2010, Insel et al., 2013, Drumond et al., 2014, Fiorella et al., 2015, Spracklen et al., 2012). Trajectories have also been used in conjunction with GCMs (Sturm et al., 2007) and satellite isotope data (Brown et al., 2008) to track isotope changes during atmospheric transport. Furthermore, transport analysis has previously been used to identify climate controls on water isotopes in precipitation in the western Amazon (Vimeux et al., 2005, Villacís et al., 2008). In both of these studies upstream rainout was identified as the most important factor in determining the isotopic composition of precipitation, with local environmental variables having little or no effect on the signal. However, these studies, which spanned 5 years and 22 months respectively, specifically looked at controls on seasonal isotope

variability and were too short to thoroughly investigate controls on isotope variation at interannual timescales.

Here we aim to resolve the ambiguity surrounding the interpretation of tree-ring $\delta^{18}O$ records from the Amazon, and thus strengthen the use of these, and other $\delta^{18}O$ proxy records, in palaeoclimate reconstructions and for possible use in validating climate models. Existing records of $\delta^{18}O_P$ in the region (e.g. in the Global Network of Isotopes in Precipitation (GNIP) database, IAEA/WMO, 2016) are often short and discontinuous, preventing a detailed assessment of climate controls at interannual timescales. The $\delta^{18}O_{TR}$ record that we use here is continuous and annual, and can therefore be calibrated against modern climate data and used to identify mechanisms driving interannual variability. To achieve this, we use air-mass back-trajectories combined with satellite observations of precipitation and leaf area index (LAI), which is a good proxy for evapotranspiration in the tropics (Spracklen et al., 2012), and fields from the ERA-Interim reanalysis (which combines model data with observations) to investigate the causal drivers of interannual variation in $\delta^{18}O_{TR}$ over a 32-year period.

5.2 Data and Methodology

This study uses a $\delta^{18}O_{TR}$ chronology developed from nine trees from Selva Negra, Bolivia (10°5'S, 66°18'W; 160 m.a.s.l.), which has been shown to record local precipitation $\delta^{18}O$ (see Baker et al., 2015, Brienen et al., 2012). We used two approaches to identify the influence of Amazon basin processes on the observed $\delta^{18}O_{TR}$ signal: 1) trajectory modelling to reconstruct air-mass histories and 2) large-scale water vapour transport analysis.

To assess the relationship between $\delta^{18}O_{TR}$ and air mass history we used a Lagrangian atmospheric transport model to calculate kinematic back-trajectories. ERA-Interim reanalysis wind fields were retrieved from the European Centre for Medium-Range Weather Forecasts (ECMWF; http://www.ecmwf.int/en/research/climate-reanalysis/era-interim) to drive the model, with trajectory position output every 6 hours. We calculated 10-day back-trajectories arriving daily (12.00 UT) 2 km above the surface (800 hPa) at Selva Negra for the period 1998–2011. This height is likely to be within the bounds of low-level moisture advection and close to the height of

precipitation onset (Andreae et al., 2004). There are uncertainties associated with trajectories as they are inherently simplistic, and may struggle to capture all of the complexities of tropical atmospheric circulation, particularly sub-grid-scale convective transport processes (Stohl, 1998). Here we use 3-dimensional trajectories, which have been shown to be more accurate than other calculation methods (Stohl and Seibert, 1998). Altitude sensitivity analysis confirms our results to be robust within 1–4 km above the surface (Appendix 5.1).

Trajectories were used to reconstruct air-mass histories, including precipitation and exposure to vegetation. Precipitation data come from the Tropical Rainfall Measuring Mission (TRMM) 3B42 V7 product, which combines data from TRMM and other satellites (Huffman et al., 2007). We summed precipitation along each back-trajectory for 10 days or until it reached the coast (whichever of these came first). This was done by accumulating precipitation at the trajectory latitude (*lat*) and longitude (*lon*) for every 6-hr time-step (*t*) and then averaging these values across a number of trajectories (*n*) to find mean accumulated precipitation (∑Precip), according to the equation: $\sum_{t=0}^{-40} Precip\left(lat_n(t), lon_n(t)\right)\Delta(t)$. Trajectories were averaged across different time periods (3-months, wet season (October–April) and dry season (May–September)) to extract the relative influence of ∑Precip on $\delta^{18}O_{TR}$ for different periods of the year. The analysis was limited to those trajectories arriving on days with rain >0 mm at Selva Negra, as these are the air-mass histories that contribute to the $\delta^{18}O_{TR}$ signal. LAI data from the Moderate Resolution Imaging Spectroradiometer (MODIS, Myneni et al., 2002) were used to calculate accumulated LAI (∑LAI) using the same methodology. The influences of other climatic variables, including temperature, were also analysed (see Appendix 5.2).

In our second approach, we used ERA-Interim data to conduct an analysis of large-scale moisture transport into and out of the Amazon basin. Wind fields from 0–4 km above the surface were averaged and used to identify the dominant atmospheric transport patterns for the wet season (October–April), and define basin inflow and basin outflow transects (Fig. 5.3a). Column-integrated northward and eastward water vapour fluxes were used to estimate average wet season moisture flow across these transects for the period 1979–2010/11. Wind and moisture transport anomalies were calculated for years with high and low $\delta^{18}O_{TR}$ values to qualitatively characterise differences in

circulation. A more detailed discussion of the methodology can be found in Appendix 5.2 (Sternberg, 2009, Sternberg and DeNiro, 1983, Bruijnzeel et al., 2011, Callède et al., 2008, Huffman, 1997, LeGrande and Schmidt, 2006, Majoube, 1971, Samanta et al., 2011, Smith et al., 2006, Yan et al., 2016).

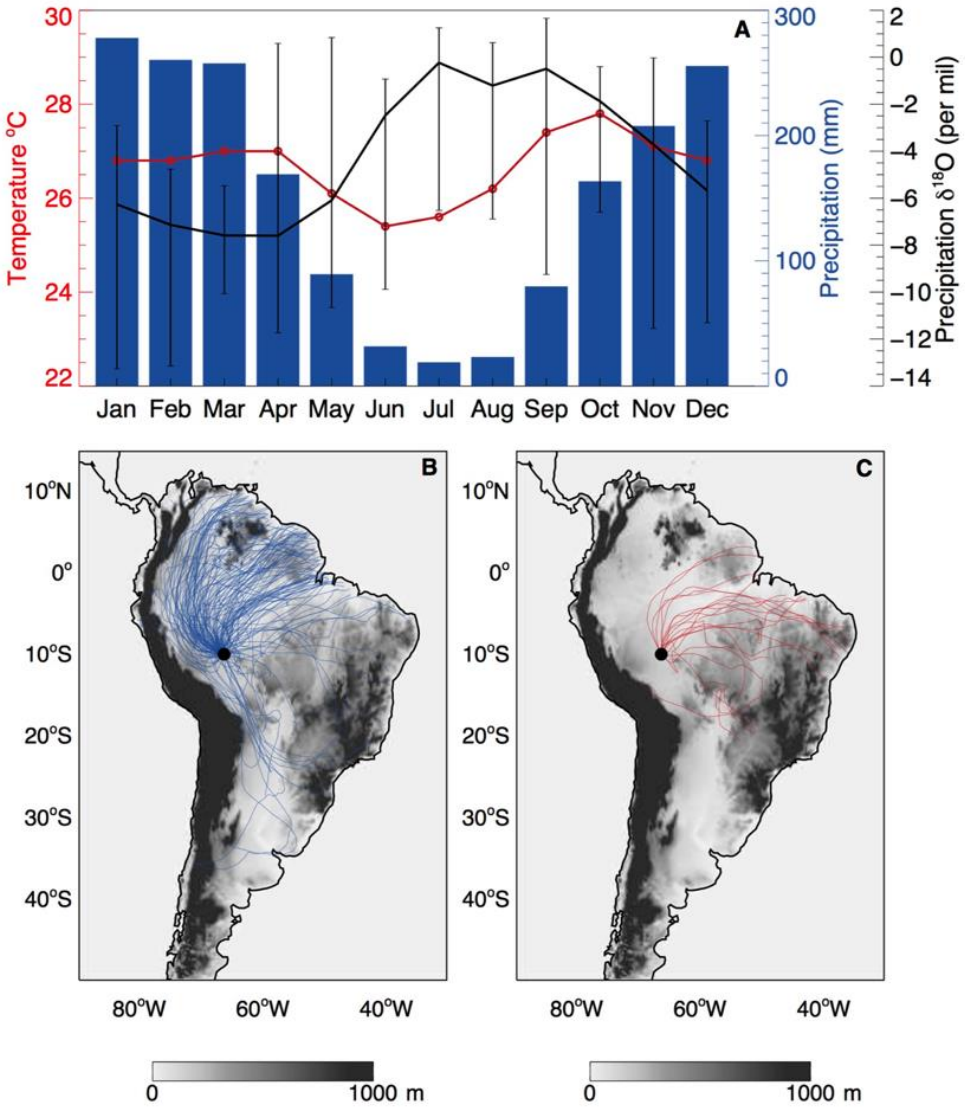

Figure 5.1 – Annual climate for the tree-ring sample site in northern Bolivia, and example wet and dry season back trajectories. (a) Climate diagram for Selva Negra, Bolivia (10°5'S, 66°18'W). Temperature and precipitation data are from 65–67.5°W, 9–11.5°S CRU TS3.21, 1960–2010. Monthly $\delta^{18}O_P$ data are averaged from 4 stations in the GNIP database (IAEA/WMO, 2016). Error bars represent the maximum and minimum observations in each month across all sites. **(b)** Daily trajectories arriving at 800 hPa on days with precipitation >0 mm at Selva Negra (black circle) during the 2010/11 wet season (Oct-Apr). **(c)** As in b but for the 2010 dry season (May-Sep). Trajectories are plotted over a topographical map of South America (Shuttle Radar Topographic Mission data).

5.3 Results

The mean climatology for our tree-ring sampling-site, Selva Negra, is shown in Figure 5.1a, based on data from the Climatic Research Unit (CRU). Temperature is fairly constant throughout the year but precipitation is highly seasonal, and there is a distinct dry season (precipitation <100 mm month^{-1}) from May–September. The tree species used to construct the $\delta^{18}O_{TR}$ chronology (*Cedrela odorata*) grows primarily during the wet season, with growth usually beginning in September/October and ending in April/May (Dünisch et al., 2003, Brienen and Zuidema, 2005). Air-mass histories from this period are therefore likely to have most influence on $\delta^{18}O_{TR}$. Seasonal variation in $\delta^{18}O_P$ is also shown in Figure 5.1. The lowest values are reached towards the end of the wet season, with a 2-month lag between peak rainfall and minimum $\delta^{18}O_P$. The highest $\delta^{18}O_P$ values are in the driest months, sometimes exceeding 0 ‰. Atmospheric transport is predominantly from the north and northwest during the wet season (Fig. 5.1b), while dry season trajectories are more easterly.

A three-month moving window correlation analysis between interannual precipitation and interannual $\delta^{18}O_{TR}$ reveals significant relationships between ∑Precip and $\delta^{18}O_{TR}$ throughout the wet season months, coinciding with the main growing period of *Cedrela odorata* (Fig. 5.2a). Correlations are consistently negative, so larger upstream precipitation corresponds with smaller $\delta^{18}O_{TR}$ values, and vice versa. The strongest three-month correlation occurs in November–January (r=–0.84, p<0.001, 1998–2010/11, n=13) when precipitation is reaching its annual peak (Fig. 5.1a). When trajectories from the dry and wet seasons are considered separately only $\sum Precip_{WET}$ is significantly related to $\delta^{18}O_{TR}$. This close relationship is shown in Figure 5.2b. Although the time series is relatively short (13 years) the relationship is highly significant (r=–0.85, p<0.001, n=13) with >70% of the interannual variation in $\delta^{18}O_{TR}$ explained by $\sum Precip_{WET}$. This provides a clear indication that the mechanism driving variation in $\delta^{18}O_{TR}$ on interannual timescales is rainout during moisture transport over the Amazon basin.

To determine whether the correlation between $\delta^{18}O_{TR}$ and $\sum Precip_{WET}$ is driven by interannual variation in the position and speed of the transport pathway or interannual variation in the precipitation amount over the basin we conducted two sensitivity experiments where we systematically controlled for variation in precipitation

and trajectory position in the calculation of $\sum Precip_{WET}$. Experiment 1 used climatological precipitation (i.e. not interannually varying) from the observed trajectories and experiment 2 used observed precipitation data from trajectory paths kept constant from year to year (see Appendix 5.2). Significant relationships between $\sum Precip_{WET}$ and $\delta^{18}O_{TR}$ were found in both of these experimental scenarios, suggesting that interannual variation in Amazon basin precipitation and variation in atmospheric circulation are both important in driving the relationship (Appendix 5.3).

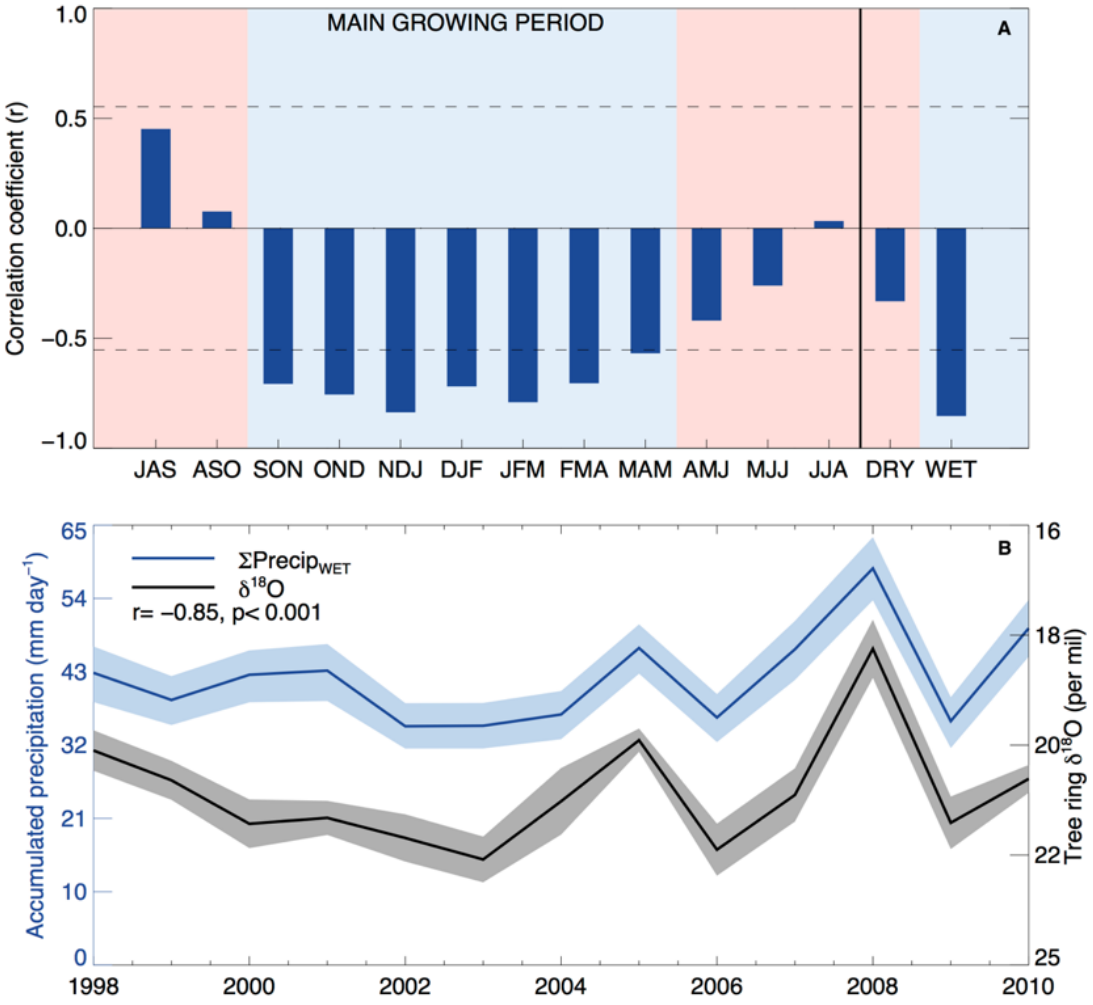

Figure 5.2 – Relationships between $\delta^{18}O_{TR}$ and precipitation along air-mass back-trajectories. (a) Three-month moving correlation coefficients between $\delta^{18}O_{TR}$ and mean accumulated TRMM precipitation ($\sum$Precip, trajectories from 1998–2010/11). Pink and blue boxes show the dry and wet seasons respectively. The bars at the right side of the plot show the mean correlation coefficients for the dry season (May-Sep) and wet season (Oct-Apr). Broken horizontal lines mark the significance threshold (p<0.05). **(b)** Interannual variation in $\sum Precip_{WET}$ and $\delta^{18}O_{TR}$ from 1998–2010. Shading indicates 95% confidence intervals. Pearson's r is –0.85 (p<0.001). Note that the scale for $\delta^{18}O_{TR}$ has been reversed.

The effects of other air-mass history attributes on $\delta^{18}O_{TR}$ were also investigated. A positive relationship between $\delta^{18}O_{TR}$ and ∑LAI (which is directly associated with evapotranspiration, see Spracklen et al. (2012)) was anticipated since evaporative recycling might be expected to return isotopically heavy water back to the atmosphere, and thus reduce continental rainout (Salati et al., 1979). In fact, $\delta^{18}O_{TR}$ and ∑LAI were found to anti-correlate during the wet season (Appendix 5.4). This may be due to the positive correlation between ∑LAI and ∑Precip across all wet season trajectories from 2000–2011 (r=0.31, p<0.001, n=1981). Further analysis showed ∑LAI also correlated strongly with trajectory time spent over land (r=0.82, p<0.001, n=1981), thus the relationship between ∑LAI and $\delta^{18}O_{TR}$ arises because ∑LAI is a proxy for travel time, and longer times provide more opportunity for fractionation processes such as rainout to occur. The effects can be teased apart by controlling for the effect of ∑Precip on $\delta^{18}O_{TR}$ and ∑LAI, resulting in mostly non-significant relationships between ∑LAI and $\delta^{18}O_{TR}$ (Fig. A5.4.1). We also looked at the influence of temperature during atmospheric transport. Temperature data were from ERA-Interim and specific to the horizontal and vertical position at each trajectory time-step. Mean back-trajectory temperature was found to have no significant relationship with $\delta^{18}O_{TR}$.

To complement the analysis above, and to overcome the limitations of a short temporal record of remote-sensing data, a basin-scale analysis of water vapour transport was carried out using ERA-Interim reanalysis data from 1979–2011 (Fig. 5.3, Appendix 5.5). Figure 5.3d shows a strong negative relationship between net wet season moisture balance (water vapour inflow – water vapour outflow) and both Selva Negra $\delta^{18}O_{TR}$ (r=–0.76, p<0.001, n=32), and the $\delta^{18}O_{TR}$ record from Brienen et al. (2012) (r=–0.73, p<0.001, n=23). The difference between water vapour inflow and outflow should be approximately equal to net rainout, and indeed correlates strongly with annual Amazon River discharge measured at Óbidos (r=0.80, p<0.001, n=32, Appendix 5.6). These results further support the idea that tree rings from the southern Amazon capture large-scale patterns of precipitation and moisture recycling. When inflow and outflow are considered separately it becomes clear that the relationship between $\delta^{18}O_{TR}$ and basin moisture balance is entirely driven by variation in the amount of outflowing water vapour as $\delta^{18}O_{TR}$ correlates strongly with moisture outflow, and only weakly with inflow (r=0.80, p<0.001 vs. r=–0.35, n=32, p<0.05, Selva Negra record). This is

consistent with the results from our trajectory analysis, since variation in outflow will be directly affected by variation in rainout over the basin. Compared with the variation in the outflow, moisture inflow shows relatively low interannual variation (5.8 vs. 14.7 %), which may further explain why $\delta^{18}O_{TR}$ correlates poorly with inflow. These findings confirm that convection and moisture removal over the basin drive interannual variability in $\delta^{18}O_{TR}$.

5.4 Discussion

Amazon climate is characterised by highly seasonal precipitation, with moisture transported in from the tropical Atlantic and then moving westward and southward over the basin (Figs. 5.1, 5.3a & Appendix 5.7). The significant anti-correlations between $\delta^{18}O_{TR}$ and $\sum Precip_{WET}$ (Fig. 5.2b), and between $\delta^{18}O_{TR}$ and basin moisture balance (Fig. 5.3d), demonstrate a clear link between the amount of moisture removed from the atmosphere during transport across the basin and isotopic variability. The analysis provides a mechanistic link to explain why tree rings at the far end of the Amazon basin can record precipitation over a region approximately 6 M km^2 (Brienen et al., 2012). The preferential removal of heavy isotopes during each precipitation event during moisture transport depletes the water vapour remaining in the atmosphere according to the Rayleigh model (Dansgaard, 1964), and thus years with more rainout correspond with more depleted values in the $\delta^{18}O_{TR}$ record. This large-scale control on the isotope signal can account for the excellent coherence between $\delta^{18}O_{TR}$ records from sites >300 km apart (Baker et al., 2015). Our results are also in agreement with studies examining the climatic drivers of isotope variability in South American precipitation on shorter timescales (Vimeux et al., 2005, Villacís et al., 2008). Correlation coefficients are strongest during the wettest months (Fig. 5.2a), which is in line with previous findings from regional circulation models (Sturm et al., 2007). It is worth observing that the severe droughts of 2005 and 2010 are not distinguishable in our isotope record as these were predominantly dry season phenomena (Marengo et al., 2011, Espinoza et al., 2011).

Interannual variation in basin-wide precipitation and interannual variation in transport route are both shown to be important factors affecting variation in $\delta^{18}O_{TR}$ in

the Amazon (Appendix 5.3). This confirms that within-basin processes determine the isotope signal in north Bolivia. Circulation changes have been highlighted before as a potential source of variation in South American $\delta^{18}O_P$. Firstly, variation in the contribution of moisture from isotopically distinct sources has been suggested as an important control on $\delta^{18}O_P$ at interglacial (Pierrehumbert, 1999, Cruz et al., 2005) but also interannual (Insel et al., 2013, c.f. Vuille et al., 2003) timescales. However, spatial variation in ocean surface $\delta^{18}O$ ($\delta^{18}O_{SW}$) in the main moisture source region for the Amazon is <1 ‰ (Appendix 5.8), and thus variation in trajectory origin is unlikely to explain much of the 4–6 ‰ variability in $\delta^{18}O_{TR}$. Alternatively, different transport pathways may be associated with different amounts of rainout (e.g. due to differences in topography, path length over land and climate), and thus interannual variation in circulation may drive interannual variation in $\delta^{18}O_P$ (Fiorella et al., 2015). Wind and moisture transport anomalies suggest it is this second source of variability that is important at our sample site and over the timescale of our study (Fig. 5.3, Appendix 5.5). Although there is substantial spatial variability in circulation between years, high $\delta^{18}O_{TR}$ years show a clear pattern of strengthened winds and enhanced moisture outflow from the southwest corner of the Amazon basin, along the path of the South American Low-Level Jet. Conversely, in low $\delta^{18}O_{TR}$ years the anomalies are reversed, with weaker wind flow and less moisture transported out of the basin. These circulation changes in the south of the basin explain why interannual variation in outflowing moisture is strongly related to $\delta^{18}O_{TR}$. Furthermore, this analysis can explain why $\delta^{18}O_{TR}$ from Bolivia correlates strongly with ENSO (Brienen et al., 2012): during a positive (negative) ENSO phase such as 1997/98, (2008/09) circulation changes accelerate (decelerate) transport out of the Amazon basin, thus leading to lower (higher) basin precipitation and higher (lower) $\delta^{18}O_{TR}$ values (Fig. 5.3). This shows how a pan-tropical climate phenomenon like ENSO influences basin-scale processes, which in turn control interannual variation in $\delta^{18}O_{TR}$. This ENSO influence on $\delta^{18}O_{TR}$ has been reported at other sites in the tropics due to ENSO's far-reaching impact on precipitation (e.g. Xu et al., 2015, Volland et al., 2016, Schollaen et al., 2015, Anchukaitis and Evans, 2010, Sano et al., 2012, Poussart et al., 2004).

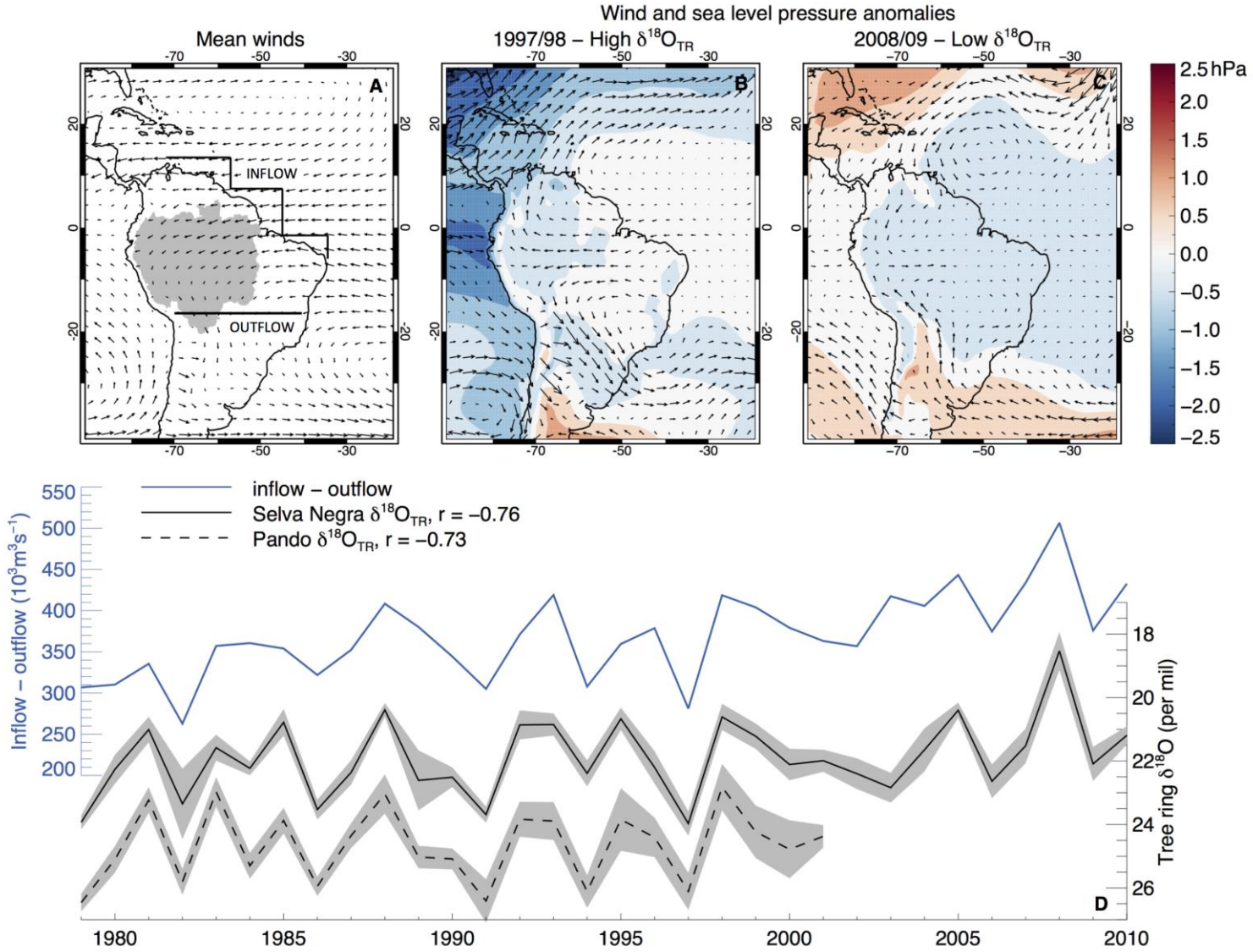

Figure 5.3 – Relationship between $\delta^{18}O_{TR}$ and mean wet season Amazon basin moisture balance. (a) Map of mean wet season (Oct-Apr, 1979-2010/11) wind vectors 0–4 km above the surface and the transects used to calculate water vapour inflow to, and outflow from, the Amazon basin (shaded in grey). **(b)** Map of wet season wind and sea level pressure anomalies in 1997/98 (a high $\delta^{18}O_{TR}$ year). **(c)** As in b but for 2008/09 (a low $\delta^{18}O_{TR}$ year). **(d)** Interannual variation in net wet season water vapour import (inflow – outflow) and $\delta^{18}O_{TR}$ from two sites in northern Bolivia (see Baker et al. (2015) for a detailed comparison of these records). Shading indicates 95% confidence intervals. Correlation coefficients between $\delta^{18}O_{TR}$ and (inflow – outflow) are given (p<0.001). Note that the scale for $\delta^{18}O_{TR}$ has been reversed. All climate data are from the ERA-Interim reanalysis.

We find a negative relationship between $\delta^{18}O_{TR}$ and air mass exposure to vegetation during the wet season, driven by a positive correlation between ∑LAI and ∑Precip. We had anticipated $\delta^{18}O_{TR}$ to positively correlate with ∑LAI, which is a proxy for evapotranspiration (Spracklen et al., 2012), since evapotranspiration reduces the effective rainout by returning heavy isotopes to the atmosphere. Indeed, previous studies report a low continental gradient in $\delta^{18}O_P$ over the Amazon due to large-scale water recycling offsetting the rainout of heavy isotopes (Salati et al., 1979, Insel et al., 2013). However, ∑Precip and ∑LAI are not in fact independent: ∑LAI is a function of travel time over land, which influences the degree of fractionation likely to have occurred along the trajectory. The negative correlations between $\delta^{18}O_{TR}$ and ∑LAI largely disappear when controlling for the effect of ∑Precip, though a significant negative relationship persists during November–January (Appendix 5.4). This result illustrates that disentangling confounding influences on $\delta^{18}O_{TR}$ can sometimes prove a challenge.

The findings in this study have implications for the interpretation of palaeoproxies in the Amazon beyond $\delta^{18}O_{TR}$. Specifically, they add support to the growing evidence base that $\delta^{18}O$ recorded in, e.g., tropical ice cores and speleothems, seem to largely reflect hydroclimate variability and not temperature variability (Grootes et al., 1989, Pierrehumbert, 1999, Hoffmann, 2003a, Vimeux et al., 2005, Moquet et al., 2016, Samuels-Crow et al., 2014, Hurley et al., 2015, Hurley et al., 2016, Hoffmann, 2003b), though it must be noted that the timescales of these studies vary from interglacial scales to just a few years. However, others have argued against trying to disentangle the effects of precipitation and temperature on $\delta^{18}O$, due to the strong correlation between these variables at interannual timescales in the tropics (e.g. Vuille et al., 2003). To complete our analysis, we used a simple Rayleigh-based model to simulate interannual variation in $\delta^{18}O_{TR}$ (Appendix 5.9). The Rayleigh model predicts isotopic composition as a function of the fraction (*f*) of water vapour remaining in the atmosphere. Outputs from our trajectory analysis were used to calculate *f* keeping all temperature-dependent parameters constant from year to year. Figure A5.9.1 shows the evolution of water vapour isotopes along a sample trajectory, and the Rayleigh-predicted $\delta^{18}O_{TR}$ value in each year. Our simulated $\delta^{18}O_{TR}$ values match well with observations (r=0.91, p<0.001, 2000–2010, root-mean-square error ≈1.6 ‰, n=11), but were twice as variable (range =

8.8 vs. 4.3 ‰). This analysis shows that the factors controlling Amazon $\delta^{18}O_{TR}$ are well understood. To some degree the same factors are likely to influence $\delta^{18}O_{ICE}$ records from the Andes, as suggested by the relationships between lowland $\delta^{18}O_{TR}$ and $\delta^{18}O_{ICE}$ from Quelccaya and Huascarán over recent times (r=0.77 and 0.68 respectively (Brienen et al., 2012)). A direct correlation between a composite $\delta^{18}O_{ICE}$ record and Amazon River discharge measured at Óbidos shows that Amazon precipitation can explain about 50 % of the variation in $\delta^{18}O_{ICE}$ from 1950–1984 (Appendix 5.2). The shift of ~6 ‰ in $\delta^{18}O_{ICE}$ since the Last Glacial Maximum (LGM) (Thompson et al., 2000) is comparable to between-year differences of <5.5 ‰ (e.g., 1997 vs. 2008) seen within one decade of our $\delta^{18}O_{TR}$ record, which can be almost entirely explained by changes in Amazon moisture balance. It is therefore feasible that variation in Amazon hydrology could account for most of the change in $\delta^{18}O_{ICE}$ since the LGM (i.e. a decrease in rainout since the LGM causing an increase in $\delta^{18}O_{ICE}$), without needing to invoke large shifts in temperature (Pierrehumbert, 1999). However, it should be noted that during the LGM $\delta^{18}O_{SW}$ would have been ~1 ‰ higher due to the difference in global ice volume, though spatial gradients in tropical $\delta^{18}O_{SW}$ were similar to the present day (Holloway et al., 2016).

The results presented here show that basin rainout is the most important mechanism driving interannual variability in Amazon $\delta^{18}O_{TR}$ over the duration of our tree-ring records, though other factors may be important at longer timescales. For example, occasional very depleted $\delta^{18}O_P$ values have been reported from rain events in the wet season at eastern coastal sites (Salati et al., 1979, Matsui et al., 1983), thought to be caused by a southward shift of the inter-tropical convergence zone (ITCZ) reducing the initial isotope value of incoming moisture. In a review of South American monsoon history inferred from stable isotopes, Vuille et al. (2012) suggest that latitudinal shifts in the ITCZ may be influential at the scale of several decades to centuries. In addition, sea surface temperature anomalies in the Pacific and Atlantic oceans are well known to affect Amazon climate (Richey et al., 1989, Yoon and Zeng, 2010, Marengo and Espinoza, 2016), and are therefore likely to influence $\delta^{18}O_{TR}$ indirectly, by causing more or less precipitation and driving changes in circulation (Vuille et al., 2003, Thompson et al., 2013). Longer $\delta^{18}O_{TR}$ records than that presented in this paper could possibly shed more light on these decadal-scale influences.

5.5 Summary

Trajectory modelling and large-scale water vapour transport analysis have been used to identify climatic controls on interannual variation in $\delta^{18}O_{TR}$. The most important single control on $\delta^{18}O_{TR}$ is rainout during moisture transport over the Amazon basin. Interannual variation in atmospheric circulation is another important influence, providing further evidence that within-basin processes regulate $\delta^{18}O_{TR}$. These results provide a mechanistic link to explain why a $\delta^{18}O_{TR}$ chronology from a single site at the end of the basin can be good proxy for precipitation over the entire Amazon region, with wider implications for the interpretation of other palaeoproxies in the Amazon.

5.6 References

Anchukaitis, K. J. & Evans, M. N. 2010. Tropical cloud forest climate variability and the demise of the Monteverde golden toad. *Proceedings of the National Academy of Sciences,* 107**,** 5036-5040.

Andreae, M. O., Rosenfeld, D., Artaxo, P., Costa, A. A., Frank, G. P., Longo, K. M. & Silva-Dias, M. a. F. 2004. Smoking rain clouds over the Amazon. *Science,* 303**,** 1337-1342.

Baker, J. C. A., Hunt, S. F. P., Clerici, S. J., Newton, R. J., Bottrell, S. H., Leng, M. J., Heaton, T. H. E., Helle, G., Argollo, J., Gloor, M. & Brienen, R. J. W. 2015. Oxygen isotopes in tree rings show good coherence between species and sites in Bolivia. *Global and Planetary Change,* 133**,** 298-308.

Ballantyne, A. P., Baker, P. A., Chambers, J. Q., Villalba, R. & Argollo, J. 2011. Regional differences in South American monsoon precipitation inferred from the growth and isotopic composition of tropical trees. *Earth Interactions,* 15**,** 1-35.

Barbour, M. M., Roden, J. S., Farquhar, G. D. & Ehleringer, J. R. 2004. Expressing leaf water and cellulose oxygen isotope ratios as enrichment above source water reveals evidence of a Péclet effect. *Oecologia,* 138**,** 426-35.

Boysen, B. M. M., Evans, M. N. & Baker, P. J. 2014. $\delta^{18}O$ in the tropical conifer *Agathis robusta* records ENSO-related precipitation variations. *Plos One,* 9**,** 1-9.

Brienen, R. J. W. & Zuidema, P. A. 2005. Relating tree growth to rainfall in Bolivian rain forests: a test for six species using tree ring analysis. *Oecologia,* 146**,** 1-12.

Brienen, R. J. W., Helle, G., Pons, T. L., Guyot, J. L. & Gloor, M. 2012. Oxygen isotopes in tree rings are a good proxy for Amazon precipitation and El Niño-Southern Oscillation variability. *Proceedings of the National Academy of Sciences,* 109**,** 16957-16962.

Brown, D., Worden, J. & Noone, D. 2008. Comparison of atmospheric hydrology over convective continental regions using water vapor isotope measurements from space. *Journal of Geophysical Research: Atmospheres,* 113**,** 1-17.

Bruijnzeel, L., Mulligan, M. & Scatena, F. N. 2011. Hydrometeorology of tropical montane cloud forests: emerging patterns. *Hydrological Processes,* 25**,** 465-498.

Callède, J., Ronchail, J., Guyot, J.-L. & Oliveira, E. D. 2008. Déboisement amazonien: son influence sur le débit de l'Amazone à Óbidos (Brésil). *Revue des sciences de l'eau/Journal of Water Science,* 21**,** 59-72.

Cernusak, L. A., Barbour, M. M., Arndt, S. K., Cheesman, A. W., English, N. B., Feild, T. S., Helliker, B. R., Holloway-Phillips, M. M., Holtum, J. A., Kahmen, A., McInerney, F. A., Munksgaard, N. C., Simonin, K. A., Song, X., Stuart-Williams, H., West, J. B. & Farquhar, G. D. 2016. Stable isotopes in leaf water of terrestrial plants. *Plant, Cell and Environment,* 39**,** 1087-1102.

Cruz, F. W., Burns, S. J., Karmann, I., Sharp, W. D., Vuille, M., Cardoso, A. O., Ferrari, J. A., Dias, P. L. S. & Viana, O. 2005. Insolation-driven changes in atmospheric circulation over the past 116,000 years in subtropical Brazil. *Nature,* 434**,** 63-66.

Dansgaard, W. 1964. Stable isotopes in precipitation. *Tellus,* 16**,** 436-468.
Drumond, A., Marengo, J., Ambrizzi, T., Nieto, R., Moreira, L. & Gimeno, L. 2014. The role of the Amazon Basin moisture in the atmospheric branch of the hydrological cycle: a Lagrangian analysis. *Hydrol. Earth Syst. Sci,* 18**,** 2577-2598.
Dünisch, O., Montóia, V. R. & Bauch, J. 2003. Dendroecological investigations on *Swietenia macrophylla* King and *Cedrela odorata* L.(Meliaceae) in the central Amazon. *Trees,* 17**,** 244-250.
Espinoza, J. C., Ronchail, J., Guyot, J. L., Junquas, C., Vauchel, P., Lavado, W., Drapeau, G. & Pombosa, R. 2011. Climate variability and extreme drought in the upper Solimões River (western Amazon Basin): Understanding the exceptional 2010 drought. *Geophysical Research Letters,* 38**,** 1-6.
Fiorella, R. P., Poulsen, C. J., Pillco Zolá, R. S., Barnes, J. B., Tabor, C. R. & Ehlers, T. A. 2015. Spatiotemporal variability of modern precipitation $\delta^{18}O$ in the central Andes and implications for paleoclimate and paleoaltimetry estimates. *Journal of Geophysical Research: Atmospheres,* 120**,** 4630-4656.
Grootes, P., Stuiver, M., Thompson, L. & Mosley-Thompson, E. 1989. Oxygen isotope changes in tropical ice, Quelccaya, Peru. *Journal of Geophysical Research: Atmospheres,* 94**,** 1187-1194.
Henderson-Sellers, A., McGuffie, K. & Zhang, H. 2002. Stable isotopes as validation tools for global climate model predictions of the impact of Amazonian deforestation. *Journal of Climate,* 15**,** 2664-2677.
Hoffmann, G. 2003a. Coherent isotope history of Andean ice cores over the last century. *Geophysical Research Letters,* 30**,** 1-4.
Hoffmann, G. 2003b. Taking the pulse of the tropical water cycle. *Science,* 301**,** 776-777.
Holloway, M. D., Sime, L. C., Singarayer, J. S., Tindall, J. C. & Valdes, P. J. 2016. Reconstructing paleosalinity from $\delta^{18}O$: Coupled model simulations of the Last Glacial Maximum, Last Interglacial and Late Holocene. *Quaternary Science Reviews,* 131**,** 350-364.
Huffman, G. J. 1997. Estimates of root-mean-square random error for finite samples of estimated precipitation. *Journal of Applied Meteorology,* 36**,** 1191-1201.
Huffman, G. J., Bolvin, D. T., Nelkin, E. J., Wolff, D. B., Adler, R. F., Gu, G., Hong, Y., Bowman, K. P. & Stocker, E. F. 2007. The TRMM multisatellite precipitation analysis (TMPA): Quasi-global, multiyear, combined-sensor precipitation estimates at fine scales. *Journal of Hydrometeorology,* 8**,** 38-55.
Hurley, J., Vuille, M., Hardy, D., Burns, S. & Thompson, L. G. 2015. Cold air incursions, δ18O variability, and monsoon dynamics associated with snow days at Quelccaya Ice Cap, Peru. *Journal of Geophysical Research: Atmospheres,* 120**,** 7467-7487.
Hurley, J., Vuille, M. & Hardy, D. 2016. Forward modeling of $\delta^{18}O$ in Andean ice cores. *Geophysical Research Letters,* 43**,** 8178-8188.
IAEA/WMO. [Online]. Global Network of Isotopes in Precipitation. The GNIP Database. Available: http://www.iaea.org/water [Accessed 2016].
Insel, N., Poulsen, C. J., Sturm, C. & Ehlers, T. A. 2013. Climate controls on Andean precipitation $\delta^{18}O$ interannual variability. *Journal of Geophysical Research: Atmospheres,* 118**,** 9721-9742.
Kahmen, A., Sachse, D., Arndt, S. K., Tu, K. P., Farrington, H., Vitousek, P. M. & Dawson, T. E. 2011. Cellulose $\delta^{18}O$ is an index of leaf-to-air vapor pressure difference (VPD) in tropical plants. *Proceedings of the National Academy of Sciences,* 108**,** 1981-1986.
Kanner, L. C., Burns, S. J., Cheng, H., Edwards, R. L. & Vuille, M. 2013. High-resolution variability of the South American summer monsoon over the last seven millennia: insights from a speleothem record from the central Peruvian Andes. *Quaternary Science Reviews,* 75**,** 1-10.
Legrande, A. N. & Schmidt, G. A. 2006. Global gridded data set of the oxygen isotopic composition in seawater. *Geophysical Research Letters,* 33**,** 1-5.
Majoube, M. 1971. Fractionnement en oxygène-18 et en deutérium entre l'eau et sa vapeur. *Journal de Chimie Physique et de Physico-Chimie Biologique,* 58**,** 1423-1435.
Marengo, J. A., Tomasella, J., Alves, L. M., Soares, W. R. & Rodriguez, D. A. 2011. The drought of 2010 in the context of historical droughts in the Amazon region. *Geophysical Research Letters,* 38**,** 1-5.
Marengo, J. A. & Espinoza, J. C. 2016. Extreme seasonal droughts and floods in Amazonia: causes, trends and impacts. *International Journal of Climatology,* 36**,** 1033-1050.
Maslin, M. A. & Burns, S. J. 2000. Reconstruction of the Amazon Basin effective moisture availability over the past 14,000 years. *Science,* 290**,** 2285-2287.

Matsui, E., Salati, E., Ribeiro, M., Ris, C., Tancredi, A. & Gat, J. 1983. Precipitation in the Central Amazon Basin: the isotopic composition of rain and atmospheric moisture at Belem and Manaus. *Acta Amazonica,* 13**,** 307-369.

McCarroll, D. & Loader, N. J. 2004. Stable isotopes in tree rings. *Quaternary Science Reviews,* 23**,** 771-801.

Methven, J. 1997. Offline trajectories: Calculation and accuracy. UK Universities Global Atmospheric Modelling Programme.

Moquet, J., Cruz, F., Novello, V., Stríkis, N., Deininger, M., Karmann, I., Santos, R. V., Millo, C., Apaestegui, J., Guyot, J.-L., Siffedine, A., Vuille, M., Cheng, H., Edwards, R. & Santini, W. 2016. Calibration of speleothem $\delta^{18}O$ records against hydroclimate instrumental records in Central Brazil. *Global and Planetary Change,* 139**,** 151-164.

Myneni, R., Hoffman, S., Knyazikhin, Y., Privette, J., Glassy, J., Tian, Y., Wang, Y., Song, X., Zhang, Y. & Smith, G. 2002. Global products of vegetation leaf area and fraction absorbed PAR from year one of MODIS data. *Remote sensing of environment,* 83**,** 214-231.

Pierrehumbert, R. T. 1999. Huascaran $\delta^{18}O$ as an indicator of tropical climate during the Last Glacial Maximum. *Geophysical Research Letters,* 26**,** 1345-1348.

Poussart, P. F., Evans, M. N. & Schrag, D. P. 2004. Resolving seasonality in tropical trees: multi-decade, high-resolution oxygen and carbon isotope records from Indonesia and Thailand. *Earth and Planetary Science Letters,* 218**,** 301-316.

Richey, J. E., Nobre, C. & Deser, C. 1989. Amazon river discharge and climate variability: 1903 to 1985. *Science,* 246**,** 101-103.

Roden, J. S., Lin, G. & Ehleringer, J. R. 2000. A mechanistic model for interpretation of hydrogen and oxygen isotope ratios in tree-ring cellulose. *Geochimica et Cosmochimica Acta,* 64**,** 21-35.

Salati, E., Dall'olio, A., Matsui, E. & Gat, J. R. 1979. Recycling of water in the Amazon basin: an isotopic study. *Water Resources Research,* 15**,** 1250-1258.

Samanta, A., Costa, M. H., Nunes, E. L., Vieira, S. A., Xu, L. & Myneni, R. B. 2011. Comment on "Drought-Induced Reduction in Global Terrestrial Net Primary Production from 2000 Through 2009". *Science,* 333**,** 1093.

Samuels-Crow, K. E., Galewsky, J., Hardy, D. R., Sharp, Z. D., Worden, J. & Braun, C. 2014. Upwind convective influences on the isotopic composition of atmospheric water vapor over the tropical Andes. *Journal of Geophysical Research: Atmospheres,* 119**,** 7051-7063.

Sano, M., Xu, C. & Nakatsuka, T. 2012. A 300-year Vietnam hydroclimate and ENSO variability record reconstructed from tree ring $\delta^{18}O$. *Journal of Geophysical Research: Atmospheres,* 117**,** 1-11.

Schollaen, K., Karamperidou, C., Krusic, P., Cook, E. & Helle, G. 2015. ENSO flavors in a tree-ring $\delta^{18}O$ record of Tectona grandis from Indonesia. *Climate of the Past,* 10**,** 3965-3987.

Smith, T. M., Arkin, P. A., Bates, J. J. & Huffman, G. J. 2006. Estimating bias of satellite-based precipitation estimates. *Journal of Hydrometeorology,* 7**,** 841-856.

Spracklen, D. V., Arnold, S. R. & Taylor, C. M. 2012. Observations of increased tropical rainfall preceded by air passage over forests. *Nature,* 489**,** 282-285.

Sternberg, L. D. S. L. & Deniro, M. J. 1983. Biogeochemical implications of the isotopic equilibrium fractionation factor between the oxygen atoms of acetone and water. *Geochimica et Cosmochimica Acta,* 47**,** 2271-2274.

Sternberg, L. D. S. L. 2009. Oxygen stable isotope ratios of tree-ring cellulose: the next phase of understanding. *New Phytologist,* 181**,** 553-562.

Stohl, A. & Seibert, P. 1998. Accuracy of trajectories as determined from the conservation of meteorological tracers. *Quarterly Journal of the Royal Meteorological Society,* 124**,** 1465-1484.

Stohl, A. 1998. Computation, accuracy and applications of trajectories—a review and bibliography. *Atmospheric Environment,* 32**,** 947-966.

Sturm, C., Hoffmann, G. & Langmann, B. 2007. Simulation of the stable water isotopes in precipitation over South America: Comparing regional to global circulation models. *Journal of Climate,* 20**,** 3730-3750.

Thompson, L. G., Mosley-Thompson, E. & Davis, M. E. 1995. Late glacial stage and Holocene tropical ice core records from Huascaran, Peru. *Science,* 269**,** 46-50.

Thompson, L. G., Mosley-Thompson, E. & Henderson, K. A. 2000. Ice-core palaeoclimate records in tropical South America since the Last Glacial Maximum. *Journal of Quaternary Science,* 15**,** 377-394.

Thompson, L. G., Mosley-Thompson, E., Brecher, H., Davis, M., León, B., Les, D., Lin, P.-N., Mashiotta, T. & Mountain, K. 2006. Abrupt tropical climate change: Past and present.

Proceedings of the National Academy of Sciences, 103**,** 10536-10543.
Thompson, L. G., Mosley-Thompson, E., Davis, M. E., Zagorodnov, V. S., Howat, I. M., Mikhalenko, V. N. & Lin, P. N. 2013. Annually resolved ice core records of tropical climate variability over the past ~1800 years. *Science,* 340**,** 945-50.
Van Der Ent, R. J., Savenije, H. H., Schaefli, B. & Steele-Dunne, S. C. 2010. Origin and fate of atmospheric moisture over continents. *Water Resources Research,* 46**,** 1-12.
Villacís, M., Vimeux, F. & Taupin, J. D. 2008. Analysis of the climate controls on the isotopic composition of precipitation ($\delta^{18}O$) at Nuevo Rocafuerte, 74.5 W, 0.9 S, 250 m, Ecuador. *Comptes Rendus Geoscience,* 340**,** 1-9.
Vimeux, F., Gallaire, R., Bony, S., Hoffmann, G. & Chiang, J. C. 2005. What are the climate controls on δD in precipitation in the Zongo Valley (Bolivia)? Implications for the Illimani ice core interpretation. *Earth and Planetary Science Letters,* 240**,** 205-220.
Volland, F., Pucha, D. & Braeuning, A. 2016. Hydro-climatic variability in southern Ecuador reflected by tree-ring oxygen isotopes. *Erdkunde,* 70**,** 69-82.
Vuille, M., Bradley, R. S., Werner, M., Healy, R. & Keimig, F. 2003. Modeling $\delta^{18}O$ in precipitation over the tropical Americas: 1. Interannual variability and climatic controls. *Journal of Geophysical Research: Atmospheres,* 108**,** 1-24.
Vuille, M., Burns, S., Taylor, B., Cruz, F., Bird, B., Abbott, M., Kanner, L., Cheng, H. & Novello, V. 2012. A review of the South American monsoon history as recorded in stable isotopic proxies over the past two millennia. *Climate of the Past,* 8**,** 1309-1321.
Xu, C., Sano, M. & Nakatsuka, T. 2011. Tree ring cellulose $\delta^{18}O$ of *Fokienia hodginsii* in northern Laos: A promising proxy to reconstruct ENSO? *Journal of Geophysical Research,* 116**,** 1-12.
Xu, C., Sano, M. & Nakatsuka, T. 2013. A 400-year record of hydroclimate variability and local ENSO history in northern Southeast Asia inferred from tree-ring delta O-18. *Palaeogeography Palaeoclimatology Palaeoecology,* 386**,** 588-598.
Xu, C., Pumijumnong, N., Nakatsuka, T., Sano, M. & Li, Z. 2015. A tree-ring cellulose $\delta^{18}O$-based July–October precipitation reconstruction since AD 1828, northwest Thailand. *Journal of Hydrology,* 529**,** 433-441.
Yan, K., Park, T., Yan, G., Chen, C., Yang, B., Liu, Z., Nemani, R. R., Knyazikhin, Y. & Myneni, R. B. 2016. Evaluation of MODIS LAI/FPAR Product Collection 6. Part 1: Consistency and Improvements. *Remote Sensing,* 8**,** 1-16.
Yoon, J.-H. & Zeng, N. 2010. An Atlantic influence on Amazon rainfall. *Climate Dynamics,* 34**,** 249-264.

Chapter 6: The changing Amazon hydrological cycle – inferences from over 200 years of tree-ring oxygen isotope data

Unpublished

Jessica C.A. Baker[1], Manuel Gloor[1], Arnoud Boom[2], David Neill[3], Santiago J. Clerici[1], Bruno B.L. Cintra[1], Julia C. Tindall[4], Melanie J. Leng[5], Robert J. Newton[4], Simon H. Bottrell[4] and Roel J.W. Brienen[1]

[1] School of Geography, University of Leeds, Leeds, UK
[2] Department of Geography, University of Leicester, Leicester, UK
[3] Universidad Estatal Amazónica, Puyo, Pastaza, Ecuador
[4] School of Earth and Environment, University of Leeds, Leeds, UK
[3] NERC Isotope Geosciences Facilities, British Geological Survey, UK

Abstract

Changes to the Amazon hydrological cycle may have important consequences for world's largest tropical forest, and the biodiversity contained therein. However, a scarcity of long-term climate data in the region can make it hard to evaluate recent climatic variability. Two tree-ring oxygen isotope ($\delta^{18}O_{TR}$) chronologies, from northern Bolivia and the Ecuadorian Andes, which may offer insights on Amazon hydrology over the past two centuries, are presented here. The Ecuador record spans 1799–2012 (<16 trees) and the Bolivia record spans 1860–2014 (<32 trees), making them the longest $\delta^{18}O_{TR}$ records from the Amazon, and the best-replicated $\delta^{18}O_{TR}$ records from the tropics to date. The two chronologies correlated well at interannual and decadal timescales, despite coming from sites >1500 km apart. Both $\delta^{18}O_{TR}$ records were strongly related to Amazon River discharge measured at Óbidos, and upwind precipitation, suggesting a common climatic driver of interannual variability. In both records a strong increase in $\delta^{18}O_{TR}$ was observed up until approximately 1950. The increase is consistent with positive trends in other $\delta^{18}O$ proxy records from across the Amazon. A factorial approach was used to quantify all possible drivers of this long-term increase, as $\delta^{18}O_{TR}$ may not be governed by the same controls at centennial and interannual timescales. Results from this analysis suggested a reduction in rainout fraction over the basin as the most likely cause for the increase, driven by rising sea surface temperatures (SSTs) in the North Atlantic. The upward trend in $\delta^{18}O_{TR}$ reverses

over the past 1–2 decades, with the lowest $\delta^{18}O_{TR}$ value recorded in Bolivia in 2008. These changes are consistent with the observed strengthening of the Amazon hydrological cycle since approximately 1990. Overall, it was shown that while the link between $\delta^{18}O_{TR}$ and the hydrological cycle is intricate, such tree-ring-derived records provide unique constraints about hydrological cycling in the past.

6.1 Introduction

The water and carbon cycles are closely coupled in the Amazon basin (Gatti et al., 2014), which is the largest freshwater drainage basin in the world. Perturbations in one cycle can therefore have important consequences for the other (e.g. Phillips et al., 2009, Lewis et al., 2011, Marengo and Espinoza, 2016, Gatti et al., 2014). The fate of Amazon vegetation under future change scenarios has been the subject of much discussion in the literature, with some model-based analyses suggesting climate feedbacks could cause precipitation reductions, system destabilisation and possible widespread forest loss (Cox et al., 2004, Malhi et al., 2009, Huntingford et al., 2008, Zemp et al., 2017). However, an analysis of rain gauge and river flux data from the region instead shows that precipitation in the Amazon has actually increased since approximately 1990 (Gloor et al., 2013), though wet and dry season precipitation anomalies are becoming increasingly variable (Marengo and Espinoza, 2016, Fu et al., 2013, Espinoza et al., 2014), and are projected to continue to do so into the future (Boisier et al., 2015).

Despite the importance of assessing climate change for the conservation of carbon stocks and biodiversity, the number of monitoring stations in the Amazon reporting data has fallen since the late 1980s (see Appendix 6.1), and there are few long-term instrumental records. This makes it hard to assess recent changes in hydrology in the context of historic variability. Proxy climate data, such as oxygen isotopes ($\delta^{18}O$), can potentially provide some insight on past hydrological variation (Mook, 2000). However, conventional $\delta^{18}O$ archives such as tropical ice cores can be affected by post-depositional processes (Hardy et al., 2003), may have little or no replication due to the expense and time needed to retrieve samples (Bradley, 2011) and are becoming increasingly threatened by anthropogenic warming (Thompson et al., 2000). There have been a growing number of speleothem $\delta^{18}O$ records from the Amazon in recent years

(e.g. Vuille et al., 2012, Kanner et al., 2013, Moquet et al., 2016, Novello et al., 2016, Wang et al., 2017 and references therein), though these also have low replication, and highly variable temporal resolution (e.g. <1–150 years). Thus, it is desirable to identify other tropical proxies that can provide a reliable record of on-going change, as well as helping to improve our understanding of past hydrological variation.

It was shown in a previous study that $\delta^{18}O$ preserved in tree rings ($\delta^{18}O_{TR}$) from northern Bolivia correlate well with interannual variation in precipitation over the whole Amazon basin and could therefore be used to better understand Amazon hydrology in the past (Brienen et al., 2012). Trajectory modelling has since been used to provide a mechanistic link to explain this relationship, with $\delta^{18}O_{TR}$ inversely related to the amount of precipitation along transport pathways (Baker et al., 2016). This is due to the controls on isotopes in precipitation ($\delta^{18}O_P$) in the Amazon, which have long been known (e.g. Dansgaard, 1964, Salati et al., 1979). During tranport of moisture across the basin, the water molecules containing heavy isotopes are more likely to condense and fall as rain, depleting the isotope composition of water vapour remaining in the atmosphere following a Rayleigh distribution (Dansgaard, 1964). However, although $\delta^{18}O_{TR}$ show promise as a proxy for reconstructing interannual variation in precipitation, as yet there have been no well-replicated $\delta^{18}O_{TR}$ chronologies from the region that extend beyond the limit of instrumental data (though Ballantyne et al. (2011) did develop a 184-year-long record from a single individual of *C. odorata*).

While the climate controls on interannual variation in $\delta^{18}O_{TR}$ from the Amazon are well understood, the factors influencing long-term trends have not yet been examined. Previous studies on $\delta^{18}O$ records from the Amazon have tended to apply known drivers of interannual variation to interpret longer-term (e.g. centennial) trends in $\delta^{18}O$ (Bird et al., 2011, Vuille et al., 2012, Kanner et al., 2013). This approach to proxy data interpretation is not reliable because it assumes that the same factors drive variation at different timescales, and that all alternative drivers of variation have remained constant through time (i.e. the assumption of uniformitarianism; Bradley, 2011), while neither of these assumptions may be valid in reality. To accurately reconstruct palaeoclimate from long proxy records all potential sources of variability must be carefully considered.

The aim of this paper was to use $\delta^{18}O_{TR}$ records from the Amazon to improve our understanding of temporal variation in regional hydrology and its controls since the early 1800s. Long $\delta^{18}O_{TR}$ records can also provide insights about how recent changes to the hydrological cycle compare with natural climatic variability. Two annually resolved and well-replicated $\delta^{18}O_{TR}$ chronologies from the western margin of the Amazon basin are presented. These records span the last two centuries making them the longest $\delta^{18}O_{TR}$ records from the region to date. Comparisons with climate data were made to analyse and assess whether the records are influenced by a common climatic driver, and a factorial approach was to investigate the cause of a long-term increase in $\delta^{18}O_{TR}$ since the early 1800s.

6.2 Methods

6.2.1 Sample collection

This study combines samples from three lowland rainforest sites in northern Bolivia and a montane forest in the eastern Ecuadorian Andes (Fig. 6.1). The Bolivian samples are from primary forests in Purisima (11.40°S, 68.72°W, 170 m above sea level (a.s.l.) and Selva Negra (10.10°S, 66.31°W, 160 m a.s.l.), and a secondary forest in El Tigre (10.98°S, 65.72°W, 165 m a.s.l.). $\delta^{18}O_{TR}$ chronologies from Purisima and Selva Negra have been presented in previous publications (see Brienen et al., 2012, Baker et al., 2015, Baker et al., 2016), though the present study uses additional samples and extends the analysis further back in time. All of the Bolivia sites are located relatively close together and thus have a similar climate. Total annual precipitation is approximately 1700 mm and highly seasonal, with a wet season (defined here as months with precipitation >100 mm) from October to April, which coincides with the main growing season for trees here (Brienen and Zuidema, 2005). Mean annual temperature is 26.2 °C with little seasonal variation (climate data are from 1960–2004, from the Riberalta meteorological station in the Global Historical Climatology Network-Monthly (GHCN-M) database (Peterson and Vose, 1997) accessed via KNMI (Koninklijk Nederlands Meteorologisch Instituut) Climate Explorer: http://climexp.knmi.nl).

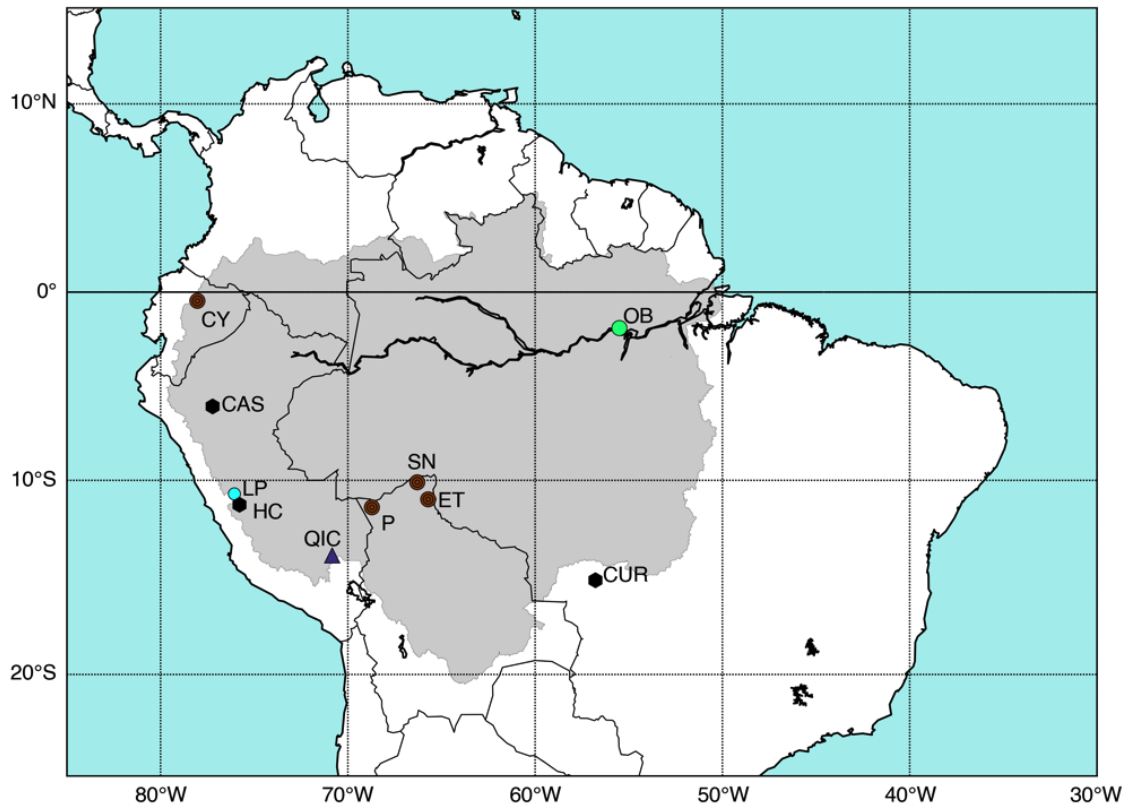

Figure 6.1 – Map of $\delta^{18}O$ proxy records from the Amazon. The Amazon basin (grey shading), tree-ring sampling sites (brown circles; CY=Cuyuja, P=Purisima, SN=Selva Negra, ET=El Tigre), the meteorological station at Óbidos (green circle; OB) and the locations of other $\delta^{18}O$ proxy records, including records from speleothems (black hexagons; CAS=Cascayunga cave (Reuter et al., 2009), HC=Huagapo cave (Kanner et al., 2013), CUR=Curupira cave (Novello et al., 2016)), a lake sediment record (blue circle; LP=Laguna Pumacocha (Bird et al., 2011)) and an ice-core record (dark blue triangle; QIC=Quelccaya ice core (Thompson et al., 2013)) are shown.

The Ecuadorian samples are from Cuyuja (0.45°S, 78.04°W, 2950m a.s.l.), which is much cooler on account of its higher elevation (mean annual temperature is 10.5 °C). Annual precipitation is approximately 1500 mm, which is similar to that of the Bolivian sites, though precipitation seasonality is lower in Ecuador (climate data are from the Papallacta meteorological station (3150 m a.s.l., 20 km away from sample site) from the period 1949–2008 (discontinuous) and available from the INAMHI (Instituto Nacional de Meteorologia e Hidrologia): http://www.serviciometeorologico.gob.ec). The wet season in Cuyuja is from March to September, and although there are no observations of leaf phenology or seasonal growth rhythms in this location, studies have shown that *C. montana* trees in southern Ecuador grow from December/January to April/May (Bräuning et al., 2009) before losing their leaves, with senescence possibly triggered by reduced light intensities at the height of the wet season (Bräuning et al., 2008).

Stem discs were collected from Purisima in 2002, from Selva Negra in 2011 and from Cuyuja in 2013, from trees that had already been felled. Living trees in Selva Negra and Cuyuja were also sampled using a 10-mm increment borer to collect cores approximately 130 cm from the ground in 2–4 directions around the circumference of the tree. In 2015 cores were also taken from living trees in El Tigre to capture more recent tree growth. *Cedrela odorata* trees were sampled in Bolivia and the closely related species *C. montana* was sampled in Ecuador.

6.2.2 Sample preparation

Discs were polished with sandpaper (up to grit 600) using a Bosch orbital sander, to improve the visibility of the tree rings. On each disc rings were counted along 2–4 radii, with every 10th ring interconnected between radii to ensure that no rings had been missed or misidentified. This was particularly important in samples from Ecuador where wedging (locally absent) rings were common. The oldest discs with the clearest rings were selected for isotope analysis (17 trees from Bolivia and 10 trees from Ecuador). Cores from younger trees were also analysed to assess the effect of ontogeny on $\delta^{18}O_{TR}$ signals. Cores were prepared using a core-microtome (Gärtner and Nievergelt, 2010) and on each core rings were marked and measured in the perpendicular direction to the ring boundaries using a LINTAB measuring stage. Ring widths were visually crossdated (Stokes and Smiley, 1968) between 2–4 cores from each tree to identify where rings might have been missed/misidentified. Cores with the widest and clearest rings were chosen for isotope analysis (17 cores from Bolivia and 13 cores from Cuyuja).

Isotope analysis was conducted on α-cellulose, which was extracted from whole wood using two different methods. First, samples from Bolivia were prepared using a scalpel to isolate and cut up the wood from each individual tree ring, making sure that the full width of the ring was evenly sampled. Wood from each ring was then put into separate filter funnel and cellulose extraction was conducted following the batch method of Wieloch et al. (2011). After extraction cellulose samples were transferred to Eppendorf tubes for homogenisation using a Retsch MM 301 mixer mill and then freeze-dried before being packed into silver cups for isotope analysis (see below).

The samples from Ecuador were analysed following an alternative technique whereby cellulose is extracted before the rings are separated from each other. The followed protocol was based on the methods of Kagawa et al. (2015) and Li et al. (2011), which build on earlier work by Loader et al. (2002). In brief, a bandsaw was used to cut sections of wood approximately 10 mm wide, 1 mm thick and between 50 and 100 mm long. These wood laths were scanned at high resolution and then sewn into perforated polytetrafluoroethylene (PTFE) cases, prior to chemical treatment to extract the cellulose following the procedure of Wieloch et al. (2011). This methodology permits much higher throughput of samples (in one week approximately 1000 tree rings could be treated, with the potential for even more than this) and the process of chemical exchange during the extraction process is also greatly accelerated. After extraction, the cellulose laths were freeze-dried while still inside their PTFE cases. Dried laths were inspected using a stereomicroscope with a transparent stage and mirror to reflect transmitted light and optimise ring visibility. Rings were carefully separated using a scalpel with reference to the wood scans to identify each ring correctly. Purified cellulose from each ring was then homogenised and freeze-dried as above, before being packed into silver cups.

6.2.3 Oxygen isotope analysis

The isotope series presented here were measured in four laboratories. Samples from Purisima were analysed at the German Research Centre for Geosciences (GFZ) in Potsdam, Germany; Selva Negra samples were analysed at the British Geological Survey's Stable Isotope Facility (part of the NERC Isotope Geosciences Facilities (NIGF)) in Keyworth, Nottingham, UK; the El Tigre samples were analysed in the School of Earth and Environment (SEE) at the University of Leeds; and Ecuador samples were analysed in the Department of Geography at the University of Leicester. Methods for $\delta^{18}O$ analysis at GFZ, NIGF and SEE have been described at length in a previous study (Baker et al., 2015), thus for brevity only describe the methods employed at the University of Leicester are described.

Cellulose $\delta^{18}O$ values were determined by pyrolysis in a high temperature furnace equipped with a glassy carbon reactor. Cellulose encapsulated in silver cups was converted to CO at a temperature of 1350 °C using a SerCon HT (high temperature)

furnace coupled to a SerCon Hydra 20-20 continuous flow isotope-ratio mass spectrometer (IRMS). $\delta^{18}O$ values (where $\delta = ((((^{18}O/^{16}O_{sample})/(^{18}O/^{16}O_{standard})) - 1) \times 1000$) were calculated with reference to two standards: cellulose from Sigma-Aldrich, UK (Lot#SLBD2972V) and whole wood Spruce Powder from Elemental Microanalysis. Precision was typically <0.2 ‰ (n=12).

6.2.4 Dating $\delta^{18}O_{TR}$ series

Crossdating $\delta^{18}O_{TR}$ series against an established $\delta^{18}O_{TR}$ chronology from the same region has been shown to be a cheap and effective way to verify tree-ring dates (Baker et al., 2015). $\delta^{18}O_{TR}$ chronologies from Purisima and Selva Negra have already been established (e.g. Baker et al., 2015, Brienen et al., 2012), and new $\delta^{18}O_{TR}$ records from Selva Negra and El Tigre were aligned with these published records. Where dating errors were suspected, the original samples of wood were then re-inspected to see whether any tree rings had been missed or miscounted. For the development of the Ecuador $\delta^{18}O_{TR}$ chronology a different procedure was followed: trees were matched against each other, since the site at Cuyuja is too far (>1500 km) from the Bolivia sites to assume that trees show similar interannual $\delta^{18}O_{TR}$ signals. Some of the $\delta^{18}O_{TR}$ data from Ecuadorian increment cores could not be crossdated, probably due to the high incidence of wedging rings, which could only be identified by careful scrutiny of complete discs. The non-matching series, which were all from small trees (2 from El Tigre and 7 from Cuyuja) were thus excluded from the composite chronologies.

Finally, one tree from Selva Negra and three trees from Cuyuja were selected for 'bomb-peak' radiocarbon (^{14}C) analysis to independently validate tree-ring dates. The ^{14}C measured in tree rings from both of these sites show excellent agreement with existing ^{14}C calibration curves, proving trees have been precisely dated (Baker et al., 2007).

6.2.5 Data analysis

Mean $\delta^{18}O_{TR}$ chronologies were constructed for Ecuador and Bolivia, with a minimum of three trees averaged at any point along each chronology (Appendix 6.2). The Bolivia record combines $\delta^{18}O_{TR}$ data from all three sites (a total of 32 trees) and spans 1860–2014 (data from 1901–2010 has been published previously (see Baker et

al., 2016, Baker et al., 2015, Brienen et al., 2012)). $\delta^{18}O_{TR}$ signals in trees from Purisima correlate strongly with trees from Selva Negra (Baker et al., 2015) and they have a similar standard deviation (0.9 ‰ and 1.1 ‰ respectively), but the trees from Purisima are consistently more enriched (by ~2.7 ‰). At least 1 ‰ of this offset is attributable to the fact that the series were measured in different laboratories, which assigned different isotope values to the same standard (for full details refer to the interlaboratory comparison in Baker et al., 2015). The cause for the rest of the offset is unclear, though it could be related to differences in soils between the two sites affecting soil water residence times, or due to physiological differences between sub-populations of *C. odorata*. Before constructing the mean chronology for Bolivia all Purisima $\delta^{18}O_{TR}$ values were thus offset by 2.7 ‰ to standardise the means between the different sites. The Ecuador record combines data from 16 trees, spans 1799–2012 and is presented here for the first time.

Mean inter-tree correlation coefficients (r_{mean}) and 'Expressed Population Signal' (EPS) statistics were used to measure $\delta^{18}O_{TR}$ chronology reliability. EPS is a measure of the extent to which a chronology is dominated by individual tree-level (EPS<0.85) or stand-level (EPS>0.85) signals (Wigley et al., 1984) and is calculated using the formula: $EPS = (N * r_{mean}) / (1 + (N - 1) * r_{mean})$ where N is the number of individual trees. A moving-window analysis was used to calculate running r_{mean} and EPS statistics, using a window of 30 years, to show changes in chronology quality through time.

$\delta^{18}O_{TR}$ records were compared against each other, and with climate data, to identify controls at interannual, decadal and centennial timescales. Spatial correlation analyses were performed to reveal relationships between $\delta^{18}O_{TR}$ records and regional climate. All correlations presented use the Pearson's product-moment correlation method and are between the unfiltered, interannual time series, unless otherwise indicated. Linear trends were identified using ordinary least squares (OLS) regression. To visualise low frequency trends in $\delta^{18}O_{TR}$ records and climate data, a second order, low-pass Butterworth filter with a cut-off frequency of 0.2 was applied in forward and reverse directions to each data series. Data analysis was conducted using Python 3.5.2 in the Scientific PYthon Development EnviRonment (Spyder) 3.1.2, and Interactive Data Language (IDL) version 8.2.3.

Climate data were downloaded via KNMI Climate Explorer, unless otherwise stated. Monthly precipitation and temperature observations (1901–2015) come from the Climatic Research Unit (CRU) TS3.24.01 product at 0.5° x 0.5° resolution (Harris et al., 2014). Spatial correlation analyses only used CRU data from the period 1953–1989 when the interpolated precipitation product includes data from >50 stations in the Amazon region (defined here as 15°S–5°N, 50–80°W, Appendix 6.1). Monthly sea surface temperature (SST) data are from the National Oceanic and Atmospheric Administration (NOAA) Extended Reconstruction Sea Surface Temperature (ERSST) dataset version 4 at 2° x 2° resolution (Huang et al., 2015). ERSST data were used from 1880 onwards, due to increasing uncertainty before this time (Huang et al., 2016). In addition, reconstructed North Atlantic SST anomalies for the period 1799–2006 from Mann et al. (2009) were used. This reconstructed dataset is based on multiple proxy records, including tree rings, ice cores, corals, speleothems and marine sediments. Monthly Amazon flow data, measured at Óbidos, are from the Agência Nacional de Águas (ANA) in Brazil (HidroWeb, 2017) with missing values reconstructed using linear relationships with hydrometric data from stations at Taperinha and Manaus (Antico and Torres, 2015). Lastly, monthly mean international sunspot number data for 1799–2015 were accessed from the Solar Influences Data Analysis Centre (SIDC, 2017).

6.3 Results and Discussion

6.3.1 Record description and inter-comparison

The $\delta^{18}O_{TR}$ series and composite chronologies from Ecuador and Bolivia are presented in Figure 6.2. These records span two centuries (1799–2014) and are the longest and best-replicated $\delta^{18}O_{TR}$ records from tropical South America to date. The *C. odorata* trees comprising the Bolivia chronology show high inter-tree synchronicity in $\delta^{18}O_{TR}$ (r_{mean}=0.69) and an EPS of 0.99 (Fig. 6.2b), which strongly indicates that $\delta^{18}O_{TR}$ signals are governed by an external control. There is slightly more variability between *C. montana* $\delta^{18}O_{TR}$ series from Ecuador (r_{mean}=0.45), possibly due to the different cellulose extraction method used (see section 2.2.1), though an EPS of 0.93 still suggests that the chronology is dominated by stand-level influences (Fig. 6.2a; Wigley

et al., 1984, N.B. EPS calculated using the raw, unadjusted series = 0.73). Moving window r_{mean} and EPS statistics decline for the most recent part of the Ecuador chronology (Fig. A6.2.1), probably due to the inclusion of the six increment cores, which could not be as carefully dated as the discs (see section 6.2.4), and because the rings in the discs tended to be very compressed in the outside edge, possibly resulting in errors during ring counting or when isolating the cellulose from each ring. However, in general both chronologies are well replicated, show coherent signals between trees and are sufficiently robust for further analysis.

The Ecuador and Bolivia records correlate well at interannual timescales (r=0.57, p<0.001, 1860–2012, n=153), despite coming from sites which are >1500 km apart and have an elevation difference of approximately 2750 m. Low-pass filters also reveal close similarities in their decadal and long-term trends (Appendix 6.3). Correlations between nearby $\delta^{18}O_{TR}$ records can be caused by changes in local relative humidity (RH)

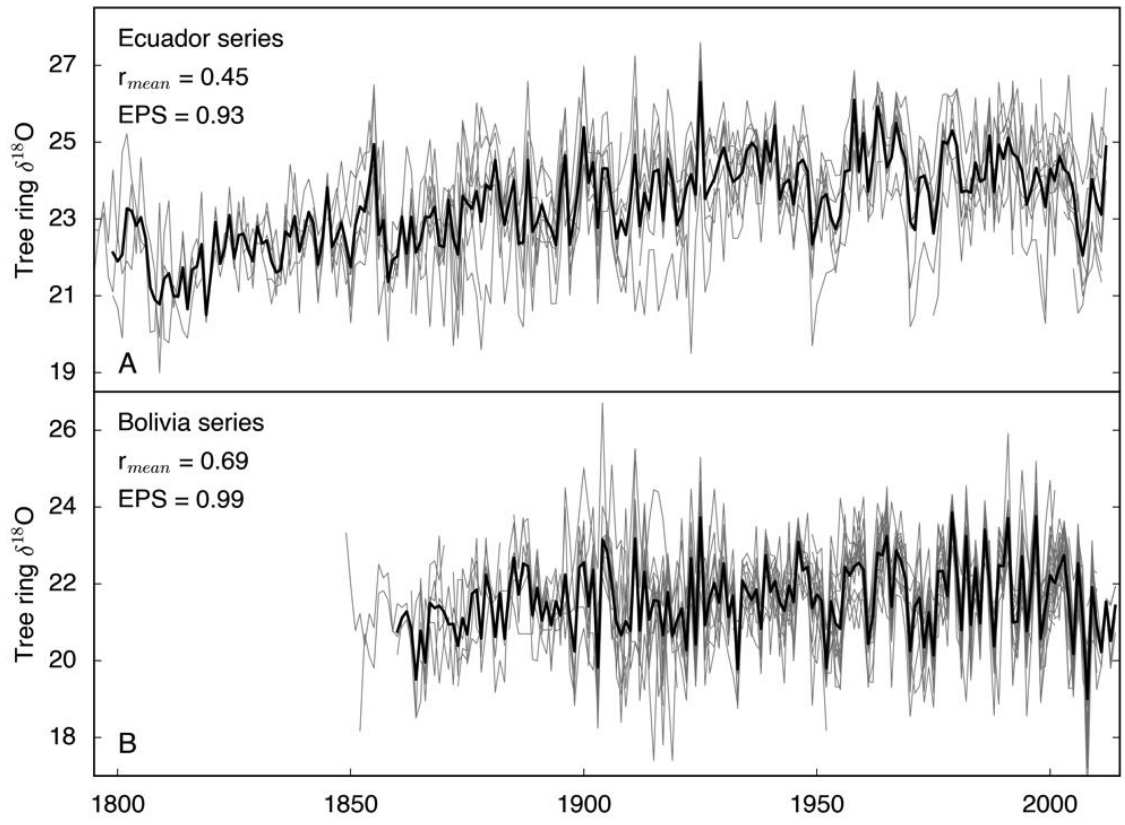

Figure 6.2 – New $\delta^{18}O_{TR}$ chronologies from Ecuador and Bolivia. Grey lines represent individual trees (16 for Ecuador, 32 for Bolivia) and the black lines show the mean composite chronologies. The mean inter-tree correlation (r_{mean}) and expressed population signal (EPS) values for the composite chronologies are indicated.

affecting stomatal conductance and consequently leaf water isotope enrichment (e.g. Andreu-Hayles et al., 2016, Labuhn et al., 2014, Xu et al., 2011). However, the large distance between the sample sites suggests another climatic control on the signal, which is independent of local conditions. Similarity between $\delta^{18}O_{TR}$ records from far distant sites, and between $\delta^{18}O_{TR}$ and other stable isotope proxy records, have been reported before in the Amazon (Ballantyne et al., 2011, Brienen et al., 2012, Baker et al., 2015, Volland et al., 2016). These connections have been attributed to strong regional coherence of $\delta^{18}O$ in precipitation ($\delta^{18}O_P$), caused by the link between precipitation in the basin and the location and strength of large-scale atmospheric overturning cells (i.e. Hadley and Walker cells, e.g. Nobre et al., 2009). This same reason is the likely explanation for the close correspondence between the records in this study, with the $\delta^{18}O_P$ signal recorded in cellulose with minimal modification of the signal in response to local climate effects (Barbour et al., 2004).

6.3.2 What drives interannual and decadal variation in $\delta^{18}O_{TR}$ from Ecuador?

The climatic factors controlling interannual variation in $\delta^{18}O_{TR}$ records from northern Bolivia are already well understood (e.g. Baker et al., 2016, Brienen et al., 2012): rainout of heavy isotopes during moisture transport across the Amazon basin,

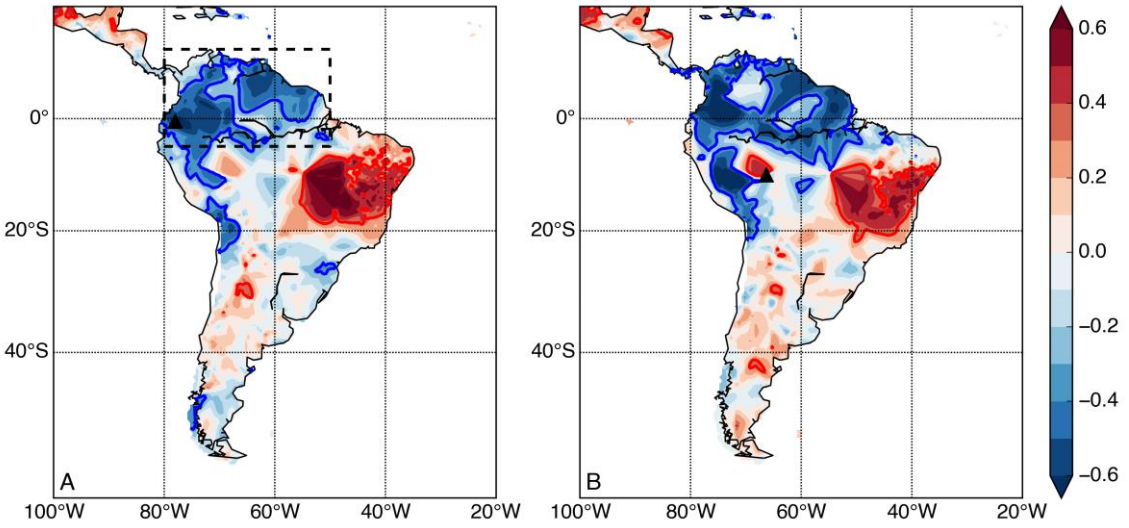

Figure 6.3 – Correlations between $\delta^{18}O_{TR}$ and gridded precipitation. Maps show the relationship between the Ecuador **(a)** and Bolivia **(b)** $\delta^{18}O_{TR}$ records and precipitation from CRU for four months during the growing season (Dec–Mar, 1953–1989). Black triangles show the location of the tree-ring sample sites. The colour bar indicates the strength of the correlation coefficients and blue and red contours show where correlations are significant (p<0.05). The broken black line in (a) shows the area from which precipitation data were averaged in the time series shown in Fig. 6.4.

and strong recycling of water vapour through vegetation, drive variation in $\delta^{18}O_P$ (Dansgaard, 1964, Salati et al., 1979, Insel et al., 2013, Villacís et al., 2008, Vimeux et al., 2005, Pierrehumbert, 1999), and this signal is preserved in tree rings. Since the Ecuador and Bolivia $\delta^{18}O_{TR}$ chronologies correlate well with each other and since both records are from the far west of the basin, it is likely they are controlled by a similar mechanism, though this has yet to be shown. This section focuses on identifying the factors controlling interannual and decadal variation in Ecuador $\delta^{18}O_{TR}$, and show how these differ from / relate to the known controls on $\delta^{18}O_{TR}$ from Bolivia.

Maps showing correlations between $\delta^{18}O_{TR}$ and gridded climate data can provide guidance about the causes of interannual variation and trends in $\delta^{18}O_{TR}$. Figure 6.3 shows correlations between Ecuador and Bolivia $\delta^{18}O_{TR}$ records and December–March CRU precipitation time series. These months coincide with the mature phase of the South American summer monsoon (SASM; Raia and Cavalcanti, 2008), and the growing season for *Cedrela* at each site. The emerging patterns for the two records are very similar, though the region of negative correlation extends further south for the Bolivia record. This corresponds to differences in pathways of moisture transport, with air parcels travelling to Ecuador over the more northern part of the basin (Appendix 6.4). Both maps also show a clear dipole, with $\delta^{18}O_{TR}$ anticorrelated with precipitation over northern South America, but positively correlated with precipitation in the southeast of the Amazon basin. This anti-phasing between precipitation in the northeast Brazil and the rest of the basin has been observed before, and is driven by the balance between moisture convergence and updraft over the basin, and subsidence and divergence of moisture in the surrounding regions (Cruz et al., 2009, Bordi et al., 2015). The dipole is modulated on orbital timescales by insolation affecting the intensity of the SASM: when summer insolation is high (low) in the southern hemisphere, a strong (weak) SASM strengthens (weakens) the Hadley and Walker circulations, increasing (reducing) subsidence and aridity in the region over northeast Brazil (Cruz et al., 2009).

Precipitation averaged over the north of the Amazon from December to March (region indicated in Fig. 6.3a) correlates well with Ecuador $\delta^{18}O_{TR}$ (r=–0.57, p<0.001, 1901–2012, n=112), as does Amazon River discharge measured at Óbidos, which integrates precipitation over approximately 80% of the Amazon basin (r=–0.63, p<0.001, 1903–2012, n=110; Fig. 6.4). Correlations with the Bolivia record are slightly

stronger (Appendix 6.5), but this may be because the Bolivia record is slightly better constrained, as it has higher replication and lower inter-tree variability. A recent study analysing climate signals in a $\delta^{18}O_{TR}$ chronology from the south of Ecuador found a better correlation with local CRU precipitation than with local station data, but the authors did not test for relationships with precipitation over a wider area (Volland et al., 2016). The authors hypothesise that moisture transported into the Andes from the Amazon is likely to influence $\delta^{18}O_{TR}$ in Ecuador, and the results presented here support this suggestion, with precipitation over the whole of northern South America affecting Ecuador $\delta^{18}O_{TR}$. No significant correlation between $\delta^{18}O_{TR}$ and local or regional temperature was found once variation in regional precipitation had been accounted for (Appendix 6.6). This is in agreement with previous studies showing that temperature does not have an important influence on $\delta^{18}O_{TR}$ in the Amazon (Volland et al., 2016, Brienen et al., 2012). Overall, these results provide a strong indication that the Ecuador $\delta^{18}O_{TR}$ chronology is subject to the same controls as the Bolivia $\delta^{18}O_{TR}$ chronology, i.e. successive precipitation events during moisture transport across the Amazon cause the progressive depletion of water vapour isotopes (e.g. Dansgaard, 1964, Salati et al., 1979), and this signal is recorded in cellulose.

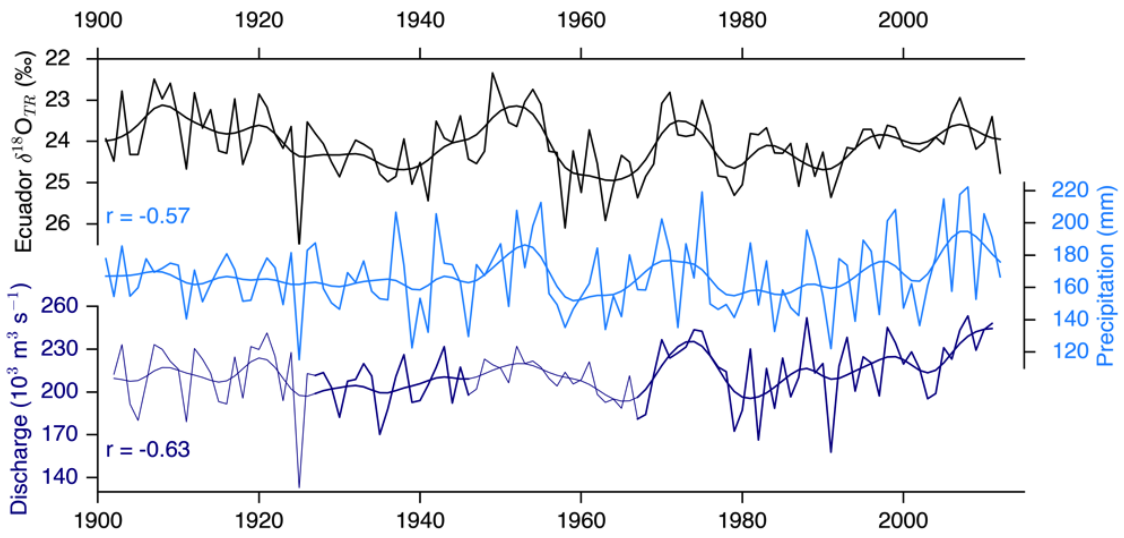

Figure 6.4 – Effect of Amazon precipitation and runoff on $\delta^{18}O_{TR}$ from Ecuador. Interannual variation in the $\delta^{18}O_{TR}$ record from Ecuador (black line, scale reversed), precipitation from CRU averaged over the region indicated in Fig. 6.3a (Dec–Mar, light blue line) and Amazon River discharge measured at Óbidos, which integrates precipitation over approximately 80% of the Amazon basin (Jun–Aug, dark blue line, line is thinner where data has been reconstructed from other river records). A low-pass Butterworth filter was applied to each series to visualize decadal variation. Values indicate the interannual Pearson correlation coefficients between $\delta^{18}O_{TR}$ and the other time series for the full period shown (p<0.001). Note that the river data is offset because peak river flow lags peak precipitation by 4–6 months.

To test the skill of potential regression-based reconstructions of Amazon hydrology from $\delta^{18}O_{TR,}$ split-period regression statistics, including the reduction of error (RE) and the coefficient of efficiency (CE) were calculated (National Research Council, 2006). Each isotope chronology was divided into two equal-length subsets (i.e. 1903–1957 and 1958–2012), which were used alternately for model calibration and verification. To calibrate the model, one subset of the $\delta^{18}O_{TR}$ data was regressed against Amazon River discharge data from the equivalent period (this dataset was used as it is the longest and most reliable record of Amazon hydrology), while the second subset was used to independently verify the model. Positive RE and CE statistics were returned for both the Bolivia and Ecuador chronologies, regardless of which subset was used to calibrate the regression model (Table A6.7.1), indicating that both records can generate models with skill in predicting Amazon river discharge. The statistics for models developed using the Ecuador chronology are lower than for models based on the Bolivia chronology, possibly due to diverging trends in the Ecuador calibration and validation periods. For this reason, and because it cannot be assumed that the factors driving interannual variability in $\delta^{18}O_{TR}$ operate on longer timescales (see section 6.4), this study refrains from applying a transfer function to explicitly reconstruct Amazon hydrology.

To investigate larger-scale controls on Ecuador $\delta^{18}O_{TR}$ the record was correlated with SST data (Fig. 6.5). The pattern of correlation is similar to that between the Quelccaya ice-core $\delta^{18}O$ record and SSTs (Fig. 3 in Thompson et al., 2013), indicating that these Andean records have similar large-scale controls. The two main regions of influence are the equatorial Pacific, and the tropical North Atlantic (TNA). SST data extracted from these two regions (marked by broken lines in Fig. 6.5a) were plotted as time series (Figs. 6.5b & c). Previous work in the Amazon has highlighted the influence of Pacific SSTs on $\delta^{18}O_{TR}$ via the influence of the El Niño-Southern Oscillation (ENSO; Brienen et al., 2012, Volland et al., 2016, Ballantyne et al., 2011), and the effect on the $\delta^{18}O_{TR}$ record from Bolivia is particularly strong (Appendix 6.8). However, this is the first time an important Atlantic influence has been shown, and thus the focus here. TNA SSTs correlate with Ecuador $\delta^{18}O_{TR}$ at interannual and decadal timescales (Fig. 6.5b). The start points of 10-day back-trajectories from the sample site were over-plotted to provide some indication of the origin of water vapour relative to the regions of highest

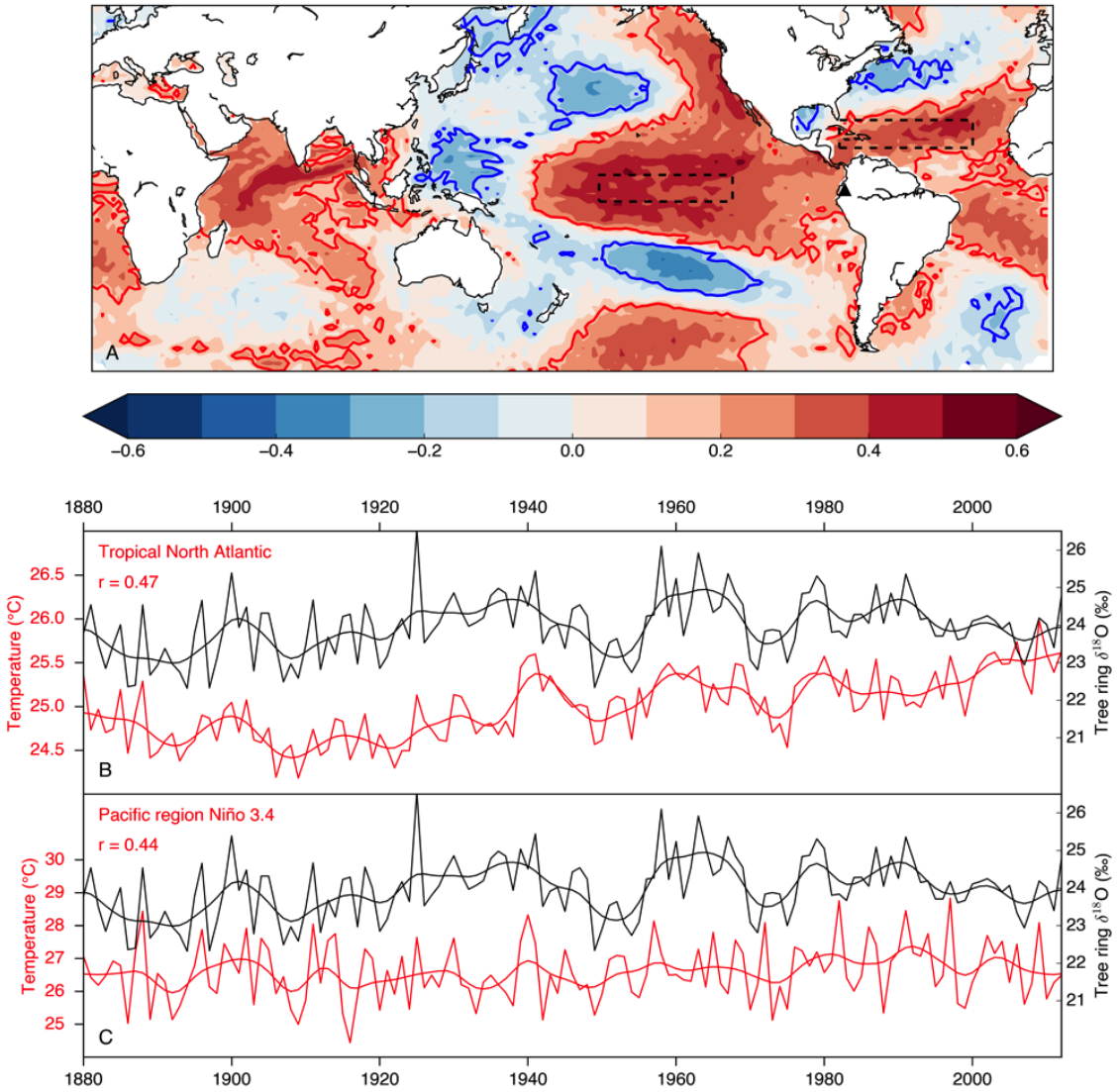

Figure 6.5 – Correlation between $\delta^{18}O_{TR}$ from Ecuador and sea surface temperature (SST) data. (a) Map showing the relationship between the $\delta^{18}O_{TR}$ record from Ecuador and gridded SST data from NOAA for four months during the growing season (Dec-Mar, 1880–2012). The location of the $\delta^{18}O_{TR}$ sample site is indicated by a black triangle. The colour bar indicates the strength of the correlation coefficients and blue and red contours show where correlations are significant (p<0.05). Broken black lines indicate regions from which SST data were averaged in the time series shown in panels b and c. **(b)** Interannual variation in SSTs from the tropical North Atlantic (red line) and the Ecuador $\delta^{18}O_{TR}$ record (black line). **(c)** As in b, but for SSTs from the Niño 3.4 region of the Pacific. A low-pass Butterworth filter was applied to each series to visualize decadal variation. Values indicate the interannual Pearson correlation coefficients between $\delta^{18}O_{TR}$ and the other time series for the full period shown (p<0.001).

correlation (Appendix 6.9). It is interesting to observe that most of these points fall in between the two regions of positive correlation in the Atlantic, suggesting that the effect of SSTs on $\delta^{18}O_{TR}$ is not direct (i.e. does not result from temperature-dependent fractionation during evaporation from the sea surface). Instead, it can be explained through a significant inverse relationship between TNA SSTs and precipitation upstream of the sample site, in the Guyanas and eastern Venezuela (Dec–Mar, Fig.

A6.10.1a). Pacific SSTs affect precipitation in a similar but wider area over the same time period (Fig. A6.10.1b). An Atlantic control on Amazon hydrology has only been well understood in recent decades: warm (cold) TNA SSTs cause the northward (southward) displacement of the inter-tropical convergence zone (ITCZ), thus driving lower (higher) precipitation in the southern and western parts of the basin, predominantly during the dry season (Yoon and Zeng, 2010, Espinoza et al., 2011, Marengo et al., 2011, Fernandes et al., 2011, Zeng et al., 2008, Yoon, 2016). The results show that TNA SSTs also significantly influence precipitation over the northern Amazon at the height of the wet season (Dec–Mar), which in turn affects the signal recorded in $\delta^{18}O_{TR}$.

A recent study reported a connection between solar activity and Amazon River discharge over the last century, due to the influence of sunspots on Atlantic SSTs (Antico and Torres, 2015). Specifically, they suggest that maxima and minima in the sunspot cycle respectively increase or decrease the difference between SSTs in the tropical North and tropical South Atlantic, thus weakening or strengthening the trade winds that transport moisture into the Amazon basin. In turn, this affects the amount of precipitation and runoff over the Amazon. While an interesting finding, the analysis was limited by the length of instrumental river records, which only extend back to 1903. Since the Ecuador record provides a proxy for Amazon basin hydrology over the last two centuries it can be used to conduct a more rigorous test of the relationship between sunspots and the Amazon hydrological cycle over the period 1799–2012. Following Antico and Torres (2015), the ensemble empirical mode decomposition (EEMD) method described by Wu and Huang (2009) was used to decompose the Ecuador record into its intrinsic oscillatory modes. Figure 6.6 shows the third modes of variability (as used by Antico and Torres) of annual (October–September) Amazon River discharge at Óbidos and Ecuador $\delta^{18}O_{TR}$, alongside the smoothed international sunspot number record (three-year moving average). Significance thresholds were adjusted to account for the reduced effective sample size ($n_{effective}$) of the smoothed time series. The results show good agreement with those of Antico and Torres (2015) over the 20th century, with sunspot number showing an anti-correlation with discharge (r=–0.49, p<0.01, $n_{effective}$ =32), and a positive correlation with $\delta^{18}O_{TR}$ (r=0.6, p<0.001, $n_{effective}$= 32) from 1903–2012 (note that discharge and $\delta^{18}O_{TR}$ are themselves inversely related, Fig. 6.4).

If sunspots drive variation in Amazon hydrology one would expect the positive relationship between sunspot number and $\delta^{18}O_{TR}$ to continue back in time. However, in the period before 1900 the relationship between the two records breaks down (r=–0.29, p=0.12, 1799–1902, $n_{effective}$=30). This could suggest either that the relationship between $\delta^{18}O_{TR}$ and Amazon hydrology is not robust, or that the postulated relationship between sunspots and Amazon hydrology is not robust. The mechanisms linking $\delta^{18}O_{TR}$ with Amazon hydrology are increasingly well understood, as described above (i.e. Baker et al., 2016, Brienen et al., 2012), while the means by which sunspots might affect Amazon hydrology are still relatively little studied. It is possible that the effect of sunspots on Amazon hydrology is not stationary, or else that the finding by Antico and Torres (2015) is coincidental, as the relationship over the full 200-year period is non-significant (r=0.20, p=0.12, $n_{effective}$=62). This example illustrates that long, annually resolved $\delta^{18}O_{TR}$ proxy records provide more insights than instrumental data alone.

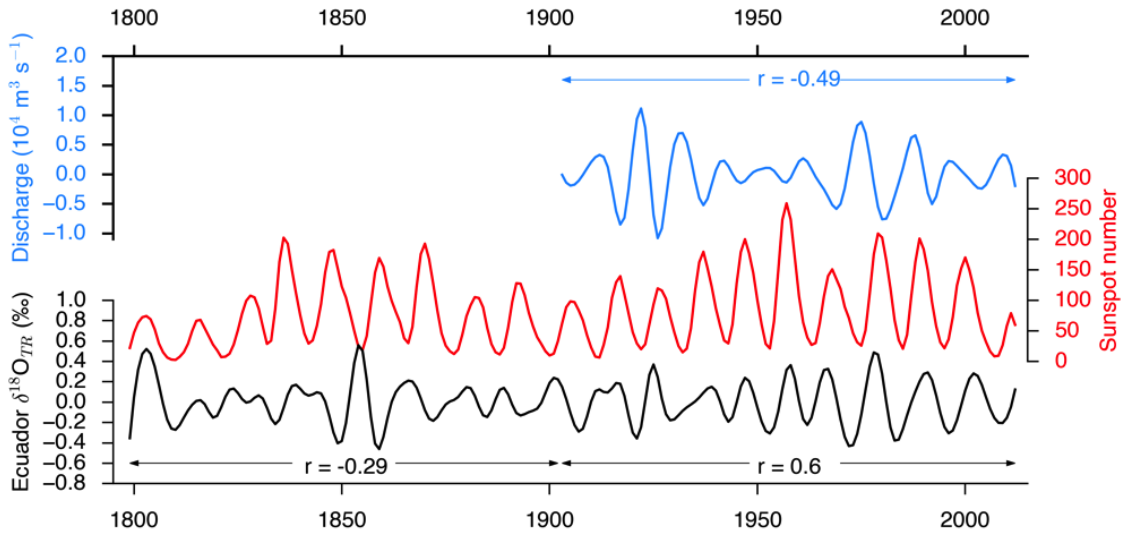

Figure 6.6 – Testing the effect of sunspots on Amazon hydrology. Decadal variation in Amazon River flow measured at Óbidos (blue line), international sunspot number (red line) and decadal variation in $\delta^{18}O_{TR}$ from Ecuador. The decadal river flux and $\delta^{18}O_{TR}$ data are the third ensemble empirical mode decomposition (EEMD) modes of the raw time series shown in Figure 6.4. Values indicate the Pearson correlation coefficients between sunspot number and the other time series for periods shown by arrows.

6.4 Long-Term Trends in $\delta^{18}O_{TR}$

Both records show a significant positive trend in $\delta^{18}O_{TR}$ over their full length. The trend in the Ecuador record is 1.24 ‰ 100yr^{-1} (p<0.001, 1799–2012) and in Bolivia 0.37 ‰ 100yr^{-1} (p<0.001, 1860–2014). However, the trends are not constant through time.

Both series show strong upward trends in $\delta^{18}O_{TR}$ in the period before 1900 (i.e. 2.11 and 2.43 ‰ $100yr^{-1}$ for 1860–1900, Ecuador and Bolivia respectively), but after 1900 the trends become gradually weaker, reaching a plateau at approximately 1950, and even becoming negative in the last 1–2 decades. The long Ecuador record, which shows approximately a 3 ‰ increase since the early 1800s, is the focus of this section. Similar (but weaker) positive trends over the past two centuries have been observed in other $\delta^{18}O$ proxy records, predominantly from the western part of the Amazon basin, including ice cores, lake sediments and speleothems (Fig. 6.7). These trends range from 0.17–1.03 ‰ $100yr^{-1}$ for the common period of 1800–1971. The common long-term increase in different proxy records suggests that at least part of the increase in $\delta^{18}O_{TR}$ is due to an increase in $\delta^{18}O_P$, although the rate of $\delta^{18}O$ increase is the strongest in the tree-ring record. This might be related to the fact the site is the furthest north, or due to some influence of tree physiology, or because the trees only grow, and thus record $\delta^{18}O$, for a few months during the Amazon wet season (i.e. are seasonally biased). Long-term increases in Amazon $\delta^{18}O$ records have previously been interpreted as showing a reduction in precipitation during the SASM (e.g. Bird et al., 2011, Vuille et al., 2012, Kanner et al., 2013). However, these studies assume that the factors driving interannual variability apply at longer timescales, and confounding sources of variation are not considered. In this study, the confounding factors that might contribute to the observed increase in $\delta^{18}O_{TR}$ are as follows:

1. Ontogenetic effects
2. Tree-level response to increasing atmospheric CO_2
3. Changes in the leaf-to-air vapour pressure difference
4. Increase in seawater $\delta^{18}O$ at moisture origin
5. Effect of increasing SSTs on fractionation during evaporation from the ocean surface
6. Change in the lapse rate
7. Change in local amount effects
8. Reduction in rainout fraction over the Amazon (i.e. the ratio of total precipitation to vapour transported into the basin)

Each of these factors is considered in turn, and the potential contribution to the trend in $\delta^{18}O_{TR}$ is quantified (summarised in Table 6.1).

Table 6.1 – Summary of factors that may contribute to the long-term increase in $\delta^{18}O_{TR}$. The estimated contribution of each factor is shown.

Factor	Predicted contribution to the increase in $\delta^{18}O_{TR}$ (‰)
Ontogenetic effects	0
Tree-level response to increasing atmospheric CO_2	0.39
Changes in the leaf-to-air vapour pressure difference	0.61
Increase in seawater $\delta^{18}O$ at moisture origin	0
Effect of increasing SSTs on fractionation during evaporation from the ocean surface	0.086
Change in the lapse rate	0.13
Change in local amount effects	0
Reduction in rainout fraction over the Amazon	1.78

6.4.1 Testing for an ontogenetic influence on $\delta^{18}O_{TR}$

When analysing long isotope series, it is important to consider the possible influence of ontogeny. The records in this study are mostly constructed from large discs, thus the early part of the record contains more juvenile rings than the later part, and therefore any age-related biases might result in erroneous trends in $\delta^{18}O_{TR}$. Work on juniper trees from Pakistan first revealed age biases in $\delta^{18}O_{TR}$, with series from juvenile trees showing negative trends in $\delta^{18}O_{TR}$ not evident in $\delta^{18}O_{TR}$ series from older trees over the same time period (Treydte et al., 2006). Since then it has become apparent that the direction of ontogenetic biases can differ between different species and across climatic zones, with negative (Esper et al., 2010) and positive (Labuhn et al., 2014) age biases being reported, and other studies which find no significant ontogenetic influence on $\delta^{18}O_{TR}$ (Young et al., 2011, Sano et al., 2013, Xu et al., 2016, Kilroy et al., 2016). Given this variability, it is important to check whether there is any evidence for an effect of ontogeny on *Cedrela* $\delta^{18}O_{TR}$ records from the Amazon.

To test for an ontogenetic influence on $\delta^{18}O_{TR}$ from Selva Negra, for each year from 2001–2010 the mean $\delta^{18}O_{TR}$ value for that year was calculated using only small trees (<20 cm diameter at breast height (DBH), 10 trees in total) and only large trees (>60 cm DBH, 9 trees in total). $\delta^{18}O_{TR}$ values in small and large trees were found to be highly correlated (R^2=0.92, Fig. A6.11.1), and the slope of the regression is not significantly different from 1 (0.85±0.21, 95% confidence interval). This is a strong indication that there is no effect of ontogeny on $\delta^{18}O_{TR}$ in *C. odorata*. It was not possible to use the same approach to test for ontogenetic effects in *C. montana* as there was insufficient data from small trees. Instead, the $\delta^{18}O_{TR}$ values from the seven old *C.*

montana trees that included isotope measurements from young rings (<20 cm DBH) and older rings (>20 cm DBH), were plotted using different colours to differentiate between the two phases. $\delta^{18}O_{TR}$ values in young rings closely follow the values and trends in older rings and there are no trailing sections, which might be expected if there were strong trends during the early years of growth (Fig. A6.11.2). Overall, it was concluded that ontogeny does not have an important influence on $\delta^{18}O_{TR}$ in either of the records presented in this study and there was thus no need to apply de-trending procedures to remove biological age trends. This means that these records can be used to assess low frequency variation in climate. Next, possible environmental drivers for the upward trend in $\delta^{18}O_{TR}$ are explored.

6.4.2 Tree-level response to rising CO_2

The upward trend in $\delta^{18}O_{TR}$ could be related to the rise in atmospheric CO_2 since the Industrial Revolution, which may have affected trees' stomatal conductance and transpiration rates (e.g. Keenan et al., 2013, van der Sleen et al., 2015). Observations from Free Air CO_2 Enrichment (FACE) experiments show that trees dynamically reduce their stomatal conductance (g_s) in response to elevated CO_2, in order to optimise carbon gain (Ainsworth and Long, 2005). Studies have also highlighted increasing structural adaptations, with plants reducing the physical capacity of their leaves to conduct water as CO_2 rises, by changing stomatal density and/or size (de Boer et al., 2011, Lammertsma et al., 2011). Experiments show that plants have higher leaf cellulose $\delta^{18}O$ when g_s is reduced (e.g. Barbour and Farquhar, 2000, Barbour et al., 2000), partly due to g_s affecting the transpiration rate. Transpiration is inversely related to the isotope enrichment of bulk leaf water ($\delta^{18}O_L$), as the flow of unenriched water from the stem opposes the back diffusion of enriched water from the site of evaporation into the rest of the leaf (i.e. the Péclet effect; Cernusak and Kahmen, 2013, Farquhar and Lloyd, 1993). Analyses on tree cores from FACE experiments in temperate sites have shown that elevated CO_2 (150–200 ppm above ambient) and the resulting reductions in g_s can cause small but significant increases in $\delta^{18}O_{TR}$, showing that $\delta^{18}O_L$ signals can be transferred to stem cellulose (Battipaglia et al., 2013). Thus, one may ask, can the $\delta^{18}O_{TR}$ increase

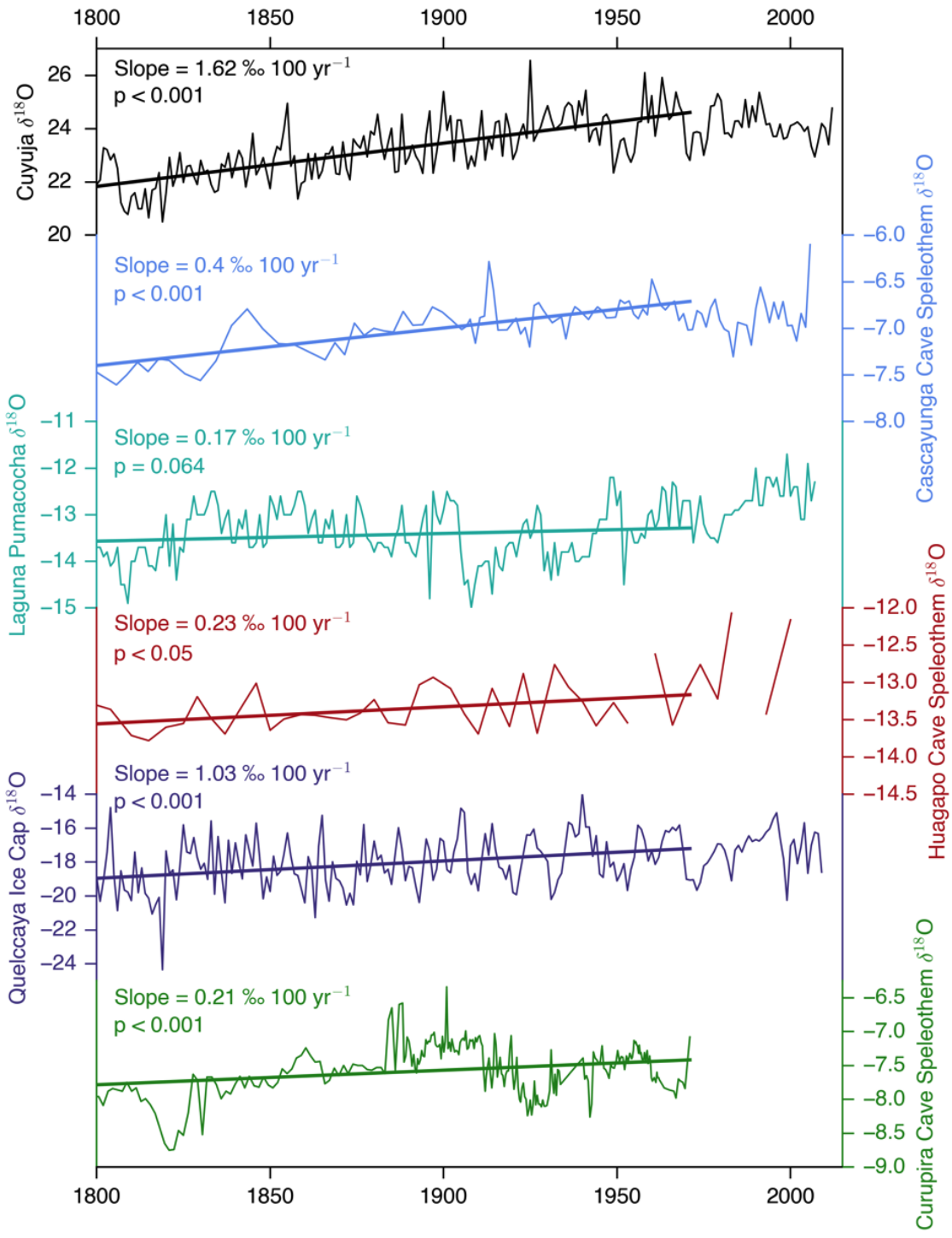

Figure 6.7 – Long-term trends in different δ^{18}O proxy records from the Amazon. Interannual variation in δ^{18}O in tree rings from Ecuador (black line, this study), Cascayunga cave speleothem (light blue line; Reuter et al., 2009), lake sediment (cyan line; Bird et al., 2011), Huagapo cave speleothem (red line; Kanner et al., 2013), Quelccaya ice core (dark blue line; Thompson et al., 2013) and Curupira cave speleothem (green line; Novello et al., 2016). The locations of these records are shown in Figure 6.1. Significant trends for the common period of 1800–1971 are shown, and the slopes of the trend lines are indicated.

of 3 ‰ be explained by this effect of rising CO_2 on transpiration rates? Increasing CO_2 has been estimated to reduce maximum g_s (g_{max}) by an average of 0.34% ppm^{-1} (Lammertsma et al., 2011), so an industrial atmospheric CO_2 increase of approximately 120 ppm, due to fossil fuel burning and cement production, might therefore be expected to have caused reductions in g_{max} on the order of 40%. Using the Péclet-modified Craig-Gordon (PMCG) model, as described by Farquhar and Lloyd (1993), Sternberg (2009) and others, a 40% reduction in g_s was estimated to cause <0.4 ‰ increase in $\delta^{18}O_{TR}$ (see Appendix 6.12). Finally, carbon isotope ($\delta^{13}C$) measurements could possibly be used to calculate changes in tree water-use efficiency (WUE = carbon assimilation/g_s), and thus infer tree-level responses to rising CO_2 in a more precise way. Hietz et al., (2005) measured $\delta^{13}C$ in *Cedrela* from Brazil and estimate a 34 % increase in WUE from the 1930s to the 1990s. If carbon assimilation remained constant over this period, then a 34 % WUE increase would correspond to a maximum decrease in g_s of 25 %, but as the authors note, the actual decrease in g_s is likely to be much smaller than this in the humid tropics, where water is unlikely to be limiting. Therefore, the estimated contribution from rising CO_2 to the trend in $\delta^{18}O_{TR}$ is probably lower than the suggested value of 0.4 ‰. In conclusion, while the increase in atmospheric CO_2 may have contributed to the observed positive trend, it is unlikely to be the primary driver.

6.4.3 Changes in leaf-to-air vapour pressure difference

Humidity and (to a lesser extent) temperature (T) changes affect the degree of fractionation during evaporation from the leaf (e.g. Cernusak et al., 2016), and thus influence $\delta^{18}O_L$. For example, controlled greenhouse experiments on cotton plants showed that a 33% reduction in relative humidity (RH) increased $\delta^{18}O_L$ by 3–4 ‰ (Barbour and Farquhar, 2000). Kahmen et al. (2011) investigated the effect of leaf-to-air water vapour pressure difference (VPD, determined by RH and T), on $\delta^{18}O$ in different plant tissues of *Metrosideros polymorpha* along an altitudinal gradient in Hawaii. They used a mechanistic model of plant physiology to explore the effect of variation in VPD on cellulose $\delta^{18}O$. Although the $\delta^{18}O$ of xylem water decreased with elevation, they found that leaf and stem cellulose $\delta^{18}O$ increased, due to increasing VPD at higher altitudes. An increase in VPD might therefore contribute to the observed long-term increase in Ecuador $\delta^{18}O_{TR}$.

We consider local changes in T and RH to quantify the potential influence of VPD on $\delta^{18}O_{TR}$. Station data from the Andes show that local temperatures have increased by an average of 0.68 °C since 1939 (Vuille et al., 2008). This can be used, together with present-day measurements of T (10.5 °C) and RH (90%) from the Papallacta meteorological station (2003–2012), to estimate the change in RH since 1939. Saturation vapour pressure (e_s) is calculated from T with the equation: $e_s = 0.6108e^{\frac{(17.27 \times T)}{(T + 237.3)}}$ (e.g. Karamouz et al., 2012) and actual vapour pressure (e_a) with: $e_a = RH \times e_s$. Assuming that e_a has remained constant, RH is estimated to have decreased by 4% over the last eight decades. The PMCG model was used to calculate that a T rise of 0.68 °C and a RH decrease of 4% would cause $\delta^{18}O_{TR}$ to increase by approximately 0.6 ‰ (Appendix 6.12). In combination with the response to increased CO_2 (section 6.4.2), plant physiological responses might thus explain circa 1 ‰ of the 3 ‰ increase in $\delta^{18}O_{TR}$ over the past 200 years. This could explain why tree rings record a stronger increase in $\delta^{18}O$ than other proxy records from the Amazon (Fig. 6.7). However, it is also necessary to acknowledge the limitations of these calculations. Typical literature-derived parameter values, which are not specific for the species or site, were used, and thus introduce a degree of uncertainty. Furthermore, recent work in the Australian tropics has cast doubt on whether enrichment at the leaf level may be preserved in stem cellulose at all, due to plasticity in the extent of post-photosynthetic exchange reactions under varying levels of humidity (Cheesman and Cernusak, 2016, Voelker and Meinzer, 2017). Therefore, the estimated 1 ‰ contribution of leaf level enrichment to the increase in $\delta^{18}O_{TR}$ could rather be considered a maximum estimate of plant physiological influence.

6.4.4 Increase in seawater $\delta^{18}O$ at moisture origin

The trend in $\delta^{18}O_{TR}$ could be driven by an increase in ocean surface $\delta^{18}O$ ($\delta^{18}O_{SW}$) in the region of evaporation. This could be due to a shift in the origin of source water, though previous work has shown that spatial variation in $\delta^{18}O_{SW}$ in the main source region for the Amazon is fairly low (<1 ‰; Baker et al., 2016). Alternatively, there could be temporal variation in $\delta^{18}O_{SW}$. This can be tested over recent decades by looking at trends in surface seawater salinity, which is often (though not always) linearly related to $\delta^{18}O_{SW}$ (Craig and Gordon, 1965, LeGrande and Schmidt, 2006).

Observations and model simulations of ocean salinity since 1950 have shown that enhanced evaporation from warming oceans has caused surface salinity to increase over most of the Atlantic (Durack and Wijffels, 2010, Durack et al., 2012). However, the main moisture source region for the sample site (inferred from the cluster of grey crosses in Fig. A6.9.1) corresponds to a region where salinity has seen a weak but significant decline since 1950 (Fig. 5b in Durack and Wijffels, 2010). Thus, it seems unlikely that $\delta^{18}O_{SW}$ would have enriched over the same time period. In addition, global seawater $\delta^{18}O$ has only changed by approximately 1 ‰ since the Last Glacial Maximum (Schrag et al., 2002), so changes larger than this in the last two centuries would also not be expected.

6.4.5 Effect of increasing SSTs on fractionation during evaporation from the ocean surface

Temperature-dependent fractionation during evaporation from the surface of a body of water is well understood (e.g. Craig and Gordon, 1965, Mook, 2000, Majoube, 1971). The relationship between fractionation and temperature is inverse, as at higher temperatures there is a smaller difference between the amount of energy needed to evaporate light and heavy molecules of water and therefore fractionation is lower (Mook, 2000). The fractionation between liquid water and water vapour ($\varepsilon_{v/l}$, approximately equal to $\delta^{18}O_{liquid} - \delta^{18}O_{vapour}$) can be calculated using the equation from Majoube (1971) reformulated as in Mook (2000): $\varepsilon_{v/l} = \frac{-7356}{T} + 15.38$ where T is the temperature in kelvin. Using this equation, it was calculated that a SST increase of 1 °C (e.g. 1900–2000, Fig. 6.5b) would result in just a 0.086 ‰ increase in the isotopic composition of evaporated vapour. To achieve the 3 ‰ increase in $\delta^{18}O$ seen in the tree-ring record an improbable 35 °C SST rise would be needed. From this it can be inferred that temperature-driven reductions in fractionation during evaporation from the moisture source are not an important driver of the long-term trend in $\delta^{18}O_{TR}$.

6.4.6 Change in the lapse rate

In a previous study an increase in the lapse rate (the rate of temperature change with altitude in °C km^{-1}) was suggested to explain an increase in the offset between lowland and highland $\delta^{18}O$ records from the Amazon during the Younger Dryas (van

Breukelen et al., 2008). Observation and model data from the Andes show rates of warming increase with altitude, and this trend is projected to continue over the next century (Vuille et al., 2003, Vuille et al., 2008, Bradley et al., 2006). Since there is less isotope fractionation at higher temperatures (e.g. Mook, 2000) it is possible that faster warming at high altitudes since 1800 has steadily reduced the depletion of atmospheric water vapour during orographic precipitation, possibly explaining the increase in the highland $\delta^{18}O_{TR}$ record. The isotope lapse rate (the rate of change in $\delta^{18}O_P$ with altitude in ‰ km^{-1}) divided by the temperature lapse rate gives the expected isotope change per degree of warming (‰ $°C^{-1}$). This allows us to calculate the temperature change that would be required to explain the 3 ‰ increase in $\delta^{18}O_{TR}$. Mean annual $\delta^{18}O_P$ and temperature data from a transect along the eastern Ecuadorian Andes, which passes close to the sample site, were used to calculate the isotope and temperature lapse rates (Garcia et al., 1998). Highland data come from Papallacta (3150 m a.s.l.) and lowland data from Lago Agrio (297 m a.s.l.). The isotope lapse rate of –1.3 ‰ km^{-1} calculated here is approximately half the global average of –2.8 ‰ km^{-1} (Poage and Chamberlain, 2001). Using the regional (global) isotope lapse rate, a 12.8 °C (5.8 °C) temperature rise would be needed at the sample site relative to the lowlands to explain the 3 ‰ rise in $\delta^{18}O_{TR}$. The Andes have seen a temperature rise of 0.68 °C from 1939–2006 (Vuille et al., 2008) while CRU temperature data shows the Amazon region as a whole has warmed by 0.14 °C over the same period. Thus, the increased warming in the highlands could only explain around 0.13 ‰ of the increase in $\delta^{18}O_{TR}$.

6.4.7 A change in local amount effects

The local ‘amount effect’ refers to the inverse relationship between precipitation amount per unit time (e.g. mm $month^{-1}$) and the isotope composition of that precipitation (Dansgaard, 1964). Raindrops become further enriched as they fall through the air, due to re-evaporation and diffusive exchange processes between the rain droplets and the surrounding water vapour (Risi et al., 2008). However, these enrichment processes are less effective during heavy precipitation events as rain falls more quickly and RH is high. A thought experiment can be conducted to imagine the influence on $\delta^{18}O_P$ (and thus $\delta^{18}O_{TR}$) of a change in local amount effects during moisture transport over the basin. In two scenarios, the same volume of precipitation

occurs along a trajectory, such that the fraction of water vapour remaining in the atmosphere at the end of the trajectory is the same in each case. In the first scenario, all of the precipitation falls during a single heavy rainfall event, while in the second scenario there is continuous light precipitation along the full length of the trajectory. Although the total rainout is the same in each case, water vapour will be isotopically heavier at the end of the trajectory in the first scenario than in the second scenario. Aerosols in smoke from fires in the Amazon have been shown to cause delays in the onset of precipitation, and increase the frequency of heavy rainfall events (Andreae et al., 2004). Therefore, an increase in biomass burning in the region may have caused changes in local amount effects (i.e. by shifting rainout patterns towards scenario 1). However, the effect of smoke on clouds in the Amazon is minimal during the wet season (Andreae et al., 2004), which is the period relevant for this study. Therefore, the Ecuador $\delta^{18}O_{TR}$ record is not expected to be strongly affected by changes in local amount effects.

6.4.8 A reduction in rainout fraction over the Amazon

The final environmental driver for increasing $\delta^{18}O_{TR}$ that is considered, is a reduction in rainout fraction over the Amazon, an idea that was first proposed by Brienen et al. (2012). It was shown in section 6.3.2 that $\delta^{18}O_{TR}$ from Ecuador and Bolivia record interannual and decadal variation in Amazon hydrology, modulated by Pacific and Atlantic SSTs. The long-term increase in $\delta^{18}O_{TR}$ and other $\delta^{18}O$ proxy records (Fig. 6.7) might therefore reflect a reduction in precipitation during the wet season. Indeed, other studies have interpreted lake sediment, ice-core and speleothem $\delta^{18}O$ records from the Amazon in this way, and suggest that the change is driven by temperature increases over the North Atlantic forcing a northward shift in the ITCZ (Bird et al., 2011, Vuille et al., 2012). However, an alternative explanation, not considered by these studies, is that the upward trend is caused by an increase in the volume of water vapour coming into the basin, thus reducing the proportion of vapour that rains out. Both of these processes would cause a reduction in rainout fraction over the Amazon. The Rayleigh equation: $\delta^{18}O_{VAP}(t) = (1000 + \delta^{18}O_{VAP}(0)) \cdot f(t)^{(\alpha-1)} - 1000)$ can be used to calculate that the fraction (f) of vapour remaining in the atmosphere at time t (i.e. at the sample site) must have increased by approximately

25% to cause a 3 ‰ rise in vapour $\delta^{18}O$ ($\delta^{18}O_{VAP}$; assuming a temperature dependent fractionation factor (α) of 1.0102 (calculated from a temperature of 15 °C), and an initial water vapour $\delta^{18}O$ ($\delta^{18}O_{VAP}(0)$) of –11 ‰). Though this sounds large, Bordi et al. (2015) used ERA-Interim reanalysis data to show that total column water vapour has increased by around 13% over the Amazon since 1979, which is comparable with another analysis (using the same reanalysis dataset) showing that wet season water vapour import to the Amazon has increased by approximately 15% over the same period, due to warming SSTs in the TNA (Gloor et al., 2015). Thus a 25% increase in incoming water vapour could feasibly explain the full 3 ‰ increase in $\delta^{18}O_{TR}$ since 1800. Alternatively, the increase could also be caused by a 25% reduction in wet season precipitation over the same timeframe, and there are insufficient instrumental data over the relevant period to confirm or refute this. Furthermore, if the 1.22 ‰ that can possibly already be explained by other hypotheses (Table 6.1) is deducted, then only a 16% reduction in rainout fraction from either mechanism is required over the last two centuries.

Since both a reduction in precipitation and an increase in incoming water vapour have been associated with increasing TNA SSTs, historical Atlantic SST data were examined to look for support that the long-term increase in $\delta^{18}O_{TR}$ could be caused by a reduction in rainout fraction through either of these mechanisms. As instrumental data is not available back to 1800, a decadal North Atlantic SST reconstruction from Mann et al. (2009) was used. It should be noted that this reconstructed SST dataset is for the full North Atlantic, not just the tropical region. The reconstruction is based on 1138 proxy datasets, including tree-ring, ice-core, speleothem, coral and marine sediment records. The filtered Ecuador $\delta^{18}O_{TR}$ chronology shows a close resemblance to the reconstructed SST record up until approximately 1970, after which the records correspond less well. Furthermore, both series show an upward trend over the past 200 years. Therefore, it is suggested that warming SSTs since 1800 have driven a long-term reduction in rainout fraction over the Amazon, which has caused an increase in wet season $\delta^{18}O_P$ and this signal is recorded in tree rings in the west of the basin. The mechanism by which Atlantic SSTs affect the rainout fraction remains ambiguous. It could be by determining the position of the ITCZ and therefore affecting the amount of precipitation over the basin (see section 6.3.2), or by controlling the amount of moisture supplied to the

Amazon region and thus influencing proportional rainout. An isotope-enabled general circulation model (GCM) may offer further insights on these potential mechanisms, and could possibly be used in future work to resolve the current ambiguity.

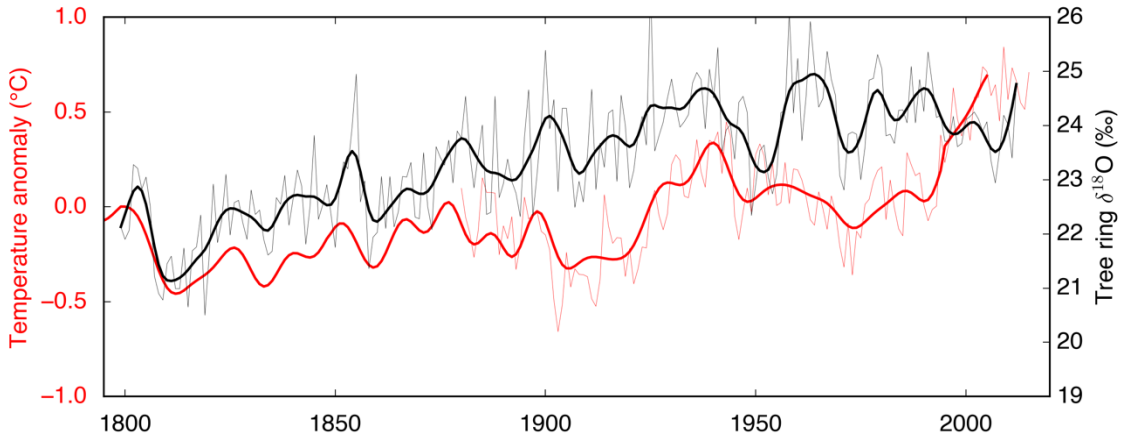

Figure 6.8 – Relationship between $\delta^{18}O_{TR}$ from Ecuador and sea surface temperatures in the North Atlantic (NA SST). The thick red line shows reconstructed decadal NA SST data from Mann et al. (2009), who estimated SSTs using a large proxy dataset. Observed annual mean NA SST anomalies from NOAA are also shown from 1880 for comparison against the reconstructed data (thin red line; averaged over 0–60°N, 75.5–7.5°W). In both cases anomalies are defined relative to a 1961–1990 reference period. Thick and thin black lines respectively indicate decadal and interannual variation in $\delta^{18}O_{TR}$ from Ecuador. A low-pass Butterworth filter was applied to the interannual $\delta^{18}O_{TR}$ record to visualize decadal variability. The Pearson correlation coefficient between the Mann NA SST reconstruction and decadal $\delta^{18}O_{TR}$ is 0.52 (1799–2006, $p<0.001$).

6.5 The Recent Intensification of the Amazon Hydrological Cycle

The long-term increase in $\delta^{18}O_{TR}$ levels out in the middle of the 20th century, and reverses over the most recent period (Figs. 6.2 & A6.3.1). This will now be explored, to see whether it is consistent with the recent amplification of the Amazon hydrological cycle, characterised by increased precipitation seasonality and thus higher wet season precipitation in recent decades (e.g. Gloor et al., 2013, Fu et al., 2013). Both records show declines in $\delta^{18}O_{TR}$ over the past 1–2 decades, though this is particularly notable in the Bolivia record, with a decline in the maxima since the mid-1990s and the lowest value in the whole chronology observed in 2008. The 2008/2009 wet season coincided with one of the most severe flood events ever recorded in the Amazon, and the highest ever maximum water level at Óbidos (Marengo and Espinoza, 2016). The difference between the Ecuador and Bolivia records may be due to the fact that Ecuador $\delta^{18}O_{TR}$ is more influenced by precipitation in the northern part of the basin (Fig. 6.3) and

precipitation over this region (light blue line in Fig. 6.4) hasn't increased as much as it has over the whole basin (dark blue line in Fig. 6.4; see also Gloor et al., 2013). Gloor et al. (2015) suggest the amplification of Amazon hydrology may be due to increased warming in the Atlantic, coupled with a switch to the cold phase of the Pacific Decadal Oscillation (PDO) in the 1990s. Model experiments have revealed an important teleconnection between the Atlantic and Pacific oceans, with increased Atlantic warming driving an acceleration of Pacific trade winds, subduction of heat in the Pacific and colder Pacific SSTs (McGregor et al., 2014, England et al., 2014). The Atlantic Multidecadal Oscillation (AMO) also changed from a cold to a warm phase in the 1990s, which, superimposed on anthropogenic warming has resulted in an 'unprecedented' cross-basin difference in SSTs and increased precipitation over the Amazon basin (Kucharski et al., 2016, McGregor et al., 2014). It is argued that the recent flattening, or even decline, in $\delta^{18}O_{TR}$ is a result of the increase in wet season precipitation associated with a strengthened Amazon hydrological cycle, which has reversed the long-term upward trend in $\delta^{18}O_{TR}$ over the past two centuries.

6.6 Summary

The two longest and best-replicated $\delta^{18}O_{TR}$ records from the Amazon basin to date have been presented in this study. The chronologies from Bolivia (<32 trees, 1860–2014) and Ecuador (<16 trees, 1799–2012) show coherent isotope signatures, indicating they are both governed by the same large-scale climate controls. Analyses have confirmed that $\delta^{18}O_{TR}$ can be used to monitor hydrological changes over the whole Amazon region on short- and long-term timescales. Furthermore, since the chronologies extend substantially beyond the limit of regional hydrological data, they can provide new insights on Amazon hydrology and the factors that control it. Specifically, both records were found to show a long-term increase in $\delta^{18}O_{TR}$, which is the clearest evidence yet of a long-term increase in wet season $\delta^{18}O_P$ in the western Amazon over the past 200 years. The increase in $\delta^{18}O_{TR}$ is related to a gradual rise in SSTs in the North Atlantic over the same period. The mechanism behind the Atlantic influence could either be through a reduction in precipitation over the basin caused by a northward shift of the ITCZ, or by rising SSTs causing an increase in water vapour

imported to the basin. Both of these mechanisms would result in a reduction in the rainout fraction over the Amazon basin, but they cannot be distinguished without additional evidence, possibly from an isotope-enabled GCM. The upward trend has reversed in recent decades, consistent with an intensification of the Amazon hydrological cycle since the 1990s. These records provide proof of long-term changes in Amazon hydrology, although careful analysis is required to correctly interpret these complex datasets.

6.7 References

HidroWeb [Online]. Agência Nacional de Águas. Available: http://hidroweb.ana.gov.br [Accessed 2017].

Ainsworth, E. A. & Long, S. P. 2005. What have we learned from 15 years of free-air CO_2 enrichment (FACE)? A meta-analytic review of the responses of photosynthesis, canopy properties and plant production to rising CO_2. *New Phytologist,* 165**,** 351-372.

Andreae, M. O., Rosenfeld, D., Artaxo, P., Costa, A. A., Frank, G. P., Longo, K. M. & Silva-Dias, M. a. F. 2004. Smoking rain clouds over the Amazon. *Science,* 303**,** 1337-1342.

Andreu-Hayles, L., Ummenhofer, C. C., Barriendos, M., Schleser, G. H., Helle, G., Leuenberger, M., Gutiérrez, E. & Cook, E. R. 2016. 400 Years of summer hydroclimate from stable isotopes in Iberian trees. *Climate Dynamics***,** 1-19.

Antico, A. & Torres, M. E. 2015. Evidence of a decadal solar signal in the Amazon River: 1903 to 2013. *Geophysical Research Letters,* 42**,** 10782-10787.

Apaéstegui, J., Cruz, F. W., Sifeddine, A., Vuille, M., Espinoza, J. C., Guyot, J.-L., Khodri, M., Strikis, N., Santos, R. V., Cheng, H., Edwards, L., Carvalho, E. & Santini, W. 2014. Hydroclimate variability of the northwestern Amazon Basin near the Andean foothills of Peru related to the South American Monsoon System during the last 1600 years. *Climate of the Past,* 10**,** 1967-1981.

Baker, J. C. A., Hunt, S. F. P., Clerici, S. J., Newton, R. J., Bottrell, S. H., Leng, M. J., Heaton, T. H. E., Helle, G., Argollo, J., Gloor, M. & Brienen, R. J. W. 2015. Oxygen isotopes in tree rings show good coherence between species and sites in Bolivia. *Global and Planetary Change,* 133**,** 298-308.

Baker, J. C. A., Gloor, M., Spracklen, D. V., Arnold, S. R., Tindall, J. C., Clerici, S. J., Leng, M. J. & Brienen, R. J. W. 2016. What drives interannual variation in tree ring oxygen isotopes in the Amazon? *Geophysical Research Letters,* 43**,** 11831-11840.

Baker, J. C. A., Santos, G. M., Gloor, M. & Brienen, R. J. W. 2017. Does *Cedrela* always form annual rings? Testing ring periodicity across South America using radiocarbon dating. *Trees - Structure and Function*.

Ballantyne, A. P., Baker, P. A., Chambers, J. Q., Villalba, R. & Argollo, J. 2011. Regional differences in South American monsoon precipitation inferred from the growth and isotopic composition of tropical trees. *Earth Interactions,* 15**,** 1-35.

Barbour, M. M., Fischer, R. A., Sayre, K. D. & Farquhar, G. D. 2000. Oxygen isotope ratio of leaf and grain material correlates with stomatal conductance and grain yield in irrigated wheat. *Functional Plant Biology,* 27**,** 625-637.

Barbour, M. M. & Farquhar, G. D. 2000. Relative humidity- and ABA-induced variation in carbon and oxygen isotope ratios of cotton leaves. *Plant, Cell and Environment,* 23**,** 473-485.

Barbour, M. M., Roden, J. S., Farquhar, G. D. & Ehleringer, J. R. 2004. Expressing leaf water and cellulose oxygen isotope ratios as enrichment above source water reveals evidence of a Péclet effect. *Oecologia,* 138**,** 426-35.

Battipaglia, G., Saurer, M., Cherubini, P., Calfapietra, C., McCarthy, H. R., Norby, R. J. & Francesca Cotrufo, M. 2013. Elevated CO_2 increases tree-level intrinsic water use efficiency: insights from carbon and oxygen isotope analyses in tree rings across three forest FACE sites. *New*

Phytologist, 197**,** 544-54.
Bird, B. W., Abbott, M. B., Vuille, M., Rodbell, D. T., Stansell, N. D. & Rosenmeier, M. F. 2011. A 2,300-year-long annually resolved record of the South American summer monsoon from the Peruvian Andes. *Proceedings of the National Academy of Sciences,* 108**,** 8583-8588.
Boisier, J. P., Ciais, P., Ducharne, A. & Guimberteau, M. 2015. Projected strengthening of Amazonian dry season by constrained climate model simulations. *Nature Climate Change,* 5**,** 656-660.
Bordi, I., De Bonis, R., Fraedrich, K. & Sutera, A. 2015. Interannual variability patterns of the world's total column water content: Amazon River basin. *Theoretical and Applied Climatology,* 122**,** 441-455.
Bradley, R. S., Vuille, M., Diaz, H. F. & Vergara, W. 2006. Threats to water supplies in the tropical Andes. *Science,* 312**,** 1755-1756.
Bradley, R. S. 2011. High-Resolution Paleoclimatology. *In:* HUGHES, M. K., SWETNAM, T. W. & DIAZ, H. F. (eds.) *Dendroclimatology: Progress and Prospects.* Dordrecht: Springer Netherlands.
Bräuning, A., Homeier, J., Cueva, E., Beck, E. & Günter, S. 2008. Growth dynamics of trees in tropical mountain ecosystems. *Gradients in a Tropical Mountain Ecosystem of Ecuador.* Springer.
Bräuning, A., Volland-Voigt, F., Burchardt, I., Ganzhi, O., Nauss, T. & Peters, T. 2009. Climatic control of radial growth of *Cedrela montana* in a humid mountain rainforest in southern Ecuador. *Erdkunde,* 63**,** 337-345.
Brienen, R. J. W. & Zuidema, P. A. 2005. Relating tree growth to rainfall in Bolivian rain forests: a test for six species using tree ring analysis. *Oecologia,* 146**,** 1-12.
Brienen, R. J. W., Helle, G., Pons, T. L., Guyot, J. L. & Gloor, M. 2012. Oxygen isotopes in tree rings are a good proxy for Amazon precipitation and El Niño-Southern Oscillation variability. *Proceedings of the National Academy of Sciences,* 109**,** 16957-16962.
Cernusak, L. A. & Kahmen, A. 2013. The multifaceted relationship between leaf water O enrichment and transpiration rate. *Plant, Cell and Environment,* 36**,** 1239-1241.
Cernusak, L. A., Barbour, M. M., Arndt, S. K., Cheesman, A. W., English, N. B., Feild, T. S., Helliker, B. R., Holloway-Phillips, M. M., Holtum, J. A., Kahmen, A., McInerney, F. A., Munksgaard, N. C., Simonin, K. A., Song, X., Stuart-Williams, H., West, J. B. & Farquhar, G. D. 2016. Stable isotopes in leaf water of terrestrial plants. *Plant, Cell and Environment,* 39**,** 1087-1102.
Cheesman, A. & Cernusak, L. 2016. Infidelity in the outback: climate signal recorded in $\Delta^{18}O$ of leaf but not branch cellulose of eucalypts across an Australian aridity gradient. *Tree Physiology***,** 1-11.
Cook, E. R. & Kairiukstis, L. A. 1990. *Methods of dendrochronology: applications in the environmental sciences*, Dordrecht, The Netherlands, Kluwer Academic Publishers.
Cox, P. M., Betts, R. A., Collins, M., Harris, P. P., Huntingford, C. & Jones, C. D. 2004. Amazonian forest dieback under climate-carbon cycle projections for the 21st century. *Theoretical and applied climatology,* 78**,** 137-156.
Craig, H. & Gordon, L. I. 1965. Deuterium and oxygen 18 variations in the ocean and the marine atmosphere. *In:* TONGIOGI, E. (ed.) *Stable Isotopes in Oceanographic Studies and Paleotemperatures.* Spoleto, Italy: Consiglio nazionale delle richerche, Laboratorio de geologia nucleare.
Cruz, F. W., Vuille, M., Burns, S. J., Wang, X., Cheng, H., Werner, M., Edwards, R. L., Karmann, I., Auler, A. S. & Nguyen, H. 2009. Orbitally driven east–west antiphasing of South American precipitation. *Nature Geoscience,* 2**,** 210-214.
Dansgaard, W. 1964. Stable isotopes in precipitation. *Tellus,* 16**,** 436-468.
De Boer, H. J., Lammertsma, E. I., Wagner-Cremer, F., Dilcher, D. L., Wassen, M. J. & Dekker, S. C. 2011. Climate forcing due to optimization of maximal leaf conductance in subtropical vegetation under rising CO_2. *Proceedings of the National Academy of Sciences,* 108**,** 4041-4046.
Durack, P. J. & Wijffels, S. E. 2010. Fifty-year trends in global ocean salinities and their relationship to broad-scale warming. *Journal of Climate,* 23**,** 4342-4362.
Durack, P. J., Wijffels, S. E. & Matear, R. J. 2012. Ocean salinities reveal strong global water cycle intensification during 1950 to 2000. *science,* 336**,** 455-458.
England, M. H., McGregor, S., Spence, P., Meehl, G. A., Timmermann, A., Cai, W., Gupta, A. S., McPhaden, M. J., Purich, A. & Santoso, A. 2014. Recent intensification of wind-driven circulation in the Pacific and the ongoing warming hiatus. *Nature Climate Change,* 4**,** 222-227.
Esper, J., Frank, D. C., Battipaglia, G., Büntgen, U., Holert, C., Treydte, K., Siegwolf, R. & Saurer, M. 2010. Low-frequency noise in $\delta^{13}C$ and $\delta^{18}O$ tree ring data: A case study of *Pinus uncinata* in the Spanish Pyrenees. *Global Biogeochemical Cycles,* 24**,** 1-11.

Espinoza, J. C., Ronchail, J., Guyot, J. L., Junquas, C., Vauchel, P., Lavado, W., Drapeau, G. & Pombosa, R. 2011. Climate variability and extreme drought in the upper Solimões River (western Amazon Basin): Understanding the exceptional 2010 drought. *Geophysical Research Letters,* 38**,** 1-6.

Espinoza, J. C., Marengo, J. A., Ronchail, J., Carpio, J. M., Flores, L. N. & Guyot, J. L. 2014. The extreme 2014 flood in south-western Amazon basin: the role of tropical-subtropical South Atlantic SST gradient. *Environmental Research Letters,* 9**,** 1-9.

Farquhar, G. & Lloyd, J. 1993. Carbon and oxygen isotope effects in the exchange of carbon dioxide between terrestrial plants and the atmosphere. *Stable isotopes and plant carbon-water relations,* 40**,** 47-70.

Fernandes, K., Baethgen, W., Bernardes, S., Defries, R., Dewitt, D. G., Goddard, L., Lavado, W., Lee, D. E., Padoch, C. & Pinedo-Vasquez, M. 2011. North Tropical Atlantic influence on western Amazon fire season variability. *Geophysical Research Letters,* 38**,** 1-5.

Fu, R., Yin, L., Li, W., Arias, P. A., Dickinson, R. E., Huang, L., Chakraborty, S., Fernandes, K., Liebmann, B., Fisher, R. A. & Myneni, R. B. 2013. Increased dry-season length over southern Amazonia in recent decades and its implication for future climate projection. *Proceedings of the National Academy of Sciences,* 110**,** 18110-18115.

Garcia, M., Villalba, F., Araguas-Araguas, L. & Rozanski, K. 1998. The role of atmospheric circulation patterns in controlling the regional distribution of stable isotope contents in precipitation: Preliminary results from two transects in the Ecuadorian Andes. *Isotope techniques in the study of environmental change.* International Atomic Energy Agency (IAEA): IAEA.

Gärtner, H. & Nievergelt, D. 2010. The core-microtome: a new tool for surface preparation on cores and time series analysis of varying cell parameters. *Dendrochronologia,* 28**,** 85-92.

Gatti, L., Gloor, M., Miller, J., Doughty, C., Malhi, Y., Domingues, L., Basso, L., Martinewski, A., Correia, C. & Borges, V. 2014. Drought sensitivity of Amazonian carbon balance revealed by atmospheric measurements. *Nature,* 506**,** 76-80.

Gloor, M., Brienen, R. J. W., Galbraith, D., Feldpausch, T. R., Schöngart, J., Guyot, J. L., Espinoza, J. C., Lloyd, J. & Phillips, O. L. 2013. Intensification of the Amazon hydrological cycle over the last two decades. *Geophysical Research Letters,* 40**,** 1729-1733.

Gloor, M., Barichivich, J., Ziv, G., Brienen, R. J. W., Schöngart, J., Peylin, P., Cintra, B. B. L., Feldpausch, T. R., Phillips, O. L. & Baker, J. C. A. 2015. Recent Amazon climate as background for possible ongoing and future changes of Amazon humid forests. *Global Biogeochemical Cycles,* 29**,** 1384-1399.

Hardy, D., Vuille, M. & Bradley, R. 2003. Variability of snow accumulation and isotopic composition on Nevado Sajama, Bolivia. *Journal of Geophysical Research: Atmospheres* 108**,** 1-10.

Harris, I., Jones, P. D., Osborn, T. J. & Lister, D. H. 2014. Updated high-resolution grids of monthly climatic observations–the CRU TS3.10 Dataset. *International Journal of Climatology,* 34**,** 623-642.

Hietz, P., Wanek, W. & Dünisch, O. 2005. Long-term trends in cellulose $\delta^{13}C$ and water-use efficiency of tropical *Cedrela* and *Swietenia* from Brazil. *Tree Physiology*, 25, 745-752.

Huang, B., Banzon, V. F., Freeman, E., Lawrimore, J., Liu, W., Peterson, T. C., Smith, T. M., Thorne, P. W., Woodruff, S. D. & Zhang, H.-M. 2015. Extended reconstructed sea surface temperature version 4 (ERSST. v4). Part I: Upgrades and intercomparisons. *Journal of Climate,* 28**,** 911-930.

Huang, B., Thorne, P. W., Smith, T. M., Liu, W., Lawrimore, J., Banzon, V. F., Zhang, H.-M., Peterson, T. C. & Menne, M. 2016. Further exploring and quantifying uncertainties for extended reconstructed sea surface temperature (ERSST) version 4 (v4). *Journal of Climate,* 29**,** 3119-3142.

Huntingford, C., Fisher, R. A., Mercado, L., Booth, B. B. B., Sitch, S., Harris, P. P., Cox, P. M., Jones, C. D., Betts, R. A., Malhi, Y., Harris, G. R., Collins, M. & Moorcroft, P. 2008. Towards quantifying uncertainty in predictions of Amazon 'dieback'. *Philosophical Transactions of the Royal Society B: Biological Sciences,* 363**,** 1857-1864.

Insel, N., Poulsen, C. J., Sturm, C. & Ehlers, T. A. 2013. Climate controls on Andean precipitation $\delta^{18}O$ interannual variability. *Journal of Geophysical Research: Atmospheres,* 118**,** 9721-9742.

Kagawa, A., Sano, M., Nakatsuka, T., Ikeda, T. & Kubo, S. 2015. An optimized method for stable isotope analysis of tree rings by extracting cellulose directly from cross-sectional laths. *Chemical Geology,* 393**,** 16-25.

Kahmen, A., Sachse, D., Arndt, S. K., Tu, K. P., Farrington, H., Vitousek, P. M. & Dawson, T. E. 2011. Cellulose $\delta^{18}O$ is an index of leaf-to-air vapor pressure difference (VPD) in tropical plants.

Proceedings of the National Academy of Sciences, 108**,** 1981-1986.
Kanner, L. C., Burns, S. J., Cheng, H., Edwards, R. L. & Vuille, M. 2013. High-resolution variability of the South American summer monsoon over the last seven millennia: insights from a speleothem record from the central Peruvian Andes. *Quaternary Science Reviews,* 75**,** 1-10.
Karamouz, M., Nazif, S. & Falahi, M. 2012. *Hydrology and hydroclimatology: principles and applications*, CRC Press.
Keenan, T. F., Hollinger, D. Y., Bohrer, G., Dragoni, D., Munger, J. W., Schmid, H. P. & Richardson, A. D. 2013. Increase in forest water-use efficiency as atmospheric carbon dioxide concentrations rise. *Nature,* 499**,** 324-327.
Kilroy, E., McCarroll, D., Young, G. H., Loader, N. J. & Bale, R. J. 2016. Absence of juvenile effects confirmed in stable carbon and oxygen isotopes of European larch trees. *Acta Silvae et Ligni***,** 27-33.
Kucharski, F., Ikram, F., Molteni, F., Farneti, R., Kang, I.-S., No, H.-H., King, M. P., Giuliani, G. & Mogensen, K. 2016. Atlantic forcing of Pacific decadal variability. *Climate Dynamics,* 46**,** 2337-2351.
Labuhn, I., Daux, V., Pierre, M., Stievenard, M., Girardclos, O., Feron, A., Genty, D., Masson-Delmotte, V. & Mestre, O. 2014. Tree age, site and climate controls on tree ring cellulose delta O-18: A case study on oak trees from south-western France. *Dendrochronologia,* 32**,** 78-89.
Lammertsma, E. I., De Boer, H. J., Dekker, S. C., Dilcher, D. L., Lotter, A. F. & Wagner-Cremer, F. 2011. Global CO_2 rise leads to reduced maximum stomatal conductance in Florida vegetation. *Proceedings of the National Academy of Sciences,* 108**,** 4035-4040.
Legrande, A. N. & Schmidt, G. A. 2006. Global gridded data set of the oxygen isotopic composition in seawater. *Geophysical Research Letters,* 33**,** 1-5.
Lewis, S. L., Brando, P. M., Phillips, O. L., Van Der Heijden, G. M. & Nepstad, D. 2011. The 2010 amazon drought. *Science,* 331**,** 554-554.
Li, Z.-H., Labbé, N., Driese, S. G. & Grissino-Mayer, H. D. 2011. Micro-scale analysis of tree-ring $\delta^{18}O$ and $\delta^{13}C$ on α-cellulose spline reveals high-resolution intra-annual climate variability and tropical cyclone activity. *Chemical Geology,* 284**,** 138-147.
Loader, N. J., Robertson, I., Lucke, A. & Helle, G. 2002. Preparation of holocellulose from standard increment cores for stable carbon isotope analysis. *Swansea Geographer,* 37**,** 1-9.
Majoube, M. 1971. Fractionnement en oxygène-18 et en deutérium entre l'eau et sa vapeur. *Journal de Chimie Physique et de Physico-Chimie Biologique,* 58**,** 1423-1435.
Malhi, Y., Aragão, L. E., Galbraith, D., Huntingford, C., Fisher, R., Zelazowski, P., Sitch, S., McSweeney, C. & Meir, P. 2009. Exploring the likelihood and mechanism of a climate-change-induced dieback of the Amazon rainforest. *Proceedings of the National Academy of Sciences,* 106**,** 20610-20615.
Mann, M. E., Zhang, Z., Rutherford, S., Bradley, R. S., Hughes, M. K., Shindell, D., Ammann, C., Faluvegi, G. & Ni, F. 2009. Global signatures and dynamical origins of the Little Ice Age and Medieval Climate Anomaly. *Science,* 326**,** 1256-1260.
Marengo, J. A., Tomasella, J., Alves, L. M., Soares, W. R. & Rodriguez, D. A. 2011. The drought of 2010 in the context of historical droughts in the Amazon region. *Geophysical Research Letters,* 38**,** 1-5.
Marengo, J. A. & Espinoza, J. C. 2016. Extreme seasonal droughts and floods in Amazonia: causes, trends and impacts. *International Journal of Climatology,* 36**,** 1033-1050.
McGregor, S., Timmermann, A., Stuecker, M. F., England, M. H., Merrifield, M., Jin, F.-F. & Chikamoto, Y. 2014. Recent Walker circulation strengthening and Pacific cooling amplified by Atlantic warming. *Nature Climate Change,* 4**,** 888-892.
Mook, W. G. 2000. *Environmental isotopes in the hydrological cycle: Volume I Introduction (Theory, Methods, Review)*, International Atomic Energy Agency and United Nations Educational, Scientific and Cultural Organization.
Moquet, J., Cruz, F., Novello, V., Stríkis, N., Deininger, M., Karmann, I., Santos, R. V., Millo, C., Apaestegui, J., Guyot, J.-L., Siffedine, A., Vuille, M., Cheng, H., Edwards, R. & Santini, W. 2016. Calibration of speleothem $\delta^{18}O$ records against hydroclimate instrumental records in Central Brazil. *Global and Planetary Change,* 139**,** 151-164.
National Research Council (2006) *Surface temperature reconstructions for the last 2,000 years*. National Academies Press, USA.
Nobre, C. A., Obregón, G. O., Marengo, J. A., Fu, R. & Poveda, G. 2009. Characteristics of Amazonian Climate: Main Features. *Amazonia and Global Change.* American Geophysical Union.

Novello, V. F., Vuille, M., Cruz, F. W., Stríkis, N. M., De Paula, M. S., Edwards, R. L., Cheng, H., Karmann, I., Jaqueto, P. F., Trindade, R. I. F., Hartmann, G. A. & Moquet, J. S. 2016. Centennial-scale solar forcing of the South American Monsoon System recorded in stalagmites. *Scientific Reports,* 6**,** 1-8.

Peterson, T. C. & Vose, R. S. 1997. An overview of the Global Historical Climatology Network temperature database. *Bulletin of the American Meteorological Society,* 78**,** 2837-2849.

Phillips, O. L., Aragão, L. E., Lewis, S. L., Fisher, J. B., Lloyd, J., López-González, G., Malhi, Y., Monteagudo, A., Peacock, J. & Quesada, C. A. 2009. Drought sensitivity of the Amazon rainforest. *Science,* 323**,** 1344-1347.

Pierrehumbert, R. T. 1999. Huascaran $\delta^{18}O$ as an indicator of tropical climate during the Last Glacial Maximum. *Geophysical Research Letters,* 26**,** 1345-1348.

Poage, M. A. & Chamberlain, C. P. 2001. Empirical relationships between elevation and the stable isotope composition of precipitation and surface waters: considerations for studies of paleoelevation change. *American Journal of Science,* 301**,** 1-15.

Raia, A. & Cavalcanti, I. F. A. 2008. The Life Cycle of the South American Monsoon System. *Journal of Climate,* 21**,** 6227-6246.

Risi, C., Bony, S. & Vimeux, F. 2008. Influence of convective processes on the isotopic composition ($\delta^{18}O$ and δD) of precipitation and water vapor in the tropics: 2. Physical interpretation of the amount effect. *Journal of Geophysical Research: Atmospheres,* 113**,** 1-12.

Salati, E., Dall'olio, A., Matsui, E. & Gat, J. R. 1979. Recycling of water in the Amazon basin: an isotopic study. *Water Resources Research,* 15**,** 1250-1258.

Sano, M., Tshering, P., Komori, J., Fujita, K., Xu, C. & Nakatsuka, T. 2013. May–September precipitation in the Bhutan Himalaya since 1743 as reconstructed from tree ring cellulose $\delta^{18}O$. *Journal of Geophysical Research: Atmospheres,* 118**,** 8399-8410.

Schrag, D. P., Adkins, J. F., McIntyre, K., Alexander, J. L., Hodell, D. A., Charles, C. D. & McManus, J. F. 2002. The oxygen isotopic composition of seawater during the Last Glacial Maximum. *Quaternary Science Reviews,* 21**,** 331-342.

SIDC [Online]. *Solar Influences Data Analysis Centre.* Available: http://www.sidc.be/silso/ [Accessed 2017].

Sternberg, L. D. S. L. 2009. Oxygen stable isotope ratios of tree-ring cellulose: the next phase of understanding. *New Phytologist,* 181**,** 553-562.

Stokes, M. & Smiley, T. 1968. *An introduction to tree-ring dating*, University of Arizona Press.

Thompson, L. G., Mosley-Thompson, E. & Henderson, K. A. 2000. Ice-core palaeoclimate records in tropical South America since the Last Glacial Maximum. *Journal of Quaternary Science,* 15**,** 377-394.

Thompson, L. G., Mosley-Thompson, E., Davis, M. E., Zagorodnov, V. S., Howat, I. M., Mikhalenko, V. N. & Lin, P. N. 2013. Annually resolved ice core records of tropical climate variability over the past ~1800 years. *Science,* 340**,** 945-950.

Treydte, K. S., Schleser, G. H., Helle, G., Frank, D. C., Winiger, M., Haug, G. H. & Esper, J. 2006. The twentieth century was the wettest period in northern Pakistan over the past millennium. *Nature,* 440**,** 1179-1182.

Van Breukelen, M. R., Vonhof, H. B., Hellstrom, J. C., Wester, W. C. G. & Kroon, D. 2008. Fossil dripwater in stalagmites reveals Holocene temperature and rainfall variation in Amazonia. *Earth and Planetary Science Letters,* 275**,** 54-60.

Van Der Sleen, P., Groenendijk, P., Vlam, M., Anten, N. P., Boom, A., Bongers, F., Pons, T. L., Terburg, G. & Zuidema, P. A. 2015. No growth stimulation of tropical trees by 150 years of CO_2 fertilization but water-use efficiency increased. *Nature Geoscience,* 8**,** 24-28.

Villacís, M., Vimeux, F. & Taupin, J. D. 2008. Analysis of the climate controls on the isotopic composition of precipitation ($\delta^{18}O$) at Nuevo Rocafuerte, 74.5 W, 0.9 S, 250 m, Ecuador. *Comptes Rendus Geoscience,* 340**,** 1-9.

Vimeux, F., Gallaire, R., Bony, S., Hoffmann, G. & Chiang, J. C. 2005. What are the climate controls on δD in precipitation in the Zongo Valley (Bolivia)? Implications for the Illimani ice core interpretation. *Earth and Planetary Science Letters,* 240**,** 205-220.

Voelker, S. L. & Meinzer, F. C. 2017. Where and when does stem cellulose $\delta^{18}O$ reflect a leaf water enrichment signal? *Tree Physiology,* 00**,** 1-3.

Volland, F., Pucha, D. & Braeuning, A. 2016. Hydro-climatic variability in southern Ecuador reflected by tree-ring oxygen isotopes. *Erdkunde,* 70**,** 69-82.

Vuille, M., Bradley, R. S., Werner, M. & Keimig, F. 2003. 20th century climate change in the tropical

Andes: observations and model results. *Climate Variability and Change in High Elevation Regions: Past, Present & Future.* Springer.
Vuille, M., Francou, B., Wagnon, P., Juen, I., Kaser, G., Mark, B. G. & Bradley, R. S. 2008. Climate change and tropical Andean glaciers: Past, present and future. *Earth-Science Reviews,* 89**,** 79-96.
Vuille, M., Burns, S., Taylor, B., Cruz, F., Bird, B., Abbott, M., Kanner, L., Cheng, H. & Novello, V. 2012. A review of the South American monsoon history as recorded in stable isotopic proxies over the past two millennia. *Climate of the Past,* 8**,** 1309-1321.
Wang, X., Edwards, R. L., Auler, A. S., Cheng, H., Kong, X., Wang, Y., Cruz, F. W., Dorale, J. A. & Chiang, H.-W. 2017. Hydroclimate changes across the Amazon lowlands over the past 45,000 years. *Nature,* 541**,** 204-207.
Wieloch, T., Helle, G., Heinrich, I., Voigt, M. & Schyma, P. 2011. A novel device for batch-wise isolation of α-cellulose from small-amount wholewood samples. *Dendrochronologia,* 29**,** 115-117.
Wigley, T. M., Briffa, K. R. & Jones, P. D. 1984. On the average value of correlated time series, with applications in dendroclimatology and hydrometeorology. *Journal of Climate and Applied Meteorology,* 23**,** 201-213.
Wu, Z. & Huang, N. E. 2009. Ensemble empirical mode decomposition: a noise-assisted data analysis method. *Advances in adaptive data analysis,* 1**,** 1-41.
Xu, C., Sano, M. & Nakatsuka, T. 2011. Tree ring cellulose $\delta^{18}O$ of *Fokienia hodginsii* in northern Laos: A promising proxy to reconstruct ENSO? *Journal of Geophysical Research,* 116**,** 1-12.
Xu, C. X., Ge, J. Y., Nakatsuka, T., Yi, L., Zheng, H. Z. & Sano, M. 2016. Potential utility of tree ring delta O-18 series for reconstructing precipitation records from the lower reaches of the Yangtze River, southeast China. *Journal of Geophysical Research: Atmospheres,* 121**,** 3954-3968.
Yoon, J.-H. & Zeng, N. 2010. An Atlantic influence on Amazon rainfall. *Climate Dynamics,* 34**,** 249-264.
Yoon, J. H. 2016. Multi-model analysis of the Atlantic influence on Southern Amazon rainfall. *Atmospheric Science Letters,* 17**,** 122-127.
Young, G. H. F., Demmler, J. C., Gunnarson, B. E., Kirchhefer, A. J., Loader, N. J. & McCarroll, D. 2011. Age trends in tree ring growth and isotopic archives: A case study of *Pinus sylvestris* L. from northwestern Norway. *Global Biogeochemical Cycles,* 25**,** 1-6.
Zemp, D. C., Schleussner, C.-F., Barbosa, H. M. J., Hirota, M., Montade, V., Sampaio, G., Staal, A., Wang-Erlandsson, L. & Rammig, A. 2017. Self-amplified Amazon forest loss due to vegetation-atmosphere feedbacks. *Nature Communications,* 8**,** 1-10.
Zeng, N., Yoon, J.-H., Marengo, J. A., Subramaniam, A., Nobre, C. A., Mariotti, A. & Neelin, J. D. 2008. Causes and impacts of the 2005 Amazon drought. *Environmental Research Letters,* 3**,** 1-9.

Chapter 7: Discussion

The Amazon rainforest resides within the world's largest drainage basin and is an important global store of carbon and biodiversity (Phillips et al., 2008). Regional climate is dominated by the diverse and complex interactions between the biosphere and the atmosphere, including the extensive exchanges of water, CO_2, energy and various chemical species (Silva Dias et al., 2002, Bonan, 2008). Rain gauge and river flux data from the Amazon show that the hydrological cycle has intensified in recent decades, with a growing divergence between the climate of the wet and the dry seasons (Gloor et al., 2013), and an increase in the frequency of extreme flood and drought events (Marengo and Espinoza, 2016). Such changes have the potential to destabilise the region, and, due to the close interdependency of the forest and the climate, could result in future forest losses (Cox et al., 2004, Huntingford et al., 2008, Zemp et al., 2017). However, climate predictions for the Amazon as yet remain far from certain (Boisier et al., 2015), and understanding of regional hydrology is limited by the scarcity of instrumental climate observations, particularly long-term climate records, which would provide historical context to recent and on-going hydrological changes.

The purpose of this thesis was to develop a deeper understanding of the Amazon hydrological cycle through analysing stable oxygen isotopes in tree rings ($\delta^{18}O_{TR}$) from the region. Due to earlier misconceptions that tropical trees do not form annual rings (e.g. Whitmore, 1998) dendrochronological research is still a relatively young field in tropical South America (Boninsegna et al., 2009). Therefore, it was first necessary to test the annual character of tree rings from different sites in the study. $\delta^{18}O_{TR}$ records were then developed from a range of different tree species and compared from multiple sites across the basin. Next, to facilitate the palaeoclimate interpretation of new $\delta^{18}O_{TR}$ chronologies from the Amazon, the mechanistic drivers of interannual variability were investigated using an approach combining trajectory modelling and vapour transport analysis. Finally, Amazon $\delta^{18}O_{TR}$ records were extended backwards in time, beyond the limit of instrumental climate data.

This chapter of the thesis collates the findings from chapters 3–6, providing further in-depth critical analysis and discussion of the literature (7.1). The extent to

which the original thesis aims and research questions have been achieved and answered is assessed, while also considering some of the difficulties encountered during the course of the research (7.2). In the following sections, the limitations associated with $\delta^{18}O_{TR}$ proxy records are reviewed (7.3) and the research implications and directions for future work are discussed (7.4). Finally, the chapter closes with a summary of the overarching conclusions that can be drawn from the thesis (7.5).

7.1 Overview of Findings and General Discussion

The results presented in this thesis represent a substantial advance of tree-ring stable isotope research in tropical South America. Here, a brief synopsis of the major findings from each chapter is given, followed by a synthesis of the results in the context of the literature.

7.1.1 Chapter summaries

In Chapter 3 the radiocarbon (^{14}C) signatures of tree-ring samples from sites across the Amazon were analysed to evaluate variation in growth periodicity. *Cedrela* spp. from three out of four sites analysed (i.e. Bolivia, Ecuador and Venezuela) were shown to form one ring per year, supporting previous studies in the same (Brienen and Zuidema, 2005, Bräuning et al., 2009, Worbes and Junk, 1999) and other (Dünisch et al., 2002, Dünisch et al., 2003, Costa et al., 2013, Brienen et al., 2010) tropical locations. However, in Suriname, where dendrochronological research has not been previously undertaken, *Cedrela* trees were found to form two rings nearly every year. From analyses of climate data and phenological observations from the literature it was concluded that the seemingly anomalous growth pattern in trees from Suriname is most likely to be caused by a combination of precipitation seasonality and an influence of genetics.

The first stable oxygen isotope series of the thesis were shown in Chapter 4. This chapter focused on tree-ring samples from Bolivia, comparing interannual $\delta^{18}O_{TR}$ signatures between sites and tree species. Samples were dated by comparison to an established $\delta^{18}O_{TR}$ chronology, and also using ^{14}C dating. A new $\delta^{18}O_{TR}$ record developed from nine *Cedrela odorata* trees was presented, and it was shown that $\delta^{18}O_{TR}$

signals had higher inter-tree synchronicity than ring-width signals, indicating that $\delta^{18}O_{TR}$ preserves a coherent climate signal. In addition, the new chronology was shown to correlate strongly (r=0.80, n=101) with the $\delta^{18}O_{TR}$ record from Brienen et al. (2012), despite coming from a site over 300 km away, evidence that $\delta^{18}O_{TR}$ records in the Amazon cohere at large spatial scales. Finally, $\delta^{18}O_{TR}$ records from six of the seven other tropical tree species analysed were found to correlate significantly with *C. odorata* $\delta^{18}O_{TR}$, including a species growing in a site 1000 km away on the Bolivian Altiplano, providing further support for large-scale coherence of $\delta^{18}O_{TR}$ signatures. However, correlations of the individual species $\delta^{18}O_{TR}$ records with *C. odorata* varied (r=0.27–0.90), possibly due to species-specific partitioning of water in the soil profile, or differences in plant physiology.

The mechanisms driving interannual variability in Amazon $\delta^{18}O_{TR}$ records were investigated in Chapter 5. Remote sensing observations of precipitation and leaf area index (LAI) were combined with air-mass trajectories, and large-scale transport of water vapour, as estimated by reanalysis of meteorological data, was analysed to determine whether $\delta^{18}O_{TR}$ signals are truly controlled by processes happening over the Amazon basin. The results confirm earlier suggestions that rainout of heavy isotopes during moisture transport over the Amazon is the primary factor controlling year-to-year variation in $\delta^{18}O_{TR}$ from northern Bolivia, and that these records are able to capture basin-scale variability in Amazon hydrology (Brienen et al., 2012). These results provide the verification required for Amazon $\delta^{18}O_{TR}$ chronologies to be reliably used to reconstruct palaeoclimate at interannual timescales.

Chapter 6 presented the two longest and best-replicated $\delta^{18}O_{TR}$ records from the Amazon to date. Although the records come from sites 1500 km apart in Ecuador and Bolivia, they were found to correlate well at both interannual and decadal timescales. Correlation analyses show that the Ecuador $\delta^{18}O_{TR}$ record is controlled by the same large-scale controls as $\delta^{18}O_{TR}$ from Bolivia, namely the amount of upwind precipitation during passage of moisture over the basin. Since the records are long (214 years and 155 years for the Ecuadorian and Bolivian records respectively), the low-frequency (i.e. centennial) signals in the records could also be analysed. After quantifying all possible sources of variability, it was concluded that the observed long-term increase in $\delta^{18}O_{TR}$ since the early 1800s most likely reflects a reduction in the proportion of water vapour

that rains out over the Amazon basin. The increase in $\delta^{18}O_{TR}$ corresponded well with an increase in Atlantic sea surface temperatures (SSTs) over the same period, indicating a remote driver of change. Finally, the two long $\delta^{18}O_{TR}$ records were used to contextualise the recent intensification of the Amazon hydrological cycle.

7.1.2 Synthesis of results

This thesis fits into a wider body of tree-ring isotope studies from across the tropics (see van der Sleen et al., 2017 for a recent review). The field is still relatively new, particularly in comparison with temperate regions (see the International Tree-Ring Data Bank, ITRDB, 2015), and has only begun to develop over the past 10–15 years. Stable isotope dendroclimatology is particularly valuable in the tropics, as there is often a paucity of instrumental climate data beyond the last few decades in these regions (e.g. Boninsegna et al., 2009). There have been relatively few $\delta^{18}O_{TR}$ studies in tropical South America (i.e. Evans and Schrag, 2004, Ballantyne et al., 2011, Brienen et al., 2012, Volland et al., 2016, Ohashi et al., 2016), or in Africa, where there have been some very preliminary studies in dry tropical sites (Verheyden et al., 2004, Gebrekirstos et al., 2011, Williams et al., 2012) and, more recently some longer $\delta^{18}O_{TR}$ records from humid tropical sites (van der Sleen et al., 2015, Colombaroli et al., 2016). However, $\delta^{18}O_{TR}$ studies in tropical Southeast Asia are more numerous, with research conducted in a variety of different countries (e.g. Poussart et al., 2004, Xu et al., 2011, Sano et al., 2012, Zhu et al., 2012, Schollaen et al., 2013, Xu et al., 2013, Xu et al., 2015, Muangsong et al., 2016, Harada et al., 2017). The main findings of the thesis will be reviewed in the context of this literature, comparing the controls on $\delta^{18}O_{TR}$ from the Amazon with controls on $\delta^{18}O_{TR}$ records from elsewhere in the tropics.

One of the main results of the work presented here is that $\delta^{18}O_{TR}$ signatures in the Amazon are governed by large-scale climate controls. This is exemplified by the excellent coherence between *Cedrela* $\delta^{18}O_{TR}$ records from distant sites, first within Bolivia (sites 325 km apart, r=0.80, n=101, Chapter 4), and between sites in Bolivia and Ecuador (sites 1500 km apart, r=0.57, n=153, Chapter 6), and also the slightly weaker correlation between lowland *Cedrela* $\delta^{18}O_{TR}$ and *Polylepis* $\delta^{18}O_{TR}$ from the Bolivian Altiplano (sites 1000 km apart, r=0.39, n=60, Chapter 4). These results strongly indicate that precipitation isotopes ($\delta^{18}O_P$) in the Amazon cohere at the same large spatial scales,

and that these $\delta^{18}O_P$ signatures are recorded in tree-ring cellulose. There are insufficient data from Africa to assess spatial coherence in tropical $\delta^{18}O_{TR}$ signals here, though several studies in the monsoon region of Southeast Asia have explicitly investigated this. Sano et al. (2012) showed a strong coherence between their $\delta^{18}O_{TR}$ chronology from Vietnam with another record 150 km away in Laos (r=0.77). From this they concluded that there is a regional hydrological control on $\delta^{18}O_{TR}$. Xu et al. (2015) extended the comparison to include a record from a site in northwest Thailand, and found significant correlations with the $\delta^{18}O_{TR}$ chronologies from Laos and Vietnam, which are 500 and 700 km away from the Thailand site respectively (r=0.4 for both correlations). It should be noted that although sample replication was relatively low in both of these studies (e.g. Sano et al. (2012) measured isotope ratios in six trees and Xu et al. (2015) analysed just four trees), Expressed Population Signal (EPS) values exceeding 0.85 were reported, indicating that the constructed chronologies were adequately robust. Further north, on the high-elevation Tibetan Plateau (approximately 30°N), $\delta^{18}O_{TR}$ chronologies have also been shown to correlate at large distances (<800 km; Grießinger et al., 2011, Liu et al., 2013, An et al., 2014, Liu et al., 2014), though these relationships were weaker and the direction of low-frequency trends did not correspond between all records analysed. In these Tibetan studies, wood was pooled from multiple trees prior to isotope analysis (e.g. Grießinger et al., 2011, Liu et al., 2013, An et al., 2014). This time- and cost-saving approach is nonetheless dissatisfactory, since much valuable information is lost, and inter-tree isotope variability cannot be assessed. This makes it more difficult to assess the quality of the resulting chronologies, and could possibly explain why correlations between these records were lower than elsewhere in Southeast Asia. Overall, these studies show that $\delta^{18}O_{TR}$ signals in tropical and subtropical Southeast Asia are controlled by regional climate signals operating at a similarly large scale to that observed over the Amazon, though the distances between the compared Amazon $\delta^{18}O_{TR}$ records are larger, and the relationships stronger.

The scale of coherence between $\delta^{18}O_{TR}$ records is a good indication of the scale at which palaeoclimate data can be reconstructed, and thus the results from the Amazon provide additional support that $\delta^{18}O_{TR}$ signals can be used to reconstruct whole-basin climate (Brienen et al., 2012). However, it is important to explicitly evaluate the

reconstruction potential of the $\delta^{18}O_{TR}$ records presented in this study. First, the EPS values for the Bolivia and Ecuador chronologies are exceptionally high (0.99 and 0.93 respectively), indicating a strong inter-tree correlation in both records. A high EPS (>0.85) is an essential condition for chronologies used to reconstruct climate, as it is indicative of a strong external control on the proxy signal (Wigley et al., 1984). van der Sleen et al., (2015) report a maximum EPS of just 0.74 for their chronology from Cameroon, and although the authors demonstrate significant correlations between their five individual tree records, the low EPS value suggests that future studies in the region ought to include a higher number of trees to construct a chronology sufficiently robust for climate reconstructions. Where reported, $\delta^{18}O_{TR}$ studies in Southeast Asia tend to show EPS values higher than the generally accepted threshold of 0.85 (e.g. Sano et al., 2012; Schollaen et al., 2013; Xu et al., 2015), though not always (e.g. Xu et al., 2011), and, as noted previously, some Southeast Asian studies cannot calculate EPS statistics due to limitations of their chosen methodology (e.g. Grießinger et al., 2011, Liu et al., 2013, An et al., 2014). The Pearson correlation coefficients between Amazon $\delta^{18}O_{TR}$ chronologies and Amazon River discharge presented here are also relatively high (r=–0.63 and r=–0.75, n=110 and 112 for Ecuador and Bolivia respectively), a further indication that these records are suitable for reconstructing palaeoclimate. Indeed, these r values are some of the highest reported for $\delta^{18}O_{TR}$-climate relationships in the tropics (*cf*. Sano et al., 2012, Schollaen et al., 2013 and Xu et al., 2015), and also compare favourably with $\delta^{18}O_{TR}$-climate r values reported for temperate sites, where dendroclimatology is a much longer-established field (e.g. Treydte et al., 2007, Wilson et al., 2016). Finally, positive split-period regression statistics (e.g. reduction of error, RE, and coefficient of efficiency, CE, Appendix 6.7) indicate that regression-based models developed from the Bolivia and Ecuador $\delta^{18}O_{TR}$ chronologies have skill in predicting Amazon runoff. However, an actual reconstruction of Amazon climate was not attempted in this study, due to the various confounding factors, discussed in Chapter 6, that might have affected the $\delta^{18}O_{TR}$ records over longer timescales, and would thus introduce error to any climate reconstruction. Therefore, the $\delta^{18}O_{TR}$ chronologies were used to help understand past changes in Amazon hydrology, without reconstructing it absolutely.

In order to glean useful information from proxy records it is necessary to have a good grasp of the underlying processes that control relationships between climate and proxy data. Thus, another important outcome from this thesis is the new insight into the mechanisms driving interannual variability in $\delta^{18}O_{TR}$ records from the Amazon (Chapter 5). During the wet season, rainout of heavy isotopes during precipitation along transport pathways over the basin was shown convincingly to be the dominant factor influencing $\delta^{18}O_{TR}$, confirming an earlier hypothesis (Brienen et al., 2012). This can explain the good correlations observed between $\delta^{18}O_{TR}$ chronologies from Ecuador and Bolivia, and Amazon River discharge measured at Óbidos, which integrates precipitation over nearly 80% of the Amazon basin (Callède et al., 2004). Research by van der Sleen et al. (2015) in Cameroon identified a similar control on interannual $\delta^{18}O_{TR}$ signatures in *Etandrophragma utile*, which is in the same family as *C. odorata* (Meliaceae). The authors showed negative relationships between the $\delta^{18}O_{TR}$ chronology and wet season precipitation over a large region in Central and West Africa, predominantly to the south of their tree-ring sample site, and conclude that rainout during moisture transport over the continent determines the $\delta^{18}O_{TR}$ signal. Early work in continental Southeast Asia also suggested that $\delta^{18}O_{TR}$ recorded a regional wet season precipitation signal (Poussart and Schrag, 2005), although dating uncertainties and limited replication constrained the conclusions that could be drawn. Subsequent studies using more robust isotope chronologies have since confirmed the importance influence of wet season precipitation on $\delta^{18}O_{TR}$ in Southeast Asia (Zhu et al., 2012, Xu et al., 2013, Xu et al., 2015). Thus, large-scale regional rainout signals are recorded in $\delta^{18}O_{TR}$ records from across the tropics, including West Africa, Asia and the Amazon, by causing the depletion of heavy isotopes during atmospheric transport (Dansgaard, 1964). In contrast, $\delta^{18}O_{TR}$ records from southern Mexico show a different signal: they do not record continental rainout but are predominantly influenced by coastal storms and local amount effects (Brienen et al., 2013). This illustrates that $\delta^{18}O_{TR}$ chronologies from different tropical locations are affected by different kinds of hydrological regime, and it is important to fully understand the factors that influence the $\delta^{18}O_{TR}$ signal at each new study location.

Remote controls on interannual and decadal variability in tropical precipitation can also be inferred from $\delta^{18}O_{TR}$ records. In this thesis, spatial correlations between $\delta^{18}O_{TR}$ chronologies from Bolivia and Brazil, and SSTs in the surrounding ocean basins,

revealed important areas of influence in the equatorial Pacific and the tropical North Atlantic (TNA, Chapter 6). A Pacific influence on $\delta^{18}O_{TR}$ from tropical South America has been reported before (e.g. Evans and Schrag, 2004, Ballantyne et al., 2011, Brienen et al., 2012), and can be explained by the well-known effect of the El Niño-Southern Oscillation (ENSO) on Amazon hydrology (Garreaud et al., 2009). During a positive ENSO phase precipitation over the Amazon is suppressed, resulting in less isotope depletion during air passage across the basin, and a higher $\delta^{18}O_{TR}$ signature, with the reverse scenario during La Niña conditions (i.e. negative phase of ENSO). ENSO was shown to have a stronger effect on the $\delta^{18}O_{TR}$ chronology from Bolivia than the record from Ecuador, reflecting spatial variation in the influence of ENSO on Amazon precipitation (e.g. Yoon and Zeng, 2010). Relationships between ENSO and $\delta^{18}O_{TR}$ have also been reported for Central America (e.g. Anchukaitis and Evans, 2010), many sites in Southeast Asia (e.g. Xu et al., 2011, Zhu et al., 2012, Sano et al., 2012, Xu et al., 2013, Schollaen et al., 2015, Xu et al., 2015), and also for tropical Australia (Boysen et al., 2014). However, no ENSO signal was detected in a $\delta^{18}O_{TR}$ chronology from Cameroon (van der Sleen et al., 2015), despite a reported influence of ENSO on precipitation during the West African monsoon (Joly and Voldoire, 2009). This could be due to a mismatch between the region where ENSO affects precipitation, and the region where precipitation influences $\delta^{18}O_{TR}$, potentially suggesting that the site in Cameroon is not ideally located to capture full precipitation variability during the monsoon. There is currently poor agreement between reconstructions of ENSO in the pre-instrumental period, highlighting a need for additional robust proxy datasets (Sano et al., 2012). $\delta^{18}O_{TR}$ records from sites on both sides of the Pacific have now been shown to be sensitive to ENSO variability, and thus may be used to improve our understanding of this important driver of pantropical climate.

An influence of TNA SSTs on interannual and decadal $\delta^{18}O_{TR}$ variability has also been shown in this thesis, and is particularly evident in the high-elevation chronology from Ecuador. This is a novel result, and is thought to be related to the effect of Atlantic SSTs on the position of the inter-tropical convergence zone (ITCZ). The ITCZ is a band of mostly convective precipitation over the region where the trade winds converge close to the equator, forming the ascending branch of the Hadley circulation (Garreaud et al., 2009). Its position is determined by the location of the warmest pool of SSTs, and thus

tropical Atlantic SST anomalies can deflect it northward or southward, respectively resulting in negative or positive precipitation anomalies over the Amazon (Yoon and Zeng, 2010). Analysis of data from the Global Network of Isotopes in Precipitation (GNIP) database (IAEA/WMO, 2016) has shown that the ITCZ affects the isotope composition of precipitation ($\delta^{18}O_P$) in South America (Matsui et al., 1983, Garcia et al., 1998). Passage of the ITCZ over the Amazon is associated with strong precipitation and anomalously low $\delta^{18}O_P$ values (Salati et al., 1979, Garcia et al., 1998). Thus, its northward displacement by anomalously warm TNA SSTs would have two important effects: first, rainout of heavy isotopes upstream of the sample site would be reduced, and second, local amount effects will be weaker if precipitation events are less intense (Dansgaard, 1964). A speleothem $\delta^{18}O$ record from southern Brazil reveals an analogue to this effect over much longer timescales, with latitudinal shifts in insolation maxima, caused by the precessional cycle, driving changes in the mean position of the ITCZ (Cruz et al., 2005). Solar insolation maxima close to the study site in southern Brazil caused enhanced convective activity and more depleted $\delta^{18}O_P$ values recorded in the speleothem. The ITCZ is also known to influence $\delta^{18}O_P$ in Southeast Asia (Araguás-Araguás et al., 1998), and given that it is an important determinant of climate in tropical Africa, it is likely to affect $\delta^{18}O_P$ here as well (Lutz et al., 2011, van der Sleen et al., 2015), though $\delta^{18}O_P$ data from this region are scarce (Rozanski et al., 1993).

New multi-centennial $\delta^{18}O_{TR}$ records from the Amazon presented here have permitted an assessment of low frequency variability in Amazon hydrology. The absence of ontogenetic effects in the $\delta^{18}O_{TR}$ chronologies from Ecuador and Bolivia meant there was no need to apply de-trending procedures, and thus low frequency climate signals were retained. The main low frequency feature of the long $\delta^{18}O_{TR}$ chronologies is a long-term increase in $\delta^{18}O_{TR}$ since the early 1800s, which is thought to reflect an increase in Amazon $\delta^{18}O_P$ that is then recorded in cellulose (Chapter 6). The cause of the increase, which corresponds with a gradual rise in Atlantic SSTs over the same timeframe, was deduced to be a reduction in the rainout fraction over the basin. The positive trend in $\delta^{18}O_{TR}$ reaches a peak at around 1950, and from the 1980s it becomes weakly negative. Other $\delta^{18}O$ proxy records from the Amazon show similar but weaker long-term increases in $\delta^{18}O$ (e.g. Reuter et al., 2009, Thompson et al., 2013, Kanner et al., 2013, Novello et al., 2016, Bird et al., 2011). These increases have been

interpreted as a weakening of the South American summer monsoon (SASM; e.g. Bird et al., 2011, Vuille et al., 2012, Kanner et al., 2013), which is a term widely (but incorrectly) used interchangeably with wet season precipitation amount over the Amazon. In other words, these studies interpret Amazon $\delta^{18}O$ records as showing a long-term drying trend over the most recent warming period. However, as discussed in Chapter 6, a positive trend in $\delta^{18}O$ can only be interpreted as a reduction in wet season precipitation if there has been no change in the volume of water vapour coming into the basin, and this cannot be assumed over longer timescales. In this analysis, the increase in $\delta^{18}O_{TR}$ was interpreted more cautiously, as either reflecting a real long-term reduction in wet season precipitation amount (and there are insufficient instrumental data over the relevant period to confirm or refute this), or an increase in the volume of water vapour imported to the Amazon, thus reducing the fraction of water vapour that rains out. Additional work is needed to disentangle these possible interpretations, and this could potentially be achieved by using an isotope-enabled general circulation model (GCM) or by collecting additional $\delta^{18}O_{TR}$ data (see section 7.4).

The $\delta^{18}O_{TR}$ records presented here are the longest from the Amazon (i.e. 155 and 214 years), though 400-year-long records have been developed from Vietnam and Laos in Southeast Asia (Sano et al., 2012, Xu et al., 2013). These records also show an increase over the past 200 years (approximately 2 ‰), which Xu et al. (2013) interpret as a weakening of the Indian summer monsoon caused by warming tropical SSTs. While an interesting and potentially accurate observation with close similarities to the findings from the Amazon, the inference by Xu et al. (2013) is based on positive correlations between their $\delta^{18}O_{TR}$ record and other $\delta^{18}O_{TR}$ records from Tibet, Nepal and Vietnam, which cannot be considered entirely independent. Furthermore, as with other $\delta^{18}O$ proxy studies from the Amazon, the study lacks a thorough discussion of other potential drivers of the long-term $\delta^{18}O$ increase. A key message from the work presented in this thesis is that proxy data must be interpreted more carefully in future studies, and drivers of variation operating at different timescales should be considered separately. Articles should always include a transparent and upfront discussion of the limitations associated with $\delta^{18}O$ data, which are useful but imperfect records of past climate.

In addition to these climatic inferences, there are further methodological insights arising from the thesis, which will be mentioned here. $\delta^{18}O_{TR}$ signals were shown to be more sensitive to interannual climate and correspond better between trees than tree-ring width (TRW) signals. Formerly, tropical and subtropical dendrochronological studies have observed relationships between climate and TRW, which have been used to extrapolate backwards in time and reconstruct historical climate (e.g. studies in South and Central America: Villalba et al., 1998, Worbes, 1999, Enquist and Leffler, 2001, Brienen and Zuidema, 2005, studies in Africa: Fichtler et al., 2004, Schöngart et al., 2006, and studies in Asia: Ram et al., 2008, Schollaen et al., 2013). However, in some of these cases TRW-climate relationships were fairly weak because environmental conditions in the tropics are more generally favourable for tree growth and show lower interannual variability than in temperate regions. Furthermore, climate reconstructions from TRW were called into question by Doughty et al. (2014) who demonstrated that reductions in diameter growth of tropical trees may not necessarily reflect a reduction in whole tree productivity due to allocation trade-offs. The higher climate sensitivity of $\delta^{18}O_{TR}$ relative to TRW has been shown before in studies from across the tropics (e.g. Xu et al., 2011, Sano et al., 2012, Brienen et al., 2013, Xu et al., 2013, van der Sleen et al., 2015), confirming that $\delta^{18}O_{TR}$ are generally more suitable than TRW for low latitude palaeoclimate reconstructions.

In relation to this, it was possible to precisely date Amazon tree-ring samples by pattern matching new $\delta^{18}O_{TR}$ records against a previously established, well-dated $\delta^{18}O_{TR}$ chronology. Using this technique, samples from Bolivia were dated within and between sites, and between species. Crossdating between $\delta^{18}O_{TR}$ series from Ecuador also enabled construction of an accurate chronology. This is an important methodological observation that could potentially facilitate the development of further Amazon $\delta^{18}O_{TR}$ records. Leavitt et al. (1985) were the first to show that crossdating stable isotope series could be used to date tree rings of unknown age in a study of $\delta^{13}C$ in tree rings from Arizona. It requires isotope signals to be regionally coherent, and/or show similar patterns between tree species, although the technique is less effective when samples have missing rings. Since this early study $\delta^{18}O_{TR}$ have been used to date tree rings in both temperate (e.g. Li et al., 2015) and tropical (e.g. Xu et al., 2013) locations, and it has now been successfully applied in the Amazon. However, there are some valid

concerns with such 'tuning' of proxy archives, summarised in a review by Blaauw (2012). These include the assumption that the so-called 'established' chronology is absolutely dated, which may not be the case, and also the assumption of synchronicity between the established chronology and the new chronology, where there might be none. While acknowledging these potential issues, it is thought that the approach applied in this thesis was sufficiently careful to circumvent these problems. First, the record from Brienen et al., (2012) that was used as the 'benchmark' series is only 100 years long, and thus the dating could be validated by comparison with regional river records, which date back to 1903 (HidroWeb, 2017). This contrasts with the multi-millennia records discussed by Blaauw (2012), that are often dated using age models, which are inherently uncertain. In addition, where adjustments were made to $\delta^{18}O_{TR}$ series in this study, such as the multi-species records in Chapter 4, the newly dated records were confirmed (at least up until the 1960s) using ^{14}C dating. It is true, that the records from Bolivia were assumed to be synchronous, due to their relatively close proximity, but adjustments were only made when there was evidence in the original wood sample to support making them. Finally, it should be emphasised that the Bolivia and Ecuador records presented in Chapter 6 were not tuned or fitted to one another, but constructed independently, and were nevertheless found to correlate well. Therefore, the observed synchronicity across the Amazon region is not simply an artefact of the methodology, but a true phenomenon caused by the large-scale environmental controls on $\delta^{18}O_{TR}$ in this region.

Another dating tool that has proved useful in this work is 'bomb-peak' ^{14}C analysis. It has been used to demonstrate variation in tree-ring periodicity across tropical South America, and also used to verify dates of $\delta^{18}O_{TR}$ series from multiple tropical tree species. In some cases, major discrepancies were found between dates obtained by simple ring counting and dates inferred from ^{14}C data. For example, *C. odorata* trees from Suriname were discovered to form approximately two rings per year, and 13 indistinct rings were shown to have been missed in the outermost section of a *Peltogyne heterophylla* sample from Bolivia. Using ^{14}C measurements to independently validate tree-ring dates is particularly valuable when working with tropical trees, as wood anatomy can sometimes be challenging and may result in a high rate of errors (Worbes, 2002, Brienen et al., 2016). Several previous tropical $\delta^{18}O_{TR}$ studies have used

^{14}C measurements to check tree-ring dates estimated by ring counting (e.g. Pearson et al., 2011, Ballantyne et al., 2011), or dates estimated from isotope age models (Evans and Schrag, 2004, Poussart and Schrag, 2005, Ohashi et al., 2016). Lastly, in addition to ^{14}C measurements aiding tree-ring research, work in this thesis has shown that dendrochronology may be able to help the ^{14}C community. Measurements of ^{14}C in tree rings from Bolivia, Ecuador and Venezuela showed excellent agreement with existing ^{14}C calibration curves, and therefore tropical tree-ring records can possibly be used to refine, or even develop new regional ^{14}C calibration curves.

7.2 Appraisal of Thesis Aims

In this section, the original thesis aims, which were summarised into six key research questions set out in Chapter 1, are reviewed. The degree to which each question has been answered is evaluated, and some of the challenges that were encountered during the research are explained.

7.2.1 How consistent is annual tree-ring periodicity across the Amazon?

To answer this question tree-ring samples from four sites across the basin were dated using ^{14}C analysis, and additional growth data for four further sites were taken from the literature. These sites are relatively well distributed geographically, and are thus suitable for testing the spatial consistency of tree-ring periodicity. Within a single tree species (*C. odorata*), periodicity was found to vary between different sites, regularly forming two rings per year in Suriname and one ring per year elsewhere in the neotropics. This result is important because it shows that tropical dendrochronologists must not assume annual ring formation in a previously untested species or site, due to spatial variation in the factors controlling tree growth. These factors were investigated, to try and identify the reason why trees in Suriname form two rings per year. Precipitation seasonality and genetics were highlighted as the most likely causes, though limited phenological data made it difficult to determine the precise mechanism of control. Furthermore, the study focussed on *C. odorata* and its highland relative *C. montana* only, and growth in other Amazon tree species may be affected by different environmental factors.

7.2.2 Do different tropical tree species show similar $\delta^{18}O_{TR}$ signatures?

Interannual $\delta^{18}O_{TR}$ signatures were compared across eight tropical tree species from Bolivia, five of which had not previously been analysed for $\delta^{18}O_{TR}$. The study was the first in the tropics to explicitly investigate $\delta^{18}O_{TR}$ signals between different tree species, though it should be noted that the eight species only represent a tiny fraction of the 230 tropical tree species that are now known to form annual rings (Brienen et al., 2016). To maximise the number of species in the study only one tree from each species was analysed, with the exception of *C. odorata*. Significant relationships with *C. odorata* were identified for six out of the seven other species, showing that tropical tree species do show similar $\delta^{18}O_{TR}$ signatures, though the strength of the correlations varied among species. Since only one tree from each species was analysed, it cannot be certain whether weak or insignificant relationships were due to species-specific differences in plant physiology, or simply because the individual measured happened to show a different signal. It would have been preferable to develop well-replicated chronologies for each of the species in the study but this was not possible due to time and financial costs. Scarce data on tree characteristics, such as rooting depth, also made it challenging to determine the cause of inter-species differences. Where $\delta^{18}O_{TR}$ signals did correlate between species it was concluded that this was most likely due to a shared source water $\delta^{18}O$ signal, and suggests that species besides *C. odorata* may be suitable for reconstructing Amazon palaeoclimate.

7.2.3 Do $\delta^{18}O_{TR}$ records from the Amazon show coherence at large spatial scales?

Robust $\delta^{18}O_{TR}$ chronologies were shown to correlate well at interannual and decadal timescales between sites 325 km apart in Bolivia (r=0.80, n=101), and also between sites in Bolivia and Ecuador that were 1500 km apart and separated by 2750 m in altitude (r=0.57, n=153). This confirms that Amazon $\delta^{18}O_{TR}$ records do cohere at very large spatial scales, and is a strong indication of a similarly large-scale coherence in $\delta^{18}O_P$, which is controlled by a large-scale environmental driver. The second of these relationships is particularly notable, as rainout of heavy isotopes during orographic uplift over the Andes might have been expected to dominate the isotope signal in trees from Ecuador (Rozanski et al., 1993). These $\delta^{18}O_{TR}$ chronologies, which were shown to correlate between distant sites, originated in the far western and southwestern margins

of the basin and it was not possible to assess large-scale $\delta^{18}O_{TR}$ coherence for other parts of the Amazon. It is anticipated that $\delta^{18}O_{TR}$ from the western Amazon would show the strongest regional relationships, as precipitation isotopes here reflect cumulative fractionation processes over the basin, whereas sites on the Atlantic coast are more strongly influenced by local amount effects (Vimeux et al., 2005, Villacís et al., 2008, Vuille et al., 2012). However, additional $\delta^{18}O_{TR}$ chronologies from sites in the centre or east of the basin have not yet been developed (see section 7.2.4).

7.2.4 Can a network of $\delta^{18}O_{TR}$ chronologies from sites across the basin provide further information about interannual variation in basin rainout, or changes in the precipitation-recycling ratio?

The original intention was to develop a network of chronologies from sites across the basin, including records from strategic locations along the moisture transport pathway. It was hoped that these records would provide further insights about basin rainout, and that they might show whether there have been changes in the continental gradient in $\delta^{18}O_P$ (caused, for example, by deforestation or reduced stomatal conductance in response to rising atmospheric CO_2). The map in Chapter 2 (Fig. 2.1) showed sites in Suriname, Venezuela and Brazil where samples of *C. odorata* were collected for analysis in this thesis. Unfortunately, pilot $\delta^{18}O_{TR}$ analyses from these sites did not show promising results, as $\delta^{18}O_{TR}$ series did not match very well between trees (see Fig. 7.1). This meant that it was not possible to construct the network of robust chronologies required to address this question. The reasons why it seemed to be more challenging to construct $\delta^{18}O_{TR}$ records from these sites compared to sites in Bolivia and Ecuador are discussed in the next few paragraphs.

The samples from Venezuela came from Reserva Forestal de Caparo (RFC) and *C. odorata* trees from this reserve have already been shown to form clear annual rings (e.g. Worbes, 1999). However, preliminary $\delta^{18}O_{TR}$ series from three *C. odorata* trees from RFC showed little interannual correlation over a period of approximately 30 years (EPS=0.56), though there is some similarity between the low frequency signals (Fig. 7.1a). The dating of one of these samples (Ven_01) has been confirmed by ^{14}C analysis. The rings were clearly visible on this sample, which was a 40-mm wide disc section, while 10 mm increment cores were analysed from the other two trees. The dating of

these trees is unlikely to be wrong, thus other reasons must explain the differences between the isotope series. RFC is close to the River Caparo, which has shaped the landscape over time, causing small variations in topography, and is also known to influence the local groundwater (Worbes, 1999). Thus, the site is comprised of shallow dips/depressions with boggy, clayish soils and pools of water, and small banks where the soils are better drained. Since the river water may have a different $\delta^{18}O$ signature to precipitation falling at RFC, and pooled water is also more likely to be influenced by fractionating evaporation and water residence time, trees growing in the depressions may take up water with a different $\delta^{18}O$ signature to trees growing on the banks. Indeed, trees Ven_01 and Ven_13 both grew in depressions, while Ven_30 grew on a bank, strongly indicating that the poor correspondence between the $\delta^{18}O_{TR}$ series is due to inter-tree differences in source water $\delta^{18}O$ ($\delta^{18}O_S$). Variation in physiology between trees might also contribute to the lack of a shared signal observed between the RFC records, but since $\delta^{18}O_{TR}$ signals in *C. odorata* from other sites are dominated by $\delta^{18}O_S$ (e.g. Brienen et al., 2012), $\delta^{18}O_S$ is also expected to be the dominant control on $\delta^{18}O_{TR}$ in *C. odorata* from Venezuela.

Previous studies on *C. odorata* from Brazil have shown that trees form annual rings at sites near Manaus (Dünisch et al., 2002, Dünisch and Morais, 2002), Aripuanã (Dünisch et al., 2003), and Nova Iguaçu (Costa et al., 2013). The samples analysed here come from the Mamirauá Sustainable Development Reserve (MSDR), which is further west than these sites, and close to the main stem of the Amazon River (here called the Solimões). Preliminary $\delta^{18}O_{TR}$ series show some agreement, but insufficient to construct a robust chronology (EPS=0.48, Fig. 7.1b). It was not possible to use ^{14}C dating on these samples as they were too young, and thus there could be dating inaccuracies, particularly as cores were analysed rather than whole stem discs. As has been mentioned previously (e.g. Worbes, 2002), and as observed with the samples from Ecuador analysed in this thesis, complete discs are essential for detecting anatomical features such as wedging rings, which can cause problems in tropical dendrochronology. In addition, the trees sampled in MSDR were close to the seasonally flooded forest, but at a higher elevation. Although these trees do not experience flooding every year, it has been suggested that in years with strong flooding (approximately every five years), they could also be affected, possibly resulting in the

formation of a false (i.e. non-annual) ring during the period of inundation (J. Schöngart, personal communication). Depending on which trees are influenced by the flood, false rings may form in some trees but not in others. This could explain why it was not possible to crossdate $\delta^{18}O_{TR}$ series from this part of Brazil.

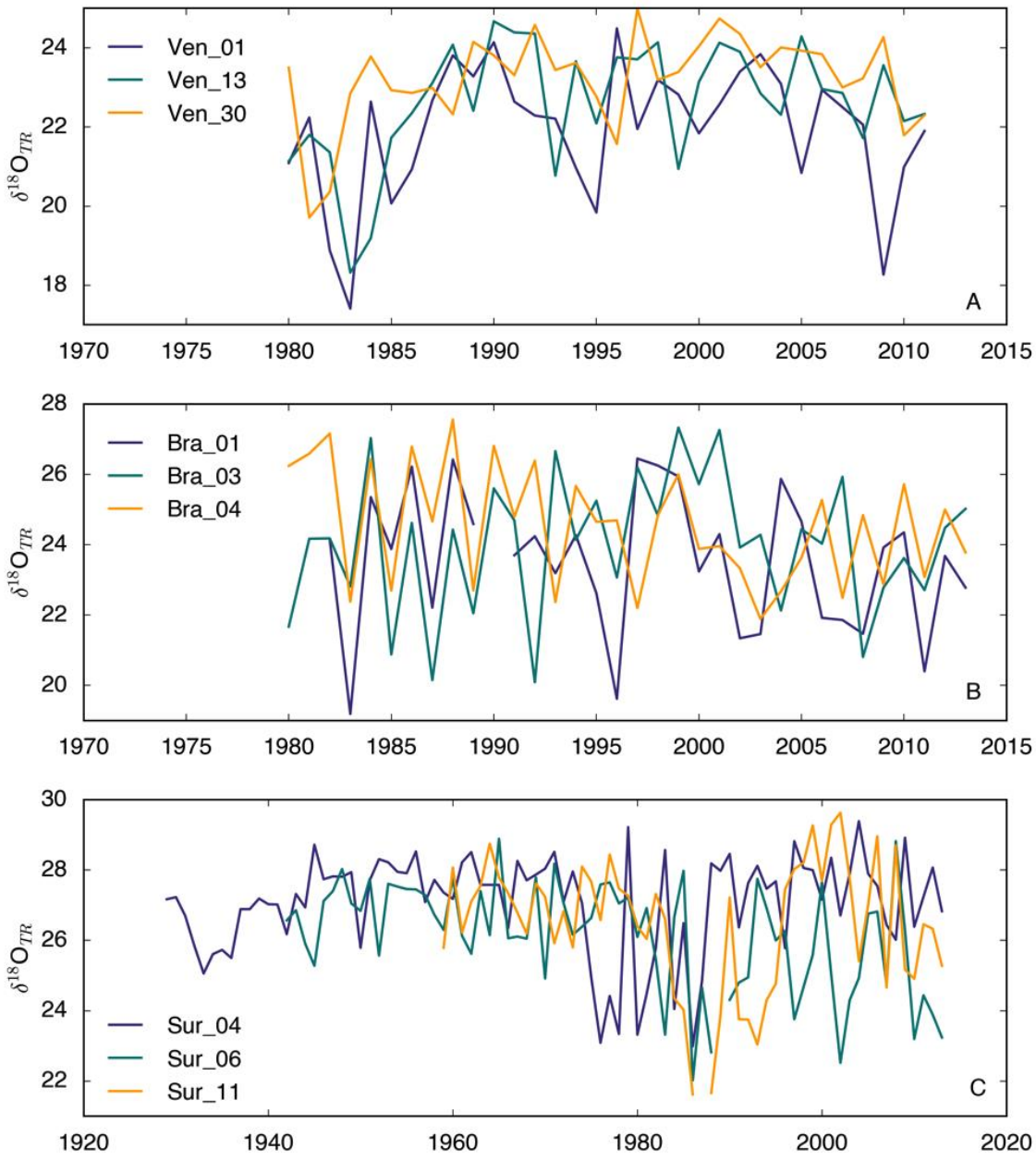

Figure 7.1 – Preliminary $\delta^{18}O_{TR}$ data from other sites in the Amazon. Interannual variation in $\delta^{18}O_{TR}$ in three *Cedrela odorata* trees from **(a)** Venezuela, **(b)** Brazil, and **(c)** Suriname.

Lastly, the samples from Suriname came from a logging concession near Matapi in the northwest of the country. Dendrochronology has not previously been conducted in Suriname, but work presented in this thesis has demonstrated that trees here form two rings nearly every year. Each ring was individually analysed for $\delta^{18}O_{TR}$, and then annual values were obtained by averaging $\delta^{18}O_{TR}$ values from two rings, weighted by their width (Appendix 7.1). There are some low frequency features in common between the $\delta^{18}O_{TR}$ series, though these features do not align, and at the interannual timescale correlations are weak or non-existent (EPS=0.27, Fig. 7.1c). Tree-ring analysis was conducted on complete discs, and ^{14}C data were used to precisely date the samples, so dating inaccuracies are unlikely to explain the very poor correspondence between the three trees. The trees may have taken up water from different sources, but as the samples were cut by a logging company, the precise origins and site conditions for the trees are not known. Without further information, it is not possible to explain the lack of a common signal in these $\delta^{18}O_{TR}$ records.

In summary, as noted in Chapter 4, it is challenging to identify the reasons why $\delta^{18}O_{TR}$ signatures don't match between trees without collecting additional data. Hypotheses to explain why trees in Venezuela, Brazil and Suriname show high inter-tree variability in comparison with sites in the western Amazon have been discussed, with suggestions including possible differential water sources and the irregular occurrence of false rings. However, these ideas must remain speculative without further data.

7.2.5 What are the most important mechanisms driving interannual variation in Amazon $\delta^{18}O_{TR}$?

Climatic drivers of variation in Amazon $\delta^{18}O_{TR}$ have previously been identified using correlation analyses, but it is also important to fully understand the mechanisms behind these relationships. Multiple approaches were employed to identify the mechanistic drivers of interannual variability in $\delta^{18}O_{TR}$, with a focus on records from Bolivia, as these had previously been suggested to be a good proxy for precipitation over the whole Amazon basin (Brienen et al., 2012). Atmospheric trajectories combined with remote sensing observations of precipitation, and insights from reanalysis data, were used to show that rainout processes during moisture transport over the basin

control interannual $\delta^{18}O_{TR}$ variability in the southwest corner of the Amazon. This confirms that these records can be reliably used to reconstruct the moisture balance of the entire region. One limitation of the approach is that the analysis was restricted to the few recent decades when satellite and reanalysis data were available. This was sufficient to investigate the causal drivers of interannual variation, but it was not possible to explore the drivers of low frequency signals in Amazon $\delta^{18}O_{TR}$ records using this methodology. One method that could possibly be used to achieve this in the future would be to use an isotope-enabled GCM (see section 7.4).

7.2.6 What can new long $\delta^{18}O_{TR}$ records presented in this thesis tell us about the Amazon hydrological cycle over the past two centuries?

Long, annually resolved and well-replicated $\delta^{18}O_{TR}$ chronologies from the Amazon, which extend beyond the instrumental record, have been presented in this thesis. In addition to investigating the drivers of interannual and decadal variability, these provided the first opportunity to analyse and interpret low frequency signals in Amazon $\delta^{18}O_{TR}$. The $\delta^{18}O_{TR}$ chronology from Ecuador shows a strong upward trend, which is also apparent in the slightly shorter record from Bolivia. Since $\delta^{18}O_{TR}$ signals have already been shown to reflect Amazon hydrology at interannual and decadal timescales, it might seem logical to assume that low frequency signals are also determined by changes in Amazon hydrology. Indeed, previous studies have interpreted long $\delta^{18}O$ proxy records by developing simple linear regression models over the period of available instrumental data, and using these to reconstruct climate over multiple centuries (e.g. Xu et al., 2013, Thompson et al., 2013). However, there are actually numerous confounding sources of variation over long timescales, and these must be carefully considered to ensure that proxy records are correctly interpreted. In this thesis, an attempt was made to quantify the contribution of each of these sources of variability to the 3 ‰ rise in $\delta^{18}O_{TR}$ since the early 1800s. It was concluded that a change in the rainout fraction over the Amazon was likely to be driving the majority of the increase. This could be caused by a long-term reduction in Amazon precipitation, as suggested by other $\delta^{18}O$ proxy studies (Bird et al., 2011, Vuille et al., 2012, Kanner et al., 2013), but can also be explained by an increase in the volume of water vapour coming into the basin. These results are tantalising, but it is difficult to distinguish between the two

mechanisms from $\delta^{18}O_{TR}$ data alone. However, both interpretations indicate long-term changes in the Amazon climate system over the past two centuries.

As well as using extended $\delta^{18}O_{TR}$ chronologies to positively identify drivers of hydrological variation in the Amazon, previously suggested drivers of variability can also be investigated in a more robust way. For example, the new $\delta^{18}O_{TR}$ record from Ecuador was used to interrogate an assertion that sunspots are a remote control on the Amazon hydrological cycle. The 200-year-long $\delta^{18}O_{TR}$ record was used to show that a relationship between decadal variation in Amazon River discharge measured at Óbidos and sunspot number observed over the 20th century by Antico and Torres (2015), is probably coincidental. This is an interesting result and shows that long $\delta^{18}O_{TR}$ chronologies can also provide new insights by challenging conclusions drawn from shorter instrumental climate datasets.

7.3 How Useful Are Amazon $\delta^{18}O_{TR}$ Proxy Records?

In this thesis $\delta^{18}O_{TR}$ chronologies from multiple sites in the Amazon have been developed and analysed. These records have provided valuable insights about the drivers of variation in Amazon hydrology on interannual, decadal, and even centennial timescales. These results are particularly important in a region where instrumental climate data are extremely limited. However, there are also a few limitations associated with proxy $\delta^{18}O_{TR}$ data, some of which have already been alluded to, but will be explicitly stated in the paragraphs below.

First, developing stable isotope chronologies is a costly and labour-intensive process, and the time between sample collection through to constructing a robust and well-replicated $\delta^{18}O_{TR}$ record can be considerable. Errors at any stage in the process can potentially have an impact on the final results, but particularly during the initial ring identification and counting. Tropical trees often have challenging ring structures (e.g. Worbes, 2002, Brienen et al., 2016), and in this research wedging rings were encountered especially frequently (e.g. Fig. 7.2). These could only be identified by analysing complete discs, which explains why discs were generally easier to date and produced better results than increment cores. Furthermore, trees from some of the study locations were found to form non-annual rings, illustrating the necessity for independent

dating validation of $\delta^{18}O_{TR}$ records. This could be using 'bomb-peak' ^{14}C dating, by comparing against climate data, or, as illustrated in Chapter 4, by pattern-matching $\delta^{18}O_{TR}$ signatures again a previously established $\delta^{18}O_{TR}$ chronology.

Once a $\delta^{18}O_{TR}$ chronology has been developed, care must be taken to interpret the signal correctly, although this may not always be straightforward. $\delta^{18}O_{TR}$ signals are complex and incorporate information from a large number of processes, both during the course of the hydrological cycle (e.g. Mook, 2000), and within the tree itself (e.g. Fig. 1.3 in Chapter 1). These sources of variability must be acknowledged, particularly over longer timescales when other factors affecting $\delta^{18}O_{TR}$, besides the climate variable of interest, may have changed. These factors complicate data interpretation, but if they can be accounted for it may still be possible to extract useful climate information. Though in some cases additional data may be required to completely disentangle the $\delta^{18}O_{TR}$ signal.

There are temporal and spatial limitations on the hydrological insights that can be derived from Amazon $\delta^{18}O_{TR}$ records. First, the $\delta^{18}O_{TR}$ records presented in this thesis are constructed from trees that only grow during the wet season, and thus they can only record information about climate during this part of the year. This seasonal bias is

Figure 7.2 – Example of wedging tree rings in *Cedrela montana* from Ecuador.

unavoidable with tree-ring records, which require trees to stop growing during a particular season in order to form an annual ring. However, it is important to appreciate that this also means that $\delta^{18}O_{TR}$ records do not provide a complete representation of climate throughout the year. Furthermore, while these records provide useful information about large-scale hydrological changes in the Amazon, on their own they cannot provide detail about spatial variation in hydrology. For example, analyses of river flux data have shown opposing discharge trends in northern and southern Amazon sub-basins since the mid 1970s (e.g. Espinoza et al., 2009, Gloor et al., 2015), but the $\delta^{18}O_{TR}$ records currently available are not able to reflect this regional variability. A cross-basin network of $\delta^{18}O_{TR}$ records would be needed to capture these changes, but as shown in section 7.2.4, this could be difficult to construct.

To summarise, Amazon $\delta^{18}O_{TR}$ records are useful records of past climate, provided data are interpreted carefully. Although quite a lot of effort must be expended to develop a robust chronology, the climate insights that can be gained can be very informative, and may provide important historical context for on-going hydrological changes in the region (e.g. Gloor et al., 2013), that would otherwise be lacking. Although the records developed so far are able to capture large-scale variation in wet season hydrology, further records are needed to represent dry season climate and capture historical climate variability across the basin.

7.4 Research Implications and Suggestions for Future Research

The growth periodicity of *Cedrela* spp., which are commonly used in dendrochronological studies (e.g. Worbes, 1999, Tomazello Filho. et al., 2000, Dünisch et al., 2002, Brienen and Zuidema, 2005), has been shown to vary between tropical sites, and tree rings within a species can be bi-annual as well as annual (Chapter 3). This result has relevance beyond a single species or region, as it emphasises the importance of dating verification, and that tree-ring records from new tropical locations should be interpreted with caution (Brienen et al., 2016). The factors controlling tree growth rhythms in South America were also explored, but could be investigated using a more systematic approach, for example by growing seedlings from multiple locations in a

greenhouse experiment (e.g. Ruiz et al., 2013). This would help us to better understand regional variation in ring periodicity, and possibly help to predict whether sites may be suitable or unsuitable for constructing $\delta^{18}O_{TR}$ chronologies.

Consistent $\delta^{18}O_{TR}$ signatures between different species and sites were shown in Chapter 4. This work has broadened the pool of species that can be used for $\delta^{18}O_{TR}$ chronology construction, with *Amburana cearensis* and *Tachigali vasquezii* showing particular promise. The latter would be especially suitable for high-resolution isotope analysis due to its fast growth rate (Brienen and Zuidema, 2005). Indeed, investigating seasonal $\delta^{18}O_{TR}$ signals between tropical tree species (e.g. Ohashi et al., 2016) could help to explain some of the observed inter-species differences, for example, by revealing whether trees grow and take up precipitation during slightly different periods in the year. Furthermore, crossdating new $\delta^{18}O_{TR}$ series against an established isotope record was shown to be effective, and thus existing $\delta^{18}O_{TR}$ records from Bolivia and Ecuador could facilitate future chronology development in the Amazon.

To aid the interpretation of tropical $\delta^{18}O_{TR}$ signals, trajectory modelling was combined with satellite observations of precipitation. This showed that interannual $\delta^{18}O_{TR}$ signals in the southwest Amazon are primarily controlled by the amount of precipitation during atmospheric moisture transport over the basin (Chapter 5). The success of this original methodology is such that it could be employed to investigate $\delta^{18}O_{TR}$ signals elsewhere in the tropics. The ROTRAJ trajectory model from Reading University (Methven, 1997) was used here, but there are other Lagrangian atmospheric transport models that are also freely available, for example, HYSPLIT (Stein et al., 2015) and FLEXPART (Stohl et al., 2005). In addition, it may be beneficial to use trajectories as part of a more sophisticated moisture source diagnostic approach, such as that used by Drumond et al. (2014). This could help further our understanding of interannual variation in $\delta^{18}O_{TR}$ by showing varying contributions from different ocean regions in different years, and variability in the degree of moisture recycling through vegetation.

In Chapter 6 $\delta^{18}O_{TR}$ records from Bolivia and Ecuador were shown to be good indicators of wet season precipitation in the Amazon basin. The *Cedrela* spp. used to construct these records only grow during the wet months (e.g. Brienen and Zuidema, 2005, Bräuning et al., 2009) and thus can only tell us about climate during this period.

Other Amazon tree species may record climate over a different part of the year. For example, trees in the floodplain forest predominantly grow during the non-flooded phase, which begins in the dry season, and they cease growing and form an annual ring during the flood pulse (Worbes and Junk, 1989, Schöngart et al., 2002). Studies have found positive correlations between growth increment and the duration of the non-flooded phase, in some floodplain tree species (Schöngart et al., 2004, Schöngart et al., 2005). Therefore, $\delta^{18}O_{TR}$ chronologies constructed from these species could possible provide complementary palaeoclimate evidence to the Amazon $\delta^{18}O_{TR}$ records that have already been developed.

The long $\delta^{18}O_{TR}$ records from Bolivia and Ecuador are the first from the Amazon to extend beyond the limit of instrumental data and thus provide new information about regional climate (Chapter 6). The longest of these records extends back to 1799, but it may be possible to develop records even longer than this, if sufficiently old, ring-forming trees can be found (see Worbes and Junk, 1999). The most interesting feature in the long $\delta^{18}O_{TR}$ records presented here, is the upward trend through most of the 19th century and into the first half of the 20th century. This could possibly indicate a drying trend in the Amazon over this period, or increasing water vapour over the basin, but these mechanisms cannot be distinguished without further information. Additional $\delta^{18}O_{TR}$ data could potentially help to clarify the issue. Although it was not possible to develop one during this research, a long-term $\delta^{18}O_{TR}$ record from the northeast coast of South America would provide valuable information about the isotope composition of incoming water vapour. Comparing a coastal $\delta^{18}O_{TR}$ record with existing $\delta^{18}O_{TR}$ records from the west of the basin would show whether there has been a decrease in the $\delta^{18}O_{P}$ gradient across the Amazon, which would indicate the upward trend in $\delta^{18}O_{TR}$ is caused by a reduction in rainout, rather than an increase in incoming water vapour. Although constructing a reliable $\delta^{18}O_{TR}$ chronology from this region maybe challenging, particularly if trees tend to form two rings a year, as they do in Suriname, such a record would provide valuable further insights about long-term variability in Amazon hydrology.

In addition, an isotope-enabled GCM could possibly be used to investigate the drivers of low-frequency $\delta^{18}O_{TR}$ variability, and help determine the cause of the long-term increase. Unlike the mechanistic approaches used to identify drivers of interannual

$\delta^{18}O_{TR}$ variability in this study (i.e. trajectory modelling and vapour transport analysis), which require satellite and reanalysis data that are only available over the last few decades, an isotope-enabled GCM simulates the physical processes that influence proxy isotope data, and can therefore be run over much longer periods (e.g. Tindall and Haywood, 2015). For example, isotope-enabled GCMs have previously been used to distinguish between drivers of variation in coral $\delta^{18}O$ records (Russon et al., 2013), and have also been used to interpret $\delta^{18}O$ proxy records from the Amazon (Vuille et al., 2012). However, Vuille et al. (2012) used the GCM to identify mechanisms controlling interannual variability in $\delta^{18}O_P$, and then applied these results to interpret centennial-scale trends in $\delta^{18}O$. This is not a satisfactory approach because it assumes that the same factors control variation at different timescales when this may not be the case. Future work should focus on model simulations of long-term trends in $\delta^{18}O$, in order to clarify the interpretation of the long $\delta^{18}O_{TR}$ records from the Amazon presented in this thesis.

Lastly, coherent isotope signals were observed between trees at some sites in the Amazon, but not at other sites. Possible reasons for this were discussed in section 7.2.4, but the precise reasons remain unclear. First, it is necessary to establish whether the water taken up by trees has the same isotope composition as precipitation. This could be achieved by measuring soil and xylem water $\delta^{18}O$, and comparing these values with measurements of $\delta^{18}O_P$. If source/stem water $\delta^{18}O$ ($\delta^{18}O_S$) values differ from $\delta^{18}O_P$ values then the reasons for this could also be investigated, for example by examining soil type, or variation in soil water partitioning (e.g. Schwendenmann et al., 2014). Alternatively, if $\delta^{18}O_S$ and $\delta^{18}O_P$ values are found to be similar then inter-tree differences must be caused by variation in tree physiology. Such analyses would help us to understand how tropical $\delta^{18}O_{TR}$ signals are determined, and could inform site choice in future $\delta^{18}O_{TR}$ studies.

7.5 Conclusions

During the course of this research, the field of stable isotope dendrochronology in the Amazon has been substantially expanded. The primary aim was to develop a deeper understanding of the Amazon hydrological cycle using $\delta^{18}O_{TR}$ as a palaeoclimate proxy, and specifically, to identify short- and long-term drivers of hydrological variability.

Evidence presented here has confirmed that interannual $\delta^{18}O_{TR}$ records from the Amazon capture basin-scale variation in precipitation, and can thus be reliably used to reconstruct historical climate in the region at interannual timescales. The long $\delta^{18}O_{TR}$ chronologies from Bolivia and Ecuador, which together provide over 200 years of proxy climate data, were used to investigate drivers of hydrological variability and thus address the key research question. In conclusion, the primary interannual control on Amazon wet season precipitation amount is variation in SSTs in the surrounding ocean basins. Specifically, SSTs in the central tropical Pacific were found to be positively related to $\delta^{18}O_{TR}$ in Ecuador and Bolivia, due to their negative influence on precipitation over the basin. The Ecuador $\delta^{18}O_{TR}$ record was also found to be controlled by SSTs in the tropical North Atlantic, which determine the latitudinal position of the ITCZ and thus also affect Amazon precipitation. However, interpretation of the $\delta^{18}O_{TR}$ records over longer timescales remains somewhat ambiguous. A strong upward trend in $\delta^{18}O_{TR}$ from the early 1800s up until the mid-20th century indicates a decrease in the rainout of heavy isotopes over the Amazon basin. This trend implies a change in the functioning of the Amazon hydrological cycle over this period, which could either be caused by a long-term reduction in Amazon wet season precipitation, or by an increase in incoming water vapour during the wet season. Additional data are required to resolve this uncertainty, either from further $\delta^{18}O_{TR}$ records, or by using an isotope-enabled GCM to provide mechanistic insights. Overall, these results represent an important advance in our knowledge of Amazon hydrology, and pave the way for further tree-ring research that will optimise our understanding of climate in this globally important region.

7.6 References

HidroWeb [Online]. Agência Nacional de Águas. Available: http://hidroweb.ana.gov.br [Accessed 2017].

An, W., Liu, X., Leavitt, S. W., Xu, G., Zeng, X., Wang, W., Qin, D. & Ren, J. 2014. Relative humidity history on the Batang–Litang Plateau of western China since 1755 reconstructed from tree-ring $\delta^{18}O$ and δD. *Climate Dynamics*, 42, 2639-2654.

Anchukaitis, K. J. & Evans, M. N. 2010. Tropical cloud forest climate variability and the demise of the Monteverde golden toad. *Proceedings of the National Academy of Sciences,* 107**,** 5036-5040.

Antico, A. & Torres, M. E. 2015. Evidence of a decadal solar signal in the Amazon River: 1903 to 2013. *Geophysical Research Letters,* 42**,** 10782-10787.

Araguás-Araguás, L., Froehlich, K. & Rozanski, K. 1998. Stable isotope composition of precipitation over southeast Asia. *Journal of Geophysical Research: Atmospheres,* 103**,** 28721-28742.

Ballantyne, A. P., Baker, P. A., Chambers, J. Q., Villalba, R. & Argollo, J. 2011. Regional differences in

South American monsoon precipitation inferred from the growth and isotopic composition of tropical trees. *Earth Interactions,* 15**,** 1-35.
Bird, B. W., Abbott, M. B., Vuille, M., Rodbell, D. T., Stansell, N. D. & Rosenmeier, M. F. 2011. A 2,300-year-long annually resolved record of the South American summer monsoon from the Peruvian Andes. *Proceedings of the National Academy of Sciences,* 108**,** 8583-8588.
Blaauw, M. 2012. Out of tune: the dangers of aligning proxy archives. *Quaternary Science Reviews*, 36, 38-49.
Boisier, J. P., Ciais, P., Ducharne, A. & Guimberteau, M. 2015. Projected strengthening of Amazonian dry season by constrained climate model simulations. *Nature Climate Change,* 5**,** 656-660.
Bonan, G. B. 2008. Forests and Climate Change: Forcings, Feedbacks, and the Climate Benefits of Forests. *Science,* 320**,** 1444-1449.
Boninsegna, J. A., Argollo, J., Aravena, J., Barichivich, J., Christie, D., Ferrero, M., Lara, A., Le Quesne, C., Luckman, B. & Masiokas, M. 2009. Dendroclimatological reconstructions in South America: A review. *Palaeogeography, Palaeoclimatology, Palaeoecology,* 281**,** 210-228.
Boysen, B. M. M., Evans, M. N. & Baker, P. J. 2014. $\delta^{18}O$ in the tropical conifer *Agathis robusta* records ENSO-related precipitation variations. *Plos One,* 9**,** 1-9.
Bräuning, A., Volland-Voigt, F., Burchardt, I., Ganzhi, O., Nauss, T. & Peters, T. 2009. Climatic control of radial growth of *Cedrela montana* in a humid mountain rainforest in southern Ecuador. *Erdkunde,* 63**,** 337-345.
Brienen, R. J. W. & Zuidema, P. A. 2005. Relating tree growth to rainfall in Bolivian rain forests: a test for six species using tree ring analysis. *Oecologia,* 146**,** 1-12.
Brienen, R. J. W., Zuidema, P. A. & Martínez-Ramos, M. 2010. Attaining the canopy in dry and moist tropical forests: strong differences in tree growth trajectories reflect variation in growing conditions. *Oecologia,* 163**,** 485-496.
Brienen, R. J. W., Helle, G., Pons, T. L., Guyot, J. L. & Gloor, M. 2012. Oxygen isotopes in tree rings are a good proxy for Amazon precipitation and El Niño-Southern Oscillation variability. *Proceedings of the National Academy of Sciences,* 109**,** 16957-16962.
Brienen, R. J. W., Hietz, P., Wanek, W. & Gloor, M. 2013. Oxygen isotopes in tree rings record variation in precipitation $\delta^{18}O$ and amount effects in the south of Mexico. *Journal of Geophysical Research: Biogeosciences,* 118**,** 1604-1615.
Brienen, R. J. W., Schöngart, J. & Zuidema, P. A. 2016. Tree Rings in the Tropics: Insights into the Ecology and Climate Sensitivity of Tropical Trees. *In:* GOLDSTEIN, G. & SANTIAGO, L. S. (eds.) *Tropical Tree Physiology: Adaptations and Responses in a Changing Environment.* Cham: Springer International Publishing.
Callède, J., Guyot, J. L., Ronchail, J., L'hôte, Y., Niel, H. & De Oliveira, E. 2004. Evolution of the River Amazon's discharge at Óbidos from 1903 to 1999. *Hydrological Sciences Journal,* 49**,** 85-97.
Colombaroli, D., Cherubini, P., De Ridder, M., Saurer, M., Toirambe, B., Zweifel, N. & Beeckman, H. 2016. Stable carbon and oxygen isotopes in tree rings show physiological responses of *Pericopsis elata* to precipitation in the Congo Basin. *Journal of Tropical Ecology,* 32**,** 213-225.
Costa, M. S., De Vasconcellos, T. J., Barros, C. F. & Callado, C. H. 2013. Does growth rhythm of a widespread species change in distinct growth sites? *IAWA Journal,* 34**,** 498 – 509.
Cox, P. M., Betts, R. A., Collins, M., Harris, P. P., Huntingford, C. & Jones, C. D. 2004. Amazonian forest dieback under climate-carbon cycle projections for the 21st century. *Theoretical and applied climatology,* 78**,** 137-156.
Cruz, F. W., Burns, S. J., Karmann, I., Sharp, W. D., Vuille, M., Cardoso, A. O., Ferrari, J. A., Dias, P. L. S. & Viana, O. 2005. Insolation-driven changes in atmospheric circulation over the past 116,000 years in subtropical Brazil. *Nature,* 434**,** 63-66.
Dansgaard, W. 1964. Stable isotopes in precipitation. *Tellus,* 16**,** 436-468.
Doughty, C. E., Malhi, Y., Araujo-Murakami, A., Metcalfe, D. B., Silva-Espejo, J. E., Arroyo, L., Heredia, J. P., Pardo-Toledo, E., Mendizabal, L. M., Rojas-Landivar, V. D., Vega-Martinez, M., Flores-Valencia, M., Sibler-Rivero, R., Moreno-Vare, L., Viscarra, L. J., Chuviru-Castro, T., Osinaga-Becerra, M. & Ledezma, R. 2014. Allocation trade-offs dominate the response of tropical forest growth to seasonal and interannual drought. *Ecology,* 95**,** 2192-2201.
Drumond, A., Marengo, J., Ambrizzi, T., Nieto, R., Moreira, L. & Gimeno, L. 2014. The role of the Amazon Basin moisture in the atmospheric branch of the hydrological cycle: a Lagrangian analysis. *Hydrology and Earth System Sciences,* 18**,** 2577-2598.
Dünisch, O., Bauch, J. & Gasparotto, L. 2002. Formation of increment zones and intraannual growth dynamics in the xylem of *Swietenia macrophylla*, *Carapa guianensis*, and *Cedrela odorata*

(Meliaceae). *IAWA Journal,* 23**,** 101-120.
Dünisch, O. & Morais, R. R. 2002. Regulation of xylem sap flow in an evergreen, a semi-deciduous, and a deciduous Meliaceae species from the Amazon. *Trees,* 16**,** 404-416.
Dünisch, O., Montóia, V. R. & Bauch, J. 2003. Dendroecological investigations on *Swietenia macrophylla* King and *Cedrela odorata* L.(Meliaceae) in the central Amazon. *Trees,* 17**,** 244-250.
Enquist, B. J. & Leffler, A. J. 2001. Long-term tree ring chronologies from sympatric tropical dry-forest trees: individualistic responses to climatic variation. *Journal of Tropical Ecology,* 17**,** 41-60.
Espinoza, J. C., Guyot, J. L., Ronchail, J., Cochonneau, G., Filizola, N., Fraizy, P., Labat, D., De Oliveira, E. A., Ordoñez, J. J. & Vauchel, P. 2009. Contrasting regional discharge evolutions in the Amazon basin (1974–2004). *Journal of Hydrology,* 375**,** 297-311.
Evans, M. N. & Schrag, D. P. 2004. A stable isotope-based approach to tropical dendroclimatology. *Geochimica et Cosmochimica Acta,* 68**,** 3295-3305.
Fichtler, E., Trouet, V., Beeckman, H., Coppin, P. & Worbes, M. 2004. Climatic signals in tree rings of Burkea africana and Pterocarpus angolensis from semiarid forests in Namibia. *Trees,* 18**,** 442-451.
Garcia, M., Villalba, F., Araguas-Araguas, L. & Rozanski, K. 1998. The role of atmospheric circulation patterns in controlling the regional distribution of stable isotope contents in precipitation: Preliminary results from two transects in the Ecuadorian Andes. *Isotope techniques in the study of environmental change.* International Atomic Energy Agency (IAEA): IAEA.
Garreaud, R. D., Vuille, M., Compagnucci, R. & Marengo, J. 2009. Present-day South American climate. *Palaeogeography, Palaeoclimatology, Palaeoecology,* 281**,** 180-195.
Gebrekirstos, A., Neufeldt, H. & Mitlöhner, R. Exploring climatic signals in stable isotopes of Sclerocarya birrea tree ring chronologies from the Sahel region in West Africa. TRACE conference paper, 2011. 143-148.
Gloor, M., Brienen, R. J. W., Galbraith, D., Feldpausch, T. R., Schöngart, J., Guyot, J. L., Espinoza, J. C., Lloyd, J. & Phillips, O. L. 2013. Intensification of the Amazon hydrological cycle over the last two decades. *Geophysical Research Letters,* 40**,** 1729-1733.
Gloor, M., Barichivich, J., Ziv, G., Brienen, R. J. W., Schöngart, J., Peylin, P., Cintra, B. B. L., Feldpausch, T. R., Phillips, O. L. & Baker, J. C. A. 2015. Recent Amazon climate as background for possible ongoing and future changes of Amazon humid forests. *Global Biogeochemical Cycles,* 29**,** 1384-1399.
Grießinger, J., Bräuning, A., Helle, G., Thomas, A. & Schleser, G. 2011. Late Holocene Asian summer monsoon variability reflected by $\delta^{18}O$ in tree-rings from Tibetan junipers. *Geophysical Research Letters*, 38, 1-5.
Harada, M., Watanabe, Y., Nakatsuka, T., Tazuru-Mizuno, S., Horikawa, Y., Subiyanto, B., Sugiyama, J., Tsuda, T. & Tagami, T. 2017. Assessment of sungkai tree-ring delta O-18 proxy for paleoclimate reconstruction in western Java, Indonesia. *Quaternary International,* 432**,** 33-38.
Huntingford, C., Fisher, R. A., Mercado, L., Booth, B. B. B., Sitch, S., Harris, P. P., Cox, P. M., Jones, C. D., Betts, R. A., Malhi, Y., Harris, G. R., Collins, M. & Moorcroft, P. 2008. Towards quantifying uncertainty in predictions of Amazon 'dieback'. *Philosophical Transactions of the Royal Society B: Biological Sciences,* 363**,** 1857-1864.
IAEA/WMO. [Online]. Global Network of Isotopes in Precipitation. The GNIP Database. Available: http://www.iaea.org/water [Accessed 2016].
International Tree Ring Data Bank (ITRDB) [Online]. Available: http://www.ncdc.noaa.gov/data-access/paleoclimatology-data/datasets/tree-ring [Accessed 1 March 2015].
Joly, M. & Voldoire, A. 2009. Influence of ENSO on the West African Monsoon: Temporal Aspects and Atmospheric Processes. *Journal of Climate,* 22**,** 3193-3210.
Kagawa, A., Sano, M., Nakatsuka, T., Ikeda, T. & Kubo, S. 2015. An optimized method for stable isotope analysis of tree rings by extracting cellulose directly from cross-sectional laths. *Chemical Geology,* 393**,** 16-25.
Kanner, L. C., Burns, S. J., Cheng, H., Edwards, R. L. & Vuille, M. 2013. High-resolution variability of the South American summer monsoon over the last seven millennia: insights from a speleothem record from the central Peruvian Andes. *Quaternary Science Reviews,* 75**,** 1-10.
Leavitt, S. W., Long, A. & Dean, J. S. 1985. Tree-ring dating through pattern-matching of stable-carbon isotope time series. *Tree-Ring Bulletin,* 1985**,** 1-10.
Li, Z., Nakatsuka, T. & Sano, M. 2015. Tree-ring cellulose $\delta^{18}O$ variability in pine and oak and its potential to reconstruct precipitation and relative humidity in central Japan. *Geochemical*

Journal, 49**,** 125-137.
Li, Z.-H., Labbé, N., Driese, S. G. & Grissino-Mayer, H. D. 2011. Micro-scale analysis of tree-ring $\delta^{18}O$ and $\delta^{13}C$ on α-cellulose spline reveals high-resolution intra-annual climate variability and tropical cyclone activity. *Chemical Geology,* 284**,** 138-147.
Liu, X., Zeng, X., Leavitt, S. W., Wang, W., An, W., Xu, G., Sun, W., Wang, Y., Qin, D. & Ren, J. 2013. A 400-year tree-ring $\delta^{18}O$ chronology for the southeastern Tibetan Plateau: Implications for inferring variations of the regional hydroclimate. *Global and Planetary Change,* 104**,** 23-33.
Liu, X., Xu, G., Grießinger, J., An, W., Wang, W., Zeng, X., Wu, G. & Qin, D. 2014. A shift in cloud cover over the southeastern Tibetan Plateau since 1600: evidence from regional tree-ring $\delta^{18}O$ and its linkages to tropical oceans. *Quaternary Science Reviews,* 88**,** 55-68.
Loader, N. J., Robertson, I., Barker, A. C., Switsur, V. R. & Waterhouse, J. S. 1997. An improved technique for the batch processing of small wholewood samples to α-cellulose. *Chemical Geology,* 136**,** 313-317.
Lutz, A., Thomas, J. M. & Panorska, A. 2011. Environmental controls on stable isotope precipitation values over Mali and Niger, West Africa. *Environmental Earth Sciences,* 62**,** 1749-1759.
Marengo, J. A. & Espinoza, J. C. 2016. Extreme seasonal droughts and floods in Amazonia: causes, trends and impacts. *International Journal of Climatology,* 36**,** 1033-1050.
Matsui, E., Salati, E., Ribeiro, M., Ris, C., Tancredi, A. & Gat, J. 1983. Precipitation in the Central Amazon Basin: the isotopic composition of rain and atmospheric moisture at Belem and Manaus. *Acta Amazonica,* 13**,** 307-369.
Methven, J. 1997. Offline trajectories: Calculation and accuracy. UK Universities Global Atmospheric Modelling Programme.
Mook, W. G. 2000. *Environmental isotopes in the hydrological cycle: Volume I Introduction (Theory, Methods, Review)*, International Atomic Energy Agency and United Nations Educational, Scientific and Cultural Organization.
Muangsong, C., Cai, B. G., Pumijumnong, N., Hu, C. Y. & Lei, G. L. 2016. Intra-seasonal variability of teak tree-ring cellulose delta O-18 from northwestern Thailand: A potential proxy of Thailand summer monsoon rainfall. *Holocene,* 26**,** 1397-1405.
Novello, V. F., Vuille, M., Cruz, F. W., Stríkis, N. M., De Paula, M. S., Edwards, R. L., Cheng, H., Karmann, I., Jaqueto, P. F., Trindade, R. I. F., Hartmann, G. A. & Moquet, J. S. 2016. Centennial-scale solar forcing of the South American Monsoon System recorded in stalagmites. *Scientific Reports,* 6**,** 1-8.
Ohashi, S., Durgante, F. M., Kagawa, A., Kajimoto, T., Trumbore, S. E., Xu, X., Ishizuka, M. & Higuchi, N. 2016. Seasonal variations in the stable oxygen isotope ratio of wood cellulose reveal annual rings of trees in a Central Amazon terra firme forest. *Oecologia,* 180**,** 685-696.
Pearson, S., Hua, Q., Allen, K. & Bowman, D. M. 2011. Validating putatively cross-dated *Callitris* tree-ring chronologies using bomb-pulse radiocarbon analysis. *Australian Journal of Botany,* 59**,** 7-17.
Phillips, O. L., Lewis, S. L., Baker, T. R., Chao, K.-J. & Higuchi, N. 2008. The changing Amazon forest. *Philosophical Transactions of the Royal Society of London B: Biological Sciences,* 363**,** 1819-1827.
Poussart, P. F., Evans, M. N. & Schrag, D. P. 2004. Resolving seasonality in tropical trees: multi-decade, high-resolution oxygen and carbon isotope records from Indonesia and Thailand. *Earth and Planetary Science Letters,* 218**,** 301-316.
Poussart, P. F. & Schrag, D. P. 2005. Seasonally resolved stable isotope chronologies from northern Thailand deciduous trees. *Earth and Planetary Science Letters,* 235**,** 752-765.
Ram, S., Borgaonkar, H. & Sikder, A. 2008. Tree-ring analysis of teak (*Tectona grandis* LF) in central India and its relationship with rainfall and moisture index. *Journal of Earth System Science,* 117**,** 637-645.
Reuter, J., Stott, L., Khider, D., Sinha, A., Cheng, H. & Edwards, R. L. 2009. A new perspective on the hydroclimate variability in northern South America during the Little Ice Age. *Geophysical Research Letters,* 36**,** 1-5.
Rozanski, K., Araguás-Araguás, L. & Gonfiantini, R. 1993. Isotopic patterns in modern global precipitation. *Climate change in continental isotopic records***,** 1-36.
Ruiz, V. E., Meloni, D. A., Fornes, L. F., Ordano, M., Hilal, M. & Prado, F. E. 2013. Seedling growth and water relations of three *Cedrela* species sourced from five provenances: response to simulated rainfall reductions. *Agroforestry systems,* 87**,** 1005-1021.
Russon, T., Tudhope, A. W., Hegerl, G. C., Collins, M. & Tindall, J. 2013. Inter-annual tropical Pacific

climate variability in an isotope-enabled CGCM: implications for interpreting coral stable oxygen isotope records of ENSO. *Climate of the Past,* 9**,** 1543-1557.

Salati, E., Dall'olio, A., Matsui, E. & Gat, J. R. 1979. Recycling of water in the Amazon basin: an isotopic study. *Water Resources Research,* 15**,** 1250-1258.

Sano, M., Xu, C. & Nakatsuka, T. 2012. A 300-year Vietnam hydroclimate and ENSO variability record reconstructed from tree ring $\delta^{18}O$. *Journal of Geophysical Research: Atmospheres,* 117**,** 1-11.

Schollaen, K., Heinrich, I., Neuwirth, B., Krusic, P. J., D'arrigo, R. D., Karyanto, O. & Helle, G. 2013. Multiple tree-ring chronologies (ring width, $\delta^{13}C$ and $\delta^{18}O$) reveal dry and rainy season signals of rainfall in Indonesia. *Quaternary Science Reviews,* 73**,** 170-181.

Schollaen, K., Karamperidou, C., Krusic, P., Cook, E. & Helle, G. 2015. ENSO flavors in a tree-ring $\delta^{18}O$ record of Tectona grandis from Indonesia. *Climate of the Past,* 10**,** 3965-3987.

Schöngart, J., Piedade, M. T. F., Ludwigshausen, S., Horna, V. & Worbes, M. 2002. Phenology and stem-growth periodicity of tree species in Amazonian floodplain forests. *Journal of Tropical Ecology,* 18**,** 581-597.

Schöngart, J., Junk, W. J., Piedade, M. T. F., Ayres, J. M., Huttermann, A. & Worbes, M. 2004. Teleconnection between tree growth in the Amazonian floodplains and the El Nino-Southern Oscillation effect. *Global Change Biology,* 10**,** 683-692.

Schöngart, J., Piedade, M. T., Wittmann, F., Junk, W. J. & Worbes, M. 2005. Wood growth patterns of *Macrolobium acaciifolium* (Benth.) Benth. (Fabaceae) in Amazonian black-water and white-water floodplain forests. *Oecologia,* 145**,** 454-61.

Schöngart, J., Orthmann, B., Hennenberg, K. J., Porembski, S. & Worbes, M. 2006. Climate–growth relationships of tropical tree species in West Africa and their potential for climate reconstruction. *Global Change Biology,* 12**,** 1139-1150.

Schwendenmann, L., Pendall, E., Sanchez-Bragado, R., Kunert, N. & Hölscher, D. 2014. Tree water uptake in a tropical plantation varying in tree diversity: interspecific differences, seasonal shifts and complementarity. *Ecohydrology,* 8**,** 1-12.

Silva Dias, M. a. F., Rutledge, S., Kabat, P., Silva Dias, P. L., Nobre, C., Fisch, G., Dolman, A. J., Zipser, E., Garstang, M., Manzi, A. O., Fuentes, J. D., Rocha, H. R., Marengo, J., Plana-Fattori, A., Sá, L. D. A., Alvalá, R. C. S., Andreae, M. O., Artaxo, P., Gielow, R. & Gatti, L. 2002. Cloud and rain processes in a biosphere-atmosphere interaction context in the Amazon Region. *Journal of Geophysical Research: Atmospheres,* 107**,** 1-18.

Stein, A. F., Draxler, R. R., Rolph, G. D., Stunder, B. J. B., Cohen, M. D. & Ngan, F. 2015. NOAA's HYSPLIT Atmospheric Transport and Dispersion Modeling System. *Bulletin of the American Meteorological Society,* 96**,** 2059-2077.

Stohl, A., Forster, C., Frank, A., Seibert, P. & Wotawa, G. 2005. Technical note: The Lagrangian particle dispersion model FLEXPART version 6.2. *Atmospheric Chemistry and Physics,* 5**,** 2461-2474.

Thompson, L. G., Mosley-Thompson, E., Davis, M. E., Zagorodnov, V. S., Howat, I. M., Mikhalenko, V. N. & Lin, P. N. 2013. Annually resolved ice core records of tropical climate variability over the past ~1800 years. *Science,* 340**,** 945-950.

Tindall, J. C. & Haywood, A. M. 2015. Modeling oxygen isotopes in the Pliocene: Large-scale features over the land and ocean. *Paleoceanography,* 30**,** 1183-1201.

Tomazello Filho, M., Botosso, P. & Lisi, C. 2000. Potencialidade da família Meliaceae para dendrocronologia em regiões tropicais e subtropicais. *F.A. Roig (ed.) Dendrocronología em América Latina. EDIUNC, Mendoza***,** 381-431.

Treydte, K., Frank, D., Esper, J., Andreu, L., Bednarz, Z., Berninger, F., Boettger, T., D'alessandro, C. M., Etien, N., Filot, M., Grabner, M., Guillemin, M. T., Gutierrez, E., Haupt, M., Helle, G., Hilasvuori, E., Jungner, H., Kalela-Brundin, M., Krapiec, M., Leuenberger, M., Loader, N. J., Masson-Delmotte, V., Pazdur, A., Pawelczyk, S., Pierre, M., Planells, O., Pukiene, R., Reynolds-Henne, C. E., Rinne, K. T., Saracino, A., Saurer, M., Sonninen, E., Stievenard, M., Switsur, V. R., Szczepanek, M., Szychowska-Krapiec, E., Todaro, L., Waterhouse, J. S., Weigl, M. & Schleser, G. H. 2007. Signal strength and climate calibration of a European tree-ring isotope network. *Geophysical Research Letters*, 34, 1-6.

Van Der Sleen, P., Groenendijk, P. & Zuidema, P. A. 2015. Tree-ring $\delta^{18}O$ in African mahogany (*Entandrophragma utile*) records regional precipitation and can be used for climate reconstructions. *Global and Planetary Change,* 127**,** 58-66.

Van Der Sleen, P., Zuidema, P. A. & Pons, T. L. 2017. Stable isotopes in tropical tree rings: theory, methods and applications. *Functional Ecology, Accepted article*.

Verheyden, A., Helle, G., Schleser, G. H., Dehairs, F., Beeckman, H. & Koedam, N. 2004. Annual

cyclicity in high-resolution stable carbon and oxygen isotope ratios in the wood of the mangrove tree *Rhizophora mucronata*. *Plant, Cell and Environment,* 27**,** 1525-1536.
Villacís, M., Vimeux, F. & Taupin, J. D. 2008. Analysis of the climate controls on the isotopic composition of precipitation ($\delta^{18}O$) at Nuevo Rocafuerte, 74.5 W, 0.9 S, 250 m, Ecuador. *Comptes Rendus Geoscience,* 340**,** 1-9.
Villalba, R., Grau, H. R., Boninsegna, J. A., Jacoby, G. C. & Ripalta, A. 1998. Tree-ring evidence for long-term precipitation changes in subtropical South America. *International Journal of Climatology,* 18**,** 1463-1478.
Vimeux, F., Gallaire, R., Bony, S., Hoffmann, G. & Chiang, J. C. 2005. What are the climate controls on δD in precipitation in the Zongo Valley (Bolivia)? Implications for the Illimani ice core interpretation. *Earth and Planetary Science Letters,* 240**,** 205-220.
Volland, F., Pucha, D. & Braeuning, A. 2016. Hydro-climatic variability in southern Ecuador reflected by tree-ring oxygen isotopes. *Erdkunde,* 70**,** 69-82.
Vuille, M., Burns, S., Taylor, B., Cruz, F., Bird, B., Abbott, M., Kanner, L., Cheng, H. & Novello, V. 2012. A review of the South American monsoon history as recorded in stable isotopic proxies over the past two millennia. *Climate of the Past,* 8**,** 1309-1321.
Whitmore, T. 1998. *An Introduction To Tropical Rain Forests*, Clarendon Press.
Wieloch, T., Helle, G., Heinrich, I., Voigt, M. & Schyma, P. 2011. A novel device for batch-wise isolation of α-cellulose from small-amount wholewood samples. *Dendrochronologia,* 29**,** 115-117.
Wigley, T. M., Briffa, K. R. & Jones, P. D. 1984. On the average value of correlated time series, with applications in dendroclimatology and hydrometeorology. *Journal of Climate and Applied Meteorology,* 23**,** 201-213.
Williams, A. P., Funk, C., Michaelsen, J., Rauscher, S. A., Robertson, I., Wils, T. H. G., Koprowski, M., Eshetu, Z. & Loader, N. J. 2012. Recent summer precipitation trends in the Greater Horn of Africa and the emerging role of Indian Ocean sea surface temperature. *Climate Dynamics,* 39**,** 2307-2328.
Wilson, R., Anchukaitis, K., Briffa, K. R., Büntgen, U., Cook, E., D'arrigo, R., Davi, N., Esper, J., Frank, D., Gunnarson, B., Hegerl, G., Helama, S., Klesse, S., Krusic, P. J., Linderholm, H. W., Myglan, V., Osborn, T. J., Rydval, M., Schneider, L., Schurer, A., Wiles, G., Zhang, P. & Zorita, E. 2016. Last millennium northern hemisphere summer temperatures from tree rings: Part I: The long term context. *Quaternary Science Reviews*, 134, 1-18.
Worbes, M. & Junk, W. J. 1989. Dating tropical trees by means of ^{14}C from bomb tests. *Ecology,* 70**,** 503-507.
Worbes, M. 1999. Annual growth rings, rainfall-dependent growth and long-term growth patterns of tropical trees from the Caparo Forest Reserve in Venezuela. *Journal of Ecology,* 87**,** 391-403.
Worbes, M. & Junk, W. J. 1999. How old are tropical trees? The persistence of a myth. *IAWA Journal,* 20**,** 255-260.
Worbes, M. 2002. One hundred years of tree-ring research in the tropics–a brief history and an outlook to future challenges. *Dendrochronologia,* 20**,** 217-231.
Xu, C., Sano, M. & Nakatsuka, T. 2011. Tree ring cellulose $\delta^{18}O$ of *Fokienia hodginsii* in northern Laos: A promising proxy to reconstruct ENSO? *Journal of Geophysical Research,* 116**,** 1-12.
Xu, C., Sano, M. & Nakatsuka, T. 2013. A 400-year record of hydroclimate variability and local ENSO history in northern Southeast Asia inferred from tree-ring delta O-18. *Palaeogeography Palaeoclimatology Palaeoecology,* 386**,** 588-598.
Xu, C., Pumijumnong, N., Nakatsuka, T., Sano, M. & Li, Z. 2015. A tree-ring cellulose $\delta^{18}O$-based July–October precipitation reconstruction since AD 1828, northwest Thailand. *Journal of Hydrology,* 529**,** 433-441.
Yoon, J.-H. & Zeng, N. 2010. An Atlantic influence on Amazon rainfall. *Climate Dynamics,* 34**,** 249-264.
Zemp, D. C., Schleussner, C.-F., Barbosa, H. M. J., Hirota, M., Montade, V., Sampaio, G., Staal, A., Wang-Erlandsson, L. & Rammig, A. 2017. Self-amplified Amazon forest loss due to vegetation-atmosphere feedbacks. *Nature Communications,* 8**,** 1-10.
Zhu, M., Stott, L., Buckley, B., Yoshimura, K. & Ra, K. 2012. Indo-Pacific Warm Pool convection and ENSO since 1867 derived from Cambodian pine tree cellulose oxygen isotopes. *Journal of Geophysical Research,* 117**,** 1-11.

Appendices

Appendix 2.1 – Cellulose extraction method comparison

Two cellulose extraction techniques were employed in this thesis: the batch extraction method from Wieloch et al. (2011) and the cross-section extraction method from Kagawa et al. (2015). The batch method involves separating and cutting up each individual tree ring with a scalpel prior to cellulose extraction. The cross-section method involves cutting sections of wood approximately 1 mm thick, which are contained within perforated polytetrafluoroethylene (PTFE) cases for the cellulose extraction process. With this method tree rings are separated with a scalpel after extraction is complete. To compare the results of these methods a sample of *Cedrela montana* from Cuyuja, Ecuador with wide and clear rings was selected. Cellulose was then extracted from a series of 21 rings using the batch method and the cross-section method. After extraction, the cellulose for each ring was homogenised, freeze-dried and weighed into silver cups for oxygen isotope analysis at the School of Earth and Environment at the University of Leeds. The results are shown in Figure 2.3.

Appendix 4.1 – Raw isotope data with original and adjusted tree-ring dates

The raw tree-ring oxygen isotope ($\delta^{18}O_{TR}$) values for each individual tree included in the multi-species analysis, and the trees used to construct the Selva Negra chronology, are presented in Tables A4.1.1 and A4.1.2 respectively. The original and adjusted tree ring dates are given to clearly show where changes have been made following crossdating against the established $\delta^{18}O_{TR}$ chronology from Brienen et al., (2012) and/or in light of the results from radiocarbon dating. In addition, the samples that had their tree ring dates adjusted were plotted to show the original and new data series (Figs. A4.1.1 and A4.1.2).

Table A4.1.1 – Raw tree-ring oxygen isotope ($\delta^{18}O_{TR}$) data from the seven tropical tree species included in the multi-species analysis presented in Chapter 4. Dates assigned following initial ring counting (original) and isotope crossdating (adjusted) are shown. Data are given in units of per mil (‰).

	Couratari		*Amburana*		*Bertholletia*	*Tachigali*
Year	**Original**	**Adjusted**	**Original**	**Adjusted**	**Unadjusted**	**Unadjusted**
2002	23.98		25.59			23.59
2001	22.34		24.12		25.92	23.44
2000	22.30	23.98	23.42	25.59	24.62	24.27
1999	24.57	22.34	25.30	24.12	23.76	22.65
1998	22.64	22.30	23.11	23.42	24.61	22.50
1997	21.85	24.57	23.58	25.30	24.24	25.23
1996	23.74	22.64	25.13	23.11	23.65	22.67
1995	21.27	21.85	24.26	23.58	23.54	22.19
1994	23.68	23.74	24.35	25.13	25.42	24.40
1993	25.31	21.27	22.03	24.26	24.09	22.60
1992	20.91	23.68	22.38		24.53	22.55
1991	20.52	25.31	24.15	24.35	23.06	24.90
1990	21.54		21.22		23.49	23.35
1989	23.61		24.56	22.03	24.96	
1988	23.88	21.54	23.97	22.38	25.46	
1987	22.72	23.61	21.37	24.15	24.02	
1986	23.50	23.88	24.56	21.22	20.03	
1985	24.30	22.72	22.21	24.56	22.99	
1984	24.25	23.50	23.19	23.97	25.99	
1983	23.94	24.30	24.48	21.37	25.50	
1982	24.82	24.25		24.56	27.08	
1981	23.57	23.94	23.16	22.21	27.03	
1980	23.36	24.82	23.90	23.19	26.08	
1979		23.57	21.43	24.48	25.93	
1978	24.39		23.42		25.71	
1977	24.65		23.43	23.16	24.52	
1976	23.37	23.36	24.69	23.90	22.99	
1975	23.38		23.48	21.43	22.67	
1974	24.41	24.39	22.66	23.42	26.79	
1973	24.86	24.65	25.04	23.43	24.98	
1972	25.24	23.37	25.98	24.69	22.73	
1971	23.65	23.38	27.00	23.48	25.63	
1970	25.58		24.63	22.66	24.78	
1969	23.95	24.41	27.24	25.04		
1968	22.94	24.86	25.87	25.98		
1967	24.16	25.24	27.64	27.00	24.50	
1966	24.32	23.65	25.64	24.63	24.13	
1965	25.46	25.58	23.97	27.24	25.33	
1964	23.77		25.32	25.87	25.21	
1963		23.95	25.57	27.64	24.53	
1962	24.82	22.94	25.76	25.64	24.25	
1961	24.29	24.16	25.73	23.97	24.09	
1960	25.48		25.52	25.32	25.32	
1959	25.69	24.32	24.22	25.57	21.89	
1958	23.82	25.46	26.03	25.76	25.44	
1957	24.35	23.77	24.85	25.73	24.54	
1956	24.23		24.53	25.52	23.96	
1955	24.56	24.82	25.52	24.22	27.83	
1954	25.20	24.29	25.33	26.03	25.00	
1953	25.52	25.48	25.08	24.85	27.08	
1952	24.52	25.69	26.70	24.53	26.45	
1951	25.74	23.82	26.26	25.52	29.04	
1950	24.02	24.35	26.59	25.33	25.48	
1949	23.98	24.23	25.27	25.08	24.64	
1948	22.56	24.56	26.59	26.70	24.59	
1947	25.11	25.20	25.54	26.26	29.04	
1946	25.80	25.52	27.37	26.59	24.69	
1945	23.22	24.52	26.34	25.27	26.02	

Table A4.1.1 – *Continued***.**

	Couratari		*Amburana*		*Bertholletia*	*Tachigali*
Year	**Original**	**Adjusted**	**Original**	**Adjusted**	**Unadjusted**	**Unadjusted**
1944	26.02	25.74	25.37	26.59	25.82	
1943	24.94	24.02	26.58	25.54	26.55	
1942	25.58	23.98	23.80	27.37	27.91	
1941	25.99	22.56	24.77	26.34	26.51	
1940	22.62	25.11	25.35	25.37	25.60	
1939	23.54	25.80	24.81	26.58	24.78	
1938	25.55	23.22	24.73	23.80	27.31	
1937	25.71	26.02	23.91	24.77	25.25	
1936	27.12	24.94	25.26	25.35	26.38	
1935	22.67	25.58	25.14	24.81	25.02	
1934	23.30	25.99	26.44	24.73	27.27	
1933	26.55	22.62	24.55	23.91	25.53	
1932	25.62		26.63	25.26	25.21	
1931	24.29	23.54	24.22	25.14	27.45	
1930	23.77	25.55	24.19	26.44	24.41	
1929	26.21	25.71	28.39	24.55	24.82	
1928	27.12		24.15	26.63	25.84	
1927	23.53	22.67	26.25	24.22	25.32	
1926	26.02	23.30	22.88	24.19		
1925	22.02	26.55	24.73	28.39	26.32	
1924	23.88	25.62	24.38	24.15	26.22	
1923	24.53	24.29	9.54	26.25	23.08	
1922	24.73	23.77	25.64	22.88	27.68	
1921	24.67	26.21	23.93	24.73	24.75	
1920	25.81	25.10	24.74	24.38	27.49	
1919	24.15	23.53	23.63		27.25	
1918	25.73	26.02	25.15	25.64	26.37	
1917	23.79	22.02	23.93	23.93	24.07	
1916	25.75	23.88	23.60	24.74	24.95	
1915	24.56	24.53	26.69	23.63	26.37	
1914	25.11	24.73	23.15	25.15	25.45	
1913	25.20	24.67	23.49	23.93	24.64	
1912		25.81	23.60	23.60	21.37	
1911	23.69	24.15	26.69	26.69	24.38	
1910	22.84	25.73	23.15	23.15	24.73	
1909	22.97	23.79	23.49	23.49	22.34	
1908	24.98	25.75	22.62	23.60	26.88	
1907	23.57	24.56	23.77	26.69	25.57	
1906	26.04	25.11	25.46	23.15	23.41	
1905	25.00	25.20	25.86	23.49		
1904	24.06			22.62	24.86	
1903	23.78	23.69	24.80	23.77		
1902	22.97	22.84	24.58	25.46	22.43	
1901	20.78	22.97	24.23	25.86	24.64	
1900	22.81	24.98	23.49		25.10	
1899		23.57	23.98	24.80	24.38	
1898		26.04	22.01	24.58	22.62	
1897		25.00	23.86	24.23	23.83	
1896		24.06		23.49	25.04	
1895		23.78		23.98		
1894		22.97		22.01		
1893		20.78		23.86		
1892		22.81				

Table A4.1.1 – *Continued***.**

	Peltogyne		*Cedrelinga*		*Polylepis*
Year	**Original**	**Adjusted**	**Original**	**Adjusted**	**Unadjusted**
2002	21.08		29.73		23.28
2001	24.33		26.48		21.11
2000	20.99		29.46		21.95
1999	24.51		26.87	29.73	17.82
1998	25.52		26.58	26.48	22.47
1997	21.76		26.83	29.46	24.49
1996	24.58		26.71	26.87	19.89
1995	21.03		25.09	26.58	24.24
1994	24.95		25.63	26.83	23.37
1993	21.50		26.00	26.71	19.18
1992	26.33		25.77	25.09	20.20
1991	24.23		25.97	25.63	23.29
1990	24.14	21.08	26.70	26.00	21.89
1989		24.33	26.12	25.77	23.60
1988	24.91	20.99	25.40	25.97	21.61
1987	23.23	24.51	32.73	26.70	22.24
1986	23.59	25.52	24.34	26.12	18.61
1985	24.11	21.76	26.50	25.40	18.93
1984	23.59	24.58	24.67	32.73	17.61
1983	24.46	21.03	28.11	24.34	22.28
1982	23.17	24.95	26.25	26.50	27.31
1981	25.57	21.50	27.58	24.67	22.98
1980	25.29	26.33	25.78	28.11	21.99
1979	25.40	24.23	25.32	26.25	22.18
1978	27.13	24.14	24.14	27.58	19.39
1977	24.04		24.32	25.78	19.79
1976	25.96	24.91	22.99	25.32	18.54
1975	25.37	23.23	25.58	24.14	18.54
1974	25.06	23.59	24.92	24.32	16.57
1973	24.24	24.11	23.97	22.99	19.92
1972	24.07	23.59	26.14	25.58	18.88
1971	21.86	24.46	26.96	24.92	17.63
1970	25.83	23.17	28.25	23.97	19.31
1969	23.95	25.57	22.81	26.14	22.01
1968	26.52	25.29	22.73	26.96	19.59
1967	23.27	25.40	28.37	28.25	19.49
1966	24.14	27.13	27.84	22.81	22.45
1965	21.48	24.04	29.98	22.73	23.40
1964	24.22	25.96	24.63	28.37	23.18
1963	23.21	25.37	28.86	27.84	20.27
1962	23.60	25.06	24.75	29.98	18.36
1961	23.95	24.24	25.82	24.63	19.83
1960	24.13	24.07	27.59	28.86	20.96
1959	25.75	21.86	24.62	24.75	19.45
1958	23.21	25.83	21.97	25.82	22.68
1957	23.10	23.95	25.45	27.59	23.21
1956	24.45	26.52	25.77	24.62	23.61
1955	23.12		24.80	21.97	20.28
1954	25.56	23.27	22.20	25.45	19.32
1953	24.91	24.14	26.03	25.77	18.81
1952	24.67	21.48		24.80	19.19
1951	24.42	24.22		22.20	20.42
1950	25.43	23.21		26.03	23.03
1949	24.26	23.60			21.06
1948	25.14	23.95			24.53
1947	24.34	24.13			22.88
1946	21.27	25.75			21.35
1945	22.64	23.21			21.99
1944	22.73	23.10			21.63
1943	25.26	24.45			20.77

Table A4.1.1 – *Continued***.**

	Peltogyne		***Cedrelinga***		***Polylepis***
Year	**Original**	**Adjusted**	**Original**	**Adjusted**	**Unadjusted**
1942	26.26	23.12			21.85
1941		25.56			26.66
1940		24.91			25.56
1939		24.67			23.59
1938		24.42			20.96
1937		25.43			22.76
1936		24.26			22.22
1935		25.14			22.38
1934		24.34			19.81
1933		21.27			18.89
1932		22.64			18.14
1931		22.73			17.26
1930		25.26			
1929		26.26			

Table A4.1.2 – Raw tree-ring oxygen isotope ($\delta^{18}O_{TR}$) data from the nine *Cedrela odorata* trees from Selva Negra. For some trees isotopes were measured in multiple radii. Data are given in units of per mil (‰).

	Tree_11		Tree_12	Tree_13		Tree_14_a		Tree_14_c
Year	**Original**	**Adjusted**	**Unadjusted**	**Original**	**Adjusted**	**Original**	**Adjusted**	**Unadjusted**
2010	20.82	20.82	21.25	22.78				20.37
2009	23.12	23.12	22.73	19.14	22.78			20.54
2008	19.43	19.43	17.20	22.41	19.14			18.19
2007	21.54	21.54	21.27	23.25	22.41	19.66		20.23
2006	23.56	23.56	22.76	20.54	23.25	21.33		21.58
2005	20.92	20.92	20.52	21.47	20.54	22.21		19.59
2004	21.84	21.84	21.06	23.49	21.47	21.87		21.72
2003	22.95	22.95	23.38	22.05	23.49	21.58		21.85
2002	23.35	23.35	22.25	21.54	22.05	21.71		21.43
2001	22.44	22.44	22.07	21.53	21.54	21.21		20.93
2000	23.27	23.27	21.09	21.01	21.53	20.52		20.89
1999	21.29	21.29	21.59	21.21	21.01	23.84		
1998	20.49	20.49	20.64	23.84	21.21	20.71		
1997	23.99	23.99	24.25	21.95	23.84	20.64	23.84	
1996	22.13	22.13	21.34	20.58	21.95	21.72	20.71	
1995	20.16	20.16	20.27	22.96	20.58	20.06	20.64	
1994	23.07	23.07	22.60	21.56	22.96	20.36	21.72	
1993	20.28	20.28	21.05	21.21	21.56	23.09	20.06	
1992	21.38	21.38	19.36	23.14	21.21	21.61	20.36	
1991	23.83	23.83	23.57	22.57	23.14	22.50	23.09	
1990	22.56	22.56	22.41	23.07	22.57	20.02	21.61	
1989	23.16	23.16	18.87	20.42	23.07	21.55	22.50	
1988	20.72	20.72	20.55	22.27	20.42	23.18	20.02	
1987	22.96	22.96	22.18	23.84	22.27	20.50	21.55	
1986	23.23	23.23	23.96	20.20	23.84	21.49	23.18	
1985	21.31	21.31	20.48	21.92	20.20	21.94	20.50	
1984	22.40	22.40	22.39	21.22	21.92	20.98	21.64	
1983	24.00		21.43	23.50	21.22	23.46	20.98	
1982	21.31	24.00	18.94	20.99	23.50	21.00	23.46	
1981	22.79	21.31	20.25	22.43	20.99	20.22	20.42	
1980	24.09	22.79	20.61	24.31	22.43	22.06	22.06	
1979	22.08	24.09	24.30	21.87	24.31	23.25	23.32	
1978	23.54	22.08	22.47	22.74	21.87	23.40	21.07	
1977	22.70	23.54	22.68	22.78	22.74	21.07	21.69	
1976	20.03	22.70	23.50	20.11	22.78	21.69	21.73	
1975	22.16	20.03	19.85	20.94	20.11	21.73	18.79	
1974	20.44	22.16	20.99	20.52	20.94	18.79	19.83	
1973	23.59	20.44	19.87	21.26	20.52	19.83	18.92	
1972	22.16	23.59	21.56	21.71	21.26	18.92	20.51	
1971	20.43	22.16	21.63	19.91	21.71	20.51	19.78	
1970	22.63	20.43	19.19	22.71	19.91	19.78	18.56	
1969	23.90	22.63	21.66	22.61	22.71	18.56	20.72	
1968	22.90	23.90	23.33	22.95	22.61	20.72	21.65	
1967	21.31	22.90	23.21	20.54	22.95	21.65	21.72	
1966	23.72	21.31	21.63	24.53	20.54	21.72	19.31	
1965	22.62	23.72	24.44	21.67	24.53	19.31	23.02	
1964	22.71	22.62	22.81	23.70	21.67	23.02	21.24	
1963	21.34	22.71	22.98	20.71	23.70	21.24	21.66	
1962	20.27	21.34	21.23	20.36	20.71	21.66	19.90	
1961	22.29	20.27	21.07	22.01	20.36	19.90	19.41	
1960	23.75	22.29	22.38		22.01	19.41	21.00	
1959	22.49	22.49	23.34			21.00	21.76	
1958	22.49	22.68	22.30			21.76	21.51	
1957	22.68	22.68	22.59			21.51	21.76	
1956	22.68	21.62	22.76			21.76	21.28	
1955	21.62	19.32	20.19			21.28	19.69	
1954	19.32	19.32	20.73			19.69	20.42	
1953	19.32	21.47	22.08			20.42	20.78	

Table A4.1.2 – *Continued*.

	Tree_11		Tree_12	Tree_13		Tree_14_a		Tree_14_c
Year	Original	Adjusted	Unadjusted	Original	Adjusted	Original	Adjusted	Unadjusted
1952	21.47	19.65	20.05			20.78	19.33	
1951	19.65	22.93	21.40			19.33	20.42	
1950	22.93	22.78	22.57			20.42	22.04	
1949	22.78	23.29	21.00			22.04	20.47	
1948	23.29		22.27			20.47	21.68	
1947	21.94	21.94	22.58			21.68	21.94	
1946	22.99	22.99	23.68			21.94	22.28	
1945	21.92	21.92	21.94			22.28	20.49	
1944	22.77	22.77	21.05			20.49	21.19	
1943	22.25	22.25	21.05			21.19	21.29	
1942	20.11	20.11	21.24			21.29	20.61	
1941	22.48	22.48	21.84			20.61	21.42	
1940	22.05	22.05				21.42	21.67	
1939	23.42	23.42				21.67	22.50	
1938	21.39	21.39				22.50	20.26	
1937	21.88	21.88				20.26	20.40	
1936	21.92	21.92				20.40	20.71	
1935	20.62	20.62				20.71	21.76	
1934	25.10					21.76	22.02	
1933	20.17	20.17				22.02	18.86	
1932	22.06	22.06				18.86	21.83	
1931	20.39	20.39				21.83	21.01	
1930	21.49	21.49				21.01	22.32	
1929	22.66	22.66				22.32	20.33	
1928	20.28	20.28				20.33	20.95	
1927	19.68	19.68				20.95	20.81	
1926	22.22	22.22				20.81	19.36	
1925	23.31	23.31				19.36	23.86	
1924	21.73	21.73				23.86	19.72	
1923	18.99	22.13				19.72	22.24	
1922	25.27	20.59				22.24	19.42	
1921	20.59	23.70				19.42	20.51	
1920	23.70	20.94				20.51	20.26	
1919	20.94					20.26	20.21	
1918	17.40					20.21	21.58	
1917	19.43					21.58	17.81	
1916	22.34					17.81	21.27	
1915	20.87					21.27	20.75	
1914						20.75	20.71	
1913						20.71	22.18	
1912						22.18	19.88	
1911						19.88	23.17	
1910						23.17	20.27	
1909						20.27	19.81	
1908						19.81	19.31	
1907						19.31	18.48	
1906						18.48		
1905							21.87	
1904						21.87	19.46	
1903						19.46	22.07	
1902						22.07	18.01	
1901						18.01	19.30	
1900						19.30	20.05	
1899						20.05	20.16	
1898						20.16	20.71	
1897						20.71	19.83	
1896						19.83	22.03	
1895						22.03	20.18	
1894						20.18	19.32	
1893						19.32	20.74	

Table A4.1.2 – *Continued.*

	Tree_11		Tree_12	Tree_13		Tree_14_a		Tree_14_c
Year	**Original**	**Adjusted**	**Unadjusted**	**Original**	**Adjusted**	**Original**	**Adjusted**	**Unadjusted**
1892						20.74	22.29	
1891						22.29	20.62	
1890						20.62	18.79	
1889						18.79	19.26	
1888						19.26	21.57	
1887						21.57	20.53	
1886						20.53	17.77	
1885						17.77	22.14	
1884						22.14		

Table A4.1.2 – *Continued*.

	Tree_16	Tree_20		Tree_21_c2	Tree_21_c1		Tree_21_c
Year	Unadjusted	Original	Adjusted	Unadjusted	Original	Adjusted	Unadjusted
2010	21.37	21.49	21.49	21.69			
2009	22.62	21.79	21.79	21.59			
2008	17.65	18.98	18.98	19.59			
2007	22.24	20.24	20.24	21.81			
2006	21.05	22.78	22.78	23.04			
2005	20.25	20.37	20.37	20.73			
2004	19.28	22.12	22.12	22.85			
2003	22.21	22.49	22.49	23.55			
2002	23.21	22.49	22.49	21.06			
2001	21.71	21.43	21.43	22.79			
2000	22.32	22.21	22.21	21.69			
1999	19.86	21.03	21.03	22.05			
1998	19.81	20.58	20.58	20.61			
1997	24.47	23.85	23.85	24.61			
1996	23.04	22.16	22.16	22.57			
1995	21.40	19.81	19.81	21.38			
1994	22.03	21.96	21.96	22.67			
1993	20.83	20.44	20.44	21.30			
1992	21.01	20.44	20.44	21.06			
1991	24.02	23.50	23.50	23.81			
1990	23.04	22.00	22.00	22.56			
1989	23.49	22.46	22.46	23.40			
1988	20.52	19.67	19.67	20.52			
1987	22.74	21.41	21.41	22.32			
1986	23.73	23.21	23.21	23.76			
1985	20.08	20.03	20.03	21.32			
1984	22.77	22.09	22.09	22.46			
1983	22.44	20.75	20.75	21.74			
1982	24.56	23.35	23.35	24.12			
1981	20.78	20.64	20.64	20.92			
1980	22.11	22.17	22.17	22.77			
1979	24.15	23.69	23.69	24.10			
1978	21.97	21.16	21.16	21.66			
1977	22.68	22.79	22.79	22.74			
1976	20.61	22.27	22.27	22.48			
1975	20.61	19.31	19.31	19.17			
1974	21.57	20.84	20.84	21.84			
1973	20.02	19.21	19.21	20.02			
1972	19.35	21.95	21.95	22.00			
1971	19.15	21.33	21.33	21.32			
1970	20.26	19.24	19.24	20.56			
1969	22.12	21.98	21.98	21.75		22.30	
1968	23.16	22.82	22.82	22.96	22.30	23.00	
1967	22.70	23.24	23.24	23.29	23.00	23.00	
1966	20.85	20.67	20.67	20.96	23.00	21.10	
1965	23.23	23.46	23.46	24.21	21.10	23.80	
1964	22.39	22.31	22.31	21.82	23.80	21.90	
1963	23.24	22.39	22.39	23.17	21.90	23.10	
1962	21.12	20.47	20.47	22.97	23.10	21.00	
1961	20.82	20.50	20.50		21.00	20.70	
1960	21.92	21.70	21.70		20.70	22.00	
1959	22.84	23.15	23.15		22.00	23.90	
1958	22.76	22.00	22.00		23.90	22.50	
1957	22.42	22.89	22.89		22.50	22.40	
1956	22.30	20.05			22.40	22.00	
1955	19.25				22.00	20.50	
1954	19.65				20.50	20.10	
1953	21.50	20.59			20.10	22.90	
1952	19.64				23.50	19.50	

Table A4.1.2 – *Continued*.

	Tree_16	Tree_20		Tree_21_c2	Tree_21_c1		Tree_21_c
Year	Unadjusted	Original	Adjusted	Unadjusted	Original	Adjusted	Unadjusted
1951	21.55	23.76			21.50	21.90	
1950	22.02	22.78			19.50	22.30	
1949	21.99	22.87			21.90	22.10	
1948	22.76	22.93	22.78		22.30	22.60	
1947	22.38	21.81	22.87		22.10	22.70	
1946	23.60	21.40	22.93		22.60	22.90	
1945	22.25	22.34	21.81		22.70	21.40	
1944	22.27	21.45	21.40		22.90	22.10	
1943	22.30	22.33	22.34		21.40	22.00	
1942	21.36	21.93	21.45		22.10	21.70	
1941	22.00	23.27	22.33		22.00	22.70	
1940	22.60	20.06	21.93		21.70	22.40	
1939	23.05	21.55	23.27		22.70	23.00	
1938	19.66	21.43	20.06		22.40	21.40	
1937	21.64	22.31	21.55		23.00	22.20	
1936	21.70	22.25	21.43		21.40	22.50	
1935	21.29	18.91	22.31		22.20	22.80	
1934	21.73	22.05	22.25		22.50	22.60	
1933	18.76	21.67	18.91		22.80	20.30	
1932	22.05	22.55	22.05		22.60	22.90	
1931	20.66	21.15	21.67		20.30	21.80	
1930	22.70	20.36	22.55		22.90	24.10	
1929	20.52	20.50	21.15		21.80	22.00	
1928	22.17	20.33	20.36		24.10	22.60	
1927	21.66	23.77	20.50		22.00	22.10	
1926	22.68	19.88	20.33		22.60	20.90	
1925	22.31	22.25	23.77		22.10	25.30	
1924	19.63	19.66	19.88		20.90	21.30	
1923	22.02	20.66	22.25		25.30	23.40	
1922	18.97	22.04	19.66		21.30	20.20	
1921	19.79	20.45	20.66		23.40	22.00	
1920	20.47		22.04		20.20	22.60	
1919	21.17	18.84	20.45		22.00	21.50	
1918	22.70	21.04			22.60	22.80	
1917	20.56	21.79	18.84		21.50	20.00	
1916	21.32	20.60	21.04		22.80	22.10	
1915	22.11	23.94	21.79		20.00	22.70	
1914	19.78	20.51	20.60		22.10	22.00	
1913	20.69	20.09	23.94		22.70	24.10	
1912	18.97	19.41	20.51		22.00	21.90	
1911	23.87	20.49			24.10	24.20	
1910	20.19	20.64			21.90	20.10	
1909	18.80	22.70	20.09		24.20	22.00	
1908	20.49	22.67	19.41		20.10	18.40	
1907	21.66		20.49		22.00	21.50	
1906	22.78		20.64		18.40	22.30	
1905	23.40		22.70		21.50	23.40	
1904	22.82		22.67		22.30	22.40	
1903	19.97				23.40	20.80	
1902	23.01				22.40	24.00	
1901	21.74				20.80	22.90	
1900	22.23				24.00	22.50	
1899	23.13				22.90	23.50	
1898	19.12				22.50	21.30	
1897	19.74				23.50	21.40	24.90
1896	23.99				21.30	22.10	22.20
1895	20.84				21.40		24.50
1894	20.78				22.10		20.40
1893	21.13						22.40

Table A4.1.2 – *Continued*.

	Tree_16	Tree_20		Tree_21_c2	Tree_21_c1		Tree_21_c
Year	**Unadjusted**	**Original**	**Adjusted**	**Unadjusted**	**Original**	**Adjusted**	**Unadjusted**
1892	22.10						22.00
1891	21.38						22.20
1890	22.29						21.50
1889	21.64						22.90
1888	22.62						21.70
1887	23.72						23.70
1886	22.39						23.60
1885	22.82						22.50
1884	22.39						23.80

Table A4.1.2 – *Continued*.

	Tree_23		Tree_27
Year	**Original**	**Adjusted**	**Unadjusted**
2010	21.22	21.22	21.29
2009	21.45	21.45	22.22
2008	19.12	19.12	17.46
2007	21.56	21.56	22.41
2006	23.11	23.11	22.62
2005	20.22	20.22	20.43
2004	22.42	22.42	22.26
2003	23.65	23.65	21.82
2002	22.61	22.61	22.91
2001	22.18	22.18	22.49
2000	23.04	23.04	22.52
1999	21.69	21.69	21.28
1998	21.86	21.86	19.81
1997	24.28	24.28	22.60
1996	23.02	23.02	22.83
1995		21.05	20.71
1994	21.05	23.12	21.41
1993	23.12	21.46	20.71
1992	21.46	21.65	21.26
1991	21.65	24.06	24.18
1990	24.06	23.13	22.70
1989	23.13	23.37	23.14
1988	23.37	20.60	20.45
1987	20.60	22.64	23.14
1986	22.64	24.17	22.68
1985	24.17	21.42	21.66
1984	21.42	22.30	22.12
1983	22.30	22.19	21.89
1982	22.19	24.14	24.05
1981	24.14	21.57	22.24
1980	21.57	22.51	22.93
1979	22.51	23.67	23.70
1978	23.67	21.33	21.71
1977	21.33	22.95	23.24
1976	22.95	23.57	22.70
1975	23.57	20.88	20.27
1974	20.88	21.27	20.78
1973	21.27	20.37	20.58
1972	20.37	22.88	22.02
1971	22.88	22.28	21.46
1970	22.28	20.45	20.25
1969	20.45	22.66	21.89
1968	22.66	23.25	22.88
1967	23.25	23.06	22.56
1966	23.06	21.03	21.55
1965	21.03	21.14	23.49
1964	21.14	21.89	22.41
1963	21.89	22.22	21.85
1962	22.22	21.37	21.36
1961	21.37	20.38	20.38
1960	20.38	21.93	22.35
1959	21.93	22.87	22.99
1958	22.87	23.08	22.31
1957	23.08	23.06	22.86
1956	23.06	23.41	22.12
1955	23.41	24.23	20.01
1954	24.23	21.79	20.36
1953	21.79	19.68	21.57
1952	19.68	19.67	19.73

Table A4.1.2 – *Continued*.

	Tree_23		Tree_27
Year	**Original**	**Adjusted**	**Unadjusted**
1951	19.67	21.75	20.87
1950	21.75	21.91	22.72
1949	21.91	21.56	21.74
1948	21.56	22.38	22.44
1947	22.38	22.60	23.01
1946	22.60	23.34	23.35
1945	23.34	21.92	22.01
1944	21.92		21.26
1943	22.72		21.84
1942	22.72		21.92
1941	22.72		22.72
1940	22.72		22.76
1939	22.72		23.36
1938	22.72		21.09
1937	21.84		20.98
1936	23.35		21.77
1935	21.86		22.58
1934	22.78		22.32
1933	21.93		20.08
1932	20.18		21.40
1931	24.40	21.84	21.42
1930	20.37	23.35	22.39
1929	22.80	21.86	21.19
1928	20.11	22.78	21.76
1927	21.00	21.93	21.35
1926	21.10	20.18	20.91
1925	20.69	24.40	24.41
1924	22.60	20.37	20.21
1923	20.42	22.80	22.75
1922	21.78	20.11	20.89
1921	21.72	21.00	21.32
1920	21.91	21.10	20.88
1919	22.91	20.69	21.08
1918	25.21	22.60	21.56
1917	20.96	20.42	19.35
1916	23.96	21.78	22.11
1915	20.26	21.72	22.30
1914	22.07	21.91	21.88
1913	20.55	22.91	22.06
1912	23.59		20.18
1911	24.02	25.21	20.50
1910	19.77	20.96	20.50
1909	22.93	23.96	21.70
1908	19.86	20.26	20.80
1907	22.35	22.07	21.10
1906	22.90	20.55	20.70
1905	19.59	23.59	23.30
1904	20.94	24.02	23.20
1903		19.77	19.40
1902		22.93	
1901		19.86	
1900		22.35	
1899		22.90	
1898		19.59	
1897		20.94	

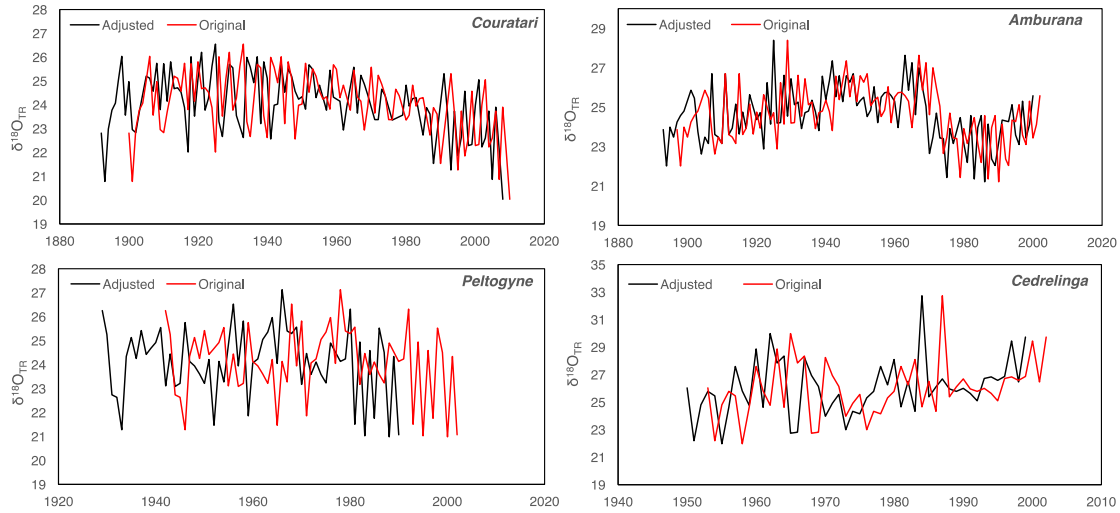

Fig. A4.1.1 – The original (red) and adjusted (black) time series for the four trees in the multi-species analysis that had their tree ring dates revised following isotope-crossdating and/or radiocarbon dating.

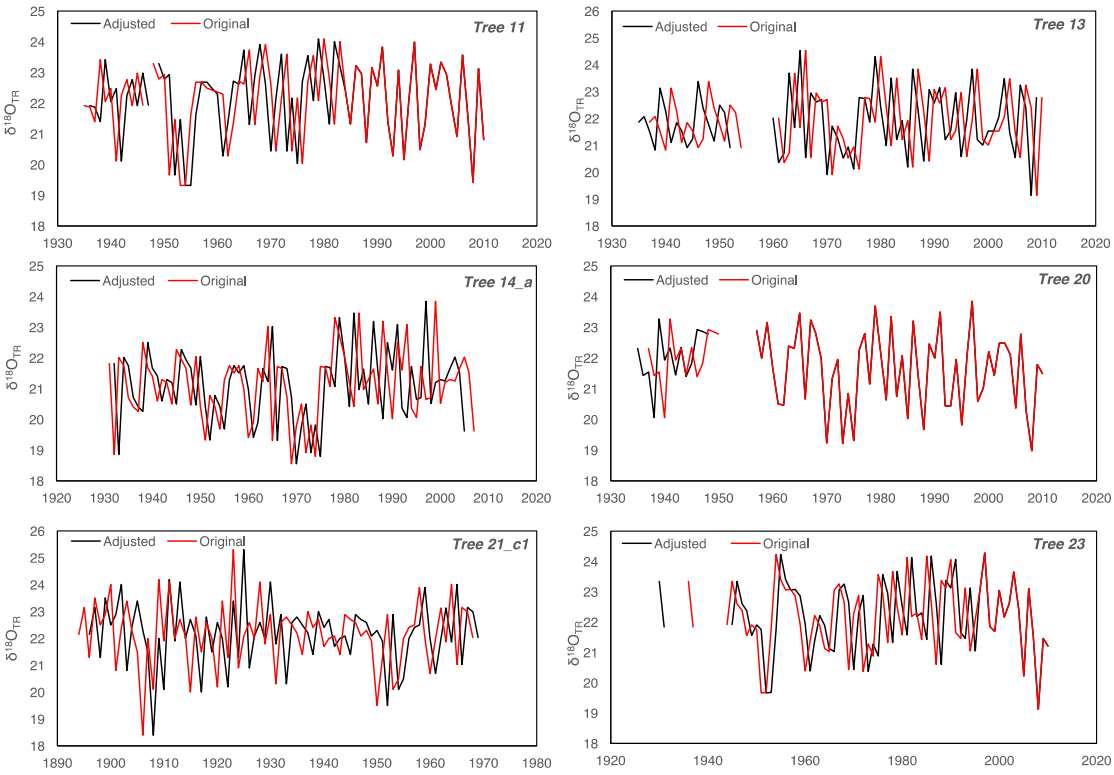

Fig. A4.1.2 – The original (red) and adjusted (black) time series for the six *Cedrela* trees that had their tree ring dates revised following isotope-crossdating.

Appendix 5.1 – Altitude sensitivity analysis

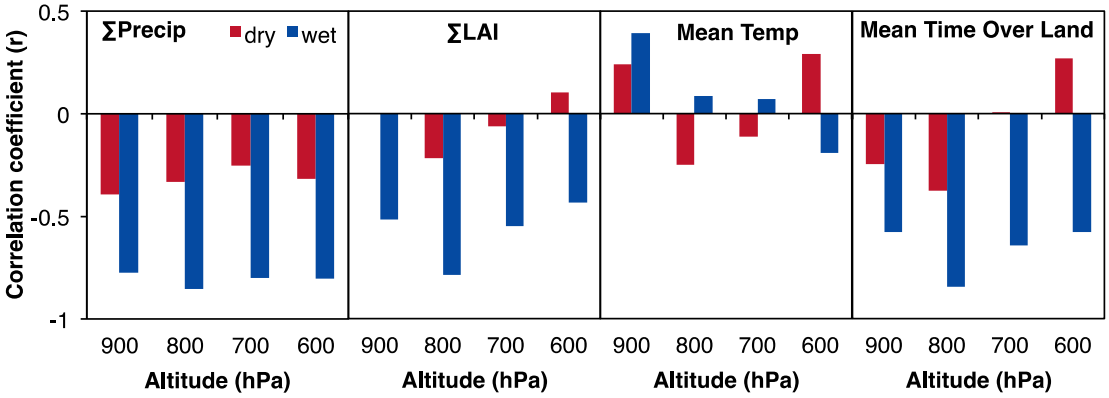

Figure A5.1.1 – Plots showing the sensitivity of correlations between tree-ring cellulose $\delta^{18}O$ ($\delta^{18}O_{TR}$) and trajectory variables (accumulated precipitation (∑Precip), accumulated leaf area index (∑LAI), mean trajectory temperature and mean travel time over land) to changes in altitude. A pressure of 900 hPa is equivalent to approximately 1 km above the surface, and 600 hPa equivalent to approximately 4 km above the surface.

Appendix 5.2 – Supplementary methods for Chapter 5

Site: The $\delta^{18}O_{TR}$ record used in this study is a composite of nine trees from Selva Negra, a lowland rainforest site in northern Bolivia. The site and $\delta^{18}O_{TR}$ record (1901–2001) are described in detail by Baker et al. (2015), including methods for isotope analysis. The most recent part of the record (2002–2010) is presented here for the first time.

Data: Precipitation data are from the Tropical Rainfall Measuring Mission (TRMM; http://trmm.gsfc.nasa.gov/) multi-satellite 3B42 V7 3-hr product available at 0.25° x 0.25° resolution. Data were retrieved online from http://mirador.gsfc.nasa.gov/cgi-bin/mirador/presentNavigation.pl?tree=project&dataset=3B42:%203-Hour%200.25%20x%200.25%20degree%20merged%20TRMM%20and%20other%20satellite%20estimates&project=TRMM&dataGroup=Gridded&version=007&CGISESSID=b42f21c2e1ea87f58ea24190e943e910. The 3B42 product combines data from TRMM and other satellites to estimate precipitation (Huffman et al., 2007). Three-hourly data were summed to daily data for use in the analysis. Monthly mean leaf area index (LAI) data are from the Moderate Resolution Imaging Spectroradiometer (MODIS; http://modis.gsfc.nasa.gov/data/dataprod/mod15.php; Myneni et al., 2002). We use the Collection 5 Boston University 0.25° x 0.25° product (MODIS C5_BU), which uses strict data quality flags (Samanta et al., 2011) and is available for the period 2000–present. A monthly LAI climatology was calculated using data from 2000–2011 to overcome missing data pixels in some years and unrealistic temporal variation (Yan et al., 2016). Temperature and precipitation data for Figure 1 are from 65–67.5°W, 9–11.5°S Climatic Research Unit TS3.21 at 0.5° x 0.5° resolution for the period 1960–2010 (downloaded through Climate Explorer: https://climexp.knmi.nl). Monthly precipitation $\delta^{18}O$ data are averaged from 4 stations in the Global Network of Isotopes in Precipitation (GNIP; IAEA/WMO, 2016) database (Porto Velho, Rurrenabaque, Rio Branco and Trinidad), downloaded through WISER (Water Isotope System for Data Analysis, http://www-naweb.iaea.org/napc/ih/IHS_resources_isohis.html). Shuttle Radar Topographic Mission (SRTM) data were downloaded from USGS (U.S. Geological Survey) EarthExplorer (http://earthexplorer.usgs.gov/) and spatially averaged to 0.25° x 0.25° resolution.

Transport model: We used the Reading Offline TRAJectory (ROTRAJ) Lagrangian atmospheric transport model developed by John Methven (http://www.met.reading.ac.uk/~swrmethn/offline/UGAMP_tech44.ps) to calculate kinematic back-trajectories. 3D wind fields from the ECMWF ERA-Interim reanalysis dataset were used to drive the model, with trajectory position output every 6 hours. The ERA-Interim reanalysis assimilates model output and observations, creating a best estimate of the state of the climate through time while constraining the trajectories to have a rooting in reality. 10-day back-trajectories (40 x 6-hour time-steps) were calculated arriving once a day at four altitudes above the surface (corresponding to air pressures of 900, 800, 700 and 600 hPa). Our results were consistent from 900–600 hPa (approximately 1–4 km above the surface, Supplementary Figure 2). As well as accumulating precipitation and LAI along each trajectory, at each time-step the temperature specific to the horizontal and vertical position of the trajectory was extracted from ERA-Interim, and these values were subsequently averaged to find the mean trajectory temperature. We used a 1° resolution land-ocean mask from the National Oceanic & Atmospheric Administration (NOAA) to constrain our analysis over land (http://www.esrl.noaa.gov/psd/data/gridded/data.noaa.oisst.v2.html). For each trajectory, we calculated the distance and travel time over land. Trajectories were found to travel at similar speeds in both the wet (October–April) and dry (May–September) seasons (mean ($\pm 1\sigma$) = 6.1±1.7 and 6.3±1.7 m s^{-1} respectively). Mean trajectory time over land was found correlate well with to $\delta^{18}O_{TR}$ (Figure S2).

Trajectory experiments: Trajectory experiments were conducted to determine whether correlations between $\delta^{18}O_{TR}$ and $\sum$Precip are driven by interannual variation in transport pathway or interannual variation in basin precipitation. To resolve this, we systematically controlled for variation in precipitation (experiment 1) and variation in trajectories (experiment 2) in the calculation of $\sum Precip_{WET}$ (Table S1). Experiment 1 used the observed daily trajectories with a daily precipitation climatology (1998–2011) to calculate $\sum Precip_{WET}$. In experiment 2 a fixed random selection of trajectories and the observed precipitation data were used to calculate $\sum Precip_{WET}$. All trajectories were used in these calculations, not only those arriving on wet days as this would have retained some information about the interannual variability in rainfall amount.

Vapour transport analysis: Amazon water vapour inflow and outflow were calculated using the 'vertical integral of northward water vapour flux' and 'vertical integral of eastward water vapour flux' variables from the ERA-Interim reanalysis dataset (http://apps.ecmwf.int/datasets/data/interim-full-mnth/levtype=sfc/). These integrate water vapour fluxes across all model levels, from the surface to 0.1 hPa. ERA-Interim wind data averaged from 0–4 km above the surface (1000, 900, 800, 700, 600 and 500 hPa pressure levels) were used to calculate wet season (October–April) anomalies relative to the 1979-2010/11 mean. Column-integrated moisture transport and mean sea level pressure anomalies were calculated using the same methodology (data also from ERA-Interim). All data were downloaded at monthly resolution from 1979–2011. River discharge data measured at Óbidos were downloaded from the Agência Nacional de Águas (ANA) in Brazil (http://hidroweb.ana. gov.br; maximum monthly discharge) and averaged from October–September.

Rayleigh calculation: The isotopic composition of atmospheric vapour ($\delta^{18}O_{VAP}$) at Selva Negra, Bolivia was calculated for each year using the Rayleigh equation:

$$\delta^{18}O_{VAP}(t) = (1000 + \delta^{18}O_{VAP}(0)) \cdot f(t)^{(\alpha-1)} - 1000 \text{ where } \delta = \left(\frac{\left(\frac{^{18}O}{^{16}O}\right)_{sample}}{\left(\frac{^{18}O}{^{16}O}\right)_{standard}} - 1 \right) \times 1000$$

and $\delta^{18}O_{VAP}(0)$ is the initial isotope composition of the water vapour (in units of per mil), *f(t)* is the fraction of the original vapour remaining in air travelling across the Amazon, (equivalent to (1 – r), where r is runoff) and α is the temperature-dependent fractionation factor during condensation. Parameter details and associated references are given in Table S2. Vapour isotope values were then converted to $\delta^{18}O_P$ values following the equation $\delta^{18}O_P = \alpha(1000 + \delta^{18}O_{VAP})$ -1000, and finally to $\delta^{18}O_{TR}$ values, $\delta^{18}O_{TR} \approx \delta^{18}O_P + 27$. The 27 ‰ constant used to convert $\delta^{18}O_P$ to $\delta^{18}O_{TR}$ accounts for biological fractionation during cellulose synthesis (Sternberg, 2009, Sternberg and DeNiro, 1983). This is not a species-specific value and offsets <4 ‰ have been observed, even between $\delta^{18}O_{TR}$ records from the same species at different sites (Baker et al., 2015). Therefore, this value of 27 may be considered somewhat arbitrary. Thus, to calculate the root-mean-square error reported in the manuscript we first removed the offset (~4 ‰) between our simulated and observed $\delta^{18}O_{TR}$ values. In these Rayleigh calculations, we kept temperature and all temperature-dependent parameters constant with *f* the only source of interannual variability.

Ice-core analysis: Isotope data from the Huascarán and Quelccaya ice cores in the Peruvian Andes were downloaded from the NOAA Ice Core Gateway (http://www.ncdc.noaa.gov/paleo/icecore/trop,(Thompson et al., 1995, Thompson et al., 2013)). A composite of these was correlated with Amazon River discharge measured at Óbidos (which correlates precipitation over ~77% of the Amazon basin (Callède et al., 2008)) giving a Pearson correlation coefficient of –0.71 (1950–1984).

Error analysis: 95% confidence limits were calculated for the mean time series presented in Figures 2 and 3. Confidence intervals for $\delta^{18}O_{TR}$ were estimated from the standard deviation of isotope values from individual trees, assuming a normal distribution. ∑Precip values were not normally distributed and thus confidence limits for this series were obtained by bootstrap resampling. There are no error estimates available for ERA-Interim so confidence limits for net wet season water vapour import could not be calculated. Ocean source regions for the Amazon (inferred from van der Ent and Savenije, 2013) were used to select ocean surface $\delta^{18}O$ ($\delta^{18}O_{SW}$) data (LeGrande and Schmidt, 2006) to quantify spatial variability in source $\delta^{18}O$ (Figure S7). To estimate the error in our Rayleigh simulation we propagated the errors in four key terms of the model ($\delta^{18}O_{VAP}(0)$, P, ET and q0) according to the following equation:

$$\sigma\delta^{18}O_{VAP}(t)^2 = f^{(2\alpha-2)} \cdot \sigma\delta^{18}O_{VAP}(0)^2 + (\delta^{18}O_{VAP}(0)(\alpha-1) \cdot f^{(\alpha-2)})^2 \cdot (((N^2\Delta t^2)/q0^2) \cdot (\sigma P^2 + \sigma E^2) + ((((\sum P-E)\Delta t)^2)/q0^4) \cdot \sigma q0^2)$$

The values we used for each of these terms and their relevant sources are given in Table S3. The influence of temperature (which affects the α term) was found to be minimal and thus it was not included in the error analysis. We estimate the error to be 0.43 ‰, which is much less than the interannual variation of our simulation.

Appendix 5.3 – Determining whether basin climate or air transport pathway has a more important influence on $\delta^{18}O_{TR}$

Experiments were conducted to isolate the influence of interannual variation in precipitation on wet season accumulated precipitation ($\sum Precip_{WET}$) from the influence of interannual variation in circulation (see Appendix 5.2 for full details). In each experiment $\sum Precip_{WET}$ is calculated for each year using the defined criteria and the resulting series correlated with $\delta^{18}O_{TR}$.

Table A5.3.1 – Results from trajectory sensitivity experiments.

Experiment description	Correlation with $\delta^{18}O_{TR}$
Control (regular wet season calculation)	–0.85 (p<0.001)
Experiment 1: interannual variation in climate removed (observed trajectories, daily precipitation climatology)	–0.83 (p<0.001)
Experiment 2: interannual variation in transport pathway removed (fixed random trajectories, correct precipitation)	–0.75 (p<0.01)

Appendix 5.4 – Relationships between tree-ring oxygen isotope composition ($\delta^{18}O_{TR}$) and leaf area index accumulated along back trajectories

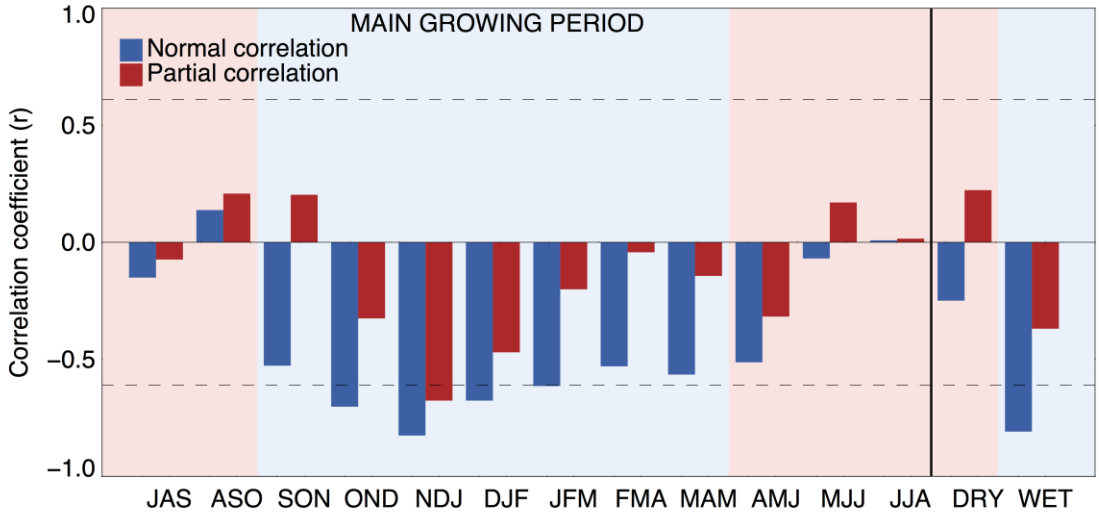

Figure A5.4.1 – Three-month moving correlation coefficients between $\delta^{18}O_{TR}$ and mean accumulated MODIS leaf area index (∑LAI, trajectories from 2000–2010/11). Blue bars show the values for the normal correlation, and red bars show the partial correlation coefficients (controlling for the effect of ∑Precip on $\delta^{18}O_{TR}$). Pink and blue boxes show the dry and wet seasons respectively. The bars at the right side of the plot show the mean correlation coefficient for the dry season (May–Sep) and wet season (Oct–Apr). Broken horizontal lines mark the significance threshold (p<0.05).

Appendix 5.5 – Wind and moisture transport anomalies over the Amazon in years with high and low tree-ring oxygen isotope ($\delta^{18}O_{TR}$) values

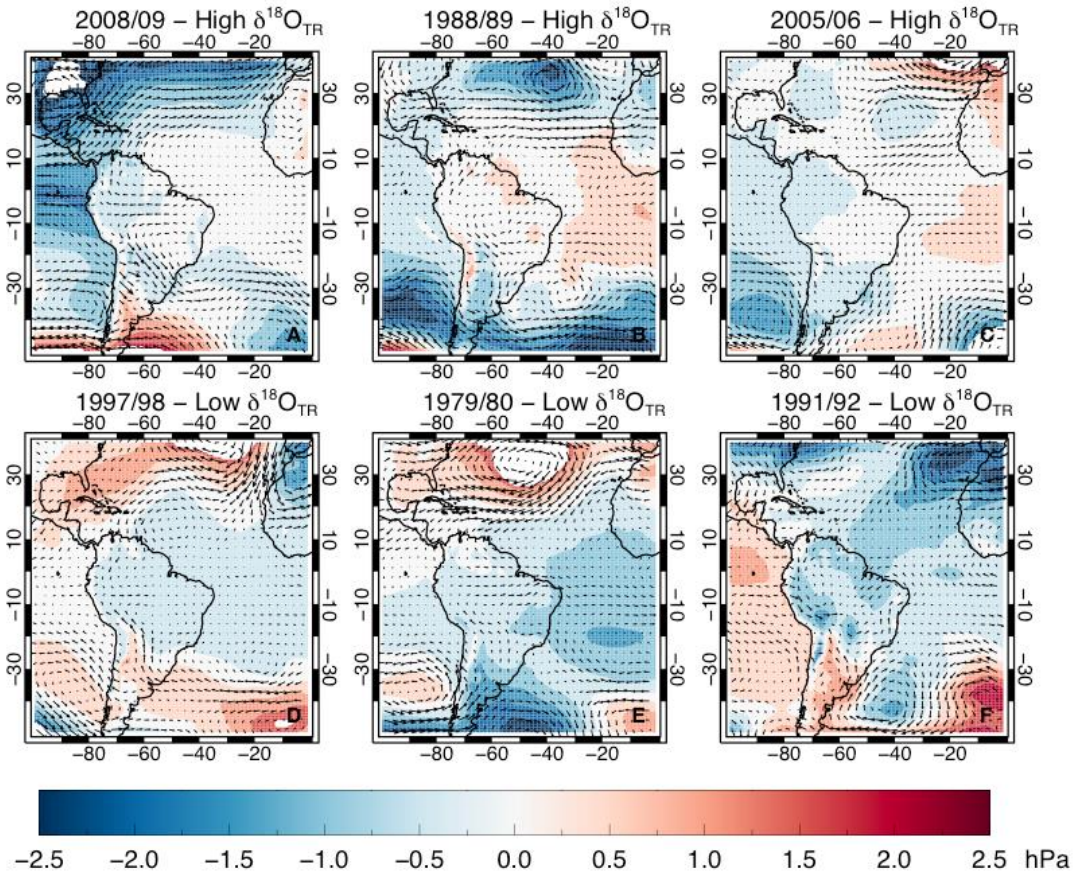

Figure A5.5.1 – **(a–c)** Wind anomalies (vectors) and sea level pressure anomalies (shaded contours) for the three years with the highest $\delta^{18}O_{TR}$ values from 1979–2010/11. **(d–f)** As in a–c but for the three years with the lowest $\delta^{18}O_{TR}$ values from 1979–2010/11. Data are from the ERA-Interim reanalysis dataset, 1979-2010/11.

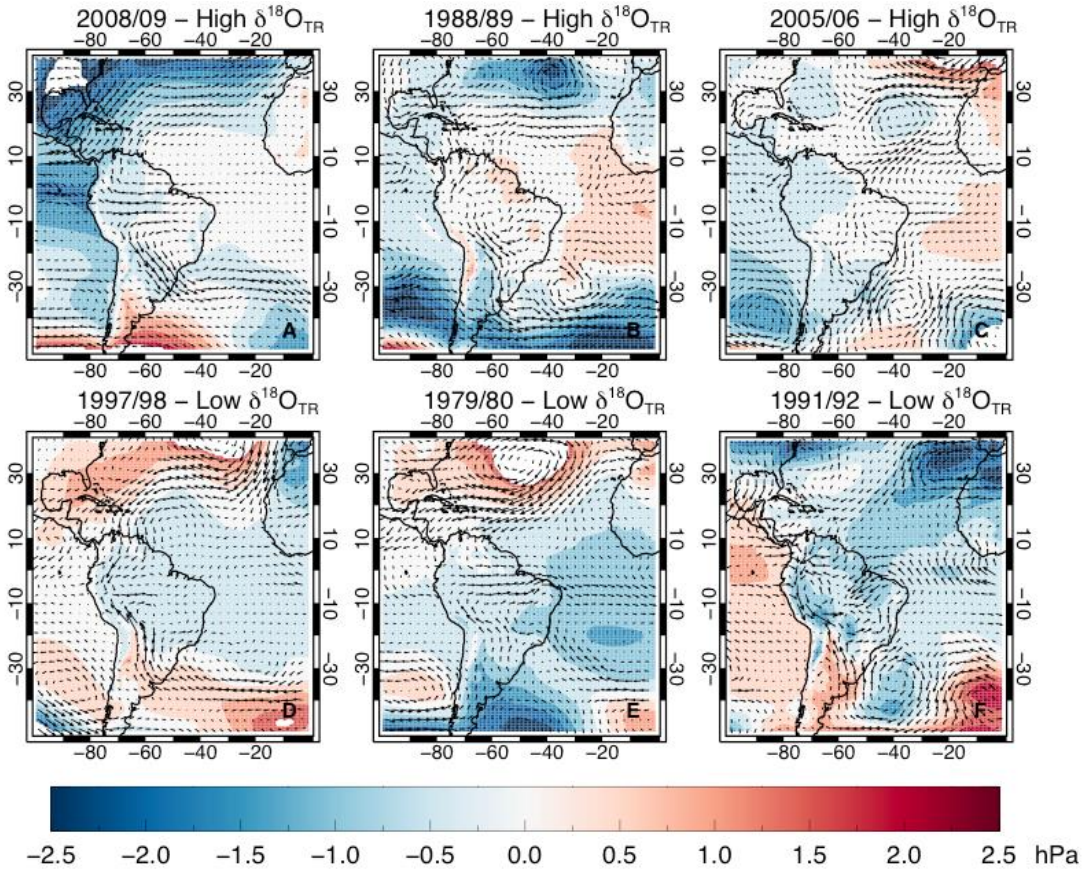

Figure A5.5.2 – **(a–c)** Moisture transport anomalies (vectors) and sea level pressure anomalies (shaded contours) for the three years with the highest $\delta^{18}O_{TR}$ values from 1979–2010/11. **(d–f)** As in a–c but for the three years with the lowest $\delta^{18}O_{TR}$ values from 1979–2010/11. Data are from the ERA-Interim reanalysis dataset, 1979-2010/11.

Appendix 5.6 – Comparing interannual variation in vapour inflow to and outflow from the Amazon basin with variation in Amazon River discharge

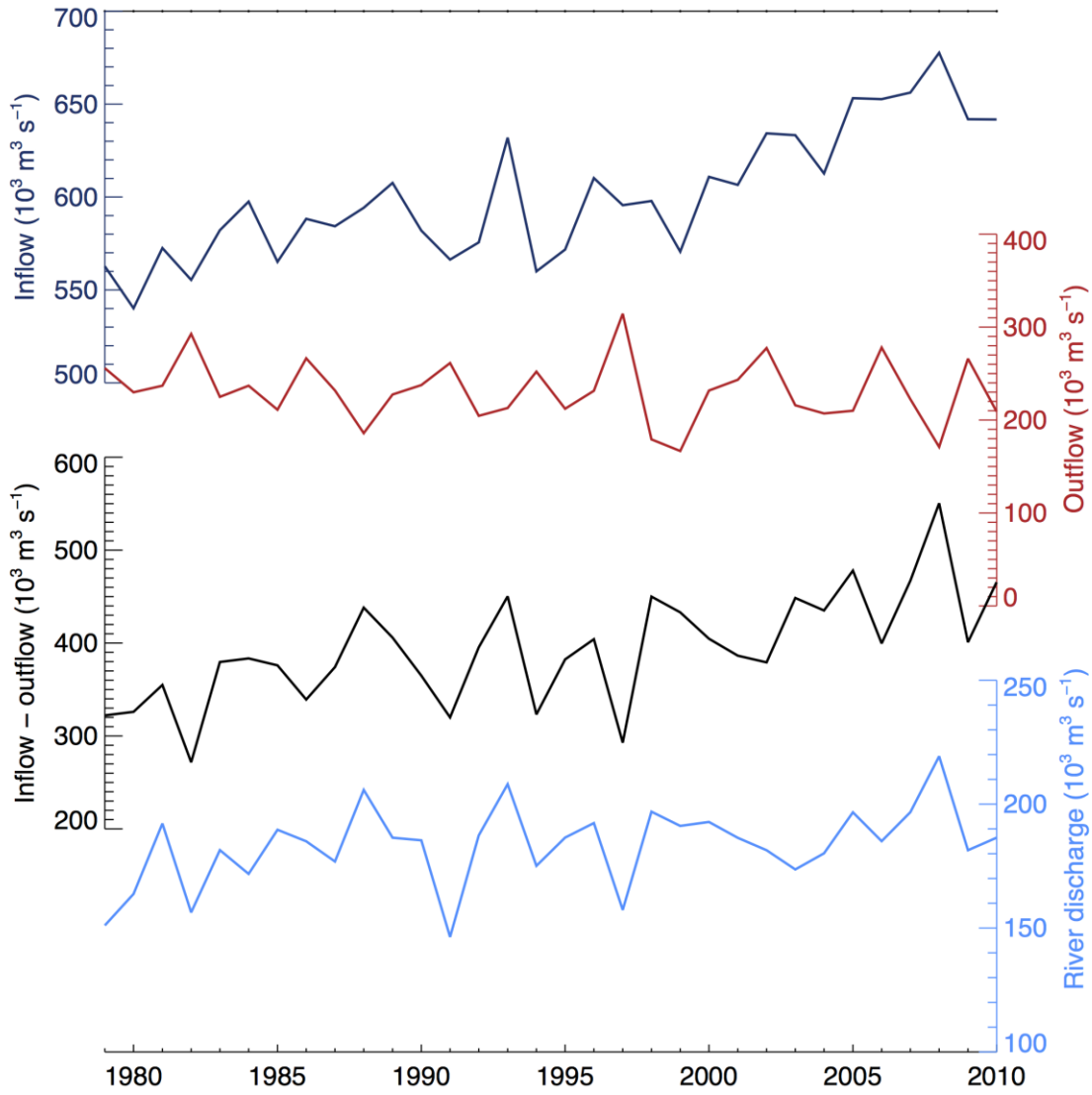

Figure A5.6.1 – Interannual variation in mean wet season water vapour inflow (dark blue line) and outflow (red line) along the transects shown in Figure 3, the difference between inflow and outflow (black line) and Amazon river discharge measured at Óbidos (light blue line).

Appendix 5.7 – Interannual variation in air transport pathways to sample site in northern Bolivia

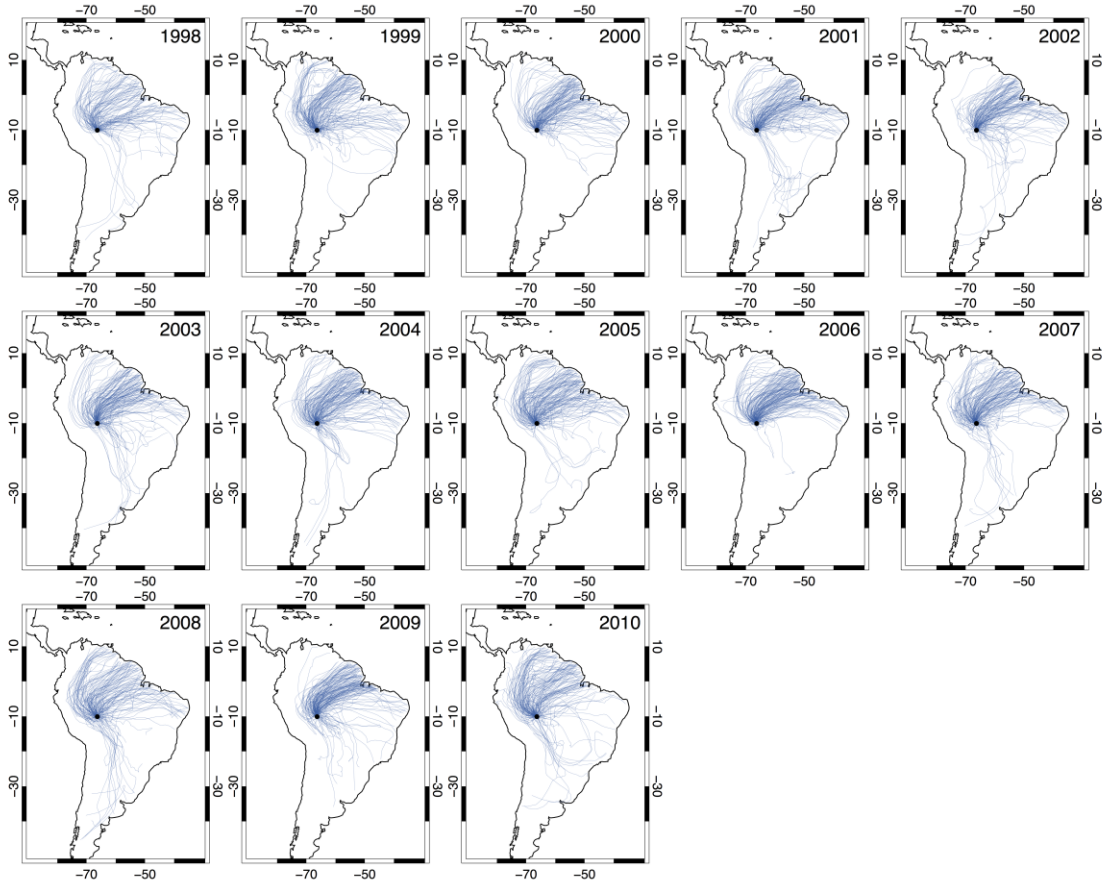

Figure A5.7.1 – Plots showing back trajectories arriving on days with precipitation >0 mm at Selva Negra, Bolivia (10°5'S, 66°18'W; 160 m.a.s.l.) during the wet season (Oct–Apr) for the years 1998-2010/11.

Appendix 5.8 – Spatial variation in isotope composition at moisture origin

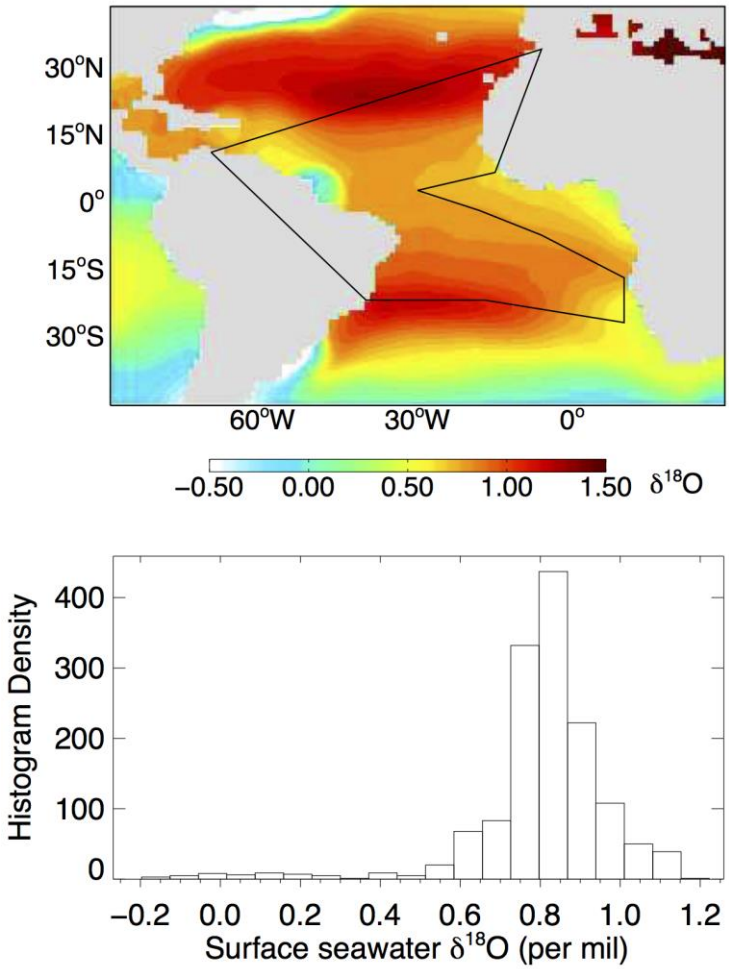

Figure A5.8.1 – **(a)** Map of spatial variation in ocean surface $\delta^{18}O$ ($\delta^{18}O_{SW}$; data from LeGrande and Schmidt (2006)). Black box shows the approximate source regions for the Amazon basin (inferred from van der Ent and Savenije (2013)). **(b)** Histogram of $\delta^{18}O_{SW}$ values extracted from the Amazon source region indicated in panel a.

Appendix 5.9 – Rayleigh-based simulation of interannual variation in tree-ring oxygen isotope composition ($\delta^{18}O_{TR}$)

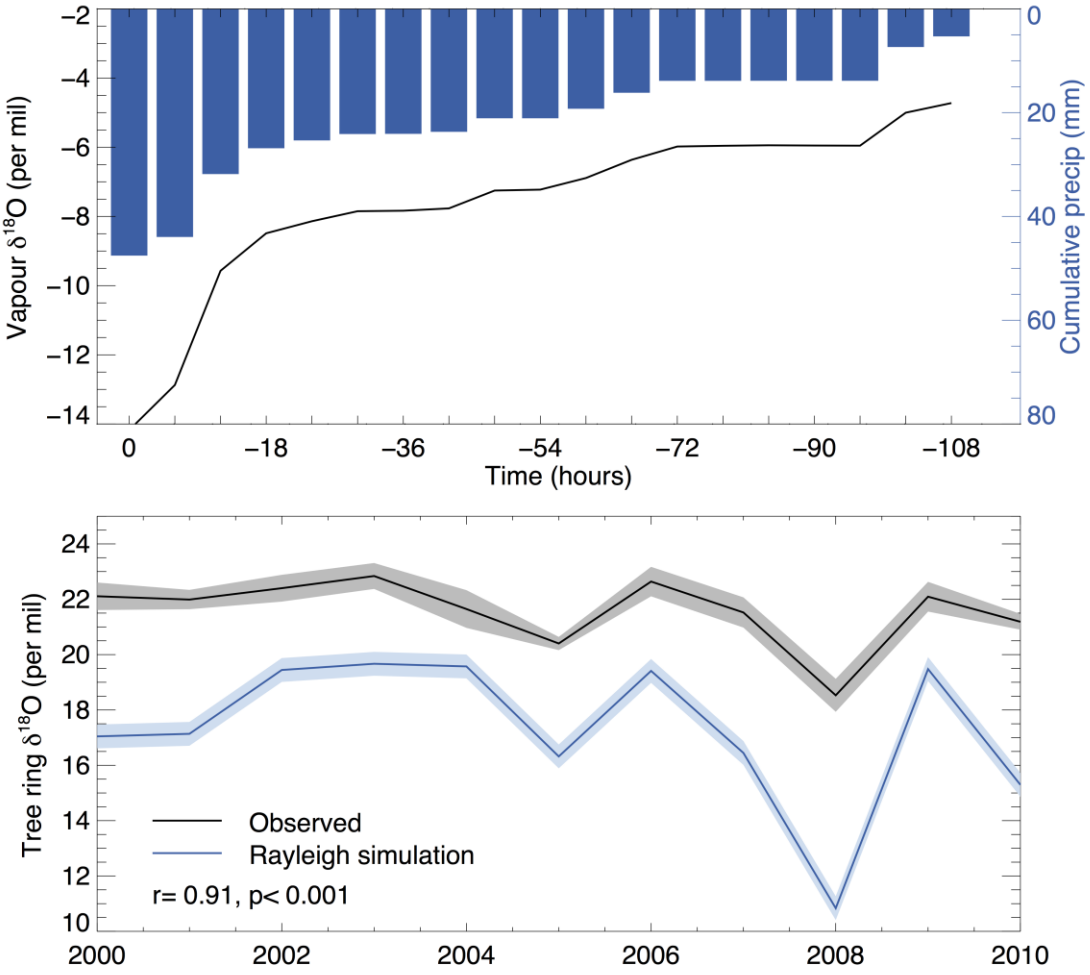

Figure A5.9.1 – **(a)** Rayleigh-predicted evolution of atmospheric water vapour $\delta^{18}O$ along a sample back-trajectory. **(b)** Interannual variation in observed (black line) and Rayleigh-simulated (blue line) $\delta^{18}O_{TR}$. The Pearson correlation coefficient is 0.91 (p<0.001). Root-mean-square error ≈1.6 ‰ (calculated with offset between simulated and observed values removed). Shading indicates the estimated error for the observed and simulated values (see Appendix 5.1).

Table A5.9.1 – Parameters used in Rayleigh simulation and their associated references.

Parameter	Description	Value (unit)	Source (if applicable)
$\delta^{18}O_{VAP}(0)$	Initial isotopic composition	–11.92 (‰)	Matsui et al. (1983), Belem mean wet season value
f	Fraction of water vapour remaining in atmosphere (equivalent to (1 - r) where r is runoff)	$1 - \left(\frac{\sum Precip - \sum ET}{q_0}\right)$	n/a
∑ET	Cumulative evapotranspiration	∑ET = 0.44 x ∑LAI – 0.25 (kg m^{-2})	Equation from Bruijnzeel et al. (2011)
q0	Initial specific humidity	61.57 (kg m^{-2})	Maximum wet season total column water vapour over Atlantic Ocean in Amazon coastal region. Data from ERA-Interim.
α	Equilibrium fractionation factor from vapour to liquid	ln α = 1.137 T^{-2} – 0.4156 T^{-1} – 0.0020667	Majoube (1971)
T	Temperature	288.3 (K)	Mean wet season trajectory temperature

Table A5.9.2 – Parameters used in error propagation for Rayleigh simulation.

Parameter	Description	Value (unit)	Source (if applicable)
f	Fraction of water vapour remaining in atmosphere (equivalent to (1 - r) where r is runoff)	0.48	Mean value from Rayleigh model
α	Equilibrium fractionation factor	1.0102	Value at mean wet season trajectory temperature
$\delta^{18}O_{VAP}(0)$	Initial isotopic composition	–11.92 (‰)	Matsui et al. (1983), Belem mean wet season value
$\sigma\delta^{18}O_{VAP}(0)$	Error in $\delta^{18}O_{VAP(0)}$	0.17 (‰)	Assumed from variation in ocean surface $\delta^{18}O$ (LeGrande and Schmidt, 2006).
N	Average number of trajectory time-steps over land	24.89	Calculated from trajectories
Δt	Length of 1 trajectory time-step	0.25 (days)	Technical Report (http://www.met.reading.ac.uk/~swrmethn/offline/UGAMP_tech44.ps)
q0	Initial specific humidity	61.57 (kg m^{-2})	Wet season total column water vapour over Atlantic Ocean in Amazon coastal region. Data from ERA-Interim.
σq0	Error in initial specific humidity	1.86 (kg m^{-2})	σ of ERA-Interim data
P	Typical TRMM precipitation value under trajectory over land	9.88 (kg m^{-2})	Average across all wet season trajectories, all years.
σP	Error in TRMM precipitation estimated as random error plus systematic error, combined in quadrature.	4.96 (kg m^{-2})	(Huffman, 1997, Smith et al., 2006, Spracklen et al., 2012)
LAI	Typical MODIS LAI value under trajectory over land	5.36 (m^2 m^{-2})	Average across all wet season trajectories, all years.
ET	Typical evapotranspiration value, estimated from LAI	2.11 (kg m^{-2})	(Bruijnzeel et al., 2011)
σET	Error in ET estimated as error in LAI measurement and error in conversion, combined in quadrature	0.66 (kg m^{-2})	(Bruijnzeel et al., 2011, Yan et al., 2016)

Appendix 6.1 – Number of climate stations in CRU precipitation dataset over time

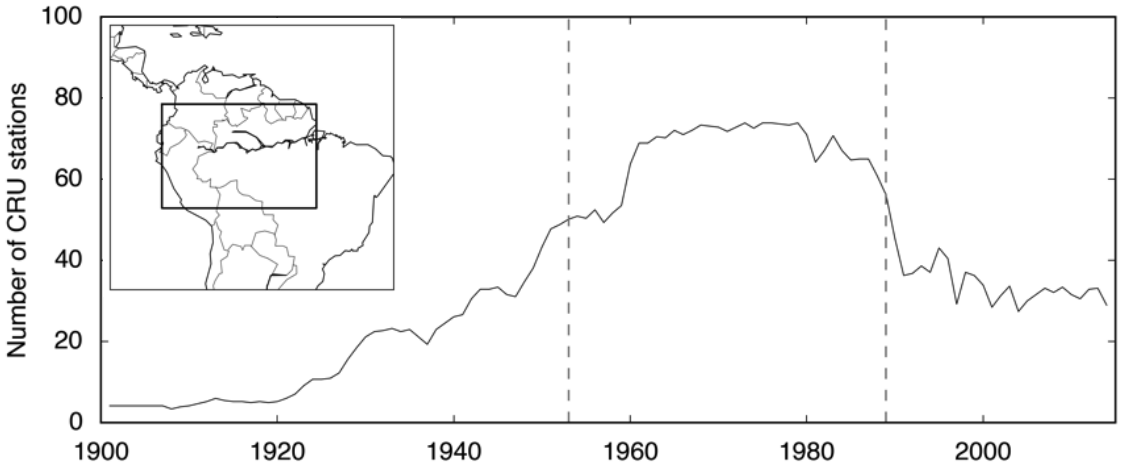

Figure A6.1.1 – Number of stations in the CRU precipitation dataset over the Amazon region indicated in the inset map.

Appendix 6.2 – Statistical analysis of tree-ring oxygen isotope ($\delta^{18}O_{TR}$) chronology quality

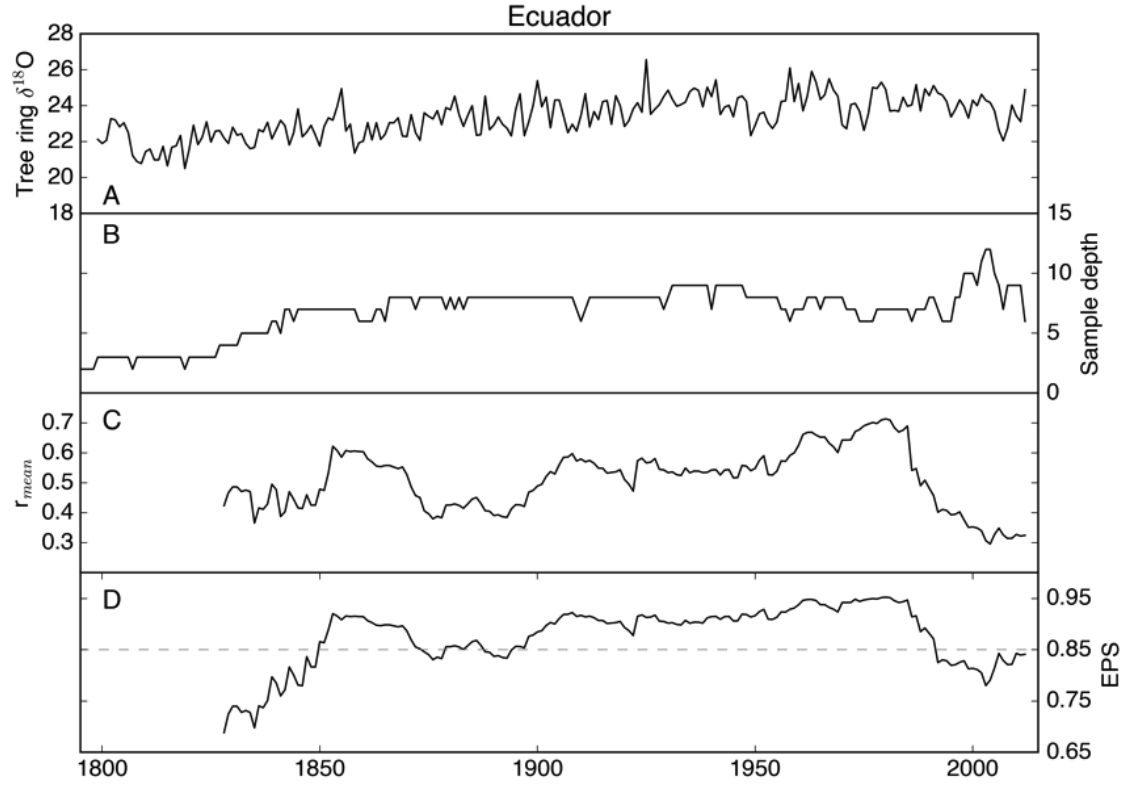

Figure A6.2.1 – **(a)** Mean interannual variation in $\delta^{18}O_{TR}$ from Ecuador; **(b)** sample depth; **(c)** moving window inter-tree correlation calculated using a 30-year window and **(d)** moving window EPS calculated using a 30-year window.

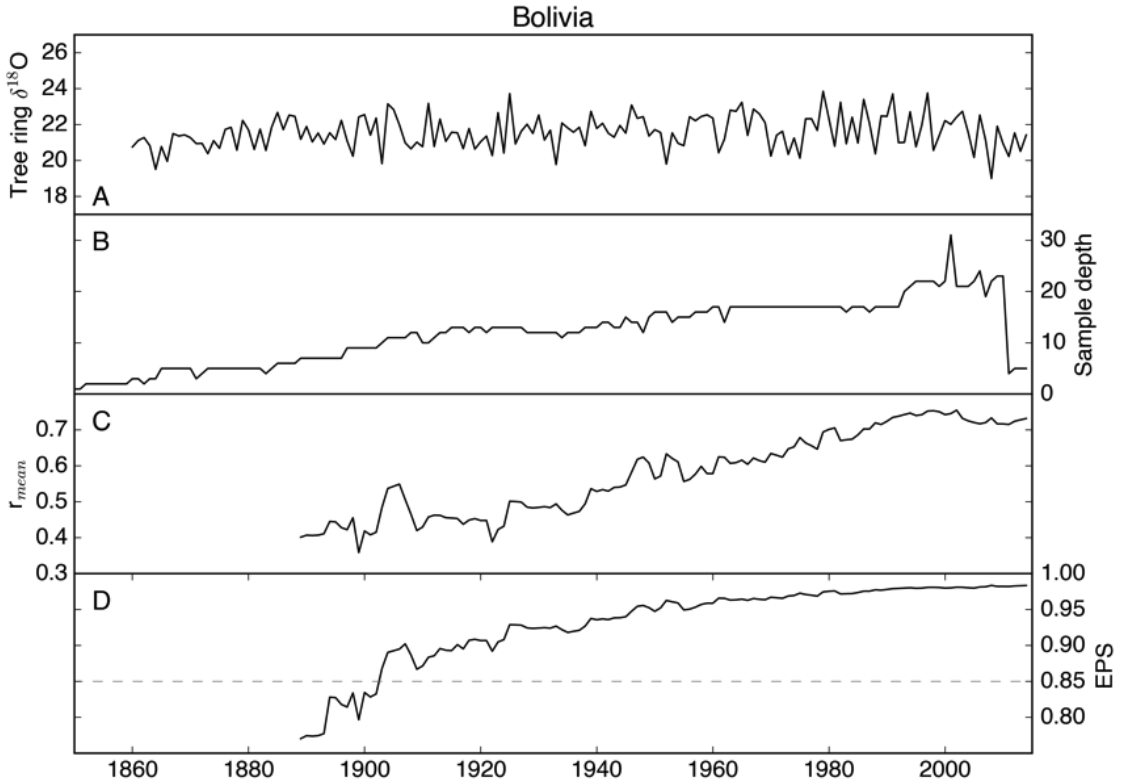

Figure A6.2.2 – (a) Mean interannual variation in $\delta^{18}O_{TR}$ from northern Bolivia; (b) sample depth; (c) running inter-tree correlation calculated using a 30-year window and (d) running EPS calculated using a 30-year window.

Appendix 6.3 – Correlation between tree-ring oxygen isotope ($\delta^{18}O_{TR}$) records from Ecuador and Bolivia

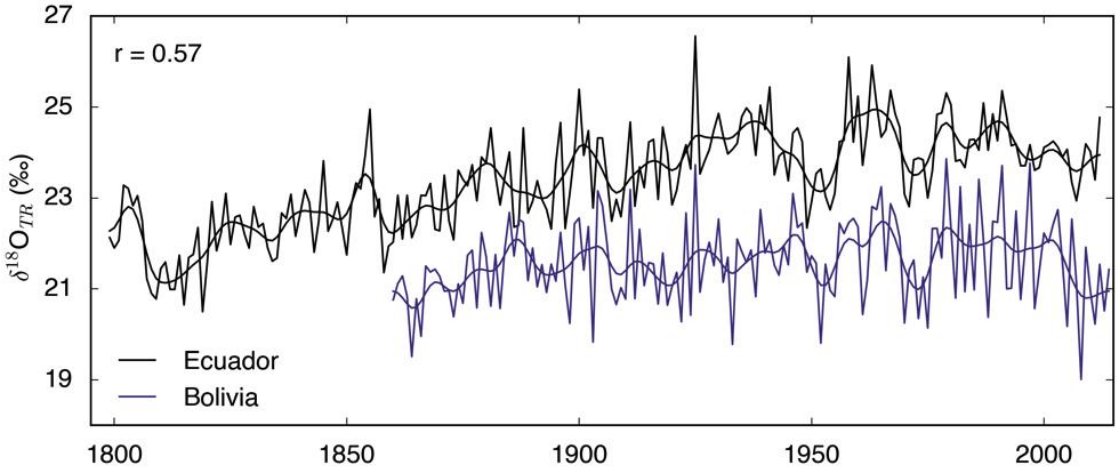

Figure A6.3.1 – Mean $\delta^{18}O_{TR}$ chronologies from Ecuador (black line) and Bolivia (dark blue line). The interannual Pearson correlation coefficient is 0.57 (p<0.001, 1860–2012). A low-pass Butterworth filter was applied to each series to visualize decadal variation.

Appendix 6.4 – Air transport pathways to sample sites in Ecuador and Bolivia

To identify the main moisture transport pathways to each of our sites (Fig. S5), 10-day kinematic back trajectories were calculated using the Reading Offline Trajectory model (ROTRAJ; Methven, 1997). ERA-Interim reanalysis wind fields were downloaded from the European Centre for Medium-Range Weather Forecasts (ECMWF, http://www.ecmwf.int/en/research/climate-reanalysis/era-interim) to drive the model. We calculated trajectories for the period 1998–2013, arriving daily (12.00 UT) at 800 hPa at each site (equivalent to 2 km above the surface in Bolivia, and at the surface in Ecuador). Precipitation data from the Tropical Rainfall Measuring Mission (TRMM) 3B42 v7 product (Huffman et al., 2007) were averaged to daily resolution and used to select only those trajectories that arrived on days with rain at the sample site, as these are the air mass histories expected to affect the $\delta^{18}O_{TR}$ signal.

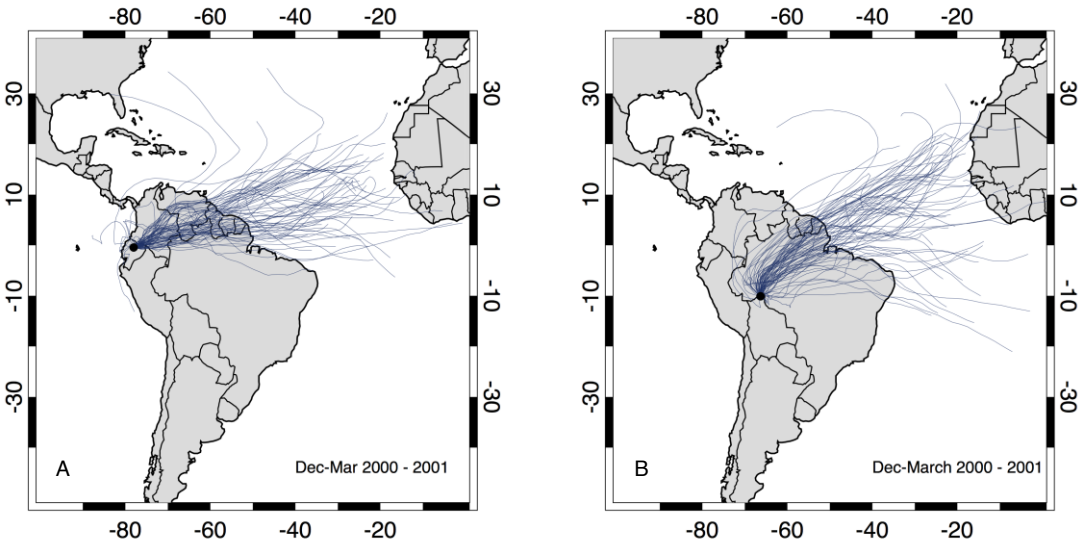

Figure A6.4.1 – Plots showing 10-day back-trajectories arriving on days with precipitation >0 mm at Cuyuja, Ecuador **(a)** and Selva Negra, Bolivia **(b)** from December to March in 2000/2001.

Appendix 6.5 – Effect of Amazon precipitation and runoff on the tree-ring oxygen isotope ($\delta^{18}O_{TR}$) record from Bolivia

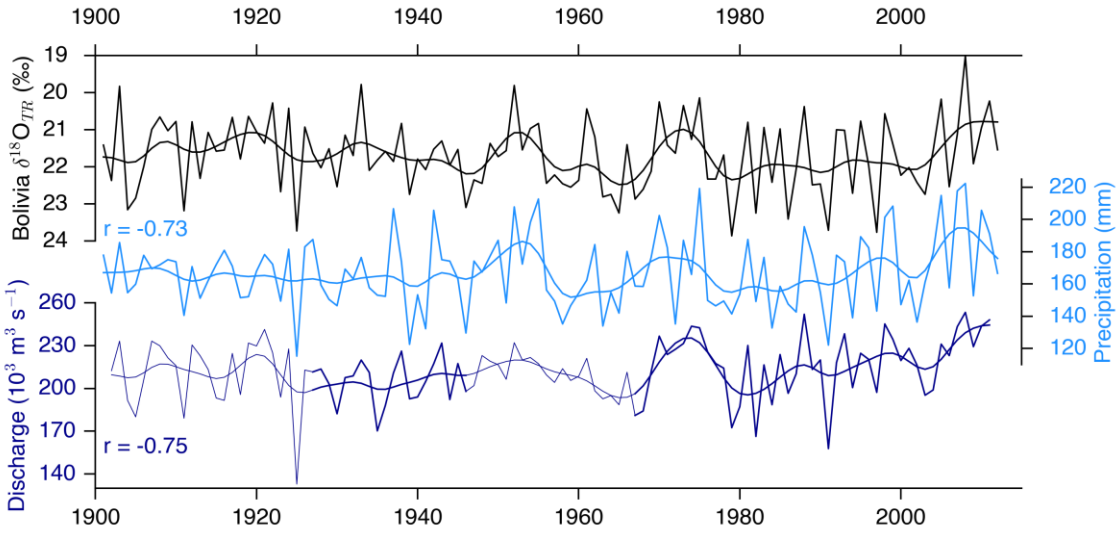

Figure A6.5.1 – Interannual variation in the $\delta^{18}O_{TR}$ record from Bolivia (black line, scale reversed), precipitation from CRU averaged over the region indicated in Fig. 2 (Dec–Mar, light blue line) and Amazon river discharge measured at Óbidos, which integrates precipitation over approximately 80% of the Amazon basin (Jun–Aug, dark blue line, line is thinner where data has been reconstructed from other river records). A low-pass Butterworth filter was applied to each series to visualize decadal variation. Values indicate the interannual Pearson correlation coefficients between $\delta^{18}O_{TR}$ and the other time series for the full period shown (p<0.001). Note that the river data is offset because peak river flow lags peak precipitation by 4–6 months.

Appendix 6.6 – Testing for local and regional temperature effects on tree-ring oxygen isotopes ($\delta^{18}O_{TR}$) from Ecuador

Table A6.6.1 – Pearson correlation coefficients and *partial correlation coefficients* between the $\delta^{18}O_{TR}$ record from Ecuador and local and north Amazon temperature data from CRU (Dec–Mar).

	Correlation with $\delta^{18}O_{TR}$	**Correlation with $\delta^{18}O_{TR}$ controlling for North Amazon precipitation**
Local temperature (1.5°S–0°N, 77.5–79°W)	0.31 (p=0.058)	*–0.079 (p=0.64)*
North Amazon temperature (5°S–12.5°N, 50–80°W)	0.52 (p<0.001)	*0.12 (p=0.48)*

Appendix 6.7 – Split-period regression statistics

Table A6.7.1 – Summary statistics for the split-period regression of the Ecuador and Bolivia $\delta^{18}O_{TR}$ chronologies against June–August Amazon River discharge measured at Óbidos.

Ecuador	r^2 for OLS model	n	Mean squared error (MSE)	Reduction of error (RE)	Coefficient of efficiency (CE)
Model 1					
Calibration 1958–2012	0.36	44	303.99	0.36	-
Verification 1903–1957	-	-	281.01	**0.28**	**0.23**
Model 2					
Calibration 1903–1957	0.58	44	152.65	0.58	-
Verification 1958–2012	-	-	429.06	**0.14**	**0.09**
Bolivia	r^2 for OLS model	n	Mean squared error (MSE)	Reduction of error (RE)	Coefficient of efficiency (CE)
Model 1					
Calibration 1958–2012	0.66	55	160.46	0.66	-
Verification 1903–1957	-	-	256.70	**0.35**	**0.30**
Model 2					
Calibration 1903–1957	0.52	55	177.11	0.52	-
Verification 1958–2012			236.99	**0.52**	**0.50**

Appendix 6.8 – Correlating the tree-ring oxygen isotope ($\delta^{18}O_{TR}$) record from Bolivia with sea surface temperature (SST) data

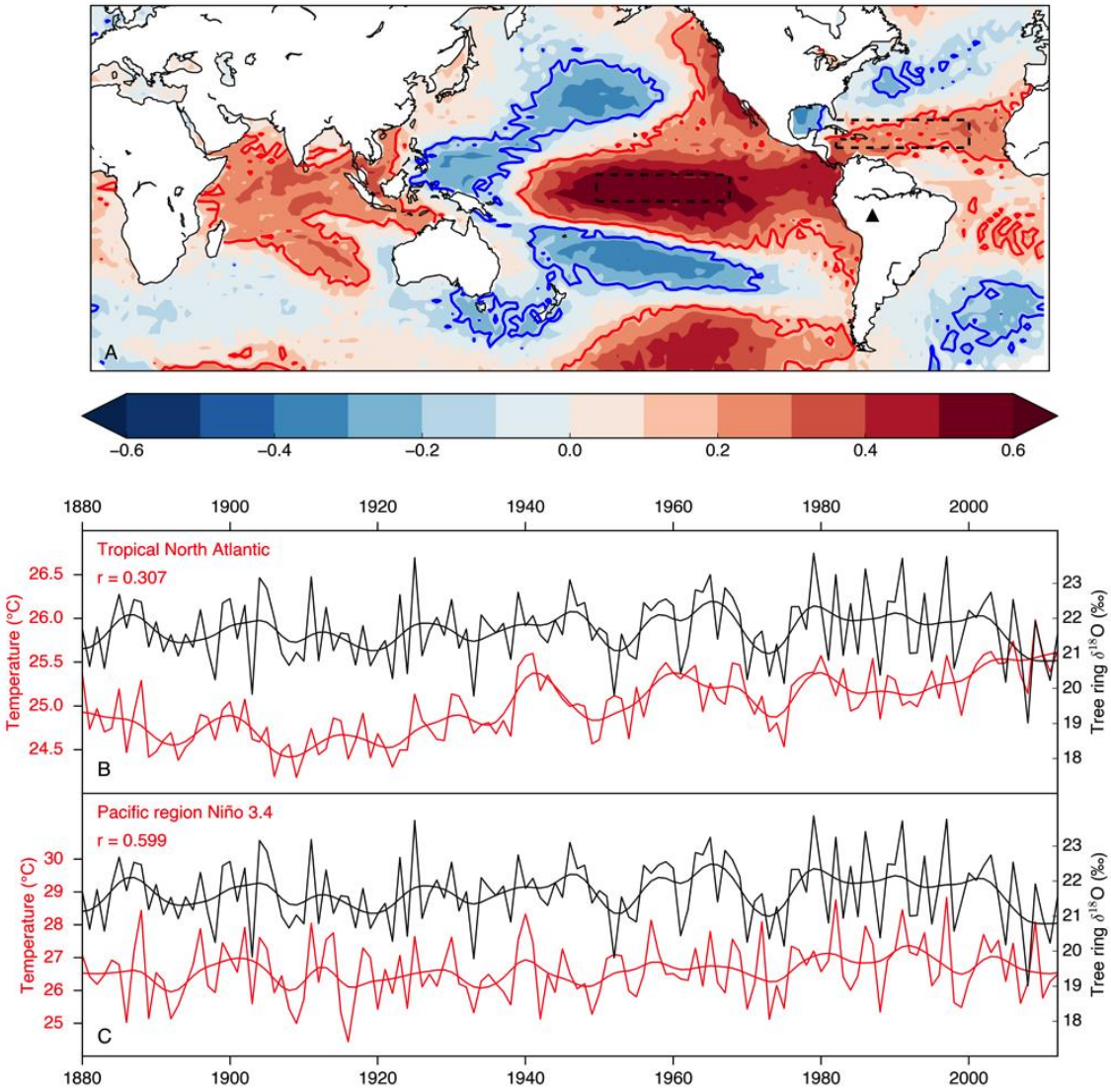

Figure A6.8.1 – (a) Map showing the relationship between the $\delta^{18}O_{TR}$ record from Ecuador and gridded SST data from NOAA for four months during the growing season (Dec-Mar, 1880–2012). The location of the $\delta^{18}O_{TR}$ sample site is indicated by a black triangle. The colour bar indicates the strength of the correlation coefficients and blue and red contours show where correlations are significant (p<0.05). Broken black lines indicate regions from which SST data were averaged in the time series shown in panels b and c. (b) Interannual variation in SSTs from the tropical North Atlantic (red line) and the Ecuador $\delta^{18}O_{TR}$ record (black line). (c) As in b, but for SSTs from the Niño 3.4 region of the Pacific. A low-pass Butterworth filter was applied to each series to visualize decadal variation. Values indicate the interannual Pearson correlation coefficients between $\delta^{18}O_{TR}$ and the other time series for the full period shown (p<0.001).

Appendix 6.9 – Comparing trajectory-inferred moisture origins with the ocean regions that influence tree-ring oxygen isotopes ($\delta^{18}O_{TR}$) in Ecuador

The start points of 10-day back trajectories from our sample site in Ecuador (see Appendix 6.4) were plotted onto a map of correlations between Ecuador $\delta^{18}O_{TR}$ and sea surface temperatures (SSTs). This provides some indication of the origin of water vapour relative to the regions where SSTs have an important influence on $\delta^{18}O_{TR}$.

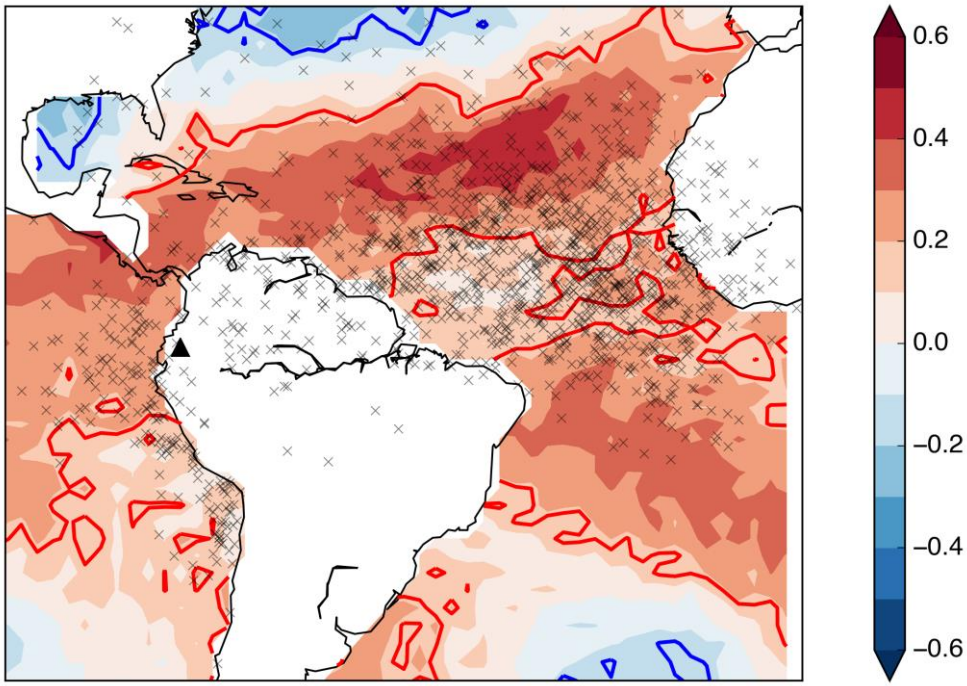

Figure A6.9.1 – Map showing the relationship between the $\delta^{18}O_{TR}$ record from Ecuador and gridded sea surface temperature (SST) data from NOAA (close-up of Fig. S7), for four months during the growing season (Dec-Mar, 1880–2012). Grey crosses show the end-points of daily 10-day back trajectories from the $\delta^{18}O_{TR}$ sample site (black triangle) for Dec–Mar, 1998–2013 (Text S1). The colour bar indicates the strength of the correlation coefficients and blue and red contours show where correlations are significant (p<0.05).

Appendix 6.10 – Effect of sea surface temperatures (SSTs) on Amazon precipitation

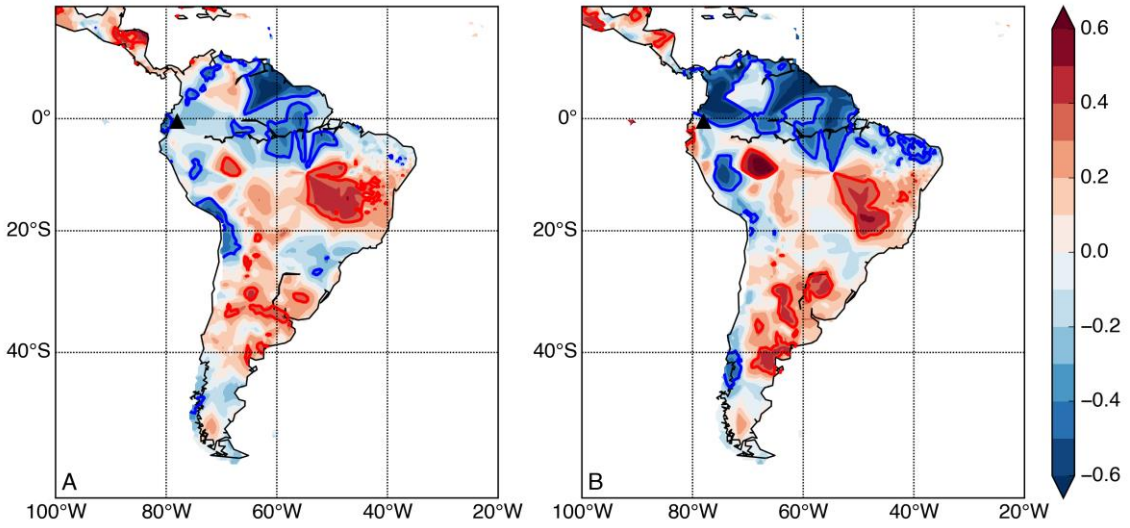

Figure A6.10.1 – Maps showing the correlation between tropical North Atlantic (a) and Pacific (b) SSTs from NOAA (averaged over regions indicated in Figs. 5a & S7a) and gridded precipitation from CRU for four months during the growing season (Dec-Mar, 1953–1989). The Ecuador sample site is indicated by a black triangle.

Appendix 6.11 – Testing for ontogenetic effects on tree-ring oxygen isotopes ($\delta^{18}O_{TR}$) from Bolivia and Ecuador

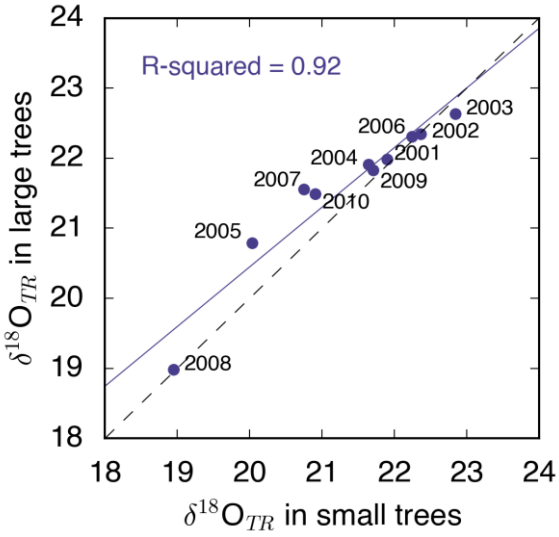

Figure A6.11.1 – Relationship between the mean $\delta^{18}O_{TR}$ value calculated from small trees (<20 cm dbh) and large trees (>60 cm dbh) from Selva Negra, Bolivia, for each year from 2001 to 2010.

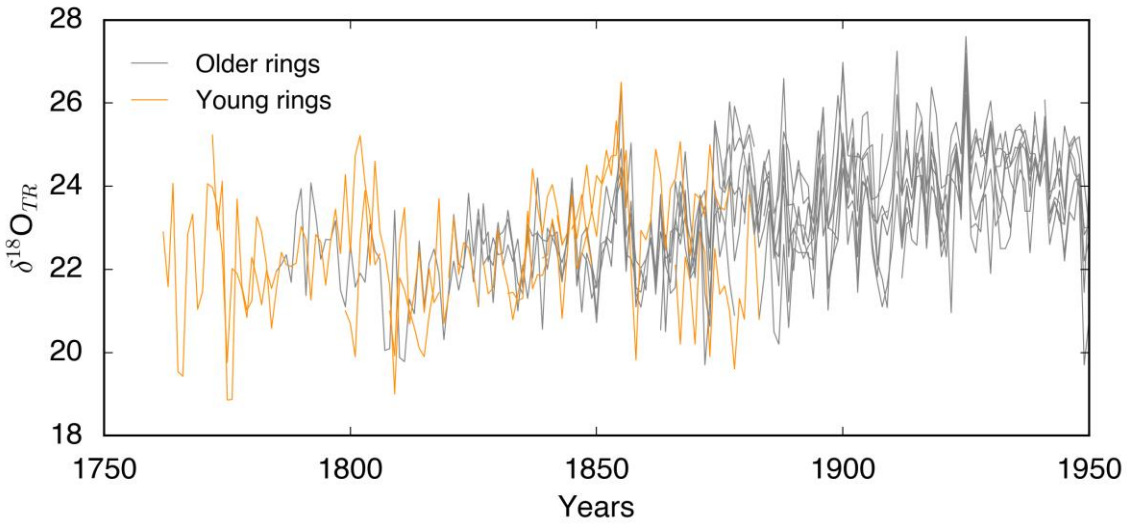

Figure A6.11.2 – $\delta^{18}O_{TR}$ series from Cuyuja, Ecuador with young rings (<20 cm dbh) and older rings (>20cm dbh) plotted in yellow and grey respectively.

Appendix 6.12 – The Péclet-modified Craig-Gordon (PMCG) model.

The PMCG model was used to quantify: i) the effect of rising atmospheric CO_2 on $\delta^{18}O_{TR}$, and ii) the effect of increasing local temperature (T) and decreasing relative humidity (RH) on $\delta^{18}O_{TR}$. For (i) the 120-ppm rise in atmospheric CO_2 since the start of the Industrial Revolution was assumed to have reduced stomatal conductance (g_s) by 40% (e.g. Lammertsma et al., 2011), while all other parameters were kept constant. For (ii) T was reduced by 0.68 °C (Vuille et al., 2008) and RH increased by 4% (see calculations in text), while all other parameters were kept constant.

Table A6.12.1 (opposite) – Equations and parameter values in the PMCG model. Calculated values are given in italics. References for literature-derived values and equations are given.

Factor	Present-day (400 ppm CO_2)	Lower CO_2 (280 ppm)	Lower T and higher RH	Unit	References
Stomatal conductance (g_s)	0.16	*0.27*	0.16	mol m^{-2} s^{-1}	Motzer et al. (2005)
Stem water ($\delta^{18}O_S$; assumed to have the same composition at precipitation)	-6.4	-6.4	-6.4	‰	Garcia et al. (1998)
Temperature (T)	10.5	10.5	9.82	°C	Papallacta station data
Relative humidity (RH)	0.9	0.9	0.94	%	
Atmospheric vapour $\delta^{18}O$ ($\delta^{18}O_V$)	-11.3	-11.3	-11.3	‰	Clark et al. (2014)
Stomatal resistance $r_s = \frac{1}{g_s}$	*6.25*	*3.75*	*6.25*	m^2 s mol^{-1}	
Boundary layer resistance (r_b)	0.2	0.2	0.2	m^2 s mol^{-1}	Barbour and Farquhar (2000)
Equilibrium fractionation: $\varepsilon^* = 2.644 - 3.206\left(\frac{10^3}{T}\right) + 1.534\left(\frac{10^6}{T^2}\right)$	*10.41*	*10.41*	*10.47*	‰	Bottinga and Craig (1968) Barbour (2007)
Kinetic fractionation: $\varepsilon_k = \frac{(32r_s+22r_b)}{(r_s+r_b)}$	*31.69*	*31.49*	*31.69*	‰	Farquhar et al. (2007)
Ambient vapour pressure: $e_a = \left(0.61365 \times e^{\frac{17.502 \times T}{T + 240.97}}\right) \times RH$	*1.15*	*1.15*	*1.14*	kPa	Cernusak et al. (2016) We assume that leaf temperature is the same as ambient temperature
Intercellular vapour pressure: $e_i = \left(0.61365 \times e^{\frac{17.502 \times T}{T + 240.97}}\right)$	*1.27*	*1.27*	*1.22*	kPa	
Ratio of ambient and intercellular vapour pressures: $\left(\frac{e_a}{e_i}\right)$	*0.9*	*0.9*	*0.94*		
Leaf water $\delta^{18}O$ at the site of evaporative enrichment: $\delta^{18}O_E = \delta^{18}O_S + \varepsilon^* + \varepsilon_k + (\delta^{18}O_V - \varepsilon_k - \delta^{18}O_S)\left(\frac{e_a}{e_i}\right)$	*2.77*	*2.75*	*1.37*	‰	Sternberg et al (2009)
Evapotranspiration rate: $ET = \frac{-2 \times 10^{-5}(g_s \times 1000)^2 + 0.0125(g_s \times 1000) - 0.2351}{1000}$	*0.0013*	*0.0017*	*0.0013*	mol m^{-2} s^{-1}	Relationship with g_s determined using data from Motzer et al. (2005) fitted with a polynomial function
Effective path length (L)	0.08	0.08	0.08	m	Barbour and Farquhar (2000)
Molar concentration of water (C)	55600	55600	55600	mol m^{-3}	Sternberg (2009)
Diffusivity of $H_2{}^{18}O$ in water (D)	2.66×10^{-9}	2.66×10^{-9}	2.66×10^{-9}	m^2 s^{-1}	
Péclet number: $\rho = \frac{ET \times L}{C \times D}$	*0.68*	*0.91*	*0.68*		Barbour and Farquhar (2000)
Fraction of enriched water: $\alpha = \left(\frac{1-e^{-\rho}}{\rho}\right)$	*0.73*	*0.66*	*0.73*		
Bulk leaf water $\delta^{18}O$: $\delta^{18}O_L = ((1-\alpha) \times \delta^{18}O_S) + (\alpha \times \delta^{18}O_E)$	*0.26*	*-0.39*	*-0.76*	‰	Sternberg (2009)
$\delta^{18}O$ of carbohydrates synthesised in the leaf: $\delta^{18}O_{CARB} = \delta^{18}O_L + 27$	*27.26*	*26.61*	*26.24*	‰	
Proportion of carbohydrate $\delta^{18}O$ that exchanges with stem water (ϕ)	0.4	0.4	0.4		
Tree-ring cellulose $\delta^{18}O$: $\delta^{18}O_{TR} = \phi \times (\delta^{18}O_S + 27) + (1-\phi)(\delta^{18}O_{CARB})$	*24.73*	*24.33*	*23.98*	‰	
Difference in $\delta^{18}O_{TR}$ from present-day	–	***0.39***	***0.61***	‰	

Appendix 7.1 – Preliminary $\delta^{18}O_{TR}$ data from Venezuela, Brazil and Suriname

One of the aims of this thesis was to develop a network of $\delta^{18}O_{TR}$ records from sites across tropical South America. In sites where stable isotope dendrochronology had not previously been conducted pilot $\delta^{18}O_{TR}$ series were initially developed for three trees, to test the potential for chronology development. This was to avoid investing too much time or too many resources trying to construct robust chronologies in unsuitable sites. If these pilot $\delta^{18}O_{TR}$ series did not show a strong common signal then no further isotope measurements would be made in that location.

Results from radiocarbon (^{14}C) analysis showed that trees in Suriname form two rings each year. Isotope measurements were conducted on each ring individually, so to obtain annual $\delta^{18}O_{TR}$ values it was necessary to use weighted averaging. Each $\delta^{18}O_{TR}$ value was weighted by the width of that ring as a fraction of the full growth in that year.

Appendix 7.2 – References for the Appendices

HidroWeb [Online]. Agência Nacional de Águas. Available: http://hidroweb.ana.gov.br [Accessed 2017].

Baker, J. C. A., Hunt, S. F. P., Clerici, S. J., Newton, R. J., Bottrell, S. H., Leng, M. J., Heaton, T. H. E., Helle, G., Argollo, J., Gloor, M. & Brienen, R. J. W. 2015. Oxygen isotopes in tree rings show good coherence between species and sites in Bolivia. *Global and Planetary Change,* 133**,** 298-308.

Barbour, M. M. & Farquhar, G. D. 2000. Relative humidity- and ABA-induced variation in carbon and oxygen isotope ratios of cotton leaves. *Plant, Cell and Environment,* 23**,** 473-485.

Barbour, M. M. 2007. Stable oxygen isotope composition of plant tissue: a review. *Functional Plant Biology,* 34**,** 83-94.

Bottinga, Y. & Craig, H. 1968. Oxygen isotope fractionation between CO_2 and water, and the isotopic composition of marine atmospheric CO_2. *Earth and Planetary Science Letters,* 5**,** 285-295.

Bruijnzeel, L., Mulligan, M. & Scatena, F. N. 2011. Hydrometeorology of tropical montane cloud forests: emerging patterns. *Hydrological Processes,* 25**,** 465-498.

Callède, J., Ronchail, J., Guyot, J.-L. & Oliveira, E. D. 2008. Déboisement amazonien: son influence sur le débit de l'Amazone à Óbidos (Brésil). *Revue des sciences de l'eau/Journal of Water Science,* 21**,** 59-72.

Cernusak, L. A., Barbour, M. M., Arndt, S. K., Cheesman, A. W., English, N. B., Feild, T. S., Helliker, B. R., Holloway-Phillips, M. M., Holtum, J. A., Kahmen, A., McInerney, F. A., Munksgaard, N. C., Simonin, K. A., Song, X., Stuart-Williams, H., West, J. B. & Farquhar, G. D. 2016. Stable isotopes in leaf water of terrestrial plants. *Plant, Cell and Environment,* 39**,** 1087-1102.

Clark, K. E., Torres, M. A., West, A. J., Hilton, R. G., New, M., Horwath, A. B., Fisher, J. B., Rapp, J. M., Robles Caceres, A. & Malhi, Y. 2014. The hydrological regime of a forested tropical Andean catchment. *Hydrology and Earth System Sciences,* 18**,** 5377-5397.

Farquhar, G. D., Cernusak, L. A. & Barnes, B. 2007. Heavy water fractionation during transpiration. *Plant Physiology,* 143**,** 11-18.

Garcia, M., Villalba, F., Araguas-Araguas, L. & Rozanski, K. 1998. The role of atmospheric circulation patterns in controlling the regional distribution of stable isotope contents in precipitation: Preliminary results from two transects in the Ecuadorian Andes. *Isotope techniques in the study of environmental change.* International Atomic Energy Agency (IAEA): IAEA.

Huffman, G. J. 1997. Estimates of root-mean-square random error for finite samples of estimated precipitation. *Journal of Applied Meteorology,* 36**,** 1191-1201.

Huffman, G. J., Bolvin, D. T., Nelkin, E. J., Wolff, D. B., Adler, R. F., Gu, G., Hong, Y., Bowman, K. P. & Stocker, E. F. 2007. The TRMM multisatellite precipitation analysis (TMPA): Quasi-global, multiyear, combined-sensor precipitation estimates at fine scales. *Journal of Hydrometeorology,* 8**,** 38-55.

IAEA/WMO. [Online]. Global Network of Isotopes in Precipitation. The GNIP Database. Available: http://www.iaea.org/water [Accessed 2016].

Lammertsma, E. I., De Boer, H. J., Dekker, S. C., Dilcher, D. L., Lotter, A. F. & Wagner-Cremer, F. 2011. Global CO_2 rise leads to reduced maximum stomatal conductance in Florida vegetation. *Proceedings of the National Academy of Sciences,* 108**,** 4035-4040.

Legrande, A. N. & Schmidt, G. A. 2006. Global gridded data set of the oxygen isotopic composition in seawater. *Geophysical Research Letters,* 33**,** 1-5.

Majoube, M. 1971. Fractionnement en oxygène-18 et en deutérium entre l'eau et sa vapeur. *Journal de Chimie Physique et de Physico-Chimie Biologique,* 58**,** 1423-1435.

Matsui, E., Salati, E., Ribeiro, M., Ris, C., Tancredi, A. & Gat, J. 1983. Precipitation in the Central Amazon Basin: the isotopic composition of rain and atmospheric moisture at Belem and Manaus. *Acta Amazonica,* 13**,** 307-369.

Methven, J. 1997. Offline trajectories: Calculation and accuracy. UK Universities Global Atmospheric Modelling Programme.

Motzer, T., Munz, N., Kuppers, M., Schmitt, D. & Anhuf, D. 2005. Stomatal conductance, transpiration and sap flow of tropical montane rain forest trees in the southern Ecuadorian Andes. *Tree Physiology,* 25**,** 1283-1293.

Myneni, R., Hoffman, S., Knyazikhin, Y., Privette, J., Glassy, J., Tian, Y., Wang, Y., Song, X., Zhang, Y. & Smith, G. 2002. Global products of vegetation leaf area and fraction absorbed PAR from year one of MODIS data. *Remote sensing of environment,* 83**,** 214-231.

Samanta, A., Costa, M. H., Nunes, E. L., Vieira, S. A., Xu, L. & Myneni, R. B. 2011. Comment on

"Drought-Induced Reduction in Global Terrestrial Net Primary Production from 2000 Through 2009". *Science,* 333**,** 1093.

Smith, T. M., Arkin, P. A., Bates, J. J. & Huffman, G. J. 2006. Estimating bias of satellite-based precipitation estimates. *Journal of Hydrometeorology,* 7**,** 841-856.

Spracklen, D. V., Arnold, S. R. & Taylor, C. M. 2012. Observations of increased tropical rainfall preceded by air passage over forests. *Nature,* 489**,** 282-285.

Sternberg, L. D. S. L. & Deniro, M. J. 1983. Biogeochemical implications of the isotopic equilibrium fractionation factor between the oxygen atoms of acetone and water. *Geochimica et Cosmochimica Acta,* 47**,** 2271-2274.

Sternberg, L. D. S. L. 2009. Oxygen stable isotope ratios of tree-ring cellulose: the next phase of understanding. *New Phytologist,* 181**,** 553-562.

Thompson, L. G., Mosley-Thompson, E. & Davis, M. E. 1995. Late glacial stage and Holocene tropical ice core records from Huascaran, Peru. *Science,* 269**,** 46-50.

Thompson, L. G., Mosley-Thompson, E., Davis, M. E., Zagorodnov, V. S., Howat, I. M., Mikhalenko, V. N. & Lin, P. N. 2013. Annually resolved ice core records of tropical climate variability over the past ~1800 years. *Science,* 340**,** 945-950.

Van Der Ent, R. J. & Savenije, H. H. 2013. Oceanic sources of continental precipitation and the correlation with sea surface temperature. *Water Resources Research,* 49**,** 3993-4004.

Vuille, M., Francou, B., Wagnon, P., Juen, I., Kaser, G., Mark, B. G. & Bradley, R. S. 2008. Climate change and tropical Andean glaciers: Past, present and future. *Earth-Science Reviews,* 89**,** 79-96.

Yan, K., Park, T., Yan, G., Chen, C., Yang, B., Liu, Z., Nemani, R. R., Knyazikhin, Y. & Myneni, R. B. 2016. Evaluation of MODIS LAI/FPAR Product Collection 6. Part 1: Consistency and Improvements. *Remote Sensing,* 8**,** 1-16.